UNIVERSITY OF CALIFORNIA, SAN DIEGO

A unified hypothesis of visual asymmetry, interhemispheric communication, and their typical development in humans

A dissertation submitted in partial satisfaction of the
requirements for the degree
Doctor of Philosophy

in

Cognitive Science (with a specialization in Anthropogeny)

by

Benjamin N. Cipollini

Committee in charge:

Professor Garrison W. Cottrell, Chair
Professor Virgina de Sa
Professor Steven Hillyard
Professor Terry Jernigan
Professor Marta Kutas
Professor Katerina Semendeferi

2014

The dissertation of Benjamin N. Cipollini is approved, and it is acceptable in quality and form for publication on microfilm and electronically:

_____

_____

_____

_____

_____

_____

Chair

University of California, San Diego

2014

DEDICATION

To my family, friends, loved ones... all those who supported me on this journey, and continue to support in what I do. You make me who I am and though this work may be incomprehensible to you, your fingerprints are all over it.

No, seriously–wash your hands before you read through this; your fingerprints are all over it from the last time!

Special love (and all that good stuff) to:

- Kelly, who (wo)mans the front lines. I appreciate you, baby.
- My mom & dad, who lovingly accepted my pure focus on what's in front of me and my inability to redirect attention to other things. I appreciate you.
- My brothers–Ned, Matt, and Jim–who also give me love and support when I need it, even as my focus has remained on this work. I appreciate you.

EPIGRAPH

There's never enough time to do all the nothing you want.

—Calvin[1]

[1] Watterson, B. (1990). The Authoritative Calvin and Hobbes (Original edition.). Kansas City: Andrews McMeel Publishing. p. 213

TABLE OF CONTENTS

[2]This chapter was published in the Journal of Cognitive Neuroscience (Hsiao, Cipollini, & Cottrell, 2013)

[3]This chapter was published in the NCPW 2013 conference proceedings (Cipollini & Cottrell, 2013a)

[4]This chapter will be published in the COGSCI 2014 conference proceedings (Cipollini & Cottrell, 2014)

[5]An early version of this chapter was published in the COGSCI 2013 conference proceedings (Cipollini & Cottrell, 2013b)

[6]This chapter was submitted as an abstract to the COSYNE 2013 conference.

[7]This proposal was originally written for my dissertation proposal and is repeated here for reference in future directions.

[8]This proposal was originally submitted for a post-doc fellowship application and is repeated here for reference in future directions.

LIST OF FIGURES

LIST OF TABLES

ACKNOWLEDGEMENTS

I am excited to have this opportunity to write about lateralization and interhemispheric communication. I feel like a ***cognitive scientist***: I read in neuroscience, anthropology, psychology, neuroscience, and computer science (sorry philosophy!), specialized in computational neuroscience *and* anthropogeny. It's been a long journey, and so many people to thank along the way.

Sometimes academia seemed so distant and closed. All my thanks to **Dr. Lourdes Anllo-Vento** for taking me seriously and reaching out to me when it seemed nobody else would. You're a mentor and like family... and I treat you like family (((silence)))! Thanks also to **Dr. Eric Halgren** for working with me and inspiring me through his research with Anders; I've been silently so impressed with what you do and how you do it, and wish I had offered more in return. Finally, thanks to **Dr. Marta Kutas** for helping bring me to the cognitive science department. for her advice and support from the very beginning. You really listen, you really care, and you're so trustworthy. I rarely use this word, but it's *lovely* to know you.

I have really enjoyed studying lateralization and interhemispheric communication. Many of these lateralized functions are the same functions that we believe make us human–skilled manual tool use, language production, face and social cue processing, even emotional processing all show lateralization in humans. The topic is so broad, I can *be* a cognitive scientist in this topic–and I enjoy it. Thanks to **Dr. Garrison Cottrell and GURU** for making a home for me and begin open to my ideas. I appreciate the openness to all of the ideas I've tried, the opportunities to learn by going to so many conferences, and the patience and trust that eventually *I will publish these results!*.

The combination of this topic, my advisors and collaborators, this university, and the community of people around it have all allowed me to explore human origins while still remaining faithful to my research topic. This broad reach has been critical to

fostering and maintaining my interests over the years of study. Thanks to **Dr. Pascal Gagneux**, **Dr. Ajit Varki**, and Anthropogeny crew for changing my life–particularly to **Dr. Leela Davies** and **Hope Morgan** for all we went through–state-side and homeland-side–together. Thanks to **Dr. Katerina Semendeferi**, **Kari Hanson**, and the rest of the Laboratory for Human Comparative Neuroanatomy for putting up with my naivet and varied interests. Thanks to the Perceptual Expertise Network, particularly **Dr. Marlene Behrmann**, **Dr. Isabel Gauthier**, **Dr. Michael Tarr**, **Dr. Thomas Palmeri** and **Dr. Jim Tanaka** for opening up your expertise to me and my interests, and all the time spent thinking together. Thanks to the iSLC cohort, particularly **Dr. Kaja Jasinska** and **Dr. Gabriella Musacchia**. When we talked, I felt excited–I love that feeling!

I've been in graduate school for a full 7 years, largely from being engaged in projects outside of academia. Thanks to **Naresh Guntupalli** for his efforts and interest in working together within the daily deals domain. Thanks to **Dr. Eugene Izhikevich** and the team at Brain Corporation for involving me in your science, engineering, and business approach–it's always been exciting, and I appreciate the opportunities! Thanks to the core FLE team–**Dr. Jamie Alexandre**, **Dylan Barth**, **Richard Tibbles**, **Liz Vu**, **Aron Asor**, **Guan Wang**, and **Rui Malheiro**–for sharing opportunities to have impact, learn new ways of doing things, and even things new things to do!

Along the way, I've struggled to take care of things needing to be taken care of. **Beverley Walton**, **Linda Nelson**, **Thanh Maxwell**, **Andrew Kovacevic**, I really appreciate the things you've done to help make this all happen for me. Without your help, patience, and kindness, I don't know what I would have done!

And finally, thanks to an unlikely source of help during the writing of this dissertation: **Otter Pops**, you rescued me! Oh, and to San Diego for being my home.

And now, some more formal acknowledgements:

I'd like to acknowledge my committee members **Dr. Virginia de Sa**, **Dr. Steven**

My home: San Diego, CA

Hillyard, **Dr. Terry Jernigan**, **Dr. Marta Kutas**, and **Dr. Katerina Semendeferi** for taking the time to review this work and my dissertation defense, and to offer your willingness, experience, and knowledge to make me a better researcher and thinker.

I'd like to acknowledge my collaborators: **Dr. Janet Hsiao**, for her openness to involve me in her differential encoding project and collaborating on a journal and conference paper together (Hsiao et al., 2013; Cipollini, Hsiao, & Cottrell, 2012), and **Dr. Garrison Cottrell** for his co-authorship of all of my publications (Cipollini et al., 2012; Cipollini & Cottrell, 2013b, 2013a; Hsiao et al., 2013; Cipollini & Cottrell, 2014) and Chapters 2 - 6, all of the feedback on presentations, posters, writing, and discussions on ideas–and how they all contributed to every chapter in this thesis. I think you underestimate your impact on these projects; though some of these may be my original ideas, if they reach anybody it will be because of how you helped me to think about them, understand them, then explain them, and you enabled me to have so many opportunities to share the ideas with others.

I'd also like to acknowledge my funding sources. CARTA fully funded me for three years. The TDLC's NSF grant funded me for this past year and funded my participation in PEN meetings and many conferences each year.

VITA

1994-1998	B. S. in Computer Science, Lehigh University, Bethlehem, PA
2003-2004	Non-degree study, University of Washington, Seattle, WA
2004-2005	Non-degree study, Yoshida Nihongo Gakuin, Tokyo, Japan.
2005-2007	Research Assistant, Lourdes Anllo-Vento, San Diego, CA.
2007-2010	M. S. in Cognitive Science, University of California, San Diego, CA
2007-2014	Ph. D. in Cognitive Science with a specialization in anthropogeny, University of California, San Diego, CA

PUBLICATIONS

Cipollini, B., Hsiao, J. H., & Cottrell, G. W. (2012). Connectivity asymmetry can explain visual hemispheric asymmetries in Local/Global, face, and spatial frequency processing. In Proceedings of the 34th annual meeting of the cognitive science society. Austin, TX: Cognitive Science Society.

Hsiao, J. H., Cipollini, B., & Cottrell, G. W. (2013). Hemispheric asymmetry in perception: A differential encoding account. Journal of Cognitive Neuroscience, 1-10.

Cipollini, B., & Cottrell, G. W. (2013). Sparse connectivity asymmetry in an autoencoder can explain visual hemispheric asymmetries in local/global, face, and spatial frequency processing. In Proceedings of the 13th annual neural computation and psychology workshop. San Sebastian, Spain: Neural Computation and Psychology Workshop.

Cipollini, B., & Cottrell, G. W. (2013). Uniquely human developmental timing may drive cerebral lateralization and interhemispheric coupling. In Proceedings of the 35th annual meeting of the cognitive science society. Austin, TX: Cognitive Science Society.

Cipollini, B., & Cottrell, G. W. (2014). A developmental model of hemispheric asymmetries of spatial frequencies. In Proceedings of the 36th annual meeting of the cognitive science society. Austin, TX: Cognitive Science Society.

ABSTRACT OF THE DISSERTATION

A unified hypothesis of visual asymmetry, interhemispheric communication, and their typical development in humans

by

Benjamin N. Cipollini

Doctor of Philosophy in Cognitive Science (with a specialization in Anthropogeny)

University of California, San Diego, 2014

Professor Garrison W. Cottrell, Chair

Lateralization is a part of virtually every function we think makes us human, yet there is no integrated neurophysiological explanation of the development of lateralization and interhemispheric integration. In this thesis I propose how development, lateralization in visual processing, and interhemispheric connectivity are all intertwined.

I begin with evidence from neurocomputational modeling that lateralization in visual processing can be accounted for by a difference in the length of long-range lateral connections brought on by typical human developmental processes. The model can explain processing asymmetries for low vs. high spatial frequencies, local vs. global

stimuli, as well as the right hemisphere lateralization of faces.

Next, I show modeling evidence against the prevailing hypothesis that lateralization and interhemispheric communication are both functions of brain size. Previous papers have argued that lateralization is related to hemispheric independence which increases with brain size, due to both longer latency and proportionally fewer interhemispheric connections in larger brains. I examine interhemispheric connectivity across species using a new allometric analysis of existing data and examine latency effects through a re-analysis of neural network modeling data. Both results suggest that interhemispheric communication is robust across brain sizes.

Along the way, I examine the neurophysiological development of long-range connections. I use neural network modeling to show that developmental changes in the physiology of axons may bias learning towards more local intrahemispheric circuits early in development, with long distance interhemispheric circuits becoming more prominent as connections mature. These modeling results are broadly consistent with the developmental trajectory of both interhemispheric communication and lateralization. I conclude by attempting to integrate these results into existing theories of developmental and adult visual lateralization.

In many domains, communication is the key to the development of specialization. I hope this work can refocus our efforts to understand how interhemispheric communication affects the development of each lateralized function in the brain and treat any relationships between hemispheric independence and lateralization as an unexpected special case worth investigating further.

Chapter 1

Introduction

Lateralization is a part of virtually every function that we think makes us human, but its evolutionary origins, neurophysiological underpinnings, and relationship to interhemispheric transfer all remain a mystery. Vision is such an important sense for primates that it takes over 50% of cortex in macaque monkeys (Sereno & Allmann, 1991), is one of the major research foci across neuroscience and psychology, and is lateralized in humans, yet no integrated neurophysiological explanation of lateralization in vision, from birth to adulthood, exists. We have cognitive (Ivry & Robertson, 1998) and neurophysiological (Hellige, 1993; Howard & Reggia, 2007) theories about where lateralization comes from, and we have computational ideas on how interhemispheric communication relates to lateralization generally (Ringo et al., 1994; Reggia & Schulz, 2002) and more specifically in the visual domain (Monaghan & Shillcock, 2004; Plaut & Behrmann, 2011). We lack a single theory to integrate across development, explain weak population-level findings, and explain how lateralization generalizes beyond lab experiments and fits into everyday vision.

This thesis is an attempt at building such an integrated theory. To do so, I drill down into neurocomputational mechanisms of visual asymmetries and interhemispheric

integration. Because insufficient neural data exist to directly tie neurophysiology to these phenomena, I closely examine the experimental paradigms that evoke behavioral asymmetries, I look at how neuroanatomy interacts with those experimental paradigms, and I consider how these potential mechanisms fit with developmental findings in the literature. I use computational modeling to investigate potential links between behavior and neuroanatomy.

Ultimately, the modeling data provide testable hypotheses on links between brain and behavior. Though speculative, such links may be used to drive experimental research as well as mechanisms for implementing high-level theories and findings in neural software and hardware. Though the value of this work will only be determined as such experiments and implementations occur, I hope this work might encourage others to approach the vast amounts of data we already have with big ideas that connect to numerous results and computational tools to test such ideas rigorously.

Approach

This thesis is driven by the view that the level of specification in current theories is too high to give an integrated account of visual asymmetry and interhemispheric integration. Because these theories fail to connect behavioral findings and computational models to specific neural mechanisms, they cannot use the richness in the neurophysiological literature to predict how mechanisms interact or change over development. The power of these physiological constraints and data is to help produce specific predictions about where, when, and how each of the relevant phenomena arise.

For this reason, the broad approach within this thesis is to create and analyze computational models that examine specific neuroanatomical and developmental mechanisms, to characterize their computational properties and their potential relationships to

behavioral data, then to use the results to create hypotheses about lateralization in visual processing and interhemispheric transfer. Though not all aspects of these hypotheses are examined and tested in this thesis, the computational models are based on measurable neuroanatomical properties and therefore capable to be used to generate quantitative predictions. Because care is taken to differentiate developmental neurophysiology from adult neurophysiology and to connect the two together, hypotheses can be generated for specific stages along the human lifespan.

Why visual asymmetries?

One of the fundamental jobs of our visual system is to parse a visual scene into an overall "global" configuration and smaller, "local" parts. This separation of large-scale, low-frequency configural information from small-scale, high-frequency detail is necessary for everyday tasks such as face recognition (Goffaux, Hault, Michel, Vuong, & Rossion, 2005), scene recognition (Bar, 2004), and reading. Since Sergent (1982)'s seminal work in the early 1980s, many behavioral studies have examined how the two hemispheres differ in perceptual processing of the visual scene. Generally, theses studies have found right hemisphere (RH) dominance of global-level / low spatial frequency / contour processing and left hemisphere (LH) dominance of local-level / high spatial frequency / detail processing (see Sergent (1983); Christman (1989); Van Kleeck (1989) for reviews). Since then, brain damage patient studies (e.g. Robertson, Lamb, and Knight (1988); Lamb, Robertson, and Knight (1990)), neuroimaging studies (e.g. Fink et al. (1997); Martinez et al. (1997); Martinez, Di Russo, Anllo-Vento, and Hillyard (2001); Hopf et al. (2006)), and computational modeling (Ivry & Robertson, 1998; Hsiao, Shahbazi, & Cottrell, 2008) have all supported the behavioral findings and helped search for underlying mechanisms.

Visual processing is more weakly lateralized, both within an individual and across the population, than other lateralized functions such as language production or skilled manual tool use. Nonetheless, lateralization of visual processing is well-suited for investigating a relationship between lateralization of function, neural asymmetries, and how neural asymmetries interact across the corpus callosum. Vision has dominated neuroanatomical studies and are prevalent in behavioral psychology, making it more plausible to discover a causal link between brain and behavior. There are ample data available to develop and test computational models, due to the wide range of behavioral studies relevant to visual processing, including studies that likely include variations in interhemispheric involvement. A number of reviews (Sergent, 1983, 1985; Christman, 1989; Van Kleeck, 1989; Ivry & Robertson, 1998) have focused the field to key issues (such as variability over stimulus parameters, task-demands, relative frequency information), helping to focus the field and set a baseline for comparing hypotheses about underlying neural mechanisms. A number of psychological, anatomical, and computational models have been proposed (Sergent, 1982; Ivry & Robertson, 1998; Hellige, 1993; Hutsler & Galuske, 2003; Howard & Reggia, 2007; Hsiao, Shahbazi, & Cottrell, 2008), providing ample ground for comparison and discussion.

Unfortunately, lateralized processing of vision is not nearly as appealing to neurophysiologists as language lateralization or handedness, and so until recently no neuroanatomical nor neurophysiological study has tried to investigate its neural origins in humans (but see Chance et al. (2013)). In addition, attempts to map experimental procedures in humans to those of animals studies have left us with more unexplained variability and very few clear results. Perhaps for these reasons, some aspects of the literature seem to have stagnated over the past 25 years.

Without data to tie behavioral findings to neurophysiological mechanisms, I became interested in the work of of Hsiao, Shahbazi, and Cottrell (2008). This preliminary

report showed an association between connection spread in visual processing and behavioral asymmetries. Though not shown in that paper, the association reported suggested that shorter connections may be biased for low spatial frequency processing–the opposite association found for center-surround receptive fields. The paper was loosely inspired by an anatomical study showing an asymmetry in long-range lateral connections in auditory cortex (R. A. Galuske, Schlote, Bratzke, & Singer, 2000), but very few links direct links between neuroanatomy and computation were reviewed in the paper, no clear data about the computational role of long-range lateral connections were cited, and so the story did not strike me as particularly compelling.

In my interest to understand neurocomputational mechanisms broadly, this represented a chance for me to learn about a type of connectivity I, and all of my colleagues, were unfamiliar with. As I delved into the details of the literature, the story became more compelling. Long-range lateral connections (LRLCs) tend to be active when stimulus strength is weak–just the situation when these visual asymmetries were strongest. LRLCs are involved in integrating contours for object detection–consistent with the asymmetric processing of "global-level" figures. LRLCs appear across cortex, and so could be involved in processing figures of different sizes by being active in different cortical areas–consistent with neuroimaging showing that lateralized processing interacts with the absolute size of stimuli in such a manner (Hopf et al., 2006). LRLCs even show variations in their connection length across visual areas, making it very plausible to find an asymmetry between the hemispheres in their length–as found in the asymmetry of these connections in auditory cortex (R. A. Galuske et al., 2000) and postulated in Hsiao, Shahbazi, and Cottrell (2008). By the time I realized that the developmental trajectory of LRLCs fit with the asymmetry that had been postulated and that the computational mechanism these networks were exploiting has not previously been described, I found myself excitedly jogging through around the yearly SfN conference, seeking out experts

like Charles Gilbert to pick their brains about how all these things work and poking computational colleagues to consider integrating them into their models.

It is important to note that the differential encoding work is collaborative work with Janet Hsiao and my advisor Garrison Cottrell. Janet conceived of the model architecture and the initial mapping to long-range lateral connections. I discovered some issues with the initial modeling work, solved those issues by making the model more neurologically plausible, discovered the spatial frequency encoding properties, generalized the findings to multiple behavioral experiments, and created a developmental version of the model. I have focused a lot of energy on fleshing out how long-range lateral connections "make sense" to describe the broader lateralization data reviewed by Ivry and Robertson (1998) and more recently Plaut and Behrmann (2011) and understanding how those literatures connect back the computational properties of long-range lateral connections in contour processing.

Why interhemispheric integration?

The prevailing view in the literature is that lateralization is driven by less communication between the hemispheres–despite the fact that lateralized functions are often complementary (Gazzaniga, 2000; Hellige, 2006) and that interhemispheric functional networks are some of the strongest found (Stark et al., 2008). Recent experimental and modeling work on complementary lateralization of face and word processing (Plaut & Behrmann, 2011; Dundas, Plaut, & Behrmann, 2012) has suggested critical interactions of the hemispheres in the development of lateralization. That work inspired me to take a more general look at findings that the hemispheres are more independent in humans than other animals, due to long conduction delays (Ringo et al., 1994) and relatively fewer connections (Rilling & Insel, 1999a).

I was surprised to find that not only is the corpus callosum diverse in its microstructure, but that the microstructure is informative to functional differences within the corpus callosum. Because the corpus callosum contains connectivity across the entire brain and is topographically organized, the microstructural map of the connections varies with the computational needs of each part of the brain (Aboitiz & Montiel, 2003; Doron & Gazzaniga, 2008). Early sensory/motor areas (vision, somatosensation) tend to interconnect along the midline with thick, myelinated fibers–good for fast transmission. When examined across species, these fast fibers increase their size with brain size, indicating that speed is important (Olivares, Montiel, & Aboitiz, 2001). On the other hand, association cortices and prefrontal cortices interconnect diffusely across the corpus callosum, using thin fibers that are more frequently unmyelinated. These thin fibers do not change across species with different brain sizes (Aboitiz & Montiel, 2003; S. S. H. Wang et al., 2008).

After delving deeply into the neuroanatomical data on the corpus callosum, I've been surprised by the paucity of human data that exist. High-quality electron microscopic data exist for cats and monkeys in developmental and adulthood (Berbel & Innocenti, 1988; LaMantia & Rakic, 1990a; LaMantia & Rakic, 1990b) and show exciting patterns of great proliferation and massive pruning of thin, unmyelinated fibers in the corpus callosum, along with age-related changes to fiber density, fiber count, and myelination. Nonetheless, only a single sample of the human corpus callosum has ever been imaged with an electron microscope and published–of a 45 year-old sample (Aboitiz et al., 1992). Only one developmental paper has been published (Luttenberg, 1965) and is marred by its use of a low-acuity light microscope, reporting fewer fibers in the human corpus callosum at birth (143 million) than reported in adulthood (200 million; Aboitiz et al. (1992)) and far below my best estimate of the fiber count at birth (800 million; see Section 5.7).

Given the diversity of connectivity across the corpus callosum, it's easy to see

that interactions over the corpus callosum can be highly task-dependent. For example, stimuli presented centrally may make use of fast, midline callosal connections, whereas stimuli presented laterally likely cannot. Therefore, in order to understand the role of interhemispheric integration in a task, one must delve into the details of the task and of the physiology. With so little human data on the microstructure of the corpus callosum available, computational tools can help map animal data to humans (see Appendix C) and test existing hypotheses of relatively weak interhemispheric interactions in humans (Ringo et al., 1994; Rilling & Insel, 1999a).

Why combine lateralization and interhemispheric integration?

For three years I was absolutely convinced that lateralization comes from less communication between the hemispheres (Ringo et al., 1994). It seemed simple–when you know how to do your own job yourself, you don't need to talk to anybody else. As one hemisphere's job becomes less functionally related to the other hemisphere's job, the need for cross-talk seems reduced.

While the story seemed simple, as white matter connectivity–and particularly the corpus callosum–became more and more prominent with the advent of DTI, resting-state MRI, and more sophisticated EEG analyses such as phase locking and causal analysis, the results simply didn't back up that story. There is evidence of robust coupling between the hemispheres in humans (Stark et al., 2008), with lateralization and interhemispheric communication both increasing over development (e.g. Benninger, Matthis, and Scheffner (1984); Petitto et al. (2012); Musacchia et al. (2013)). If anything, these results seemed to show that interhemispheric networks were stronger than any others.

Upon re-examining the two major papers supporting the independence hypoth-

esis, I noted that neither paper actually tests whether independent networks lead to lateralization. When I began to think about other fields, the hypothesis of specialization being brought about by independence started to seem absurd–specialization increases competency in one function *at the cost of others*; communication is what mediates sharing of resources between complementary specializations. When I started to think about and look into other fields, this is just what I found: in other fields such as cellular biology (Gurkan, Koulov, & Balch, 2007; Graham, Cook, & Busse, 2000; Marzec & Kurczynska, 2014; Palmer, 2002), agriculture (Qin & Zhang, 2012; Gollin & Rogerson, 2014), economics (Bolton & Dewatripont, 1994; R. Katz & Tushman, 1979; Tushman, 1978), even in design of cities in online games (*Specializations - SimCity Wiki Guide*, n.d.), and presumably government, social networks, and all other fields: specialization is dependent on robust communication.

When I found that both major proposed causes of independence–longer conduction delays (Ringo et al., 1994) and fewer interhemispheric connections (Rilling & Insel, 1999a) in larger-brained species–had good reasons to doubt them (Chapters 5 and 6, respectively), I finally let go of the hypotheses myself, and instead of trying to use those ideas to build on the neural network modeling of visual asymmetries, I focused on understanding the existing data on interhemispheric transfer and its role in lateralization. As outlined in the future work in Chapter 8, I hope that some ideas from this research (Chapter 7 may be used to move that project forward.

Thesis Outline

This thesis is written in the "independent chapters" format, as most chapters have been published in conference proceedings or are in preparation for journal publication. As such, relevant background appears in each chapter. I've also added a chapter to

integrate the primary research chapters with each other and with data from the literature; the aim of that chapter (7) is to propose a unified explanation of visual asymmetries and interhemispheric communication. Therefore, no single literature review or background is covered in this thesis; relevant background is distributed across the chapters.

The thesis encompasses three projects: neurodevelopmental modeling of visual processing asymmetries, neurodevelopmental modeling of interhemispheric communication, and allometric modeling of interhemispheric connectivity. Chapters 2 - 4 cover the Differential Encoding model[1], a neurodevelopmental model of visual processing asymmetry. Chapter 5 covers interhemispheric communication in adults and modeling work supporting a neurodevelopmental theory on the development of white matter connectivity and its relationship to lateralization. Chapter 6 covers comparative aspects of interhemispheric connectivity across mammalian species. Chapter 7 attempts to connect chapters 2 - 6 with each other and with related data and theories in the literature, to give an integrated neurodevelopmental theory of visual processing asymmetry and interhemispheric communication. Chapter 8 includes two submitted research proposals and two rough outlines for future work based on these results and techniques.

[1] Janet Hsiao is the first author of Chapter 2, published as (Hsiao et al., 2013). Please review Chapter 2's acknowledgements section (2.6) for details on my contributions to the chapter.

Chapter 2

A differential encoding account of hemispheric asymmetry in perception[1]

2.1 Abstract

Hemispheric asymmetry in the processing of local and global features has been argued to originate from differences in frequency filtering in the two hemispheres, with little neurophysiological support. Here we test the hypothesis that this asymmetry takes place at an encoding stage beyond the sensory level, due to asymmetries in anatomical connections within each hemisphere. We use two simple encoding networks with differential connection structures as models of differential encoding in the two hemispheres based on a hypothesized generalization of neuroanatomical evidence from the auditory modality to the visual modality: The connection structure between columns is more distal in the language areas of the left hemisphere and more local in the homotopic regions in the right hemisphere. We show that both processing differences and differential frequency filtering can arise naturally in this neurocomputational model with neuroanatomically inspired

[1] This chapter was published in the Journal of Cognitive Neuroscience (Hsiao et al., 2013)

differences in connection structures within the two model hemispheres, suggesting that hemispheric asymmetry in the processing of local and global features may be due to hemispheric asymmetry in connection structure rather than in frequency tuning

2.2 Introduction

The way we analyze and process the global and local forms of visual stimuli has been extensively examined. Navon (1977) proposed the "global precedence hypothesis", suggesting that the global form of a visual stimulus is unavoidably recognized before the local forms. This effect was later shown to depend on both the characteristics of the local and global forms and the hemispheric asymmetry in the perception of local and global features (Hoffman, 1980). Follow-up studies further confirm that there is a right visual field (RVF)/left hemisphere (LH) advantage for responses to local features and a left visual field (LVF)/right hemisphere (RH) advantage for responses to global features (Sergent, 1982; Ivry & Robertson, 1998; Van Kleeck, 1989; Kitterle, Christman, & Hellige, 1990; Proverbio, Minniti, & Zani, 1998; Han et al., 2002; Weissman & Woldorff, 2005). Nevertheless, studies examining grating detection did not support the existence of hemispheric specialization for particular frequency ranges (Kitterle et al., 1990; Rijsdijk, Kroon, & van der Wildt, 1980; Di Lollo, 1981; Peterzell, Harvey, & Hardyck, 1989; Fendrich & Gazzaniga, 1990). It thus remains unclear why this perceptual asymmetry exists (M. Martin, 1979; Peterzell, 1991).

Sergent (1982) used hierarchical letter patterns (Navon, 1977) to examine this hemispheric asymmetry (Figure 2.1a). Stimuli were presented to either the RVF/LH or the LVF/RH for 150 ms, and the participants' task was to judge whether they saw a target letter or not, regardless of its being in the global or local pattern. The stimuli of greatest interest in Sergent (1982)'s experiment were the conflict conditions when the

target appeared in either the local or global pattern (the L+Sand L-S+ cases in Figure 2.1a), since they were the conditions in which interference may arise. The results showed that there was a significant interaction between presented visual field and target level in response time: participants were faster at detecting a target at the global level when it was presented in the LVF/RH, and faster at detecting a target at the local level when it was presented in the RVF/LH (Figure 2.1b). She thus concluded that global precedence in form analysis1 is a property of the RH but not the LH. She also argued that "hemispheric differences as a function of spatial frequencies must result from processing taking place beyond the sensory level", since studies examining grating detection did not report a hemispheric difference in contrast sensitivity or visible persistence (Kitterle et al., 1990; Rijsdijk et al., 1980; Di Lollo, 1981; Peterzell et al., 1989; Fendrich & Gazzaniga, 1990).

A similar hemispheric asymmetry has also been consistently reported in auditory perception. For example, in dichotic listening studies of speech recognition, it has been shown that there is an advantage for responses to prosody, which rely more on low frequency information, when the stimulus is presented to the left ear/RH, and an advantage for responses to content, which reply more on high frequency information, when the stimulus is presented to the right ear/LH (Ivry & Robertson, 1998; Ley & Bryden, 1982).

Ivry and Robertson (1998) proposed a Double Filtering by Frequency (DFF) theory to account for this hemispheric asymmetry in perception. The theory argues that information entering the brain goes through two frequency filtering stages. The first stage involves attentional selection of task-relevant frequency range, and at the second stage, the LH amplifies high frequency information (i.e., a high-pass filter), whereas the RH amplifies low frequency information (i.e., a low-pass filter). They developed a computational model based on the DFF theory to account for this perceptual asymmetry (Figure 2.2a), and used one-dimensional hierarchical patterns as the stimuli in their

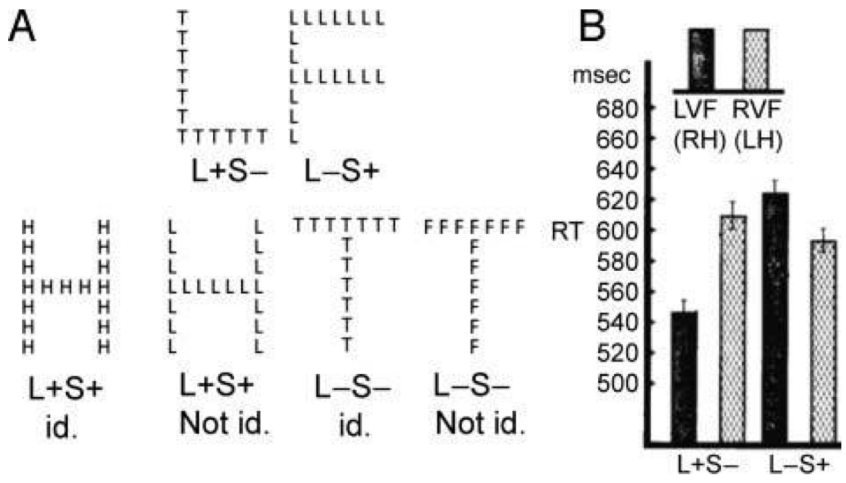

Figure 2.1: (a) Stimuli in Sergent (1982)'s experiment. A hierarchical letter pattern contains two patterns: a global pattern and a local pattern. The global pattern (the large letter) is composed of a number of local patterns (the small letters). Sergent (1982) referred to the two levels of the stimulus as having differential spatial frequency contents: low frequency for the global pattern and high frequency for the local pattern. In her experiment, she used four letters to compose the hierarchical letter patterns: "H" and "L" were designated as targets, and "T" and "F" as distracters. Given that each letter may appear as the local or the global pattern, there are in total 16 patterns, which can be put into six conditions according whether there is a target in the local or global patterns. "L+" means the large letter is a target, and "S+" means the small letters are targets. "id." means the local and the global patterns are identical. (b) The RT data for the L+S- and L-S+ stimuli in the LVF and RVF presentation conditions (Sergent, 1982).

simulation (Figure 2.2b). Their results showed that, consistent with human data, the model exhibited the hemisphere-by-level interaction after a few training epochs and an overall advantage for stimuli with a global target (Figure 2.2c) (Sergent, 1982). However, note that the overall effect pattern is different from Sergent's. Furthermore, the result is fragile; with further training, the interaction disappears–the LH network is generally better at both kinds of patterns.

A second fundamental problem with the DFF model is that there is little evidence suggesting differential frequency tuning in the neurons in the two hemispheres. Nor is there anatomical evidence supporting the existence of different frequency modules in the brain as those proposed in the model. In addition, given that it is unclear how the

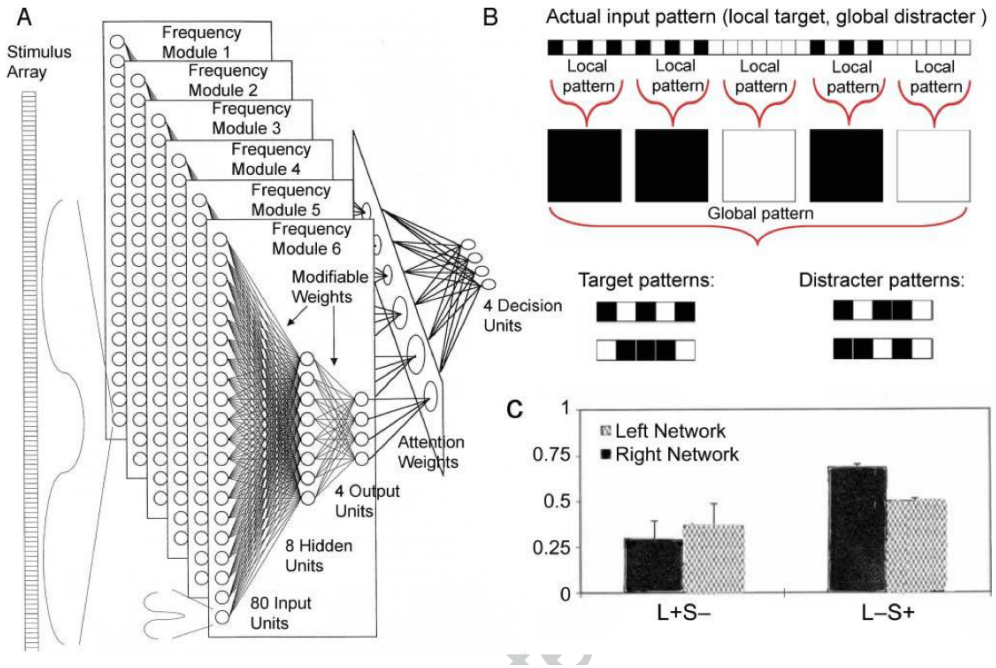

Figure 2.2: (a) Ivry and Robertson (1998)'s computational model based on the DFF theory. The model contains six different frequency modules; each module extracts information of a specific spatial frequency from the input and learns to map the extracted information to the output (Module 6 has the lowest frequency). The four decision nodes correspond to four target patterns: whether target 1 or target 2 is present, and whether it is at the global or local level. The outputs from the modules then go through an attention weight layer as a filter. The filter first selects a task-relevant frequency range (how the range is decided is unspecified). At the second stage, in the RH network, the filter amplifies the output information from the low spatial frequency modules within the frequency range, whereas in the LH network it amplifies the output information from the high spatial frequency modules, through giving different weights to different modules. The figure shows an example LH network. (b) One-dimensional hierarchical patterns. There are two target patterns (10101 and 01110) and two distracter patterns (11010 and 10110). These are composed in the input to the model. Shown at the top is an actual input pattern formed by taking the first distracter pattern and replacing each black portion with a target pattern. Thus this represents the first target pattern at the local level and the second distracter pattern at the global level. A 0 unit appears between each local pattern as a separator4. (c) Results of Ivry and Robertson (1998)'s computational model of the DFF theory with large stimuli (i.e. stimuli are enlarged by five) after 100 epochs. Note that it was not reported whether the RH advantage in L+S- was significant. In addition, inconsistent with human data, the LH network became better at identifying both local and global targets with further training.

task-relevant frequency range is decided, the model does not fully explain why there is little evidence suggesting the existence of hemispheric specialization for particular frequency ranges (Kitterle et al., 1990; Rijsdijk et al., 1980; Di Lollo, 1981; Peterzell et al., 1989; Fendrich & Gazzaniga, 1990), although Ivry and Robertson (1998) argued that it is because absolute instead of relative frequencies were used in these studies. As pointed out by Sergent (1982), given the lack of evidence of hemispheric specialization for particular frequency ranges, this hemispheric asymmetry must result from processing taking place beyond the sensory level. Contrary to the DFF theory, the two hemispheres may not differ in the way they extract visual information.

What is the process taking place beyond the sensory level that results in this perceptual asymmetry? In recent years, it has been shown that, in the posterior superior temporal lobe in the LH, a region that is associated with language processing, the width of individual cortical microcolumns and the intercolumnar distance is greater than those in the analogous regions in the RH; pyramidal cells in this region also have longer dendrite lengths and contact fewer adjacent columnar units than do those in the RH (Seldon, 1981a, 1981b, 1982; Anderson, Southern, & Powers, 1999; Buxhoeveden, Switala, Litaker, Roy, & Casanova, 2001; Hutsler & Galuske, 2003). A similar hemispheric asymmetry also exists in the macrocolumnar structures (Hutsler & Galuske, 2003). In particular, through neuronal track tracing, R. A. Galuske et al. (2000) found that in the posterior part of Brodmann area 22, an area that involves language-relevant processing of auditory signals, there were modular networks of long-range intrinsic connections linking regularly spaced clusters of neurons; while the cluster size was similar in the two hemispheres, the spacing between clusters in the modular networks in the LH was about 20% larger than those in the RH. This anatomical asymmetry was not observed in the primary auditory area (Brodmann area 41). These hemispheric differences in cortical columnar and connectional structure give rise to reasonable speculation about hemispheric asymmetry in functional

processing architecture. Indeed, assuming similar relations between anatomical and functional organization of cortical modules as in visual cortex, R. A. Galuske et al. (2000) concluded from their data that there may be more functionally distinct columnar systems included per surface unit in area 22 in the LH compared with the RH; more specifically, the representation in the RH may be more functionally overlapped compared with that in the LH (Hutsler & Galuske, 2003; R. A. Galuske et al., 2000).

According to this observation, here we test the hypothesis that the hemispheric asymmetry in perception results from differential connectivity configurations at an encoding stage beyond the sensory level. Although these anatomical data are from auditory cortex because of the researchers' interests in language processing areas, the behavioral hemispheric asymmetry has been observed in both visual and auditory processing (Ivry & Robertson, 1998; Hutsler & Galuske, 2003). Thus, we assume that the anatomical findings in the auditory processing area also apply to visual processing, build a model based on this assumption, and see where that leads.

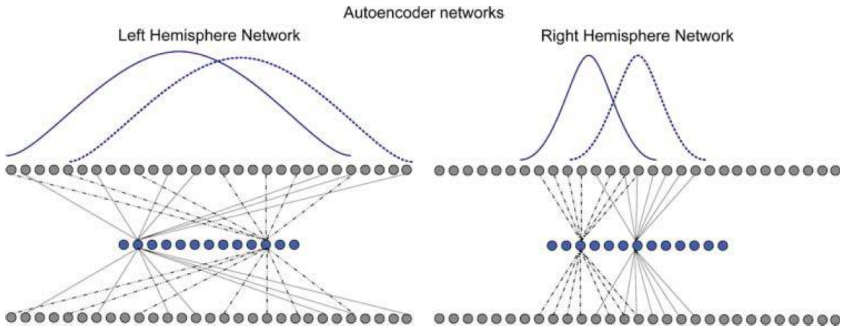

Figure 2.3: LH and RH autoencoder networks; both have the same number of connections. Each hidden node has a fixed number of symmetric connections to the input and output layers, respectively.

We use autoencoder networks to implement differential connectivity configurations at an encoding stage. An autoencoder network is a two-layer neural network that is trained to reproduce each input pattern in the output; after training, the hidden

layer activation when an input pattern is presented is used as a compressed encoding of the input pattern24. In order to simulate differential connectivity configurations, the networks have incomplete connectivity (Figure 2.3); each hidden node has a fixed number of symmetric connections to the input and output layers respectively. The distribution of the connections is determined by a Gaussian probability density function (PDF). Note that these hidden nodes are different from the radial basis function units used in some previous models (Ivry & Robertson, 1998; Monaghan & Shillcock, 2004). In those models the weights of the connections from each unit are fixed according to a Gaussian distribution (Monaghan & Shillcock, 2004) or a combination of Gaussian distributions4. In contrast, in our model the connectivity configuration from each hidden node follows a Gaussian probability distribution and the weights are adjustable through training. Also in contrast to these earlier models, in the LH network, we use a wide Gaussian PDF to simulate a sparse connectivity with adjacent neurons; in contrast, a narrow Gaussian PDF is used to simulate a dense connectivity in the RH network (Figure 2.3). The variances of the Gaussian PDFs are chosen as two extreme cases of denseness/sparseness of the connections in order to examine the qualitative differences between them. We equalize the computational power of the LH and RH networks by using the same number of hidden nodes and connections, so that the resulting differences between the two networks will reflect the functional difference between the two encoding schemes. We then use a perceptron (a one-layer neural network) to classify the encodings developed in the LH and RH networks according to whether there is a target or not in the stimulus; the error in the output layer of the perceptron reflects how good the encoding is given the detection task, analogous to human reaction time in the same task when the corresponding input stimulus is presented–greater uncertainty leads to longer reaction time.

We conducted two simulations: in the first simulation, we used the same one-dimensional hierarchical pattern stimuli as the DFF simulation (Ivry & Robertson, 1998);

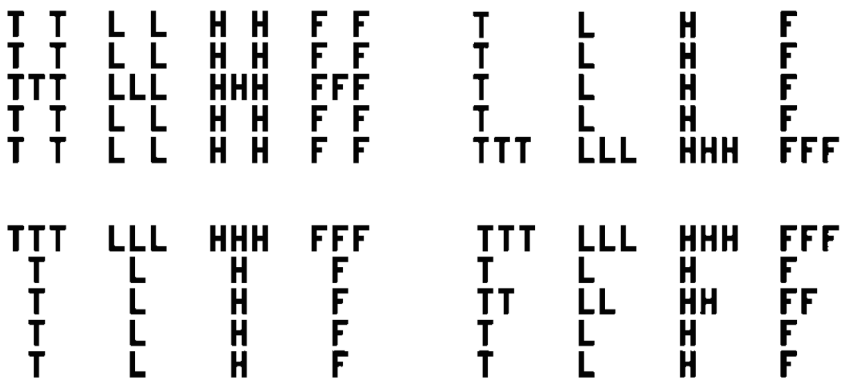

Figure 2.4: Hierarchical letter patterns used in our second simulation. Each pattern is 31 X 13 (403) pixels. They are composed of the same letters used in Sergent (1982)'s experiment.

in the second simulation, we used hierarchical letter patterns similar to those used in Sergent's experiment (Sergent, 1982) (Figure 2.4). In both simulations, training stopped after a fixed number of training epochs; the numbers of the epochs were chosen so that the error would have converged before the training stopped; in other words, there was no early stopping as in the DFF simulations.

2.3 Methods

Here we ran two types of simulations, both using two target patterns and two distracter patterns that could be combined into local targets and global distracters and vice versa. In the first experiment, we used the simplified one-dimensional hierarchical stimuli used in Ivry and Robertson (1998) simulation. Each stimulus was 29 units long, constructed by combining two patterns so that one pattern forms the local features and the other forms the global pattern of the stimulus, with a blank (0) unit between each local pattern (Figure 2.2B). In the second simulation, we replicated Sergent's experiment using two-dimensional hierarchical letter patterns. Each pattern could appear at the local or global level, for a total of 16 input patterns (Sergent, 1982). In this simulation, each

pattern was 31 X 13 (403) pixels, with the same letters and same assignments of letters to targets and distracter sets as used in Sergent's experiment (Figure 2.4).

In the simulations, we used two autoencoder networks (Cottrell, Munro, & Zipser, 2012; Rumelhart, Hinton, & Williams, 1986) with different connectivity configurations as a way to learn an efficient encoding from the input data. While holding the number of connections for each hidden unit fixed, the LH network had a comparatively wider pattern of connectivity that the RH network (Figure 3), in accordance with the asymmetry reported between long-range connections in LH and RH BA 22 (R. A. Galuske et al., 2000). More specifically, each hidden unit had a fixed number of connections to the input layer, and these connections were randomly drawn from a Gaussian pdf. Each hidden unit within a model hemisphere used a Gaussian pdf with an identical σ (variance), with the LH σ ($\sigma_{1D} = 12, \sigma_{2D} = 18$ pixels; the subscripts 1D and 2D refer to the stimulations with one- and two-dimensional stimuli, respectively) greater than the RH σ ($\sigma_{1D} = 1.8, \sigma_{2D} = 4$ pixels; see Figure 2.3). The variances were chosen as two extreme cases of denseness/sparseness of the connections to examine the qualitative differences between the LH and RH networks; a wide range of values for the variances were tested, and similar results were found. The connection pattern from the hidden layer to the output layer was completely symmetric to those from the input layer to the hidden layer. Each hidden unit was associated with a position in the input space such that the set of hidden units were evenly distributed across the input space. When selecting the connections for a particular hidden unit, the Gaussian pdf was centered at that hidden unit's location in the input space.

After selecting all connections and constructing a network, the network was trained on all 16 input patterns until the network reached a fixed error (summed across all output units and patterns; see below for more details). Similar to Monaghan and Shillcock (2004), we trained to a performance criterion, rather than for a fixed number of

iterations, because the networks with different connectivity patterns learned the patterns at different rates. Once a network was trained, hidden unit encodings for each input pattern were computed by presenting the input pattern and then recording the hidden unit activities. These hidden unit encodings were compressed encodings that reflect the result of having differential connectivity to the hidden units.

After obtaining the compressed encodings of the input stimuli, we used a perceptron (i.e., a one-layer neural network) with a sigmoidal output function to classify the encodings according to whether there was a target or not (at either level) in the input stimuli, the same task participants were required to do in Sergent (1982)'s experiment. The output layer of the perceptron had a single node; the node had value 1 when a target was present at either level (75% of the stimuli) and 0 otherwise (25% of the stimuli). The error was measured as the difference between the output of the perceptron and the desired output (0 or 1). As has been done in previous studies, this error was considered to be a measure of uncertainty, and compared directly with human RT (Dailey, Cottrell, Padgett, & Adolphs, 2002; Seidenberg & McClelland, 1989)).

In the simulation with one-dimensional stimuli, we explored the parameter space by testing the model with different combinations of the parameters, ranging from 11 to 15 hidden nodes and 5 to 10 connections from each hidden node. In the simulation with hierarchical letter patterns, the combinations ranged from 11 to 15 hidden nodes and from 170 to 220 connections from each hidden node. For both the autoencoder networks and the perceptron, the training algorithm was gradient descent (Rumelhart et al., 1986) using sum-square error (SSE) for the objective function. The learning rate started at a constant ($\eta_{1D} = \eta_{2D} = 0.1$ for the autoencoder networks; $\eta_{1D} = \eta_{2D} = 0.05$ for the perceptron) and was adapted during training: If the error decreased in the current epoch, the learning rate for the next epoch increased by a factor of 1.05; if the error increased, the new learning rate was decreased by a factor of 1.25. Training of the autoencoders proceeded

until the average SSE across all output nodes reached a predetermined threshold (0.025) within a predetermined maximum number of iterations ($max_{1D} = 1000, max_{2D} = 250$). Rare cases where the autoencoder could not reach the SSE performance criterion within the maximum number of training iterations were marked as rejections. Little effect was seen in varying this threshold in the ranges of 0.05 (requiring very few training iterations) to 0.01 (requiring many training iterations and leading to a high incidence of rejections). Training for the perceptron classifiers stopped after 250 iterations; values between 100 and 1000 iterations showed similar performance. After training the perceptron had 100% classification accuracy.

To match the statistical power found in Sergent's experiment, we ran the model 68 times in each simulation, giving us approximately the same number of total trials (68 models 16 trials per model hemisphere) as Sergent's human data (12 subjects 90 trials per visual field).

To examine encoding differences between LH and RH networks in terms of spatial frequency, output images were computed for each network. This was done by presenting each input image to a trained network and then recording the output unit activities. These output images were then analyzed for spatial frequency content. To compare and visualize, we took the log power at each frequency and then computed the difference in log power between RH and LH networks. We used hierarchical letter patterns (Sergent, 1982) for this analysis.

2.4 Results

Results of the Simulation with One-dimensional Stimuli

We first report the results of the simulation in which we used the same one-dimensional stimuli as those used in Ivry and Robertson (1998)'s model (Figure 2B). To

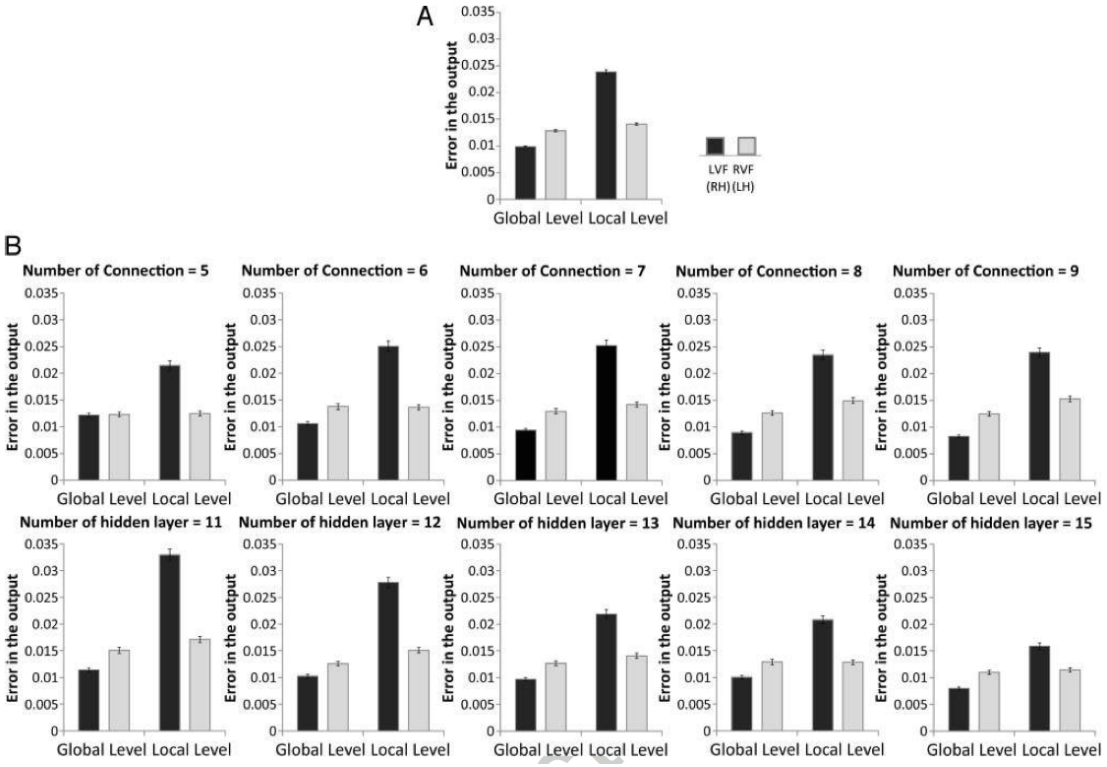

Figure 2.5: (A) Results of the simulation with one-dimensional stimuli used in the DFF model (Ivry & Robertson, 1998). (B) Results of the simulation when splitting the data according to either number of hidden nodes or number of connections.

verify that the results were robust to the parameters defining the model architecture, we ran the model with different parameter combinations, ranging from 11 to 15 hidden nodes and from 5 to 9 connections from each hidden node (in total 25 different combinations). We used repeated-measures ANOVA to analyze the data; the within-subject variable was target level (global vs. local), whereas the between-subject variables were hemisphere (LH vs. RH networks), number of hidden nodes (11, 12, 13, 14, and 15), and number of connections from each hidden node (5, 6, 7, 8, and 9). The dependent variable was the error in the output layer of the perceptron.

Consistent with human data, the results showed that the model had better performance when the target was at the global level ($F(1,3350) = 1092.823, p < .001$), and there was a significant interaction between hemisphere and target level ($F(1,3350) =$

$756.923, p < .001$; Figure 2.5A); although both of these two effects interacted with either the number of hidden nodes (Target Level × Number of Hidden Nodes, $F(4,3350) = 38.347, p < .001$; Target Level × Hemisphere × Number of Hidden Nodes, $F(4,3350) = 20.456, p < .001$) or number of Connections (Target Level × Number of Connections, $F(4,3350) = 11.927, p < .001$; Target Level × Hemisphere × Number of Connections, $F(4,3350) = 4.805, p = .001$), when we split the data according to either number of hidden nodes or number of connections, both effects were significant in all cases ($p < .001$ for all cases; Figure 2.5B). Nevertheless, in Sergent (1982)'s human data, there was no main effect of hemisphere; the two hemispheres had a similar performance level on average. In contrast, our model showed a main effect of hemisphere: the LH network performed better than the RH network, $F(1,3350) = 154.231, p < .001$; this effect interacted with number of hidden nodes, $F(1,3350) = 12.808, p < .001$: Performance difference between the two hemisphere networks was significant when the network had 11 [$F(1,670) = 69.770, p < .001$], 12 [$F(1,670) = 63.882, p < .001$], 13 [$F(1,670) = 16.954, p < .001$], or 14 hidden nodes [$F(1,670) = 19.119, p < .001$], but not when it had 15 hidden nodes [$F(1,670) = 2.383, p = .123$; Figure 2.5B]. This suggests that performance difference between the two hemisphere networks can be influenced by parameter settings.

Results of the Simulation with Hierarchical Letter Pattern Stimuli

In the second simulation, we used the hierarchical letter patterns used in Sergent (1982)'s study. We explored how the performance changed with different parameter combinations, ranging from 22 to 30 hidden nodes and 40 to 120 connections from each hidden node (in total 25 different combinations). As in the first simulation, we used repeated-measures ANOVA to analyze the data; the within-subject variable was target level (global vs. local), whereas the between-subject variables were hemisphere (LH

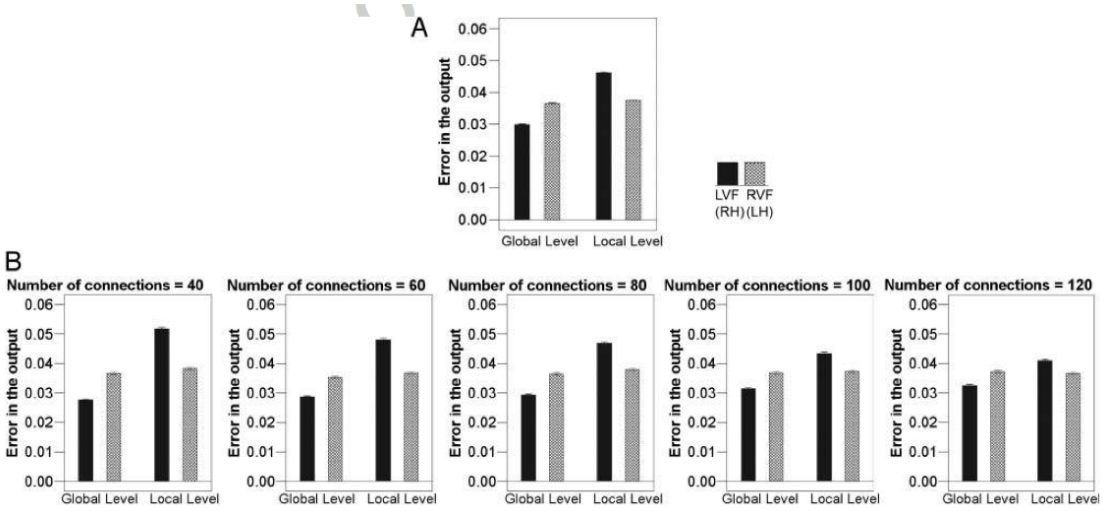

Figure 2.6: (A) Results of the simulation with hierarchical letter pattern stimuli. (B) Results of the simulation when splitting the data according to number of connections from each hidden node.

vs. RH networks), number of hidden nodes (22, 24, 26, 28, and 30), and number of connections from each hidden node (40, 60, 80, 100, and 120). The dependent variable was the error in the output layer of the perceptron.

The results showed an advantage of detecting a global level target, $F(1,3350) = 1070.838, p < .001$, and an interaction between hemisphere and target level, $F(1,3350) = 858.284, p < .001$ (Figure 2.6A); both effects interacted with number of connections, $F(4,3350) = 36.261, p < .001$, but not number of hidden nodes, $F(4,3350) = 1.933, p = .102$. When we split the data by number of connections, we found that both effects were significant across all cases (Figure 2.6B). The model also showed a main effect of hemisphere, $F(1,3350) = 91.054, p < .001$, and this effect interacted with number of connections, $F(4,3350) = 17.519, p < .001$: When the model had 40 [$F(1,670) = 58.135, p < .001$], 60 [$F(1,670) = 112.781, p < .001$], or 80 connections from each hidden node [$F(1,670) = 14.713, p < .001$], the LH network performed significantly better than the RH network; this difference was not significant when the model had 100 [$F(1,670) = 1.343, p = .247$] or 120 connections [$F(1,670) = 0.251, p = .617$].

Thus, the results from the two simulations suggested that although the global level advantage effect and the interaction between hemisphere and target level could be modulated by different parameter settings, the modulation generally only affected the size of the effects, not the direction; in other words, these effects were robust against parameter changes. In contrast, the performance difference between the LH and RH networks was sensitive to parameter settings.

We also investigated spatial frequency content preserved in the LH and RH encodings. We reproduced input images from their encodings in the output; for hierarchical letter patterns, low frequencies were better reproduced in the RH network, whereas high frequencies were better reproduced in the LH network (Figure 2.7A and 2.7B), consistent with Sergent (1982)'s hypothesis and the DFF theory (Ivry & Robertson, 1998). However, this did not result directly from frequency tuning of the neurons. Rather, differential frequency filtering behavior emerged naturally as the result of the encoding scheme, suggesting that the asymmetry in perception may be due to differences in anatomy rather than frequency tuning per se.

2.5 Discussion

In the current study, we test the hypothesis that hemispheric asymmetry in the perception of global and local features originates from differential encoding beyond the sensory level due to anatomical differences between the two hemispheres, instead of differential frequency filtering as proposed by the DFF theory (Ivry & Robertson, 1998). We first argue that the lack of evidence supporting hemispheric specialization for particular frequency ranges (Kitterle et al., 1990; Rijsdijk et al., 1980; Di Lollo, 1981; Peterzell et al., 1989; Fendrich & Gazzaniga, 1990) suggests that this hemispheric asymmetry takes place beyond the sensory level (Heinze, Hinrichs, Scholz, Burchert,

& Mangun, 1998; Sergent, 1982) and the two hemispheres do not differ in information extraction. We then argue that the difference takes place at an encoding stage due to differences in connection structures. We incorporate evidence about the anatomical differences in columnar and connectional structure in the auditory cortex between the two hemispheres (Seldon, 1981a, 1981b, 1982; Anderson et al., 1999; Buxhoeveden et al., 2001; Hutsler & Galuske, 2003) into a computational model that uses autoencoder networks to develop efficient encodings of the stimuli (Cottrell et al., 2012; Rumelhart et al., 1986): The columnar structure in the posterior superior temporal lobe in the RH has more connections among neighboring columns compared with the LH and thus may develop representations that are more functionally overlapped than those in the LH (Hutsler & Galuske, 2003). Although relevant anatomical data for the visual cortex are not currently available, similar perceptual asymmetry has been observed in both visual and auditory modalities (Poeppel, 2003). Thus, based on a hypothesized generalization across the two modalities, we use two autoencoder networks with differential connectivity configurations to simulate this differential encoding: The RH autoencoder network has a narrower connection distribution to allow more connections among neighboring nodes compared with the LH autoencoder network. We then use a perceptron to examine how efficacious the two encoding systems are in terms of detecting local and global level targets. The results match human data (Sergent, 1982) well; they show a significant hemisphere-by-level interaction: an RH advantage for responses to a global level target and an LH advantage for responses to a local level target (Sergent, 1982). They also show an overall advantage in responses to a global level target, consistent with human data (Navon, 1977). This effect is because the narrower connection distribution in the RH autoencoder network allows each hidden node to develop a compressed representation for a local region within the stimulus; because in natural images neighboring pixels are more correlated than distant ones, there may be more variance in low spatial frequencies across

the input patterns received by a hidden node, resulting in the dominance of low spatial frequency information. In contrast, with a wider and sparser connection distribution, each hidden node in the LH autoencoder network samples across a wider range of the input image and the sampled pixels are more random and less likely to be correlated; consequently, there may be comparable variance in high and low spatial frequencies across the input patterns received by a hidden node, resulting in the LH network's better ability in preserving high spatial frequencies as compared with the RH network.

In comparison with Ivry and Robertson (1998) DFF model, we show that our model provides a better account of human data (Sergent, 1982). Their model enforces a discrete separation of frequency information into modules, and hemispheric differences take place through manipulating the combination of the outputs from different frequency modules. It is unclear how these frequency ranges are combined in a certain way and how the model is able to account for the lack of evidence supporting hemispheric specialization for particular frequency ranges (Kitterle et al., 1990; Rijsdijk et al., 1980; Di Lollo, 1981; Peterzell et al., 1989; Fendrich & Gazzaniga, 1990). In addition, there is little anatomical evidence suggesting differential frequency tuning in the neurons in the two hemispheres or differential modulation by frequency channels in the two hemispheres similar to that proposed in the DFF model. In contrast, through hypothesizing that hemispheric differences take place at an encoding stage beyond the sensory level and using Gaussian probability distributions to simulate differential connection configurations at the encoding stage, our model naturally develops the hemispheric difference in the frequency content in the encoding.

In our simulation with one-dimensional stimuli as those used in the DFF model, we explored the parameter space and found that the main effect of global level advantage and the interaction between network and target level were robust against parameter changes, although in some cases there was a significant main effect of LH network

advantage. In contrast, in the DFF model, with one given parameter setting, the interaction between network and target level was fragile–the LH network became better at identifying both local and global targets with further training. Also, the simulation of the DFF model used one-dimensional hierarchical stimuli that differed greatly from Sergent's original hierarchical letter patterns. In contrast, here we used two-dimensional hierarchical letter patterns similar to those used in human studies (Sergent, 1982) and replicated the results, a test that has not been conducted with the DFF model. In addition, through analyzing the spatial frequency content preserved in the encodings from the LH and RH networks, we show that differential frequency filtering behavior emerged naturally as the result of the encoding scheme, suggesting that hemispheric asymmetry in perception may be due to hemispheric differences in connection structures rather than frequency tuning per se.

The modeling results provide support for the idea that a hemispheric difference in cortical columnar and connection structure similar to that in the auditory cortex may also exist in high-level visual areas. We speculate that it may be in the lateral occipital region. It has been reported that there is significantly greater ipsilateral activity (i.e., activation from the other hemisphere after the initial contralateral projection from the visual hemifields to the hemispheres) observed in the area anterior to the retinotopic areas (Tootell, Mendola, Hadjikhani, Liu, & Dale, 1998), suggesting that the lateral occipital region may be a convergence point after the visual field split (Hsiao, Shieh, & Cottrell, 2008). Consistent with this speculation, recent fMRI studies have suggested that the locus of this hemispheric asymmetry in local and global processing is in the occipital/occipitotemporal region (Han et al., 2002; Martinez et al., 1997). Another possibility is the inferior parietal lobe/superior temporal gyrus region, suggested by recent fMRI studies showing that the activation in this region corresponds to the asymmetry observed in human data (Weissman & Woldorff, 2005; Robertson et al., 1988). Further examinations are required to confirm these speculations.

We are currently pursuing the incorporation of more anatomical data into the model, such as using 2D Gabor filters to simulate responses of complex cells in the early visual system (Daugman, 1985), and also using the proposed autoencoder networks as the way to develop efficient encoding in the two hemispheres in modeling more complicated real world visual stimuli (such as faces; cf., the Principal Component Analysis step in many visual perception models (Hsiao, Shieh, & Cottrell, 2008; Dailey & Cottrell, 1999; Dailey et al., 2002) to further examine the cognitive plausibility of this differential encoding mechanism in accounting for other hemispheric asymmetry phenomena in perception, such as the left side bias in face perception (C. Gilbert & Bakan, 1973) and the RVF advantage in visual word recognition (Bryden & Rainey, 1963).

2.6 Acknowledgements

Author contributions: Janet Hsiao conceived of the project, wrote the paper, produced figures, and did the statistical analyses. I revised the 2D simulations to generalize over selection of target and distracter letters, conceived and wrote the spatial frequency analyses, wrote the methods section. Garrison Cottrell supervised, advised, and helped edit the content.

This research was supported by NIH grant MH 57075 and NSF grant #SBE-0542013 to the Temporal Dynamics of Learning Center (GWC, PI) and a McDonnell Foundation grant to the Perceptual Expertise Network (I. Gauthier, PI).

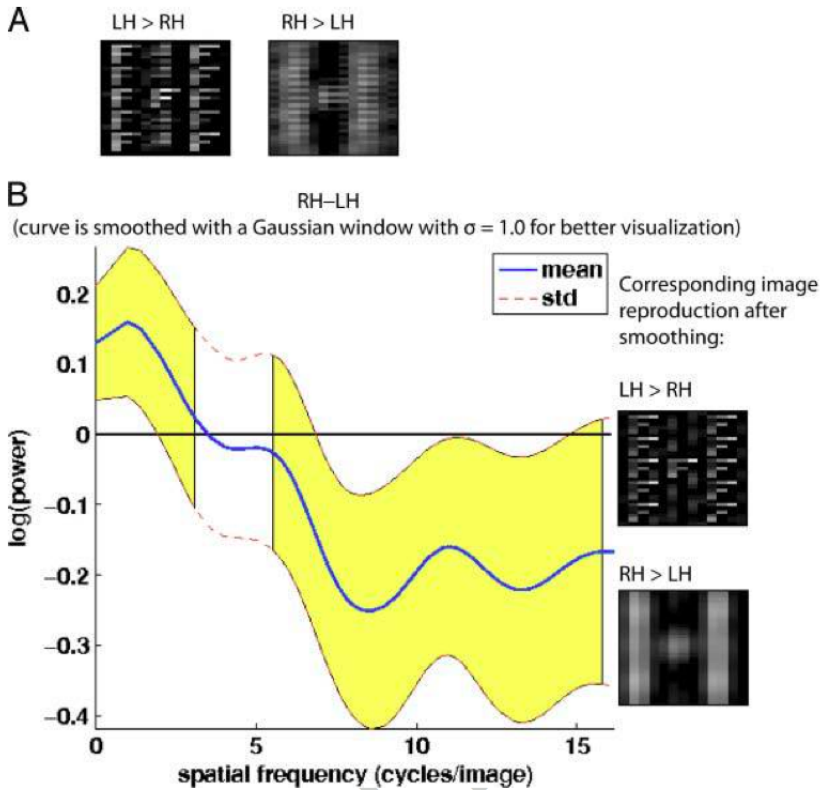

Figure 2.7: (A) Image reproduction example (global: H; local: F) showing the frequency information in which the two networks significantly differ in power. (B) Spatial frequency analysis of the output from the autoencoders with 26 hidden nodes and 100 connections to/from each hidden node in the simulation with hierarchical letter pattern stimuli. The plots show the difference in log radially averaged power spectrum (i.e., the directional independent mean spectrum) between the two networks ($RH - LH$); the blue line shows the mean, whereas the red dash line indicates one standard deviation across the 68 simulation runs. Regions marked in yellow indicate significant difference from zero.

Chapter 3

Patchy Connectivity and Visual Processing Asymmetries: A Neuro-developmental Hypothesis[1]

3.1 Introduction

A large literature of behavioral experiments and neuroimaging studies has established the existence of left-right asymmetries in classification tasks across a variety of visual stimuli. Typically, these studies have used visual half-field presentation: a stimulus is briefly presented to the left or right of a fixation point; after seeing the stimulus, subjects press a button to indicate their response to some type of classification task, such as whether a target stimulus was present or not. Because information from the left visual field (LVF) is initially directed exclusively to the right cerebral hemisphere (RH), and information from the right visual field (RVF) to the left cerebral hemisphere (LH), if the same stimulus is presented in the RVF and LVF but differences in reaction time

[1]This chapter was published in the NCPW 2013 conference proceedings (Cipollini & Cottrell, 2013a)

or accuracy are found, then a hemispheric difference in the processing of the stimulus is inferred. Across these studies, the two inferences that are generally made are that the LH shows a specialization for processing information at higher spatial frequencies (HSF), while the RH shows a specialization for processing information at lower spatial frequencies (LSF) (Sergent, 1982; Hellige, 1993; Ivry & Robertson, 1998).

Ivry and Robertson (1998) developed the Double Filtering by Frequency (DFF) theory to account for asymmetries in frequency processing of visual and auditory stimuli. They proposed that, after early sensory encoding decomposes a stimulus into its component frequencies, processing involves two filtering stages. First, each hemisphere focuses on only the frequencies relevant to the task. Then, each hemisphere is biased towards encoding information, or spectral power, in that band of task-relevant frequencies: the LH encodes more information in the higher frequencies of those selected in the first stage, while the RH encodes more spectral power in the lower frequencies of those selected.

To provide some validation their theory, Ivry and Robertson also implemented a neural network model based on the DFF theory. This model was able to account for three particular experiments from the literature, each of which Ivry and Robertson argued expresses a core feature of visual processing asymmetries. Later, Hsiao, Shahbazi, and Cottrell (2008) implemented a different neural network model of the DFF theory, and showed that it could account for a fourth study (see Table 3.1 for a summary of these studies).

While the DFF theory and associated models account for all these data, Hsiao, Shieh, and Cottrell (2008) questioned some of the assumptions and implementation details of these models, including:

- There is a lack of physiological evidence suggesting differential frequency tuning in the neurons of the two hemispheres

- The stimuli were drastically reduced in complexity: they used 1D arrays (instead of 2D images) with only 2 stimulus classes (instead of the 6 presented to human subjects)
- The classification task used to train their model differed from that given to human subjects.
- With further training, their hemisphere $\times$ level interaction disappeared or reversed.

To address this, Hsiao, Shieh, and Cottrell (2008) developed a neural network model with a simple architectural difference between the hemispheres. Specifically, they incorporated an anatomical asymmetry in long-range lateral connections between "patches" found in Wernicke's area (a language-related auditory area) and its RH homologue (R. A. Galuske et al., 2000) into a simple autoencoder neural network. When this "Differential Encoding" (DE) model was used to encode 2D images of Navon figures, and these encodings then classified with a second neural network, the same hemisphere $\times$ level interaction emerged.

While suggestive, this model was used to account for only one of the four experiments that the DFF has accounted for. In addition, the DE model did not use biologically plausible parameters, nor to justify the specific role of the connections in question in the experiment modeled. Finally, this model was never examined for spatial frequency encoding differences, and so its relationship to previous hypotheses about such differences remains unclear.

We aim to address all of these issues here. We begin by arguing that long-range lateral connections horizontal are specifically involved in the paradigms eliciting visual processing asymmetries and modeled by Ivry and Robertson and Hsiao et al, due to their differential activation under conditions of low stimulus strength. We argue that the DE model, with a specific configuration, is a reasonable implementation of the

anatomical system. We then describe modeling work where we implemented this model setup, and showed that such a model exhibits both spatial frequency differences, as well as differences on classification tasks of encoded stimuli, for three of the behavioral studies that the DFF has accounted for. We discuss why we think a failure to account for the fourth study is informative and potentially interesting. Finally, to support the plausibility of our work, we show, using a developmental version of our model, that normal neural development of visual cortex, in conjunction with changes in visual acuity and a hypothesized timing difference in the maturation of the hemispheres (Hellige, 1993), can lead to the hypothesized anatomical asymmetry.

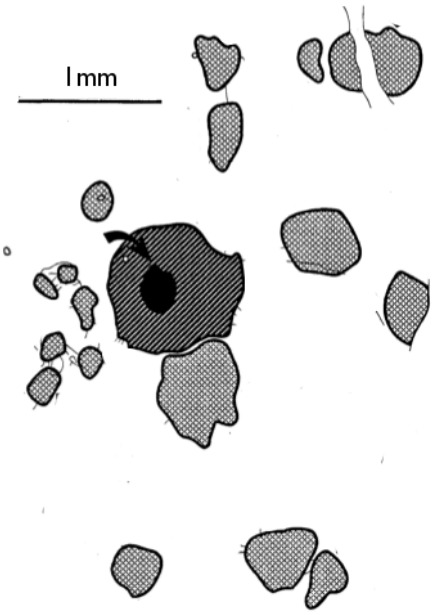

Figure 3.1: Drawing of "patches" in V4 (Amir et al., 1993). Dark arrow indicates site of dye injection.

3.2 Patchy connectivity may be involved in processing asymmetries

"Patches" are groups of locally interconnected mini-columns, spanning about 500mm in diameter in cortex. They are called "patches" because an injection of dye into the cortical surface will label cortex at the injection site, as well as a number of discrete patches of surrounding cortex. They are thought to be functional units, and somewhat akin to hypercolumns. These patches themselves interconnect with nearby patches within a cortical area through long-range horizontal connections that travel through the grey matter. These patchy connection networks are quite specific and sparse; a patch will connect with a subset of its local neighbors (see Levitt and Lund (2002) for a review).

Previously, R. A. Galuske et al. (2000) found that the distance between interconnected patches in Wernicke's area (a language-related auditory area) and its RH homologue differed, while no such differences were found in primary auditory cortex. Specifically, patches in the LH tended to connect to patches farther away than patches in the RH. Hsiao, Shieh, and Cottrell (2008) incorporated this connectivity difference into an autoencoder neural network, then encoded 2D images of Navon figures using the LH and RH networks. They showed that when these these encodings were classified with a second neural network, the same hemisphere $\times$ level interaction emerged as when human subjects were required to make a similar classification of the same stimuli, when presented laterally (Sergent, 1982).

Why might long-range horizontal connections be specifically involved in Sergent's experiment, or other experiments showing visual processing asymmetries and accounted for by Ivry and Robertson's DFF model? Looking into the literature, we found a number of reviews stating that asymmetries were quite dependent on task setup and stimulus parameters, specifically stimulus contrast and stimulus presentation duration:

stimuli must be presented with low contrast, or briefly, to elicit asymmetries (Christman, 1989; Sergent, 1983, 1985; Ivry & Robertson, 1998). When the stimulus strength is high, asymmetries disappear.

We interpret these findings to suggest that asymmetry is not in the feed-forward pathway, whose function we assume is positively correlated to stimulus strength, but instead can be found in secondary types of connections - feed-back and long-range lateral connections. We focus on long-range lateral connections between patches because they have specifically been found to be more active during low stimulus strength (H. A. Swadlow & Alonso, 2009), are modulated by top-down task demands (C. D. Gilbert & Li, 2013), are well characterized anatomically and physiologically (Levitt & Lund, 2002), are thought to help encode higher-level visual information such as contours (C. D. Gilbert, 1992; Grossberg & Williamson, 2001), and we know at least one existing asymmetry in this type of connectivity (R. A. Galuske et al., 2000).

We find that a specific implementation of the neural network employed by Hsiao et al. to be a plausible model of how long-range lateral connections affect a map-based encoding, such as a retinotopic encoding of an image. Specifically, connections from the input to hidden layer can be interpreted as a recurrent network unfolded in time, if each hidden unit connects to the input image at that hidden unit's location. In this particular model architecture, forward propagation of activity along the input-to-hidden unit connections would represent the propagation of activity laterally, over one time-step. The number of hidden units used would represent the number of local patchy connection networks used to reconstruct the image; when the number of hidden units matches the number of pixels, then all patchy connection networks are used in the reconstruction.

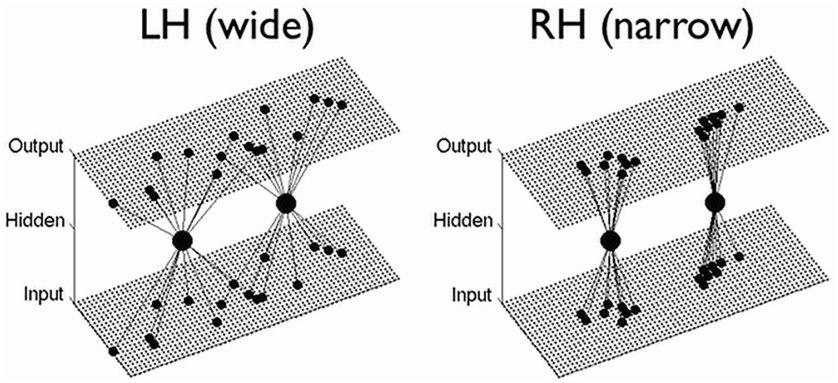

Figure 3.2: Representation of two hidden units for LH (left) and RH (right) autoencoder networks, along with their connections. The connections are randomly sampled from a Gaussian distribution centered on each hidden unit's position in the input array. The Gaussian distribution used for the LH is wider than that used for the RH. Not pictured are the classification networks, which operate on the hidden unit encodings extracted from the autoencoder networks after training.

3.2.1 Methods

The "Differential Encoding" (DE) model consists of two autoencoder neural networks, each representing one cerebral hemisphere, which differ only in the spatial spread of connections from the input to hidden, and hidden to output layers. Unlike most autoencoders, the hidden units of these models connect to a small subset of the input and output banks (see Figure 3.2). Each hidden unit has a position in the input (and output) arrays, and a fixed number of connections to the input (and output) arrays are sampled from a Gaussian distribution centered at that hidden unit's position in the input (and output). The LH and RH autoencoders have the same number of hidden units and sample the same number of connections to the input (and output) for each hidden unit. The only difference between the networks, then, is the width (σ) of the Gaussian distribution.

In accordance with the findings of R. A. Galuske et al. (2000), the LH network has a wider distribution than the RH network (see Figure 3.2). Note that this differs from previous models of hemispheric differences, where the gaussian describes the receptive

fields of Radial Basis Function units (Monaghan & Shillcock, 2004). In that work, wider receptive fields characterize the RH. Here, *whether or not there is a connection* is sampled from a Gaussian distribution. Here, our connections are sparse and there is no center-surround receptive field structure. Based on previous results in Hsiao et al., we expected to find the opposite associations in this network architecture: a wider connection distribution would favor processing of HSFs, and a more narrow connection distribution would favor processing of LSFs.

The number of hidden units was set to the number of pixels (34×25 pixels $= 850$), to allow equal spacing across the input image with enough total parameters to learn the images. The number of connections per hidden unit (15) were fixed to be close to values reported in the literature for the number of interconnecting patches labeled by a single injection in V4 (Amir et al. (1993); see Figure 3.1).[2] Each LH and RH network was constructed by randomly sampling connections for each hidden node. Gaussian distributions were used such that inter-patch distance values were similar to those reported in R. A. Galuske et al. (2000), computed as the relative width of a "patch" (here, considered to be 1 pixel) vs. the relative distance between the center of patches (1.75 for the RH, 2.05 for the LH).

We aimed to model the four datasets described in Table 3.1. Each of these four datasets were collected using brief, lateralized presentation of an image, then requiring some classification of that stimulus (e.g. whether the stimulus contained a target feature or not). We assume that asymmetries elicited in this paradigm are due to hemispheric differences in encoding these stimuli, and asymmetries in the classification of these stimuli are due to the asymmetries of the encodings. Our basic model setup, then, is to construct greyscale images for each task; to encode these images in our LH and

[2] A wide range of values (smaller and larger) was tested for each of these parameters; results did not differ qualitatively when the number of connections per hidden unit varied to allow for the same number of overall weights to be used to learn the images. If too few weights were used, the networks could not learn the training set well enough for a meaningful analysis.

Table 3.1: Citations and descriptions for the four behavioral studies addressed in our modeling work.

Reference	Description & reason for inclusion in Ivry and Robertson (1998)
Sergent (1982)	Using Navon figures, which are large "global"-level letters composed of smaller "local"-level letters, this study showed a hemisphere $\times$ level interaction, where target letters present at the larger, "global" level generally elicited a faster reaction times when presented to the LVF/RH, while target letters present at the smaller, "local" level generally elicited faster reaction times when presented to the RVF/LH.
Kitterle, Hellige, and Christman (1992)	This study showed that the same stimuli used in different tasks could elicit different hemispheric advantages. This suggests that it is not the frequencies present in the stimuli that elicits the asymmetry in processing, but rather which frequencies are relevant to the task that drive the asymmetry. They found that a task requiring HSF information elicited faster reaction times when stimuli were presented to the RVF/LH, while a task requiring LSF information elicited faster reaction times when stimuli were presented to the LVF/RH.
Christman, Kitterle, and Hellige (1991)	This study showed that when two stimuli differed by a single spatial frequency, which hemisphere showed a processing advantage didn't depend on the actual frequency of that component, but rather whether that frequency was relatively higher or lower compared to the other frequencies composing the stimuli. When the discriminative frequency was higher than the frequency content of the rest of the stimulus, responses were faster for presentation to the RVF/LH; when the discriminative frequency was lower than the frequency content of the rest of the stimulus, responses were faster for presentation to the LVF/RH.
Young and Bion (1981)	This study showed that accuracy on a face identification task was better when the probe faces were presented to the LVF/RH.

RH autoencoder models with asymmetric connectivity patterns, and then to classify these asymmetric encodings in separate, but identical, LH and RH feed-forward neural networks trained on the classification task corresponding to the encoded images for that dataset.

For each dataset, greyscale images were constructed for each task stimulus. The autoencoders were trained via backpropagation of error (Rumelhart et al., 1986), using batch processing and sum-squared error (SSE), to reproduce these greyscale images from the input to the output. Once the autoencoders reached a pre-determined performance level ($SSE = 0.02$, per output unit), training stopped. We used two types

of regularization (weight decay ($\lambda = 0.975$) and adding noise (0.01%) to our training images) to encourage good generalization. Each stimulus image was presented to the trained autoencoder network, and the activation of the hidden units was recorded. These encodings, which differed only due to the differences in connectivity structure between LH and RH networks, were then used as inputs to a separate 3-layer feed-forward neural network, which was trained to classify these encoded stimuli according to the behavioral task given to human subjects in the original experiment. The number of hidden units was different for each classification network (but identical between hemispheres), and was chosen such that the classification task could be learned well.

For a single experiment, multiple "instances" of each LH and RH network were constructed and trained; each "instance" differs only in the random sampling of its connections.[3] Performance was evaluated on each model individually, then performance for all instances of each hemisphere were averaged. Average model error for each model hemisphere was compared to average reaction time in the corresponding human experiment, with both conceived as measures of difficulty or uncertainty in processing.

In order to examine how the different connectivity distributions affect spatial frequency encoding, each stimulus image was presented to a trained autoencoder. Each output image produced was examined for spatial frequency content, and a 2D spectrogram across all images in the stimulus set was constructed. Each 2D spectrogram was translated to a 1D spectrogram.[4] Each spectrogram was compared to the spectrogram of the original image. The difference in spectrograms was then compared across hemispheres, showing for each frequency which hemisphere has encoded information closer to the original

[3]The number of model instances was chosen such that the total number of trials across all stimuli and model instances matched that reported in the corresponding behavioral experiment, to match statistical power of results. This makes sure that any asymmetry measured here is of an appropriate size that it could account for the human data.

[4]Each 2D frequency (f_x, f_y) was converted to a 1D frequency $(f_r = \sqrt{f_x^2 + f_y^2})$; for each unique value of f_r, all power/amplitude values were then averaged to create the 1D spectrogram.

image than the other.

Table 3.2: Simulation results. Column 2: comparison of human and model behavioral performance. Column 3: Spatial frequency processing difference between right (values above zero) and left (values below zero) hemisphere networks.

	Human Data	Simulation Data	Spatial Frequency Processing
Sergent (1982)	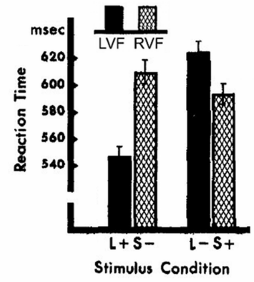	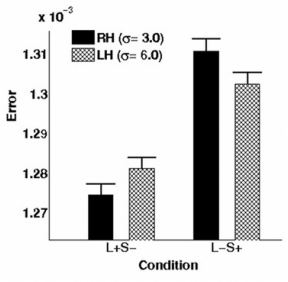	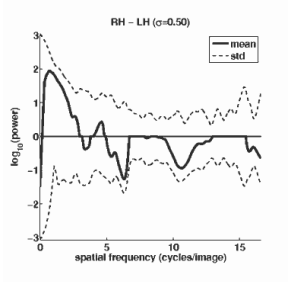
Kitterle et al. (1992)	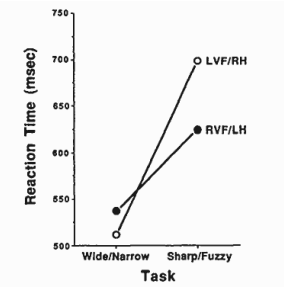	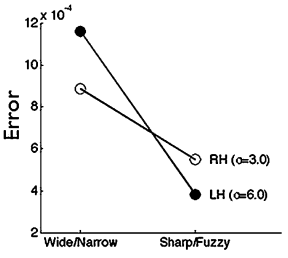	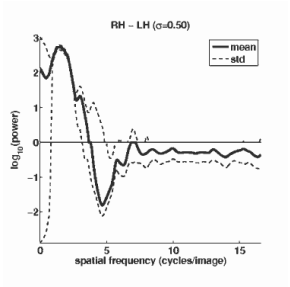
Young & Bion (1981)	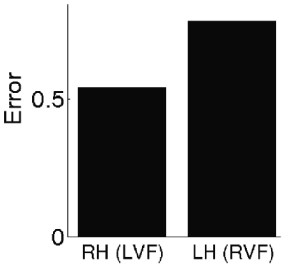	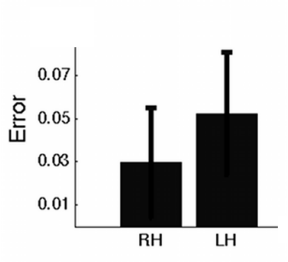	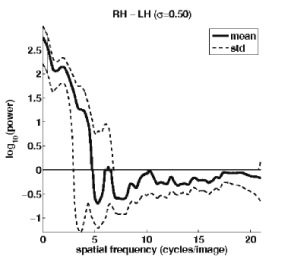
Christman et al. (1991)	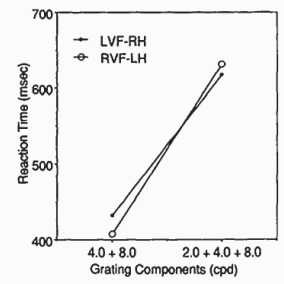	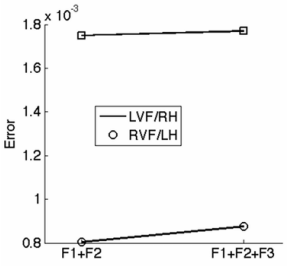	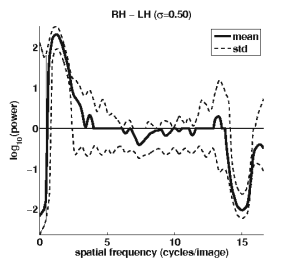

3.2.2 Results

Results are summarized in Table 3.2, showing that for 3 of the 4 tasks, the model performance (column 2) showed the interaction or performance differences found in the human behavioral measures (column 1). In addition, in all 4 tasks, the model shows an interaction between frequency band and hemisphere (column 3): greater accuracy in reproducing images for the RH networks (above zero-line) is focused in the lower spatial frequencies (towards origin), while greater accuracy for the LH networks (below zero-line) is focused in the higher spatial frequencies (away from origin).

This indicates that, somewhat counterintuitively, narrowly distributed connections are biased relatively more towards LSF processing, and widely distributed connections are biased relatively more towards HSF processing. We are investigating the cause of this relationship in current work. Preliminary results indicate that average spacing between nearest-neighbors of input/output units connecting to a single hidden unit governs this behavior. Specifically, when connection spread is small, constructive/destructive interference patterns between LSF vs HSF gratings of different phases and orientations occur: LSF gratings shows large variations in hidden unit activation based on particular orientations and phases, while HSF gratings do not. This seems to allow for more specific encoding of shapes and contours in LSF gratings, and thus a bias towards representing LSF information.

Examining these results more closely, we found two places where our models did not accurately reflect the human behavior. In our replication of (Kitterle et al., 1992), while we did show the measured hemisphere $\times$ task interaction, the relative difficulty of the two tasks did not match that in the human measures. This difficulty may depend on different sensory transformations, or other issues. In fact, in subsequent work, we have found this to be true in the modeling; changing the training dataset, or regularization parameters, does not affect the hemisphere $\times$ task interaction, but does affect the relative

difficulty of the two tasks. Therefore, we don't think that this mismatch is an important one to consider here.

We believe the second issue we found is more important, and more interesting. Our models did *not* show a hemisphere $\times$ stimulus class interaction for the Christman et al. (1991) study. We tested a few possible explanations for this. We varied the three base frequencies that composed the stimuli; this affected which model hemisphere showed better performance, but no reliable hemisphere $\times$ stimulus class interaction was found. We tried larger images, to expand the range of spatial frequencies that could be encoded and obtained similar results. Lastly, we trained the autoencoder on separate dataset, then extracting hidden unit encodings on the task-relevant stimuli. Again, this did not show any consistent interaction.

Using data from our developmental model, we discuss an alternative interpretation of Christman et al. (1991)'s study in the Discussion section below.

3.3 Patchy connection networks may develop asymmetrically in humans, under normal visual development

The results above clearly suggest an association between narrowly distributed connections and LSF processing, and widely distributed connections and HSF processing. Here, we investigated whether a developmentally-inspired model can learn these connection patterns through experience. The model incorporates three observations/constraints: 1) The right hemisphere begins maturing earlier than the left; 2) early in development, the input to the system is concentrated in the low spatial frequencies, due to low acuity in infancy; and 3) synaptic connections are subject to a pruning process to remove weak or ineffective connections.

This setup has strong parallels human visual development. Hellige (1993) has

provided evidence that the RH begins maturing earlier than the LH. We know that visual acuity changes rapidly in infants, such that visual acuity and sensitivity to high frequencies increases over time. This means that the RH will mature while visual input is more biased towards low frequencies, and the LH will mature while the visual input is less biased. L. C. Katz and Callaway (1992) have shown that connections between "patches" mature by strengthening connections consistent with visual input, and pruning (removing) connections that are not. Thus, our goal is not only to try and corroborate our previous findings, but to provide a plausible neurodevelopmental account of where both anatomical and behavioral asymmetries come from.

3.3.1 Methods

We created two sets of autoencoder neural networks, each completely identical. They each had the same connectivity pattern, consisting of 20 connections selected from a circular 2D Gaussian distribution from the hidden units to the input and output units, with a fixed number of connections from each hidden unit to the input and output layers. The only difference between these sets of neural networks was that one was trained on blurred, low-frequency-passed images (our RH networks) and the other was trained on full-fidelity images (our LH networks), to simulate extreme differences in development. As a first pass, we used a Gaussian kernel (σ=8px) to blur our images for the RH network.

Networks were trained using back propagation of error (batch mode, using the SSE error criterion), to simulate the strengthening of connections through learning. To simulate the pruning aspect of development, after every 10 epochs, we removed a constant percentage of the weakest connections (13.4%), such that after 50 epochs exactly 50% of the connections remained. At the end of training, each network had 50% reduction in its original connections, such that on average, each hidden unit had 10 connections.

3.3.2 Results

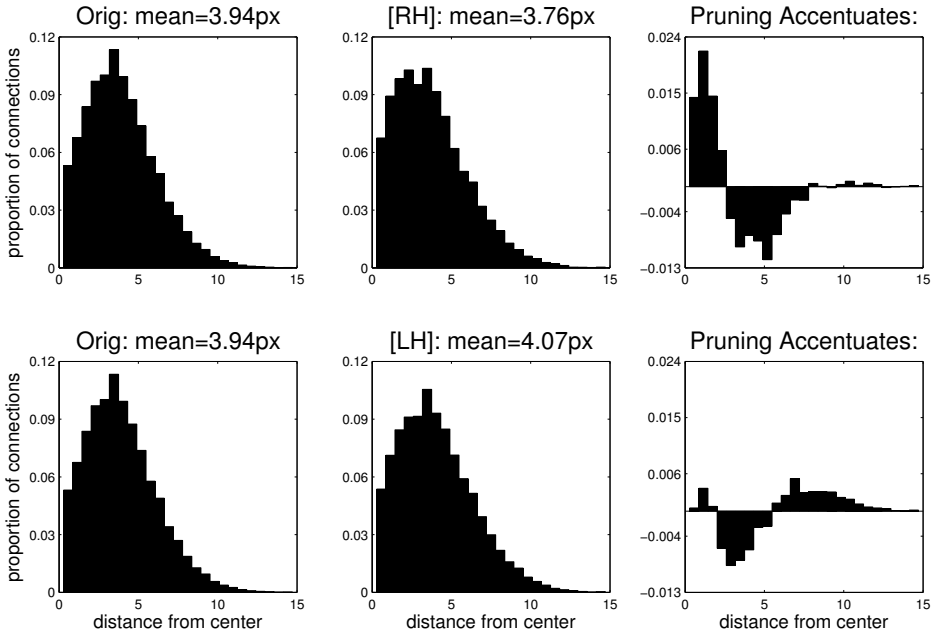

Figure 3.3: Distribution of connections for networks trained on blurry/low-pass (RH; top row) and full-fidelity (LH; bottom row) images, as well as the difference between each of those distributions from the original distribution.

After training, the network trained on low-pass/blurry images (RH) biased the original distribution towards shorter connections, while the network trained on full-fidelity images (LH) biased the original distribution towards more distant connections (see Figure 3.3). This corroborated the associations we saw in our first study, where a smaller spread of connections favored storing information in LSFs, and where a wider spread of connections favored storing information in HSFs. Analysis of the spectral power differences between the networks also showed a similar bias as described in Table 3.2.

As described above in Section 3.2.2, we are examining the computational reasons for this association in current work.

3.4 Reprising the "Relative Frequency" Effect

Christman et al. (1991) showed that when a frequency grating alone distinguished two stimulus classes, the effect of that grating depended on the frequency of that grating *relative* to the other frequencies that made up those stimuli. When the distinguishing grating was higher than the rest of the frequencies used in the stimuli, the stimulus containing the distinguishing grating showed a LH advantage; when the distinguishing grating was lower, there was a RH advantage. Ivry and Robertson's propose that this "relative frequency" effect is itself a computational mechanism: filters at different spatial scales / frequency bands are weighted and summed based on the task; a top-down bias to those weights (that differs between the hemispheres) is relative to the the frequencies selected by those weights.

An alternate hypothesis is that the same filters that select the task-based frequency range are themselves different between the hemispheres. Then, when those filters are weighted and summed based on task demands, a bias that is dependent on that weighting occurs. This alternate hypothesis is not possible in the DFF, where the filters represent bottom-up processing in all conditions (low and high stimulus strength), and therefore would predict hemispheric differences in every experiment. This alternate hypothesis is possible with our model, however. We argued that long-range lateral connections are only active during low stimulus strength, as found in the experiments detailed above. In our case, different "filters" would be different cortical areas, each of which process information at different spatial scales.

Some data exist that are consistent with our proposal. Tasks at different spatial scales do engage different cortical areas (Hopf et al., 2006), consistent with our suggestion that cortical areas can act as task-based "filters" of spatial scale / frequency. In addition, there is reason to believe that homologous cortical areas between LH and RH would

have different frequency biases *relative to the spatial scale of that area*. Data reviewed from our developmental models suggest that small reductions (due to synaptic pruning) in the average spread of long-range lateral connections biases processing towards LSFs. Further experiments with our developmental model showed that, the greater the original spread of connections, the lower the frequency at which the RH stopped showing an advantage (the "cross-over point", where RH and LH performance is similar). Thus, in our proposal, homologous areas with larger spatial scales would have to have a larger average spread of connections in order show a frequency bias relative to that spatial scale. In fact, that's exactly what's found in the macaque monkey: areas higher in the visual processing hierarchy show longer average connections, both in cortical distance, and in the percentage of the visual field they span over (Amir et al., 1993). Our modeling data also suggest that, given the small average spread found in early visual areas, little or no frequency biases could develop there. This is consistent with the idea that visual processing asymmetries are found beyond early sensory processing.

Thus, the failure of our model, representing a single cortical area, to account for Christman et al. (1991)'s data may indicate that these data represent processing in two different cortical areas, each selective for information at a particular spatial scale, each with frequency processing biases relative to that spatial scale. Our autoencoder model above represents a single cortical area; to model this, we would need multiple autoencoder models, each with information at different spatial scales (possibly different image resolutions) and with corresponding changes to the average connections spread (greater for images of lower resolutions).

3.5 General Discussion

Here we showed that an asymmetry in a specific type of intra-cortical connectivity can account for local/global behavioral data, face processing data, and matches spatial frequency asymmetries reported in the literature. This model provides a biologically grounded implementation for these phenomena, and the analyses here showing consistent frequency filtering differences in the model hemispheres are consistent with the current algorithmic explanation for visual processing asymmetries via frequency filtering. These frequency filtering differences are found at a post-sensory encoding stage, consistent with the suggestions in the literature.

We have also implemented a plausible developmental scenario for the emergence of this connectivity asymmetry, which uses only well-established principles (changes in visual acuity over development and both strengthening and pruning of long-range horizontal connections during development) and supported hypotheses (different time-courses for RH and LH maturation).

Finally, we have suggested that our failure to model the results of Christman et al. (1991) with a model of a single cortical area is not a failure of our model, but instead suggests that the "relative frequency" effect in visual processing asymmetries is itself not a mechanism in visual processing. We propose that this effect is the result of latent biases within "higher" areas in the visual hierarchy that are established developmentally and are relative to that area's spatial scale of processing. The bias of an area affects visual processing when the spatial scale of processing for a task matches that of the area, and when stimulus strength is sufficiently weak to activate these intrinsic long-range lateral connections.

3.6 Acknowledgments

Author contributions: I conceived of, implemented, and analyzed all computational simulations and analyses. Janet Hsiao and Garrison Cottrell advised on the project. Garrison Cottrell provided feedback on the final manuscript.

This work was partly funded by a Center for Academic Research and Training in Anthropogeny (CARTA) fellowship, as well as by NSF grant SMA 1041755 to the Temporal Dynamics of Learning Center, an NSF Science of Learning Center

Chapter 4

A Developmental Model of Hemispheric Asymmetries of Spatial Frequencies[1]

4.1 Abstract

Lateralization touches virtually every function we think makes us human and interacts fundamentally with development. Here we connect lateralized function to anatomical asymmetries, and connect those anatomical asymmetries to temporal asymmetries in development.

Our differential encoding (DE) model (Hsiao et al., 2013; Cipollini et al., 2012; Cipollini & Cottrell, 2013a) shows that lateralization in visual processing of spatial frequencies can be explained by a postulated asymmetry in the spatial spread of connections within retinotopic visual cortex. Here, we present three new modeling results supporting our previous conclusions. First, we show that our model results persist when

[1]This chapter will be published in the COGSCI 2014 conference proceedings (Cipollini & Cottrell, 2014)

trained on natural images, warped to match physical distortions of V1, showing that greater biological realism does not diminish our results. Second, we show that the hypothesized anatomical asymmetry can emerge from normal development, due to 1) the known temporal asymmetry in developmental pruning, coupled with 2) known acuity changes. This results in the two hemispheres being trained with images of different spatial frequency content. Third, results from this developmental model suggest that the LH is not specialized for HSF processing; rather, the RH is specialized for LSF processing to the detriment of HSF processing.

Keywords: Lateralization, local/global, high frequency, high spatial frequency, low frequency, low spatial frequency, development, double filtering by frequency, differential encoding, visual processing, asymmetry

4.2 Introduction

Lateralization is an essential part of virtually every function that we believe makes us human. Speaking, fine motor skills, spatial reasoning, emotion, reading, and face perception are all functions with an uneven representation across most individual's cortical hemispheres, but with a consistent hemispheric distribution across the human population.

Lateralization of visual processing, in particular, has long been established (see Ivry and Robertson (1998) for a review). Subjects tend to respond more quickly or accurately to to task-relevant low spatial frequency (LSF) information when presented to left of fixation (which the right hemisphere (RH) has preferred access to) vs. to the right of fixation (which the left hemisphere (LH) has preferred access to). The opposite holds for task-relevant high spatial frequency (HSF) information. These results fit nicely with LH lateralization for word reading (which contain a lot of HSF information) and

RH lateralization for face perception (which contain important configural information in LSFs). The more general inference is generally that the RH is specialized for LSF processing, while the LH is specialized for HSF processing. We believe that understanding mechanisms behind lateralization of spatial frequency (SF) processing may give insight into word reading, face perception, and general mechanisms that may lead to other lateralized functions.

Like lateralization, development is also key to understanding human cognition. Human development differs from that of any other primate (R. D. Martin, 1983; D. Geschwind & Rakic, 2013), including extinct homo species such as Neanderthal (Gunz, Neubauer, Maureille, & Hublin, 2010). Developmental disorders come with a wide variety of cognitive impairments, including many involving atypical pattern of lateralization and inter-hemispheric transfer.

How do development and learning interact with hemispheric lateralization of visual processing? Several hypotheses exist. A few are based on data showing that the right hemisphere develops earlier than the left (N. Geschwind & Galaburda, 1985; Hellige, 1993). As Hellige (1993) noted, during that time, the retina is also developing, during which acuity changes from predominantly LSF ranges to adult-like levels. Howard and Reggia (2007) theorized that during this period, magnocellular afferents to visual cortex enervate V2 in the RH, while later-developing parvocellular afferents innervate V2 in the LH to a greater extent, leading to lateralization of spatial frequency processing. Other approaches exist; Plaut and Behrmann (2011) showed that anatomical constraints on wiring length, the differential projection onto the retina of words (central) and faces (peripheral), and the left lateralization of language could lead to lateralization of faces to the RH (Fusiform Face Area) and words to the LH (Visual Word Form Area).

In this paper, we show that the hypothesized asymmetry that leads to lateralization emerges from a plausible interaction between asymmetry in the timing of connection

pruning and visual acuity changes. We show this in a biologically plausible model under "natural image" experience and with cortical distortions thought to exist in retinotopic visual areas. Then, in order to compare the results of our developmental model to our previous work, we also implemented a more biologically plausible version of our model, also using "natural image" experience and the same cortical distortions.

4.3 The Differential Encoding (DE) Model

Our approach and model of lateralization of visual processing was initially a response to the Double Filtering by Frequency (DFF) model by Ivry and Robertson (1998). Following the lead of Sergent (1982), they argued that the hemispheres are generically lateralized for SF processing across modalities, and proposed that lateralization of spatial frequency processing plays a causal role in the local/global effects in hierarchical letter stimuli and in other tasks with information at multiple spatial scales. However, their connectionist implementation of their model simply assumed a spatial frequency bias existed between the hemispheres, without any indication how such frequency biasing could be neurally implemented and exist in each relevant modality.

Inspired by the finding that long-range lateral connections differed in their spatial spread between left and right BA22 (Wernicke's area and its RH homologue) (R. A. Galuske et al., 2000), we hypothesized that the same asymmetry exists in visual cortex. We then showed in a simple connectionist model how frequency filtering could arise from such a connectivity asymmetry (Hsiao et al., 2013; Cipollini et al., 2012), and could lead to lateralization in classical behavioral tasks (Hsiao et al., 2013; Cipollini & Cottrell, 2013a). We also argued that, due to the dependence of lateralization on both task and stimulus features, that long-range lateral connections are most likely involved, as they are involved through stimulus enhancement via top-down attention (Li, Piech,

& Gilbert, 2008; Piech, Li, Reeke, & Gilbert, 2013) as well as bottom-up processing (H. A. Swadlow & Alonso, 2009).

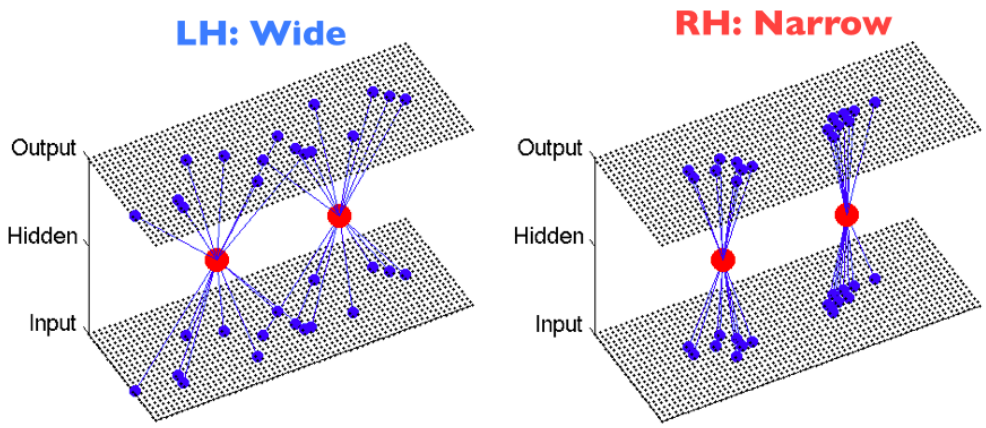

Figure 4.1: Two (of 850) hidden units for each hemispheric model, each with 8 connections. In our simulations below, each hidden unit has 15 connections.

The differential encoding model is a three layer feed-forward autoencoder model with sparse connectivity between the hidden layer and the input and output layers (Figure 4.1), where inputs and outputs are images. Each hidden unit has a 2D position in the input/output space and a small, fixed number of connections. Connections for each unit are sampled from a Gaussian distribution centered at the hidden unit's input/output location. The only difference between the LH and RH models is the standard deviation (σ) parameter of the Gaussian distribution: $\sigma_{LH} > \sigma_{RH}$, such that the spatial spread of connections is greater in the LH vs. the RH model. Note that this Gaussian PDF is used to create *connections* between layers and thus is different from the Gaussian receptive field functions used in some models of lateralization (e.g., Ivry and Robertson (1998); Monaghan and Shillcock (2004)). In fact, the difference in connection spread in our model hemispheres (more spread LH connections) are the *opposite* of theirs (e.g. more spread RH connections).

The model is trained using backpropagation of error (see Cipollini et al. (2012) for detailed methods and training parameters). The training task is to reproduce the output image from the input image through the sparse connectivity matrix described above. This forces the images to be recoded in a manner dependent on the sparse connectivity matrix. The hidden unit encoding represents the lateral interaction between nearby retinotopic locations in cortex.

For LH and RH analysis, many networks instances are generated and trained, with their results compiled and analyzed by hemisphere. After training, differences in spectral content of the input and output images indicate lateralized differences in SF encoding abilities (Hsiao et al., 2013; Cipollini et al., 2012) for detailed methods). Hidden unit encodings are computed for images related to a human behavioral task, and are then used as inputs to independent RH and LH classification networks. These classification networks are trained (using the backpropagation of error algorithm; see Cipollini et al. (2012) for detailed methods) on the same classification task as in the human behavioral task. After training, network performance is summarized over all LH and RH network instances and is then compared to the summary statistics for the human data.

4.4 The Developmental DE Model

A primary finding of our previous work is an association between connection spread and spatial frequency processing, where a more spatially constrained connection spread is biased for lower spatial frequency processing. We discovered this by querying what image information is best learned when the connection distribution is varied. Here, we explore the complementary approach: we query what connection distributions are preferred when the spatial frequency content of training images is varied.

Human visual development is an example of this complementary approach. This

is due to an interaction among the following three factors:

- Visual acuity / contrast sensitivity is initially poor and improves as the retina develops (see P. Wang and Cottrell (2012) for a summary).
- Long-range lateral connections are profuse at birth, with die-off of presumably unused connections and strengthening of the remaining connections, occurring during early visual experience (L. C. Katz & Callaway, 1992).
- The RH begins maturing earlier than the LH (for reviews, see N. Geschwind and Galaburda (1985); Hellige (1993, 2006)).

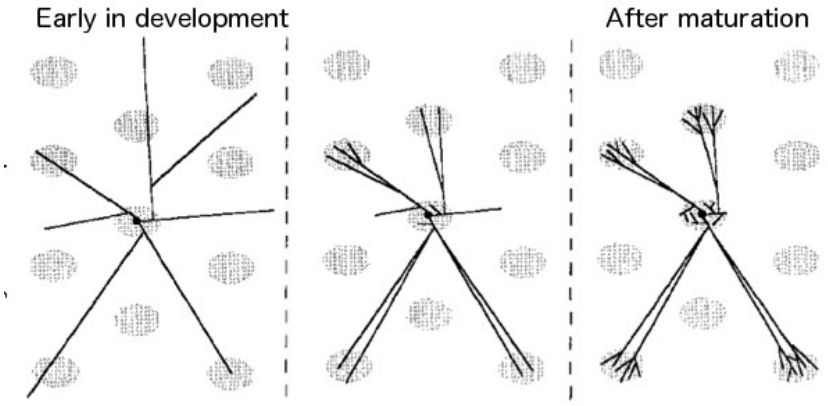

Figure 4.2: Maturation of long-range lateral connections between "patches" in the developing cat visual cortex. Through visual experience, connections are pruned and elaborated, while synapses are strengthened. Adapted from L. C. Katz and Callaway (1992).

Because the RH begins maturing earlier, RH connections are pruned more during blurrier, lower-frequency visual experience, while the LH connections are pruned more when visual acuity is better. This is just the complementary mechanism we described above.

4.5 Methods

Here, we construct LH and RH autoencoder models similarly to our previous work. Input images are 34x25 pixel images. Each model has 850 hidden units distributed across the input/output space, with connections sampled from a Gaussian distribution ($\sigma = 10$ pixels; see top row of Figure 4.3). Unlike in previous work, connections for LH and RH hidden units are selected from the same Gaussian distribution, simulating initial symmetry between the hemispheres.

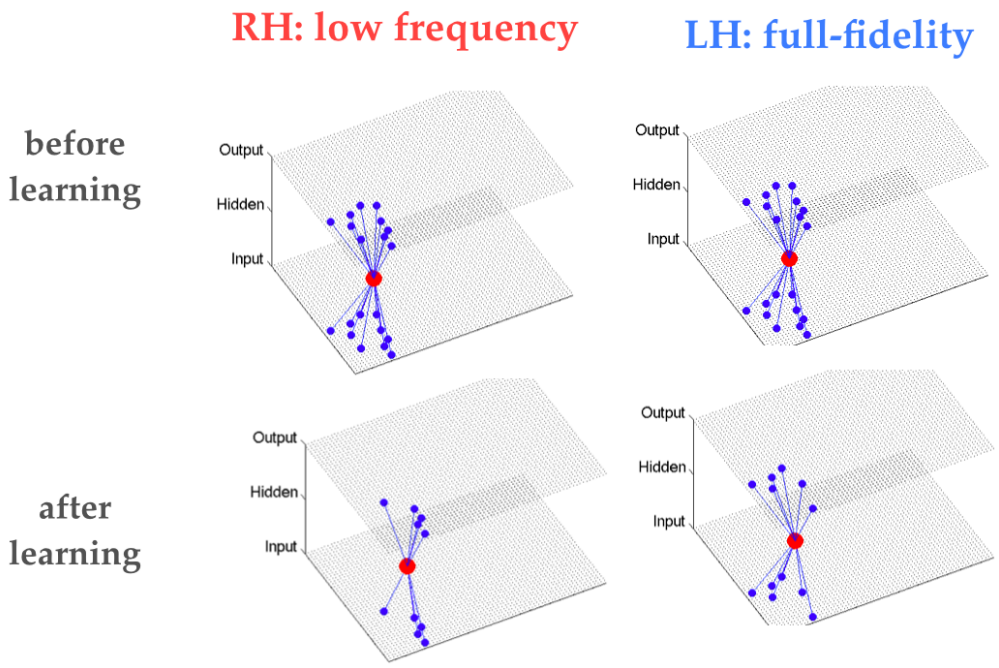

Figure 4.3: Pruning results differ in the LH and RH models, despite the original connection patterns being identical. This is due to differences in connection removal, induced by different spatial frequency content in the training images.

There are four major differences in the training methods from our previous work[2]:

- Rather than training only on task-specific images (such as hierarchical letter stim-

[2] In addition, weight decay was set to $\lambda = 0.05$, to accentuate differences between used and unused weights.

uli), we train on 250 natural image patches sampled randomly from the van Hateren database (van Hateren & van der Schaaf, 1998)[3]. This simulates more accurately the visual experienced gained during development.

- Each hidden unit has 30 connections to start–twice as many as previous models had–and will eliminate synapses until each hidden unit has, on average, 15 input/output connections (see Figure 4.3). This simulates initial connection proliferation before maturation, followed by elimination during visual experience.

- LH and RH networks differ only in the spectral content of the images they're trained on. Both networks are trained on low-pass images where the image quality improves over time (i.e. the cutoff frequency increases over time), but on average the image quality is higher for the LH network than the RH network (i.e. on average, the cutoff frequency is at a higher frequency for the LH network). The different schedules of training inputs are detailed in Figure 4.4. This simulates the interaction between changes in visual acuity and hemispheric development.

- In order to simulate the cortical expansion of the fovea, we trained on log-polar version of our original images. The log-polar transform is thought to closely represent retinotopic visual cortex that we aim to simulate (Schwartz, 1985).

After both networks are trained, we compile the empirical connectivity distribution of the unpruned connections across all hidden units within LH and RH models. We compare each distribution with the original connection distribution (before pruning) to see how training on different SF content affected pruning.

In order to compare our developmental model to our previous work, we trained our previous model with the same 250 natural image patches and with 15 connections

[3]Greater numbers of image patches were tried and made no qualitative difference in the results, but did increase training time.

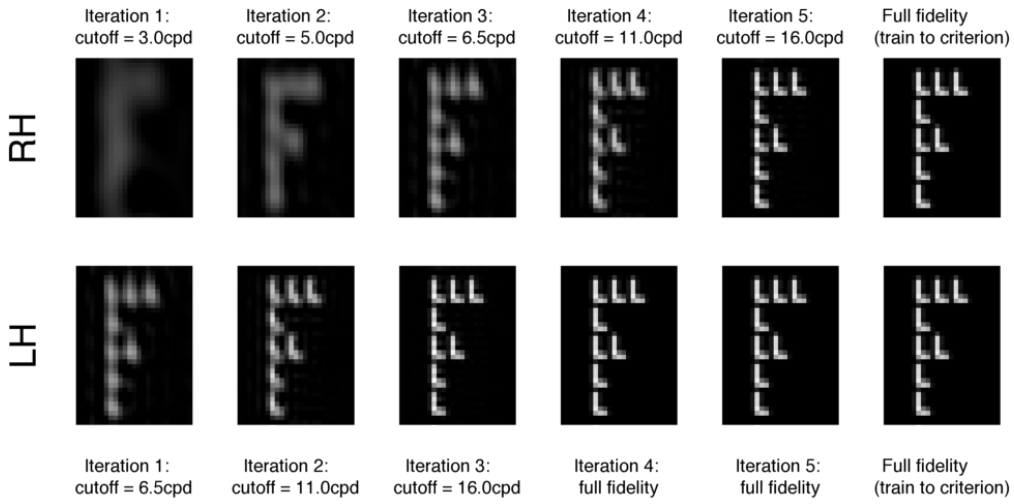

Figure 4.4: Low-pass filtering schedule of image training. During each iteration, the model was trained on all 250 natural images for 7 epochs. Before moving on to the next iteration, connections containing the smallest $(0.5)^{\frac{1}{6}}\%$ weight values were pruned, such that after the 6 iterations, 50% total connections were pruned. After these 6 training / pruning iterations, both models were trained on full-fidelity natural images until reaching an equal error criterion (summed over all input images and pixels), simulating equal visual experience. Note that hierarchical letter stimuli are pictured here as they show variations in spatial frequency content better than the natural images that were actually used throughout the simulations here.

per hidden unit, just like the developmental model after pruning occurs.[4]. We verified that this models shows qualitatively similar results in both frequency processing and behavioral modeling as previously reported (Hsiao et al., 2013), and thus was appropriate for direct comparison to this developmental model.

4.6 Results

For our network following our previous work, but trained on natural images, we found the same spatial frequency differences as previously reported. We also tested the same network (without retraining) on target detection of letters within hierarchical letter stimuli (Sergent, 1982). These networks showed the same *hemisphere* $\times$ *target level*

[4] $\sigma_{RH} = 4$ pixels, $\sigma_{LH} = 10$ pixels, weight decay $\lambda = 0.025$

interaction as previously found (see Figure 4.5)[5].

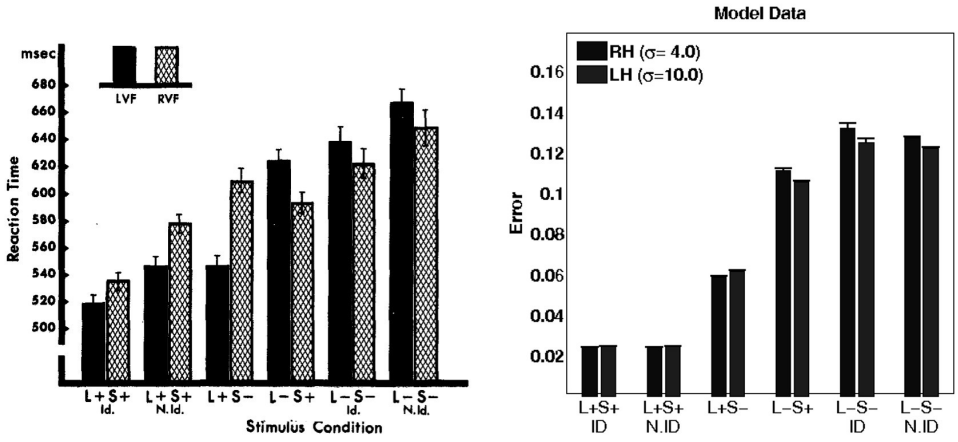

Figure 4.5: Behavioral results for our previous model, but with autoencoders trained on natural images rather than hierarchical letter stimuli. These results are more consistent with the overall pattern of behavioral results found in Sergent (1982). They are also more consistent across the 6 groupings of $[H, L, T, F]$ into groupings of 2 targets and 2 distractors. Note that we did not test our developmental model on this behavioral task.

For our developmental networks, while we used a complementary approach to the problem, we found the same association between spatial spread of connections and spatial frequency processing: networks trained and pruned under low-frequency images kept connections with a relatively smaller spatial spread than networks trained and pruned on full-fidelity images.

4.6.1 Connection Distributions

In these developmental networks, connection distributions can only differ from variations in visual experience that lead to variations in what connections are pruned. These networks show a difference pattern very similar to our previous model, which had LH and RH connections sampled from Gaussians with different standard deviations.

[5]In fact, results on this network were more robust to which letters were chosen as targets than in previous work, likely due to a reduction in overfitting of the network due to having a larger training set and more robust regularization procedures

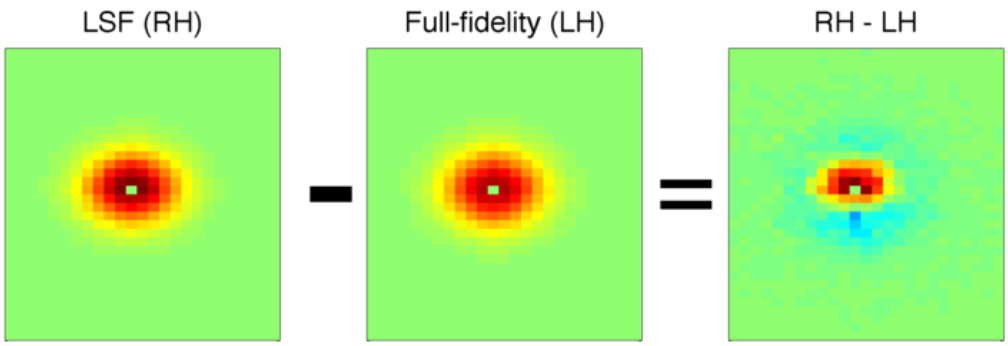

Figure 4.6: RH and LH connection distributions from the developmental model, and their difference. Here, warm colors are positive, cold colors are negative, and green is zero. To compile the RH and LH distributions, all hidden units were placed at the center of the figure, and a histogram of connections was created. Note in the difference plot the central positive values indicating more short connections in the RH model, and the surrounding blue ring indicating more spread connections in the LH model.

This shows that spatial frequency input differences can drive connectivity differences qualitatively similar to those we had previously postulated, and suggests that these connectivity differences can arise through typical human visual development.

Despite the similar appearance of these connection distributions, the size of the connectivity spread was overall smaller in our developmental model (see Figure 4.7). In our previous work, LH connections were 30% farther from their nearest connecting neighbor than RH connections on average; here, this number dropped to 5%. We note that re-running the developmental model with a greater difference in the spatial frequency content of the input images can drive connection distance differences equal or greater to the 30% postulated in our previous study.

4.6.2 Spatial Frequency Content

The developmental model also showed spatial frequency differences similar in shape, but attenuated, as compared to those found in our previous work (see Figure 4.8). We found that this was related to the smaller average connection spread reported above;

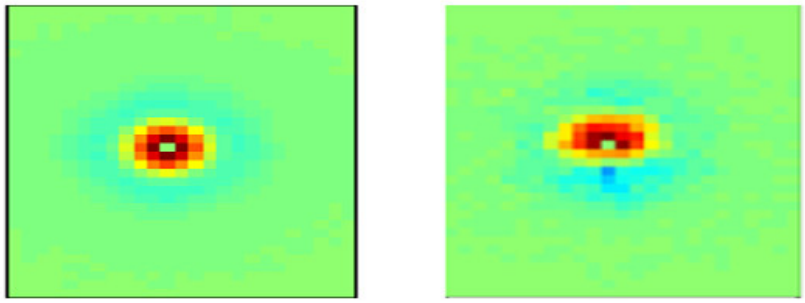

Figure 4.7: $RH - LH$ connection distribution differences between our previous model trained on natural images (left) and our developmental model (right). Warm colors show connections with greater representations in the RH, cool in the LH.

when the developmental model was re-run on a greater difference in frequency content, the spatial frequency differences met or exceeded those reported in our previous work.

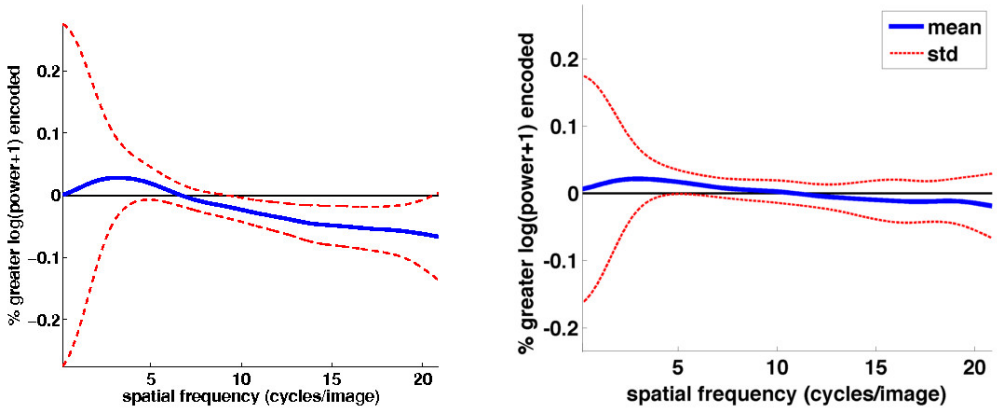

Figure 4.8: 1D spatial frequencies for our previous model trained on natural images (left) and our developmental model (right). Note the similar character of both, but attenuated in this developmental scenario. Note also that all spatial frequency differences, besides those very close to the x-axis crossing point, are statistically significant.

4.6.3 Connection Changes

In the literature we've reviewed, it has been consistently suggested that the RH is specialized for low spatial frequency (LSF) processing, and the LH for high spatial frequency (HSF) processing. However, the performance of each hemisphere is measured

relative to the other. We don't have a baseline to compare each hemisphere's abilities to, which would be necessary to determine whether both hemispheres are biased, or whether one hemisphere is biased and the other is not.

We can examine this directly issue directly in our developmental model. In Figure 4.9, the RH (top row) and LH (bottom row) changes over training are shown. We can see that the RH and LH changed similarly, but that the LH network is simply less changed from the original distribution than the right.

This suggests the novel hypothesis that, in fact, the RH is biased towards LSF information at the cost of HSF information, while the LH is essentially similarly, but less biased. Under this hypothesis, the LH only looks specialized for HSF information because it is being compared to the RH, which has sacrificed HSF processing more than the LH has (for the benefit of better LSF processing). We are currently developing a model to examine this hypothesis in greater detail.

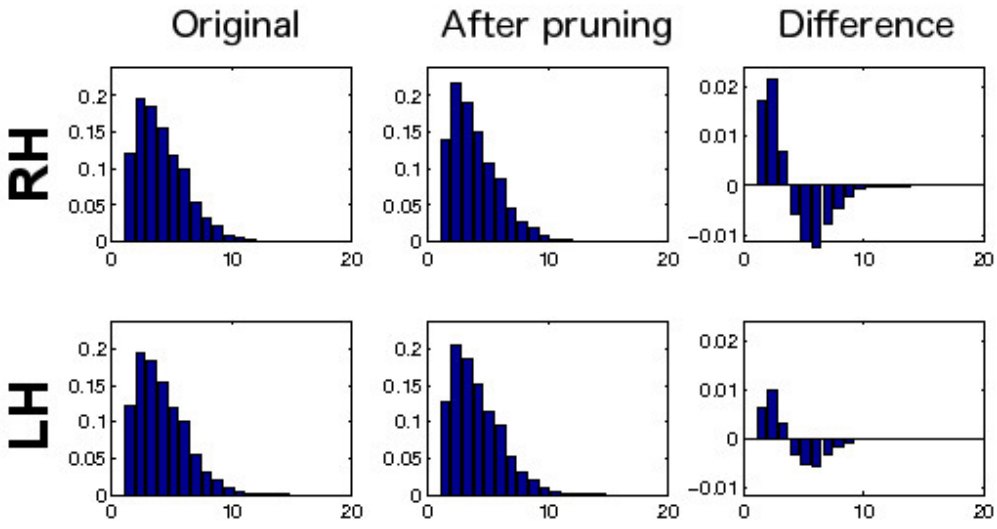

Figure 4.9: These are histograms of the distance from each connection to the hidden unit location. RH and LH networks begin with the same distribution. Each model hemisphere changes its connection distribution via connection pruning during its (differing) visual experience. The difference between beginning and ending distributions is pictured on the right. Note the similar character of the differences, with the LH network essentially being an attenuated version of the RH network.

4.7 General Discussion

Here, we described a developmental model of lateralization in visual processing, where improvements in visual acuity interacts the differential timing of connection pruning in left and right hemispheres. In this developmental model, we fixed spatial frequency content and allowing connections to vary via connection pruning during learning. This led to an association between a smaller connection spread, enhanced low spatial frequency processing, and attenuated high spatial frequency processing.

This association is consistent with those found from our adult model, where connection spread was fixed and spatial frequency processing measured. These results suggests that the assumptions of our adult model could plausibly arise during normal human visual development.

In addition to the above findings, we also saw the first indication that the RH may be specialized for LSF processing at the detriment of HSF processing, while the LH is similarly, but less strongly, biased in how it processes and represents spatial frequency content.

In the future, we plan to follow up on two issues here, and extend this work to central vision:

- We did not test the encodings from our developmental model in any behavioral paradigm. Our first order of business is to verify that the developmental model also shows the behavioral lateralization seen in humans and replicated by other versions of our model.

- We plan to implement a new model to systematically explore how spatial frequency processing relates to spatial spread of connections. This would be a simple 2-layer receptive field model–one output neuron with a sparse set of input connections. We will use this model to map out how spatial spread affects frequency tuning

preferences of the output neuron.

- We also hope to explore how interhemispheric connectivity affects the development of lateralization and the interaction between task, stimuli, and measures of functional lateralization. Specifically, we're interested to embed these connectivity differences in a model with inter-hemispheric interactions, so that we could try and model data for central fixation in the same behavioral paradigm modeled above (Sergent, 1982).

4.8 Acknowledgments

Author contributions: I conceived of, implemented, and analyzed all computational simulations and analyses. Garrison Cottrell advised on the project and provided feedback on the final manuscript.

This work was partly funded by a Center for Academic Research and Training in Anthropogeny (CARTA) fellowship, as well as by NSF grant SMA 1041755 to the Temporal Dynamics of Learning Center, an NSF Science of Learning Center

Chapter 5

Uniquely human developmental timing may drive interhemispheric coupling and cerebral lateralization[1]

5.1 Abstract

Cerebral lateralization is intertwined with virtually every cognitive function that we think makes us human, yet a clear dichotomy in a leading theory about its origins remains unexplained. Lateralized processing has been suggested to be due to independent development of local neural circuits (Ringo et al., 1994; Rilling & Insel, 1999a), but the complementary nature of these circuits, evidence of extremely strong interhemispheric functional coupling, and the similar developmental trajectories between lateralization and interhemispheric communication seem to suggest that robust interhemispheric interactions are key to the lateralized human brain.

Here, I review literature and present modeling evidence suggesting that: (1)

[1] An early version of this chapter was published in the COGSCI 2013 conference proceedings (Cipollini & Cottrell, 2013b)

Current evidence that conduction delay magnitude leads to hemispheric independence is overstated, misinterpreted, and inconsistent with experimental data on the development of lateralization and the corpus callosum. (2) Variability in conduction delays, present in early development due to a preponderance of thin, unmyelinated white matter fibers, bias developing brains towards the use of shorter, local connections; this effect can drive hemispheric independence. (3) Lateralization does not seem to spontaneously emerge from this model, nor is it induced by providing lateralized inputs or outputs. I show that results (1) and (2) are consistent with general findings from the literature encompassing both development and adulthood.

I conclude by arguing that effects of conduction delay variability early in development is greatest in humans, due to a trade-off between maximizing adult brain size while minimizing brain size at birth. This suggests that, counter to previous proposals, the physiology of interhemispheric communication in humans may be more than function of brain size shared across mammals, but instead related to the uniquely human problem of birthing a large-brained fetus through a narrow bipedal pelvis.

5.2 Introduction

A single concept, supported prominently by a single paper, has dominated thought as to the origins of cerebral lateralization and effect of conduction delays in the cognitive science literature. The modeling work of Ringo et al. (1994) has been extensively (and in many cases exclusively) cited to support the notion that long conduction delays, due to the large human brain size, enable cerebral lateralization. This “delay magnitude hypothesis” has intuitive appeal, as it supports another long-held notion: that some combination of large brains and functional lateralization has made us human.

There is no denying the importance of functional lateralization in human cognitive

abilities; we are functionally lateralized in virtually all cognitive functions that we think are special to our species, including language, high-precision manual use of tools, spatial processing abilities, even emotional processing (Gazzaniga, 2000; Craig, 2005). There is also no denying, however, that the lateralized hemispheres are also tightly coupled–both in their complementary abilities (Gazzaniga, 2000; Hellige, 2006) as well as their online functional coupling (Stark et al., 2008).

The relationship between the suggested greater hemispheric independence in humans and the hemispheres' complementary, interacting abilities is simply not captured by the delay magnitude hypothesis. Nor does the hypothesis account for the anatomical and functional asymmetries that appear throughout the animal kingdom in species of all brain sizes (Rogers & Andrew, 2002; Rogers, 2009). It cannot speak to data showing that interhemispheric coupling and functional lateralization increase during development (e.g. Benninger et al. (1984); Petitto et al. (2012); Musacchia et al. (2013)), let alone the fact that that happens while fiber length increases (Lewis & Elman, 2008). Whether or not the delay magnitude hypothesis is correct, it certainly is not complete.

Imagine throwing a ball or shooting an arrow. With greater distance, hitting the target gets harder–not because it is harder to compute the angle needed to hit the target; the equation remains the same–but rather that any variability, any small error in aim or effect of wind is amplified by the distance to the target. This *distance-dependent variance* is what drives the greater challenge of coordinating at a distance.

Traditionally, the propagation of action potentials along axons has been thought to be extremely reliable. Though this is true in some axons (H. Swadlow, 2000), it is not true for thin, unmyelinated axons, where many varieties of molecular stochasticity and noise cause trial-to-trial distance-dependent variability (Faisal, Selen, & Wolpert, 2008; S. S. H. Wang, 2008). As learning in spiking neurons is highly dependent on precise timing of pre- and post-synaptic spikes, it seems likely that distance-dependence

variability will slow learning and favor learning in more reliable fibers.

Here, I show evidence that functional lateralization is not caused by the magnitude of conduction delays, nor by hemispheric independence. Instead, I show that variability in the magnitude of conduction delay can cause hemispheric independence, and that this independence tends to delay the development of perceptual lateralization, while having a more complex pattern on lateralized motor outputs. I argue that this effect, driven by small diameter, unmyelinated axons that are prevalent through early post-natal development, is likely strongest in humans.

This paper proceeds in four parts. First I will review literature, including the original modeling of Ringo et al. (1994), that strongly question the delay magnitude hypothesis. Then I'll show results from four computational experiments, using a derivative of that model developed by Lewis and Elman (2008). In Experiments 1 and 2, I show that *variability* in delay magnitude can cause independence between the hemispheres. In Experiment 3, I show that reduction of noise over development enables a shift from intrahemispheric to interhemispheric circuits. In Experiment 4, I show how the model can be used to examine how independence might affect lateralization, with preliminary results showing no relationship. I will summarizing what these results say about human development of white matter connectivity and lateralization. I will then conclude by arguing that a unique set of circumstances cause conduction delay variability to be most severe for humans, suggesting a mechanism for what makes human lateralization unique in its strength and importance to our cognitive abilities.

5.2.1 The failure of conduction delay magnitude

Axons of the corpus callosum are especially long in large-brained mammals such as humans, due to their need to traverse through a large, highly gyrified brain to interconnect the two cerebral hemisphere. Because the average conduction velocity of

axons does not sufficiently compensate for the additional axon lengths when compared to smaller-brained animals, the resulting interhemispheric transmission delay over the majority of callosal axons is longer in large-brained species (Ringo et al., 1994; Olivares et al., 2001; Aboitiz & Montiel, 2003). The delay magnitude hypothesis postulates that this increased delay causes less interhemispheric collaboration and therefore enables cerebral asymmetry.

While the anatomy and physiology of callosal axons is well established, their seemingly intuitive effects on interhemispheric collaboration is supported by a single model in a single paper Ringo et al. (1994). Here, I argue against the delay magnitude hypothesis in two parts. First, I present 4 results from the literature that are inconsistent with the delay magnitude hypothesis. Then I show that the data reported from the model itself do not support the hypothesis either.

Increased interhemispheric collaboration is associated with an increase in slow fibers

Larger corpus callosum size is associated with less lateralization. This is true for regions of the corpus callosum, as well as the corpus callosum as a whole. The midbody of the callosum, which carries fibers to and from motor cortex, is larger for individuals with less lateralization in handedness (Witelson, 1989; Luders et al., 2010). Callosal cross-sectional area is proportionally larger for left-handers (Witelson, 1985), who show less functional lateralization than right-handers. Within humans, larger corpus callosum size is also associated with a larger number of thin fibers, not with the thickness of fibers (Aboitiz et al., 1992).

These two observations associate less lateralization with a greater number of thin, slow fibers–just the opposite of what the delay magnitude hypothesis would predict.

Homotopic areas show functional coupling

The corpus callosum largely connects corresponding (homotopic) areas between left and right cerebral hemispheres. Thus, according to the delay magnitude hypothesis, homotopic areas connected with slow, thin fibers (Aboitiz & Montiel, 2003) should show weak functional connectivity.

In fact, this is not the case at all. For example, when examining interhemispheric correlations through resting-state fMRI, Stark et al. (2008) found very strong interhemispheric correlations between association areas. Reduced interhemispheric coherence (measured with EEG) at locations away from primary sensory/motor cortices has been measured in mental disabilities or diseases, such as dyslexia (Dhar, Been, Minderaa, & Althaus, 2010) and schizophrenia (Hoptman et al., 2012).

Hellige (2006) points out that functional specializations tend to be complementary. For example, visual processing of the left hemisphere seems biased towards high frequency processing, while the right hemisphere seems biased towards low-frequency processing (Sergent, 1982; Ivry & Robertson, 1998). If there is less interhemispheric integration due to more independent processing, then why would the two hemispheres show any type of relationship at all? The delay magnitude hypothesis offers no answer.

Longer delays may support coordination

The corpus callosum in larger brains doesn't simply have longer conduction delays; it also has a broader range of conduction delays (Caminiti, Ghaziri, Galuske, Hof, & Innocenti, 2009). Innocenti (2011) reviews modeling data that a broader range of conduction delays supports a broader range of oscillations across the corpus callosum (Caminiti et al., 2009), and that a broader range of oscillations in turn may increase the stability of those oscillations (Roberts & Robinson, 2008). The current belief is that these oscillations are necessary for binding of information between two distant cortical areas

(Fries, 2005); stabilization of interhemispheric oscillations would presumably enhance interhemispheric communication. Thus, longer delays may be associated with improved ability to coordinate interhemispheric integration, rather than any reduction as predicted by the delay magnitude hypothesis.

The delay magnitude hypothesis fails to explain development.

The delay magnitude hypothesis only addresses mature, adult brains. There are a number of developmental phenomena that clearly are inconsistent with the delay magnitude hypothesis.

First and foremost, both lateralization and interhemispheric communication increase during development (e.g. Benninger et al. (1984); Petitto et al. (2012); Musacchia et al. (2013)). This is in direct conflict with the delay magnitude hypothesis, which states that decreased interhemispheric communication should lead to greater lateralization.

Additionally, delay magnitude changes over time. Lewis and Elman (2008) used a version of Ringo et al. (1994)'s model to show that, the steeper the developmental brain growth curve, the more detrimental interhemispheric connections are to learning.[2] As their model "matured", even though the magnitude of delays were longer, because they were more stable, they promoted interhemispheric collaboration.

Thus, interhemispheric collaboration develops at the same time as lateralization and delay stability improves interhemispheric collaboration. The former is inconsistent with the delay magnitude hypothesis; the latter is unaccounted for.

Delays likely matter less than has been previously stated

There are a number of reasons to question the Ringo et al. (1994) results–and their interpretation within the literature–which I detail here.

[2]This is due to the fact that, as brain size changes more quickly, the conduction delays change more as well, and those larger changes are more detrimental to learning.

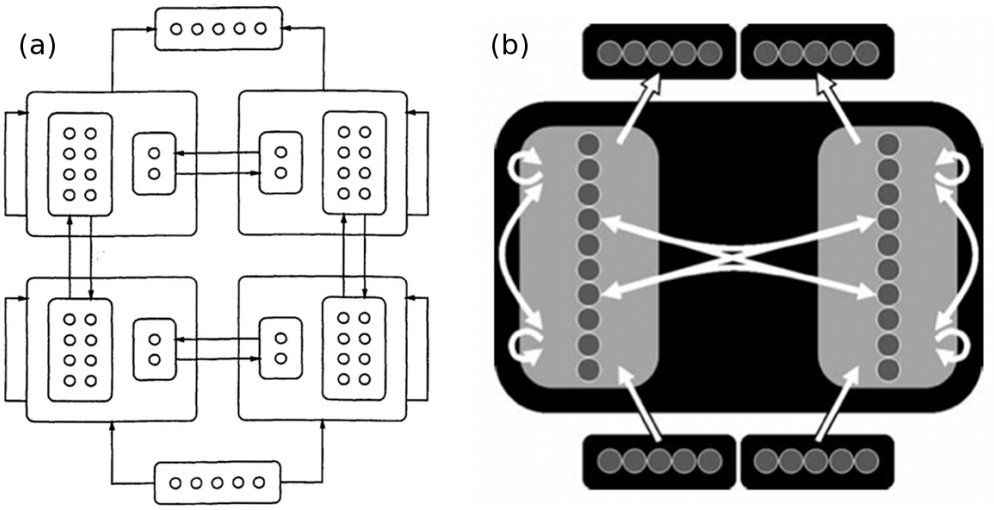

Figure 5.1: (a) The model architecture of Ringo et al. (1994). Information flows from bottom to top; left model hemisphere is to the left, and right model hemisphere is to the right. Arrows represent full connections between pre- and post-synaptic units. All delays are 1 time-step, except the interhemispheric ("callosal") connections, whose delay were varied across conditions. Note the shared output nodes, which allow an (unintended) path for fast interhemispheric coordination independent of the "callosal" connections.

(b) The model architecture of Lewis and Elman (2008) simplifies the structure and splits the inputs and outputs, allowing input and output pattern associations to differentiate between optional and obligatory interhemispheric integration.

The model failed to fully control interhemispheric transfer Although the authors aimed to separate interhemispheric communication through long conduction delays, their model setup failed to do so. In addition to their "callosal" connections that were varied with short and long delays, their model also had converging connections from the hemispheres to a shared bank of output nodes, whose delays were always short (one time-step; see Figure 5.1a). Due to the use of the backpropagation in time learning algorithm, error is calculated at the shared output nodes and propagated back through to the input through the intrahemispheric connections. Thus, even if the model was re-trained without any "callosal" connections, the hemispheres would still show interhemispheric

dependence; one hemisphere would not be able to complete the task without the other[3].

A second way in which Ringo et al. (1994) failed to control interhemispheric transfer is in their input-output associations. Because all input and output patterns were the same to each hemisphere, interhemispheric communication was never necessary. Each hemisphere received exactly the same input, and so could independently produce the shared output. In order to characterize how interhemispheric transfer happens when necessary, the need for interhemispheric transfer must be controlled.

Both of these issues were addressed by Lewis and Elman (2008). Interhemispheric transfer was controlled by simply splitting the output nodes into two separate banks, as depicted in Figure 5.1b. Interhemispheric dependence was controlled by splitting the input nodes, then controlling the training task to introduce patterns that contain output values that cannot correctly be determined without information from the other hemisphere ("inter-" patterns; Figure 5.4b), as opposed to that could be processed without any information from the opposite hemisphere ("intra" patterns; Figure 5.4a).

To control for both of these issues, all modeling work in this paper uses a similar split-output architecture to Lewis and Elman (2008)'s model, with input and output pattern association that differentiates between optional and obligatory interhemispheric transfer. See Section 5.3.1 for more details on modeling methods used in this paper.

The results of the paper are misunderstood and misinterpreted. Citations to this paper are often made to support the notion that functional lateralization is inevitable, given the human brain size. This is a misrepresentation of the Ringo et al. results. In the paper, the authors only claim that lateralization at short settling times is caused by long delays. Tasks that allow "multiple passes" across the callosum were interpreted to show indistinguishable results across delays.

[3]I verified this through simulations using a reimplementation of their model.

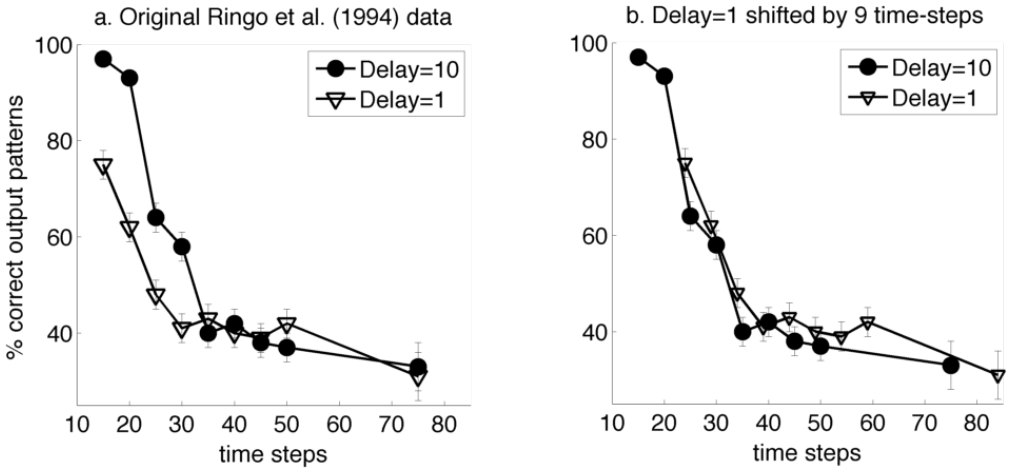

Figure 5.2: (a) Original data from Ringo et al. (1994), showing performance of networks after lesioning interhemispheric fibers, for two networks with different interhemispheric delays (1 time-step vs. 10 time-steps). Different networks were required to process across a range of times (x-axis; 15-75 time-steps), while they were trained to output binary strings that were associated with particular input binary strings. After training, "callosal" connections were lesioned, and network performance was measured. The network with the shorter interhemispheric delays ($D = 1$; empty triangles) shows poorer performance on networks running for fewer time-steps (x-axis=15-30 time-steps); this was interpreted as indicating greater interhemispheric interaction.

(b) We should expect a network with delay=1 and delay=10 to have a difference of 9 time-steps to the onset of hemispheric interaction. I shifted the $D = 1$ curve by 9 time-steps later (right on the x-axis) to allow us to visualize any qualitative difference in the interhemispheric interaction outside of this difference in onset. The overlap of the curves suggest that there is no other variation in interhemispheric communication besides this simple static delay.

Besides these citations showing misunderstandings of the results, the author interpretations of the data were not fully correct either. The authors seem to believe that interhemispheric interactions are suppressed until around 35 time-steps in the model–the point at which performance reaches chance for both networks (Figure 5.2a). In fact, the original results do not show any suppression of interhemispheric transfer; the hemisphere either operate independently or not at all. To show this, I align the results from the two models to account for the difference in timing (9 time-steps; see Figure 5.2b). When I do

so, the results from the two models are indistinguishable, showing that the only change in interhemispheric interactions is a brief, static delay in onset of interhemispheric communication, rather than any long delay or change (qualitative or quantitative) in interhemispheric interactions. Besides the static delay in the onset of communication, the models show precisely the same level of interhemispheric coordination.

In addition, the idea of "multiple passes" misunderstands the inner workings of the model. They say "The network not allowed sufficient time for multiple transfers of activations (the network with slow interhemispheric transmission trained with faster output times) ends up with two hemispheres operating fairly independently." (Ringo et al., 1994; p 340). The hemispheres will operate fully independently for the delay amount, then fully dependently after that. There are no "passes" in the model, as information is sent continuously and predictively. For example, within the network with interhemispheric delay of 10 time-steps, at $t = 1$ the interhemispheric nodes send activation across the corpus callosum that is useful for the other hemisphere to try and solve the task at $t = 11$ when that information arrives. If information were traded as "passes", then there would be lulls in interhemispheric communication during each pass. This again points out that the models are fully independent for the transfer time of a single pass (1 or 10 time-steps), then collaborate to precisely the same level after that.

A third way that the authors overstep the model results is in their suggestion that processing that must be faster than the interhemispheric transfer time, such as phoneme processing, must be done independently in the two hemispheres. Much like the "passes" idea, their idea does not take into account the predictive abilities of neural coding. The processing must be fast and unpredictable in order for slower interhemispheric communication to be rendered irrelevant. If the processing is fast but predictable, the other hemisphere can send predictions about future time-steps that will arrive to the other hemisphere at the time needed to co-process a bilateral stimulus. This is how the

model shows precisely the same level of interhemispheric communication, even with long delays.

The experimental setup of the model confounds the effect of delays and predictability. The network starts at $t = 1$ with no meaningful activation, and so the stimulus is fully unpredicted and no predictive signal is available to overcome the delay. It is at $t = 10$ that the predictive signal (sent at $t = 1$ arrives, and interhemispheric effects can be seen.

It is worth noting that this effect of unpredictability is widespread in visual perception experiments, where stimuli are presented without context in order to make them unpredictable. This will favor functional connections that don't depend on prediction as compared to if the stimulus was predictable from spatial context (like a scene), temporal priming, or other regularities. This may contribute to the overwhelming sense that visual processing is a hierarchical feed-forward system–our experiments put the neural network in situations where predictive coding cannot shape the neural response, and so an impoverished neural interaction is seen.

The relevance of the paper is often misunderstood and misinterpreted The key quantities that affect the onset of interhemispheric collaboration are the difference in onset of these interactions and predictability. Because of this, it is important to note that the model clearly exaggerates this difference (10x longer for interhemispheric vs. intrahemispheric communication). To determine the relevance of the model, a more precise assessment of intra- and interhemispheric delays must be made. Though the exact time it takes for information to be moved between the hemispheres is unknown, we do have reasons to think that even for fast, unpredictable processing, conduction delays may not be a barrier to interhemispheric collaboration.

Callosal connections between areas are not of a single delay, but instead form a

distribution of delays (see Figure 5.3). Onset of activity may be mediated by the fastest callosal fibers–which we know vary with brain size (Olivares et al., 2001; S. S. H. Wang, 2008) and keep the minimum delay close to 2 - 4 milliseconds (Innocenti, 2011). In other words, the onset of interhemispheric communication could be as short as 2 - 4 milliseconds–on the time-scale of other time delays within the brain (such as the amount of time for an excitatory post-synaptic potential to be integrated, and the time for renormalization of the membrane potential to occur, the time for long-range lateral connections to propagate action potentials). These delays may interact with conduction delays, and may smooth out many of these effects on the millisecond-level. Finally, intrahemispheric connections have their own distributions (Innocenti, Vercelli, & Caminiti, 2013) and distances (Lewis, Theilmann, Sereno, & Townsend, 2009; Markov et al., 2013), so intrahemispheric connections cannot be considered as a homogenous group whose average delay may be faster (or not) than intrahemispheric fibers, but whose fastest delay may be on the same time-scale. Taken together, it's clear that we don't know enough about the delay distributions (and their functional roles) across the entire brain to make the claim that fast, unpredictable processing is affected by the average callosal delay time.

5.2.2 My hypothesis: conduction delay *variability* affects long-distance communication

The delay magnitude hypothesis fails to address how developmental changes in white matter connectivity lead to the adult state. It also fails to explain how homotopic areas could be both more independent and complementary in function. The model implemented to support the delay magnitude hypothesis fails to support the hypothesis, as the model hemispheres communicate just as robustly with delays in the model–just with a delay to the onset of that communication that is small in real systems and, in real systems and real scenarios, may be overcome through a number of mechanisms. Lastly,

the delay magnitude hypothesis never actually tests for a causal relationship between delay magnitude and lateralization; it only assumes one.

From a computational perspective, one mechanism likely to cause reduced communication is not delay magnitude, which can be overcome through prediction, but instead delay variability. If the reliability of connections were compromised, then Hebbian learning rules that use spike timing to strengthen and weaken synapses would likely favor more reliable information sources, due to the dependence of potentiation strength on precise timing. This is similar to Bayesian models of integrating information from multiple information sources, where the relative weights from the two sources are inversely related to their variance–less reliable sources are given lower weights (Battaglia, Jacobs, & Aslin, 2003).

Surprisingly, there are very good reasons to believe that delay reliability is an issue in the brain. (Faisal et al., 2008) review a number of mechanisms that cause unreliability in conduction delays. Increased variability of conduction delay is associated with a number of biophysical properties, such as smaller soma size (Faisal, White, & Laughlin, 2005), lower spiking rates (Schneidman, Freedman, & Segev, 1998; van Rossum, O'Brien, & Smith, 2003), spontaneous spike generation in unmyelinated axons with diameter $< 0.3\mu m$ (Faisal et al., 2005), channel noise along unmyelinated axons with diameter $< 0.5\mu m$ (Faisal & Laughlin, 2007), and history-dependent spiking in unmyelinated axons.

Interestingly, in all cases increased variability is related to soma and axon size–neurons with smaller bodies tend to have smaller axon diameters (Faisal & Laughlin, 2007), tend to have lower, modulatory drive (Sherman & Guillery, 1998), and are much more likely to be unmyelinated. Therefore all factors above converge to relate variability to a small absolute projection neuron size. In adults, these phenomena have been observed in the cerebellum (as reviewed by S. S. H. Wang (2008)), where tiny granule cells project

thin, unmyelinated fibers to Purkinje cells. These small granule cells have such a weak drive that on average one Purkinje cell connects with 200,000 granule cells. This system shows up to 20% variability in spike timing along the granule cell axons. There are no reports in the literature of variability in axons within the cerebral cortex–is there any reason to think there might be?

Here, I hypothesize that small axon size may be particularly important in the cerebral cortex during early development. In the corpus callosum, high-resolution electron microscope data of cat (Berbel & Innocenti, 1988) and macaque (LaMantia & Rakic, 1990b) show that the preponderance of fibers pre- and post-natally are thin and unmyelinated. Axon diameters increase over development as the overall brain volume and callosal volume increase, and fibers myelinate over time (see Figure 5.3). Therefore, pre-natally and during development one might expect a bias for more local connectivity than long distance connectivity, with long-distance connectivity coming online as white matter fibers mature. In humans, recent functional connectivity evidence suggests that this is the case, with an early bias for shorter-range (Kelly et al., 2009; Uddin, Supekar, & Menon, 2010) and thicker, earlier myelinated early sensory-motor fibers (Fransson, den, Blennow, & Lagercrantz, 2011).

There are also good reasons to think that small axon size may be particularly important to lateralization. Lateralized functions are often located in association areas, where callosal fibers are thinnest, least likely to be myelinated, and mature the latest (Aboitiz & Montiel, 2003). Lateralization also tends to develop over time, suggesting an interaction between delay variability and lateralization. Finally, there is evidence that the development of lateralization interacts with the development of the corpus callosum. Callosal fibers are some of the longest connections in the brain (Lewis et al., 2009), and therefore would be some of the most unreliable fibers during development.

Therefore, I suggest that early in development the hemispheres should be rela-

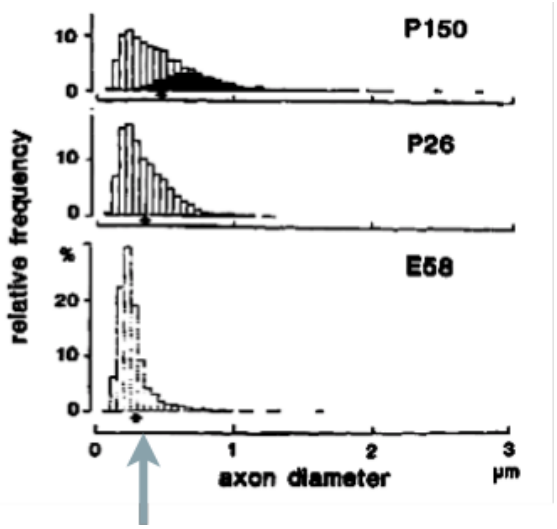

Figure 5.3: Pre-natal (E58: post-conception day 58) and post-natal (P26 and P150: post-birth days 25 and 150, respectively) axon diameter distributions in the developing cat corpus callosum (Berbel & Innocenti, 1988). Unmyelinated fibers are indicated by white bars, myelinated fibers indicated by black bars. Note the increasing mean axon diameter and percentage of fibers myelinated with age. Arrow indicates 0.3μm, approximately corresponding to 0.5μm before tissue processing for imaging, the width at which axon.

tively independent, due to greater delay variability on long interhemispheric fibers as compared to more local intrahemispheric circuits. As delay variability decreases with maturation, interhemispheric collaboration should increase. Finally, these changes should interact with the development of lateralization. I test these hypotheses over a set of four experiments. In Experiments 1 and 2, I test whether delay variability can cause a bias for more local circuits and greater hemispheric independence. In Experiment 3, I test whether decreases in delay variability increases the contribution made by long-distance connections. Finally, in Experiment 4, I explore how delay variability interacts with lateralization.

5.3 Experiment 1: Timing variability biases learning towards local circuits

This experiment aims to test the hypothesis that timing variability is detrimental to interhemispheric communication, and that such variability biases learning towards use of more local circuits.

5.3.1 Methods

Note that code for all experiments, with instructions for reproducing the published results and figures, is freely available online[4].

Model Setup

I implement a version of Lewis and Elman (2008)'s recurrent neural network model (Figure 5.1b), itself a modified version of Ringo et al. (1994)'s neural network model (Figure 5.1a). The network runs for a fixed number of time-steps (30 in this experiment[5]), with an input presented for the first 6 time-steps and an output measured at the last time-step. All connections carry a delay; in all simulations cited and implemented, intrahemispheric delays are set to 1 time-step (interhemispheric delays vary by simulation). Each hemisphere consists of 5 input units, fully connected to 15 hidden units. Similar to Ringo et al. (1994) and Lewis and Elman (2008), all units are rate-coded leaky-integrator units[6]. The hidden units have full recurrent self-connections, as well as

[4] https://github.com/bcipolli/NoisyCC

[5] As shown in Figure 5.2, results do not vary with total network run-time as long as the network has sufficient total time for interhemispheric communication to occur. Further data containing variation in total network run-time are are collected in Experiment 2.

[6] This is a plausible framework for studying interhemispheric interactions: asymmetries are linked to higher-order cortical areas (Sergent, 1982; Gazzaniga, 2000; Schenker, Sherwood, Hof, & Semendeferi, 2007) which tend to interconnect over the corpus callosum using slow fibers (Aboitiz & Montiel, 2003) that are suggested to use rate-coding, rather than spike-time coding employed by thicker, faster fibers (S. S. H. Wang, 2008).

full feed-forward connections to 5 output units. 3 hidden units from each hemisphere connect fully and reciprocally to each other as a model "corpus callosum"; these were the only shared connections between the hemispheres[7]. For all simulations, only these interhemispheric connections are manipulated.

I operationalize variability in conduction delays as Gaussian noise of the activity (instantaneous firing rate) transmitted over fixed (reliable) delays. Noise is computed on a per-synapse, per time-step basis. The amount of noise is determined by the total delay on that connection (as variability in spike time is a function of connection length (Faisal et al., 2008; S. S. H. Wang, 2008)) and the current activation value (as more spikes will lead to more variability in a rate code): $noise = \eta * [delay\ magnitude] * [current\ activation]$ where η is a constant that allows the average noise level to be manipulated. I chose this operationalization because in a rate-coding system, variation in the arrival of individual spikes (or a missing spike) leads to noise in the instantaneous firing rate.

Model Training

As in previous studies, the task for the network is to learn associations between input binary strings and output binary strings. As in Lewis and Elman (2008), the training dataset contains both intrahemispheric patterns (where one hemisphere could determine its output without receiving any information from the other; 50% of the input patterns) and interhemispheric patterns (where one hemisphere must receive information from the other hemisphere to choose between 4 possible binary output strings; 50% of the input patterns). This allows a more careful analysis about how interhemispheric communication is affected by variability. It is worth noting that there are 5 output values per interhemispheric pattern, and while some output values of each pattern are ambiguous as specified, some of the output values of interhemispheric patterns are still predictable.

[7]Lewis and Elman (2008) used 10 hidden units and 2 inter-hemispheric units; increasing these numbers facilitates task learning. Select simulations run with the original parameters showed similar effects.

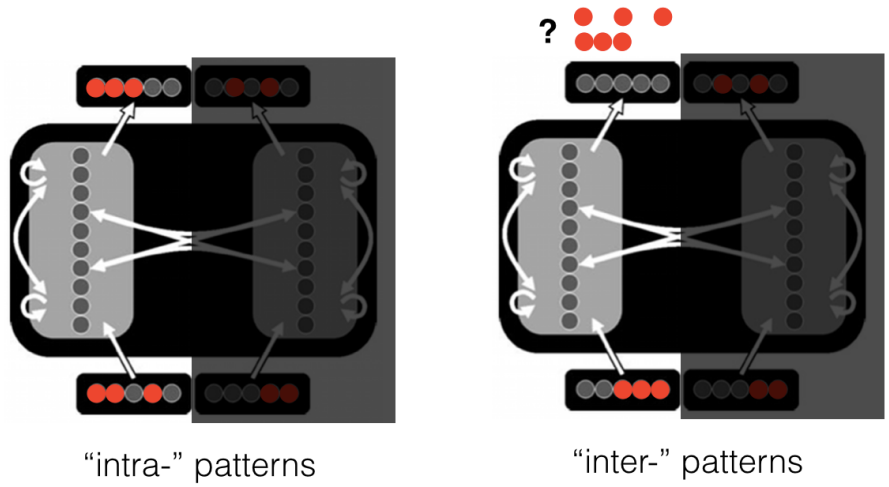

Figure 5.4: "Intra" patterns can be processed intrahemispherically, without any information from the other model hemisphere. "Inter" patterns contain output values that require information from the other hemisphere to be correctly output.

The model uses a version of backpropagation through time appropriate for learning with conduction delays (Pearlmutter, 1989) for calculating the error gradients and uses resilient backpropagation for computing gradient updates (Riedmiller & Braun, 1993). Error is reported using the sum-squared error function, but the error gradients are computed using an error function that led to more robust training [8]. The networks are trained until they have zero classification error or until 1000 training epochs have elapsed.

Learning in the networks with published learning rates is slow and the degree of interhemispheric communication is dependent on parameters that were not varied in either study (such as the exponential decay parameter of the leaky integrator units). Parameters are chosen here to optimize learning speed while balancing between intra-

[8] As in (Chapter 3), I use a gradient ($(y-t)^3$) that more severely penalizes local minima where a few patterns are learned very poorly so that the majority of the patterns are learned more quickly. Though this does not change the qualitative results of any of the experiments, this made the learning trajectories more robust and helped networks achieve 100% performance more reliably.

and interhemispheric dependencies[9]; for example, these parameters control how quickly the leaky integrator units respond to activation (rise time); a slower rise time can lead to less of an effect of conduction delay differences. The purpose of this study is to examine whether changes in intra- and interhemispheric processing occur across experimental conditions, rather than trying to precisely quantify such changes, so this method to choose parameters seemed a reasonable one for this study.

Measuring performance

Two performance measurements are computed. Classification error is the percentage of output nodes that are not within 0.5 of their expected output value ($+1$ or -1) and was the performance criterion used by Ringo et al. (1994). Training error is the average (sum-squared) error at each output node and provides a more nuanced measure of network performance.

In order to test the degree of interhemispheric interactions in a network, interhemispheric connections are temporarily lesioned and network performance is measured. The difference between intact and lesioned network performance is called the "lesion-induced error" (Lewis & Elman, 2008) and represents the degree of interaction between the networks. Higher lesion-induced errors indicate more dependence on the interhemispheric connections and therefore greater interhemispheric interactions.

Experimental Setup

25 "no-noise" networks (without any noise introduced on interhemispheric connections) are trained and performance assessed every 100 epochs, to establish baseline measures. The same procedure is used for 25 "noise" networks, which are identical to the 25 "no-noise" networks in their architecture, training procedure, and even their random

[9]Parameters: $leakyintegratortimeconstant T = 2, momentum \alpha = 10^{-3}, resilienceterm \kappa = 10^{-2}$

initial weights, except for having random Gaussian noise (1% of average unit activity) injected on the interhemispheric connections.

Introducing Gaussian noise makes interhemispheric information, with longer conduction delays and therefore more noise, to be less reliable than intrahemispheric information. I expected this to cause learning of intrahemispheric patterns to use less interhemispheric information, and learning of interhemispheric patterns to be delayed. Therefore, I predicted (1) that the learning trajectory of the noise network would be more gradual (i.e. have a smaller slope) and (2) that lesion-induced error would be lower in the no-noise vs. noise networks.

5.3.2 Results

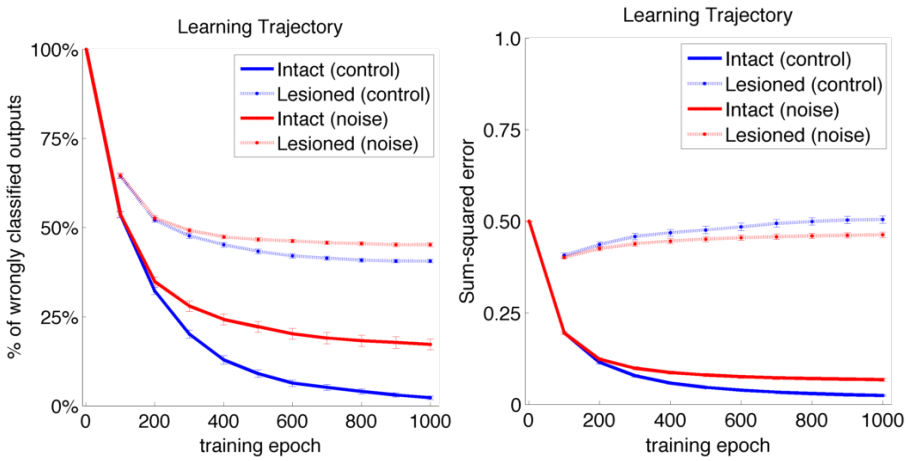

Figure 5.5: Changes in (a) classification error and (b) sum-squared error (SSE), measured every 100 epochs during training, for no-noise (blue) and noise (red) networks. "Intact" lines (solid) show average network performance with interhemispheric connections intact; "Lesioned" lines (dashed) show average network performance with interhemispheric connections temporarily removed. Error bars show the standard error of the mean.

Figure 5.5a shows performance for no-noise and noise networks on both intact and lesion conditions. Overall, the noise and no-noise networks were able to learn the

task and show a large loss in performance when interhemispheric connections removed. These networks show much less variability across different random initializations than the networks shown by Ringo et al. (1994) (see Figure 5.2a), despite fewer network instances being evaluated here (25 vs. 50 in Ringo et al. (1994)). The no-noise networks classified $> 99\%$ of outputs correctly while the noise network classified 83% of the output patterns correctly. Though this seems a large discrepancy, examining the sum-squared error (SSE) it becomes clear that the noise network performance is much closer to the no-noise network performance. Because SSE is a more nuanced measure of error, it is used for the rest of the analyses.

Figure 5.6 shows performance for no-noise and noise networks separated by pattern classification type (intra- and interhemispheric patterns). A main effect of noise is found: noise affects the learning of all patterns, even patterns that do not require the use of interhemispheric information. However, there was an interaction of noise and pattern type. Intrahemispheric patterns show almost ceiling performance on learning and very little lesion-induced errors, indicating that the network has learned to suppress interhemispheric activity and solve the mapping intrahemispherically. Examining the lesion-induced error (Figure 5.6, second row), the no-noise and noise networks were significantly different starting at epoch 600 (t-test, $p < 0.05$ for epochs 600 - 1000). The interhemispheric patterns, on the other hand, show a much stronger effect. The patterns are learned to a sub-ceiling asymptote. That asymptote is reflected equally in the lesioned network, where reduced error after lesioning indicates that the noise is suppressing interhemispheric coordination. These effects started earlier during learning and were much stronger than for the intrahemispheric patterns (t-test; $p < 0.01$ at epoch 300, $p < 0.001$ for epochs 400 - 1000).

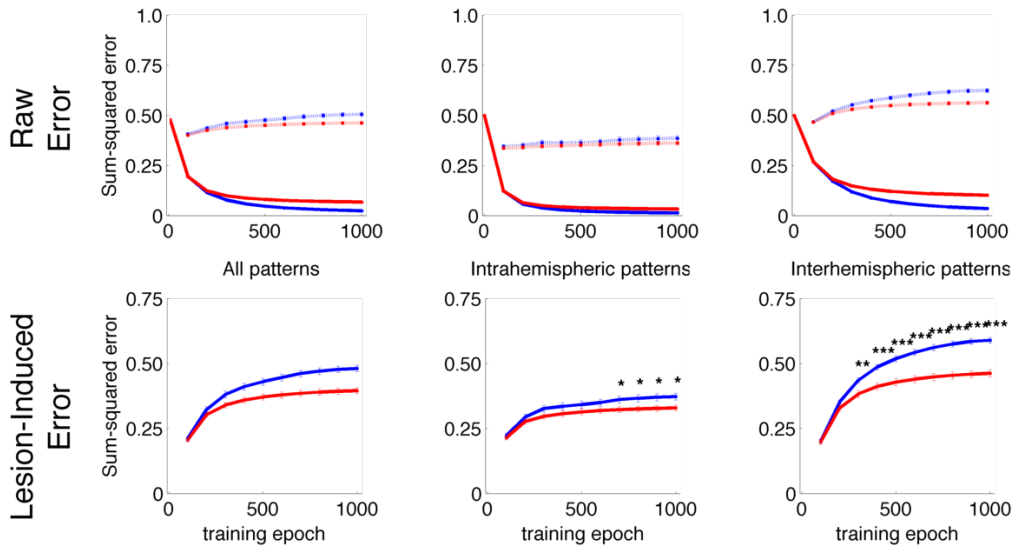

Figure 5.6: Changes in sum-squared error, measured every 100 epochs. Raw error (row 1) and lesion-induced error (row 2) for no-noise (blue) and noise (red) networks. Column 1 is for all patterns, column 2 for "intra" patterns (those that can be solved without interhemispheric information), and column 3 for "inter" patterns (those that require interhemispheric information to be solved correctly). Stars in lesion-induced error indicate significant differences between no-noise and noise networks, (* means $p < 0.05$, ** means $p < 10^{-2}$, *** means $p < 10^{-3}$). Note that lesion-induced error is the difference between curves of the same color from row 1.

5.3.3 Discussion

Noise, with strength proportional to the delay of the connection, biased the model to favor intrahemispheric connections at a shorter delay and led the model hemispheres to work more independently. Patterns that did not require interhemispheric communication were learned almost as well in no-noise vsṅoise conditions, with networks containing noise showing less lesion-induced error. A similar, but much stronger pattern was shown for patterns that did require interhemispheric communication, with noise networks showing a much smaller lesion-induced error than no-noise networks.

These findings are consistent with the hypothesis that timing variability is detrimental to learning and therefore biases networks to use connections with less variability. In the biological system, since timing variability is hypothesized to be present early in

development and timing variability is a function of axon length, this would bias circuits early in development to using more local, short-range connections.

5.4 Experiment 2: Delay variability and magnitude have differential effects on interhemispheric collaboration

This experiment aims to test the hypothesis that timing variability and delay magnitude, while both functions of axon length, have separable effects on interhemispheric coordination. Specifically, I expect delay magnitude to affect the onset of interhemispheric collaboration (as discussed in Section 5.2.1) and timing variability to affect the degree of interhemispheric collaboration. In addition, this experiment aims to compare these networks directly to the networks of Ringo et al. (1994) by varying the total network run-time, the delay magnitude of interhemispheric connections, compiling results similarly to Figure 5.2a, and performing the same analysis done in Section 5.2.1.

Before running this experiment, I generally predict that networks without noise would replicate the finding that delay magnitude causes only a delay to the onset of interhemispheric collaboration. This would be tested by showing that shifting the two curves to the difference in onset of interhemispheric collaboration shows no significant difference between the curves. I predicted that for the no-noise network, an onset delay should be present for intrahemispheric patterns (consistent with the results from Ringo et al. (1994)) and interhemispheric patterns (which require interhemispheric communication and therefore are necessarily delayed). An addition effect of noise should be seen for interhemispheric patterns, showing as a significant difference in the curves even after the shift to compensate for onset differences. This noise effect should be smaller or not present for the intrahemispheric patterns in the no-noise network.

5.4.1 Methods

In Experiment 1, the interhemispheric delay is fixed to the "long" delay from Ringo et al. (1994) (10 time-steps) and total run-time is not varied (30 time-steps). In Ringo et al. (1994), interhemispheric delays of 1 vs. 10 time-steps were compared, and total run-time was varied from 15 to 75 time-steps. These results are then compiled into the same form as Figure 5.2, for comparison purposes.

In this experiment, interhemispheric delays of 2 vs. 10 time-steps are compared, and total run-time is varied from 15 to 75 time-steps. Because noise is a function of delay, this allows testing effects due to differences in delay (for comparison to (Ringo et al., 1994)) and noise together.

5.4.2 Results

Figure 5.7 shows results for no-noise and noise networks, delay=2 vs. delay=10, with curves separated into intra- and interhemispheric patterns.

As expected, for no-noise networks (Figure 5.7, rows 2 and 3), the shifted curves show complete overlap, indicating that differences in delay magnitude only introduce an onset delay. Also as expected, the noise networks show different patterns for intra- and interhemispheric patterns. The shifted curve for the intrahemispheric patterns show the same overlap as above, with no significant effect of noise found. The interhemispheric patterns show a significant difference between the shifted curves until the point where both curves reach floor performance.

5.4.3 Discussion

Results indicate that the hemispheric independence caused by noise cannot be accounted for through a simple onset-delay mechanism. Delay magnitude leads to

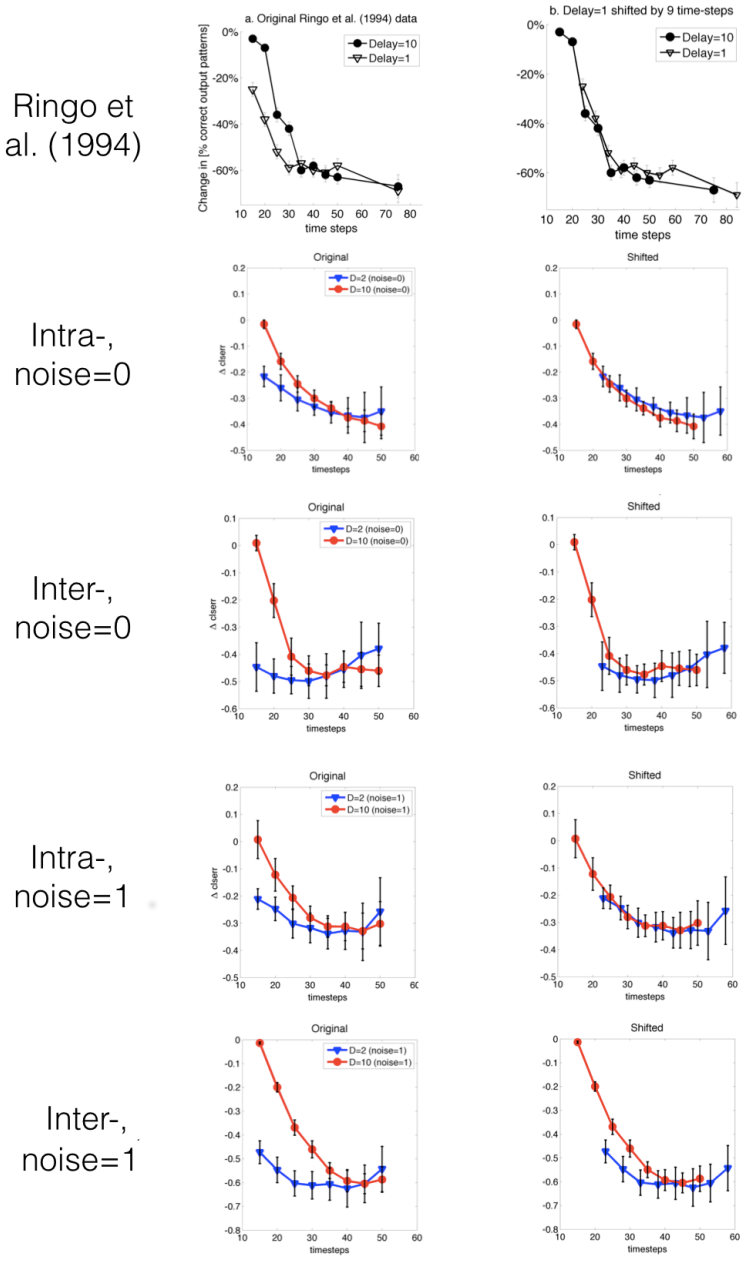

Figure 5.7: Reporting results for comparison to Ringo et al. (1994), separately for no-noise and noise networks and "intra" vs. "inter" patterns. "Intra" patterns do not require interhemispheric collaboration for a hemisphere to select the correct output for a given input; "inter" patterns are four-way ambiguous without receiving information from the other hemisphere. Error bars indicate standard deviation, not standard error of the mean as in Figure 5.6.

delayed collaboration (as in Ringo et al. (1994)), and in addition noise causes reduced collaboration (as seen in 5.6).

More generally, these results suggest that when timing variability is a concern, learning will be biased towards using shorter connections as they have shorter delays and therefore less delay-dependent variability. This should apply to both intra- and interhemispheric connections. However, since interhemispheric connections are on average longer, this should also show as an overall bias towards intrahemispheric connectivity.

5.5 Experiment 3: Reduction of timing variability in maturing brains leads to greater long-distance coordination

Experiments 1 and 2 show that conduction delay variability, implemented as instantaneous noise in the firing rate proportional to the delay of the connection, leads to a bias for connections with a shorter delay (and therefore less noise). In the developing brain, this would manifest as a bias towards shorter connections as delay is proportional to connection length.

As discussed in Section 5.2.2, I hypothesize that delay reliability should be high at birth but continually improve over development. The goal of this Experiment is to examine whether reduction of variability over time will lead to networks reducing their bias towards connections with shorter delays and incorporating more interhemispheric information. In human development, circuits gradually shift away from their initial local bias. I therefore hypothesize that in the neural network model, improving delay reliability during training will lead to greater interhemispheric interactions as measured by greater lesion-induced error.

5.5.1 Methods

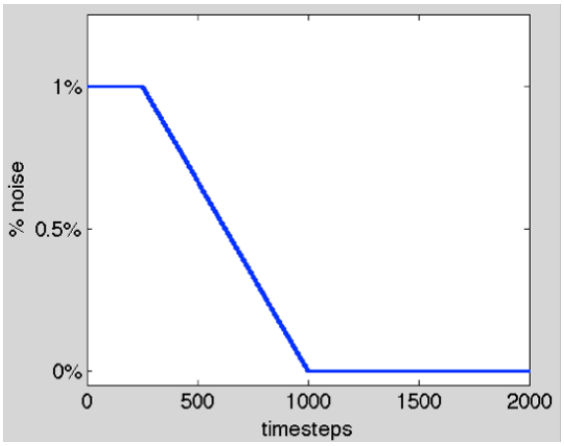

Figure 5.8: Graphical representation of changes to the relative noise level (compared to overall activation) over training, to simulate reduced conduction delay variability over developmental thickening and myelination of white matter fibers.

No-noise and noise networks are trained and tested according to the methods of Experiment 1. The networks are trained for 2000 epochs instead of 1000 to allow sufficient training time to examine the effect of dynamically manipulating noise in the networks. In Experiments 1 and 2, the noise networks are given constant noise over all training epochs. In this experiment, the noise changes over time (see Figure 5.8). Noise is held constant at 1% for the first 250 epochs (early development), then linearly reduced for 750 epochs until it hits 0% (later development). Finally, the network is trained with no noise for 1000 epochs (maturation).

As usual, lesion-induced error is measured for intra- and interhemispheric patterns separately.

5.5.2 Results

The no-noise network showed the same pattern as in Experiment 1: lesion-induced error increases during training until the network learned the task, indicating

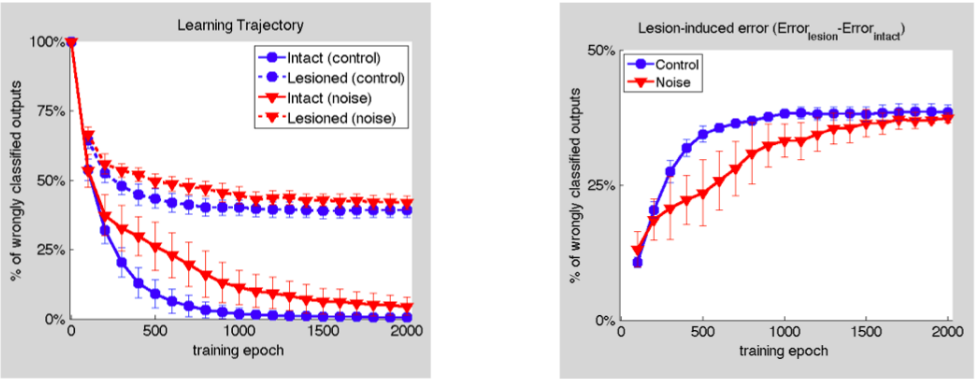

Figure 5.9: (a) Training error and (b) lesion-induced error for no-noise and noise networks. The noise network showed increases in lesion-induced error in all stages, but different rates across the three stages in learning, corresponding to the three stages in Figure 5.8: a period of quickly increasing lesion-induced error (epochs 1-250), a period of moderately increasing lesion-induced error (epochs 251-1000), and a period of reducing lesion-induced error (epochs 1001-2000).

robust interhemispheric transfer. While noise is on, the noise network has a smaller slope to approach convergence (Figure 5.9a, solid red line) than the no-noise network had at its earliest learning stages. Once the noise is turned off, the noise network slowly converges to performance (Figure 5.9a, solid red line) and interhemispheric collaboration (Figure 5.9b, solid red line) as the no-noise network.

Dividing the results up into intra- and interhemispheric patterns show the same pattern as in Experiment 1: both intra- and interhemispheric patterns are affected by noise, but the intrahemispheric patterns are less severely affected and converge to the no-noise network performance faster.

5.5.3 Discussion

These results indicate that variability during learning does not permanently bias networks to use less variable, local connections. Instead, as variability decreases the network uses more of the increasingly reliable interhemispheric information. When vari-

ability reduces to zero, the network continues to increase its use of the interhemispheric information until it matches the network trained without any noise.

More generally, these results suggest that learning is biased towards using local circuits early in development, but that as variability decreases due to increasing axon diameter size and myelination, adult-like circuits that incorporate long-distance intra- and interhemispheric integration may emerge.

5.6 Experiment 4: Lateralization and interhemispheric coordination are intertwined

In their paper, Ringo et al. (1994) did not test for a relationship between interhemispheric communication and lateralization, but instead assumed one. A general examination of lateralization and interhemispheric interactions was done by Reggia and Schulz (2002). Lateralization was assessed by examining performance of one hemisphere with the other disabled, much the same as the Ringo model with the interhemispheric connections lesioned. Lateralization was induced by varying network parameters between the left and right networks (overall activation level, number of units, etc.), then differences in performance level between the networks was measured. Under these conditions, lateralization occurred most strongly when interhemispheric connections were inhibitory.

The aim of Experiment 4 is to propose measures of lateralization in these networks, then to examine whether lateralization emerges spontaneously or when I attempt to induce it.

5.6.1 Methods

In order to measure lateralization in representations between the networks, I use an algorithm from Laakso and Cottrell (2000) that is similar to representational similarity analysis (RSA) (Kriegeskorte, Mur, & Bandettini, 2008). In this algorithm, how similar a model represents two stimuli is computed for all stimulus pairs presented to the model. Then this set of similarities are then used to compare across models; two models that regularly judge the same two stimuli as similar will be judged as models with similar representations. The mathematics behind the algorithm are simple: the similarity between the internal representations a single model has for two stimuli is computed as the euclidean distance between the hidden unit activations, while the similarity between two models is computed as the correlation between each model's vector of pairwise similarities across all stimuli.

In addition to applying this measure to the models from Experiment 1, I also want to examine how the no-noise and noise networks would perform when the two hemispheres are asymmetric. Rather than changing the computational properties of the model to test this (as done in Reggia and Schulz (2002)), I preferred to use the same model as before, but simply induce asymmetry by presenting symmetric or asymmetric inputs, and training on symmetric or asymmetric outputs. I view this as no different than receiving asymmetric visual inputs, producing asymmetric hand movements for outputs, or even receiving inputs from a brain region that is itself lateralized. Changes in behavior of the model between the different stimulus and output conditions can be attributed to the interaction between variations in the interhemispheric variability and the stimulus conditions.

In order to accomplish this, binary string stimuli are randomly generated. When an input or output needs to be symmetric, one of the random binary strings is discarded and the other is copied. Note that in conditions with symmetric outputs, one hemisphere

could always predict the output of the other (because the outputs are the same), so no interhemispheric patterns were available for analysis in those conditions. In conditions with asymmetric outputs, patterns could still be separated into intra- and interhemispheric patterns, as the predictability of the output could still be modulated.

5.6.2 Results

Representational similarity between hemispheres

I computed the similarity between left and right hemisphere models in a 2 x 2 design: for no-noise and noise models, and with interhemispheric connections intact and lesioned. As shown in Table 5.1, there is an expected main effect of intact vs. lesioned networks. When networks are intact, there is some level of similarity between their representations; when the interhemispheric connections are lesioned, all similarity between the networks is lost. Otherwise, there was no effect of no-noise vs. noise and no interaction between noise level and interhemispheric connection status.

Table 5.1: Representational similarity for left and right hemisphere networks.

	No-noise	Noise
Intact	0.38 ± 0.12	0.36 ± 0.13
Lesion	-0.03 ± 0.01	-0.03 ± 0.01

Comparison of input and output asymmetries

For input and output asymmetries, patterns between no-noise and noise networks followed those reported in Experiment 1. There were, however, some interesting results that came out of comparisons of error patterns between different symmetry / asymmetry combinations. None of these results were predicted in this exploratory data analysis.

Few results popped out as particularly salient. Most plots showed a simple

difference average correct for both intact and lesioned networks, and so showed no differences in lesion-induced error. I describe one difference as an example of what types of data were found.

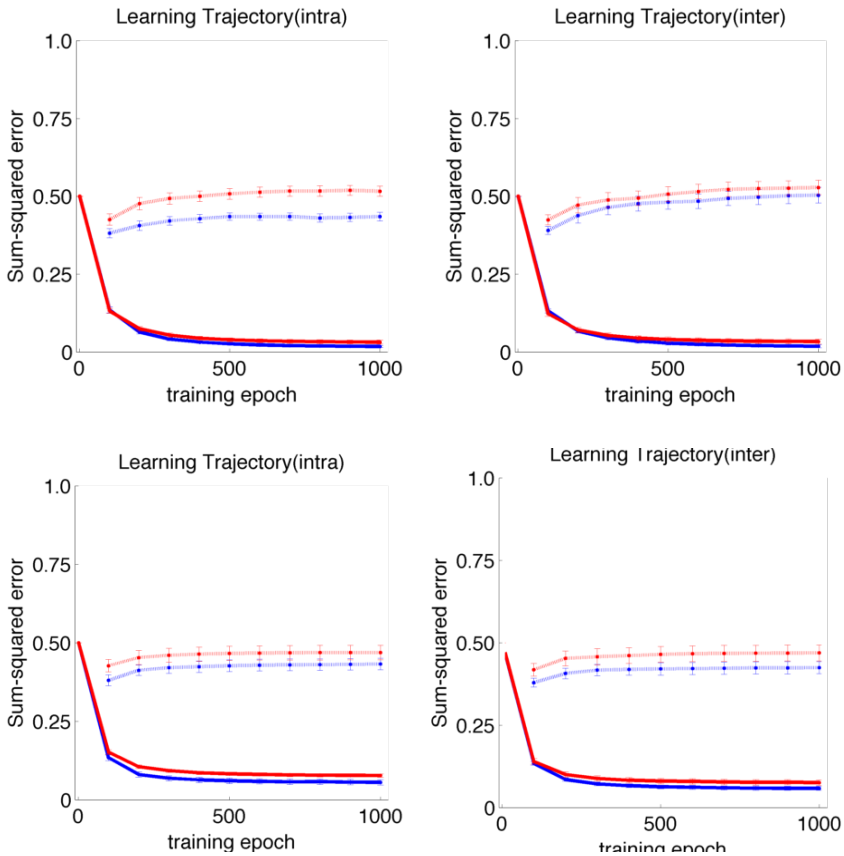

Figure 5.10: Asymmetric (blue) vs. symmetric (red) inputs, with asymmetric outputs.

Asymmetric inputs led to less interhemispheric collaboration Figure 5.10 varies inputs between symmetry and asymmetry and examines the effect of lesion and noise. For no-noise networks (top row), symmetric inputs (red) had greater hemispheric interactions for intra- vs. inter- patterns, but asymmetric inputs (blue) remained at the lower level of hemispheric interactions for both inter- and intra- patterns. With noise (bottom row), the difference in symmetric inputs between intra- and interhemispheric patterns vanished.

5.6.3 Discussion

This exploration is aimed at taking first steps to examine relationships between modulations of interhemispheric communication and the development of lateralization. I found that no spontaneous lateralization was present when computing similarity between model hemispheres, both for no-noise and noise networks. Similarity did not differ between the hemispheres in no-noise vs. noise conditions. Finally, networks with asymmetric inputs and/or outputs did not show any clear pattern of lateralization and also did not show changes in similarity as interhemispheric communication was modulated.

5.7 General Discussion

In this chapter I reviewed literature showing that interhemispheric integration is robust in humans, that there's no indication of a causal link between long conduction delays and hemispheric independence, and no evidence of a causal link between hemispheric independence and lateralization. Instead, I argued that independence could be caused by variability in conduction delays. I failed to characterize any relationship between independence and lateralization in either condition of variability or not. I also pointed out that the variability in conduction delay is likely to exist in neonates, when large numbers of thin, unmyelinated white matter fibers are prevalent and of a diameter that would exhibit variability in conduction delay.

Why is conduction delay an intuitively appealing answer? It is worth noting that conduction delay and variability are both functions of axon length and diameter, and are correlated for thin unmyelinated axons. Thin, unmyelinated axons have a special physiology as well as a special functional role in the brain, leading to correlations across a number of quantities: delay magnitude, delay reliability, energy consumption

(S. S. H. Wang, 2008), connectivity pattern (Markov et al., 2013) and volume (Zhang & Sejnowski, 2000). While each of these may play a role in overall brain architecture and physiology, it is unlikely that all play a causative role in all aspects of brain architecture and physiology. I have argued in this chapter that it is time to let go of the correlation between delay magnitude and degree of connectivity and interaction.

Is human lateralization special? There are indications that human development is unique (R. D. Martin, 1983), and the degree to which humans are functionally lateralized at the population-level for functions that are critical to our daily lives is also unique. While previous work tried to associate lateralization with brain size through this hypothesis of hemispheric independence, I've shown here that this is unlikely to be the case.

I speculate that while conduction delay variability may be an issue for all mammals, it is particularly important for humans. If true, I speculate this is due to a dual constraint in humans: the necessity to minimize head volume at birth while maximizing neural resources in adulthood, under conditions of efficient well-connectedness and no post-natal neurogenesis nor white matter fiber production. White matter volume tends to dominate in larger brained species, due to the fact that white matter volume grows exponentially faster than brain volume itself (Zhang & Sejnowski, 2000). White matter volume is also extremely plastic post-natally, as both axon diameters and the degree of myelination change drastically over development (Berbel & Innocenti, 1988; LaMantia & Rakic, 1990b) and through adulthood and aging (Aboitiz, 1991; Jernigan, Baar, Stiles, & Madsen, 2011; Riise & Pakkenberg, 2011; Hou & Pakkenberg, 2012). Therefore, we believe that white matter volume is highly compressed at birth particularly in humans and rapidly expands during the period of post-natal pruning.

Unfortunately, the only human fetal and neonate callosal samples are from a light microscope (Luttenberg, 1965), where it is clear that most fibers have been missed

due to low image resolution. Luttenberg (1965) reports 125 million callosal fibers at birth, almost half of what our best estimates of human adult fiber count is, and at odds with animal data showing that neonates have around 3x more callosal fibers than mature adults. It is in principle possible to estimate the human neonate axon diameters from human data; my attempt to do so required one final parameter from Luttenberg (1965) that unfortunately was not reported: the degree of tissue shrinkage during tissue fixation for slicing and mounting.

Future Directions In this paper I was unable to establish a developmental link between interhemispheric communication and lateralization. I note a few recent papers on the benefits of noise in learning (Ermentrout, Galan, & Urban, 2008; Faisal et al., 2008; Vincent, Larochelle, Lajoie, Bengio, & Manzagol, 2010). I intend to investigate whether initially noisy interhemispheric interactions facilitate both generalization and specialization of the hemispheres. It seems computationally advantageous to share processing of highly salient features, as it may allow each hemisphere to select secondary features that it can be more specialized to process.

5.8 Acknowledgments

Author contributions: I conceived of, implemented, and analyzed all computational simulations and analyses. Garrison Cottrell advised on the project and provided feedback on a much earlier version of this manuscript.

This work was partly funded by a Center for Academic Research and Training in Anthropogeny (CARTA) fellowship, as well as by NSF grant SMA 1041755 to the Temporal Dynamics of Learning Center, an NSF Science of Learning Center

Chapter 6

Interhemispheric connectivity endures across species: an allometric exposé on the corpus callosum.

6.1 Abstract

Are human brains lateralized because they are large? Rilling and Insel (1999a) argued that in primates, interhemispheric connectivity is selectively reduced as a function of brain size, leading to reduced functional connectivity in larger brains. They compared callosal mid-sagittal area and grey matter surface area to estimate connectivity, which ignores cross-species scaling effects for callosal fiber density and grey matter neuron density.

To address the issue, I first computed an allometric regression of callosal fiber density. Using small-brained animal data from S. S. H. Wang et al. (2008), I find callosal fiber density scales as the -0.28 power of brain size. To validate the regression values for human data, I examine the best available human data (Aboitiz et al., 1992) and note a

confound of sample age. Though an age effect on callosal fiber density is not directly reported in the neuroanatomy literature, I find it in the data (Berbel & Innocenti, 1988; LaMantia & Rakic, 1990a). I use monkey data to estimate a value for the human data LaMantia and Rakic (1990a) at sexual maturity and find that the corrected human data is within 11% of the allometric prediction for humans. I then review literature consistent with the interpretation that humans have thinner fibers than expected for our brain size. I also estimate, based on the age-correction, that the human corpus callosum has 240 million fibers, 20% more fibers than previously estimated based on the age-confounded sample (Aboitiz et al., 1992).

I then used the regression of callosal fiber density, along with others computed from data in the literature, to estimate inter- and intrahemispheric connectivity directly. I find that (1) the proportion of total connectivity that is interhemispheric is much more drastically reduced as a function of brain size than previously reported (allometric exponent 0.64 vs. previously reported 0.88, but that (2) this reduction is not selective for interhemispheric connections: axon counts per fiber tract interconnecting two cortical areas scale similarly for inter- and intrahemispheric connections. This is due to the increasing number of area-area intrahemispheric fiber tracts as brain size increases (Changizi & Shimojo, 2005) compared to the largely homotopic interhemispheric connections. Thus, any claim of a reduced role for interhemispheric connections would also have to claim that, e.g., V1$\rightarrow$V2 is less functionally relevant. On the contrary, I estimate the average interhemispheric area-area connection contains about 4x more fibers than the average intrahemispheric one, despite on average being longer–suggesting a special role for interhemispheric connections that persists over all brain sizes.

The results are inconsistent with the prevailing hypothesis that lateralization is driven by greater hemispheric independence in larger brains (Ringo et al., 1994; Rilling & Insel, 1999a). Instead, these data are consistent with neuroimaging studies and our

computational work (Chapter 5) which suggest that interhemispheric interactions play a role in the development and function of the lateralized human brain. In addition, these results suggest a special role for interhemispheric connectivity that is shared by all primates–regardless of brain size.

6.2 Introduction

Lateralization touches on virtually every function that we think makes us human, including: language, fine motor skills, spatial cognition, and social perception. The prevailing view from the literature is that lateralization in humans is a consequence of greater independence between our cerebral hemispheres, driven by architectural (Rilling & Insel, 1999a) and physiological (Ringo et al., 1994) differences between small brains and large brains.

There are a number of reasons to doubt this hypothesis. When examining the neuroimaging literature, there is evidence of robust coupling between the hemispheres in humans (Stark et al., 2008), with both lateralization and interhemispheric communication increasing over development (e.g. Benninger et al. (1984); Petitto et al. (2012); Musacchia et al. (2013)). We've shown that one major proposed cause of independence and lateralization–longer conduction delays in larger-brained species–likely does not cause either hemispheric independence nor lateralization (Chapter 5). Finally, in other fields such as cellular biology (Gurkan et al., 2007; Graham et al., 2000; Marzec & Kurczynska, 2014; Palmer, 2002), agriculture (Qin & Zhang, 2012; Gollin & Rogerson, 2014), economics (Bolton & Dewatripont, 1994; R. Katz & Tushman, 1979; Tushman, 1978), even in design of cities in online games (*Specializations - SimCity Wiki Guide*, n.d.), and presumably government and other fields: specialization is dependent on robust communication. The reason is shared and simple: specialization increases competency in

one function *at the cost of others*; communication is what mediates sharing of resources between complementary specializations.

In our reading of the literature, one final data point seems to support the hypothesis that humans have greater hemispheric independence and that independence leads to lateralization in brain function. Rilling and Insel (1999a) suggest that interhemispheric connectivity is selectively reduced (when compared to total white matter connectivity) in species with larger brains. They base this on their MRI data analysis, where they find that the proportion of mid-sagittal callosal surface area (as a proxy for interhemispheric connectivity) to the amount of grey matter surface area (as a proxy for neuron count, and therefore total white matter connectivity), decreases as a function of species brain size.

Rather than comparing surface areas, here I turn to the literature for data to estimate numbers of total and interhemispheric white matter fibers from Rilling and Insel (1999a)'s surface area data. I find that the proportion of total fibers that is interhemispheric is drastically reduced with increasing brain size–much more strongly than reported by Rilling and Insel (1999a). However, I find that this apparent proportional decrease is completely explained by the increase in cortical areas with brain size and the homotopic nature of the corpus callosum. More cortical areas means each cortical area will interconnect with a greater number of other areas within a hemisphere, while that same cortical area will largely remain restricted to connecting to the homotopic areas across the corpus callosum. That is, the number of callosal connections between areas remains fixed at one, while the number within a hemisphere is increasing with brain size.

This simple fact of homotopic callosal connectivity versus expanding intrahemispheric connectivity does not represent a proportional decrease in the number of fibers within interhemispheric inter-area connections vs. their intrahemispheric counterparts. This same apparent reduction is not specific to interhemispheric area connections (e.g. left V1 $\rightarrow$ right V1), but holds for intrahemispheric area connections (e.g. left V1 $\rightarrow$

left V2) as well. This changes the interpretation to one consistent with "efficient well-connectedness" (Changizi, 2009) and views that functional connectivity is dynamic and based on task-demands (e.g. Innocenti (2008); Doron, Bassett, and Gazzaniga (2012)). This undermines the interpretation of selective suppression of interhemispheric connectivity in larger brains, and suggests that the functional significance of an inter-area connection cannot be determined from these data.

One critical data point in our computation is a novel allometric regression of callosal axon density, computed from 6 relatively small-brained mammals (S. S. H. Wang et al., 2008), which shows clear decreasing density with increasing brain size. To corroborate our use of these small-brained animal data to extrapolate to human brains, I find limited data (a single human sample) with a mismatched age to the animal sample (Aboitiz et al., 1992). I attempt to correct for this age difference using allometry-based cross-species corrections (Clancy, Finlay, Darlington, & Anand, 2007) and find an excellent match between our human estimate using the cross-species data and the corrected human data. These two independent estimates both suggest that human young adults have approximately 240 million fibers in the corpus callosum, 20% more than reported in previous estimates (Aboitiz et al., 1992), and commonly accepted in the literature.

Previous Results & Inferences

Mammalian brains span over five orders of magnitude in size, but the structure of the smallest brains differs from the structure of the largest. The relative differences in structure are highly predicability as a function of brain size (Jerison, 1982; Clancy et al., 2007; Herculano-Houzel, Collins, Wong, Kaas, & Lent, 2008; Changizi, 2009), often as a power law ($y = A * x^B$, where A and B are constants). These "allometric" functions (functions that relate quantities to brain and body size) often follow power

laws, indicating they are "scale-free"–that a power-law relationship between quantities holds, independent of absolute size. Most microscopic (e.g. the # of synapses per neuron) and macroscopic (e.g. the total white matter volume) measures follow a power-law relationship with brain size (see Figure 6.1). These various allometric scaling functions seem to have interdependencies, suggesting that they derive from more basic principles such as trade-offs between efficient wiring and interconnectedness (Changizi, 2009).

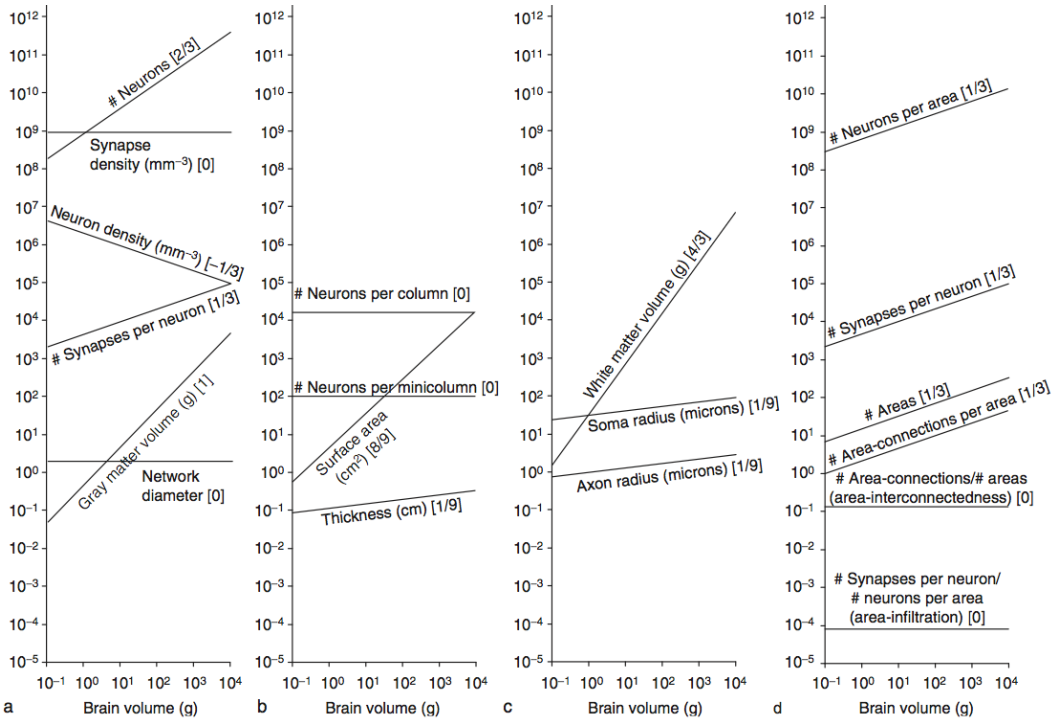

Figure 6.1: Summary of allometric scaling curves across microscopic and macroscopic brain measures in mammals (Changizi, 2009). Note that the exponent in square bracket represents the allometric exponent, which is also the slope of the line.

Rilling and Insel (1999a) imaged 18 species of primates to examine scaling laws within the taxonomic order most relevant to humans, and focused on comparing allometric scaling of interhemispheric and total connectivity. However, they did not measure connectivity directly, and could not estimate it directly from their measurements. Instead, they argued that comparing the ratio between grey matter surface area (GMSA)

and surface area of the corpus callosum at mid-sagittal section (CCA) across species could be used as an estimate of total vs. callosal connectivity. They pointed out that the two quantities match dimensions (area), and each could be roughly used as a proxy for connectivity (GMSA related to the # of neurons and therefore total connectivity, CCA related to the # of callosal axons and so callosal connectivity).

When GMSA and CCA were compared across species, Rilling and Insel (1999a) found that GMSA increases slightly faster than CCA (allometric exponent=0.88). Given the interpretation in terms of connectivity, they concluded that total intrahemispheric connectivity increases faster than total interhemispheric connectivity, suggesting a selective decrease of interhemispheric connectivity with larger brain sizes and therefore likely more independent hemispheres in primates with larger brains–specifically, humans.

My interpretation

I argue that this interpretation is flawed, due to a fundamental difference between callosal and intrahemispheric connectivity in terms of interconnecting cortical areas. Cortex can be parceled into cortical areas by cytoarchitecture (Brodmann, 1909; Bailey & Bonin, 1951; Barbas & Rempel-Clower, 1997), counts and densities of cell types and sizes (Schleicher, Morosan, Amunts, & Zilles, 2009; Uylings et al., 2010), overall cortical thickness (Rimol et al., 2010; Uylings et al., 2010), myeloarchitecture examining intrinsic (local) connectivity patterns (Vogt & Vogt, 1919; Glasser, Goyal, Preuss, Raichle, & Van Essen, 2014), density of receptor types (Zilles & Amunts, 2009) expression, and other computational methods (Schleicher, Amunts, Geyer, Morosan, & Zilles, 1999). Though area size and location does vary based on definition, the cortical area is thought to be a fundamental computational unit in systems neuroscience and is critical for understanding white matter connectivity. White matter connectivity tends to be well-defined between areas (Catani & Thiebaut de Schotten, 2008; Oishi et al., 2008; Hagler et al., 2009;

Markov et al., 2010, 2013) across individuals, traveling in fiber bundles called fascicles.

Evidence suggest that each cortical area in larger brains connects to a greater number of cortical areas (Changizi & Shimojo, 2005), likely due to an increase in the number of cortical areas (Brodmann, 1909; Changizi, 2001; Changizi & Shimojo, 2005; van Essen, Glasser, Dierker, Harwell, & Coalson, 2011) and the need to maintain "efficient well-connectedness" (Changizi, 2009). Callosal connectivity, on the other hand, tends to be homotopic (Aboitiz & Montiel, 2003), which means that for a given cortical area (e.g. V1), interhemispheric connections represent one fiber bundle, irrespective of brain size. Thus, for that given cortical area, there is one interhemispheric inter-area connection (homotopic), while the number of intrahemispheric inter-area connections are increasing with brain size (see Figure 6.2 for a schematic example).

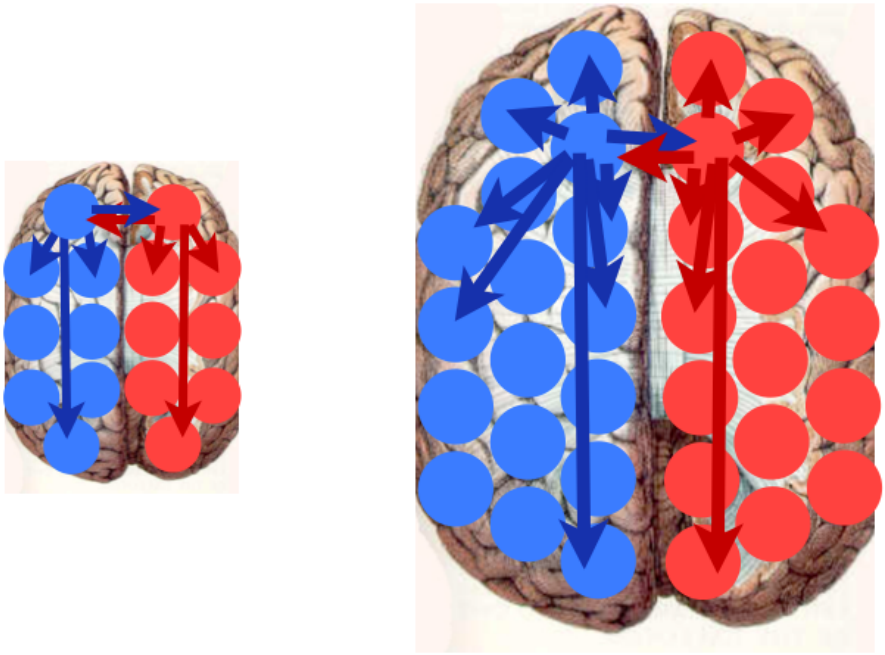

Figure 6.2: Schematic showing fewer cortical areas (8 areas per hemisphere) and inter-area connections (4 per area) in smaller brains and more cortical areas (16 areas per hemisphere) and inter-area connections (8 per area) in the larger brain. Though the number of intrahemispheric inter-area connections changing, a single interhemispheric inter-area connection (to the homotopic area in the other hemisphere) remains across all brain sizes.

This means that for any specific inter-area connection, regardless of whether interhemispheric (left V1 $\rightarrow$ right V1) or intrahemispheric (left V1 $\rightarrow$ left V2), will appear proportionally smaller as brain size increases because the number of inter-area connections a given area (e.g. V1) participates in is increasing. Because of the homotopic nature of the corpus callosum, then, even if the number of fibers within an area's interhemispheric inter-area connection is increasing with brain size at the same rate as fibers in its intrahemispheric inter-area connections, it would appear to be reduced when compared to the total of all intrahemispheric connections. Based on data from Changizi and Shimojo (2005), and consistent with a similar estimate in Changizi (2001), I estimate this apparent reduction rate (as a function of brain volume (BV)) to be $BV^{0.66}$– much smaller than Rilling and Insel (1999a)'s estimate of $BV^{0.88}$.

On this analysis, the exponent of 0.88 actually suggests that the number of fibers in any interhemispheric inter-area connection is actually proportionally increasing by $BV^{0.22}$ ($BV^{0.88}/BV^{0.66}$) compared to the average interhemispheric connection. This is the opposite of the conclusion drawn by the paper; instead of a selective decrease in interhemispheric connectivity with larger brain size, the 0.88 exponent really predicts that callosal connections are becoming relatively stronger than any intrahemispheric inter-area connection in the brain. This would stand as a very surprising result if true.

My Approach

In order to compare fiber counts from the Rilling and Insel (1999a) surface area data, I propose to use the following quantities and simple equations[1] . As detailed in Table 6.1, estimates of many of these quantities exist in the literature. The one quantity without an estimate is $Axon\ Density_{callosum}$. Once these equations are compiled, then an

[1]Note that $Volume_{grey}$ can be measured directly or computed from surface area and thickness. See discussion of this in Section 6.5.1

allometric equation for $\#\,Connections_{callosal}$ vs. $\#\,Connections_{total}$ can be computed.

$$\#\,Connections_{callosal} = [Area_{callosum}] * [Axon\ Density_{callosum}] \tag{6.1}$$

$$\#\,Connections_{white\ matter} = [\#\,Neurons_{total}] * [\%\ Neurons_{project\ to\ white\ matter}] \tag{6.2}$$

$$\#\,Neurons_{total} = [Volume_{grey}] * [Neuron\ Density_{grey}] \tag{6.3}$$

In this paper, I describe four new analysis that contribute to the literature on inter-species scaling of the corpus callosum and how humans fit into that picture. In Analysis 1, I compute an allometric regression for $Axon\ Density_{callosum}$ from a high-quality dataset of small-brained animals (S. S. H. Wang et al., 2008). In order to examine the use of this dataset for larger-brained species such as humans, in Analysis 2 I analyze the human literature on corpus callosum density and compare it to the regression results. After a few new findings regarding the human data, the comparison confirms that the allometric regression is a good fit for the human data. In Analysis 3 I select datasets from the literature to plug into Equations 6.1 - 6.3, examining each in detail. I then plug in values from the literature to directly estimate scaling of interhemispheric and total white matter connectivity, and I find that the scaling exponent is lower than that reported by Rilling and Insel (1999a). In Analysis 4, I examine whether this scaling difference can be accounted for by different scaling patterns of the number of callosal and interhemispheric inter-area connections. I find that they generally can be, and find no relative differences in the scaling fiber counts within inter-area connections. Instead, I find evidence of robust interhemispheric connectivity over brain sizes that on average contain 4x more fibers than the average intrahemispheric connection. Finally, I place these findings into a broader literature on interhemispheric collaboration in humans. I conclude that it is no longer tenable to support the hypothesis of greater hemispheric independence in humans,

and was never tenable to support the hypothesis that hemispheric independence drives lateralization in humans or any other specialized system.

6.3 Analysis 1: Allometric regression of animal callosal axon density

Most research on the corpus callosum has focused on mid-sagittal area of the corpus callosum, looking for correlations between area and brain size, intelligence, asymmetry, handedness, gender, and diseases (see (Gazzaniga, 2000) for a review). Though the corpus callosum is somewhat unique in its highly homogeneous fiber orientation and accessibility, far fewer resources have been put into examining the microstructure of the corpus callosum. These studies have pointed out a true need for electron microscopy, as the corpus callosum contains a large number of thin, unmyelinated fibers (Aboitiz et al., 1992) that are missed without use of electron microscopy. Yet only a handful of such studies exist (Berbel & Innocenti, 1988; LaMantia & Rakic, 1990a; LaMantia & Rakic, 1990b; Kim & Juraska, 1997; S. S. H. Wang et al., 2008); for humans, only one study with one *sample* exists (Aboitiz et al., 1992).

Fortunately, a dataset using electron microscopy (S. S. H. Wang et al., 2008) examined six species, carefully reported tissue processing and imaging procedures, and reported brain sizes, making it potentially usable for allometric regression. Allometric regression can be extremely challenging when combining datasets across labs, particularly for data mounted on slides, as different tissue processing techniques, imaging resolutions, protocols for measuring and counting data, and even measurements of brain size can differ and introduce great variability. Though it only contains six species, in terms of tissue quality and reporting tissue processing and imaging procedures, S. S. H. Wang et al. (2008)'s dataset is the best-case scenario.

Unfortunately, the raw data from this paper is unavailable; this was a common problem across all analyses in this paper. Instead, the data are estimated from digital processing of scatter plots and histograms from the publication. Next I describe the methods I used to "pluck" data comparing callosal density and brain mass from S. S. H. Wang et al. (2008) for all six species.

6.3.1 Methods

Density data are plotted as a function of brain diameter on S. S. H. Wang et al. (2008) Figure 1e, with individual samples and species averages visible for all six species. Average brain weights for the 6 species were published in S. S. H. Wang et al. (2008) Table S1.

In order to "pluck" data from these scatter plots, I follow the following procedure: I download the source paper in PDF form. On a 27" screen (iMac), I zoom into the figure to maximize the limiting dimension (usually vertical), then capture a screen shot (png format) of the image. I use the mouse to manually mark (using different colors) each X-axis (magenta) and Y-axis (yellow) tick-mark, the X-axis (blue) and Y-axis (green) locations, and the centroid of each datapoint. Each datapoint's centroid is determined by counting the number of pixels within the line and finding the arithmetic center; where a unique center pixel does not exist (i.e. when an even number of pixels in the line), I choose the left-most (X-axis) or bottom-most (Y-axis) of the middle two pixels.

In order to read the image and parse out values, I use the MATLAB program (version 7.10.0.499 (R2010a)). All data are available online [2]. I load each png and select the image coordinates of the different classes of marked pixels by color. I average the spacing between measured axis ticks to estimate the number of pixels per tick. I

[2] https://github.com/bcipolli/CallosalScaling/blob/c3e72194cae535acd3b6cbd7ea01f67ad9a10759/data/code/wang_etal_2008/w_data.m

normalize the tick values by the axis zero-point, then I use the tick label values to compute a mapping between pixels and values. I then use the equations for converting pixels to X and Y values to convert data points into estimated X and Y values.

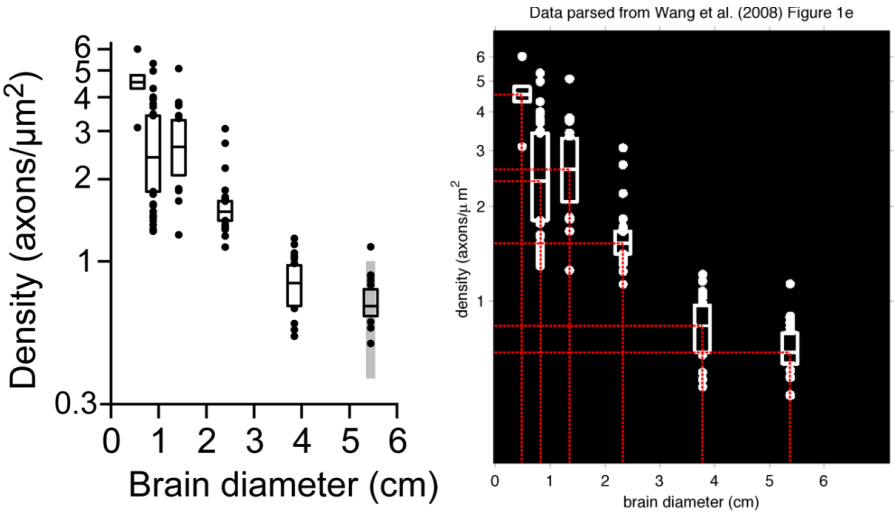

Figure 6.3: (a) Original and (b) manually marked, digitally cropped, parsed, and annotated copy of S. S. H. Wang et al. (2008) Figure 1e, used for extracting callosal density across 6 species.

In other places where I have used this method, I use the "plucked" data to estimate summary statistics or regression coefficients reported in the paper, then compare to the published values (see Section 6.5.1). This allows me to estimate error in the "plucking" procedure, which is generally less than 2%. S. S. H. Wang et al. (2008) did not report any summary statistics for callosal axon density, and so no quantitative estimate could be made. However, a qualitative "goodness-of-fit" estimate could be made by plotting "plucked" pixel values back onto the original image to show whether they match the image; see Figure 6.3 for visual inspection of S. S. H. Wang et al. (2008) Figure 1e parsing.

Once the values were available, I regressed the log_{10} estimates of brain weight and corpus callosum density using reduced major axis regression in MATLAB (Trujillo-Ortiz,

n.d.).

6.3.2 Results

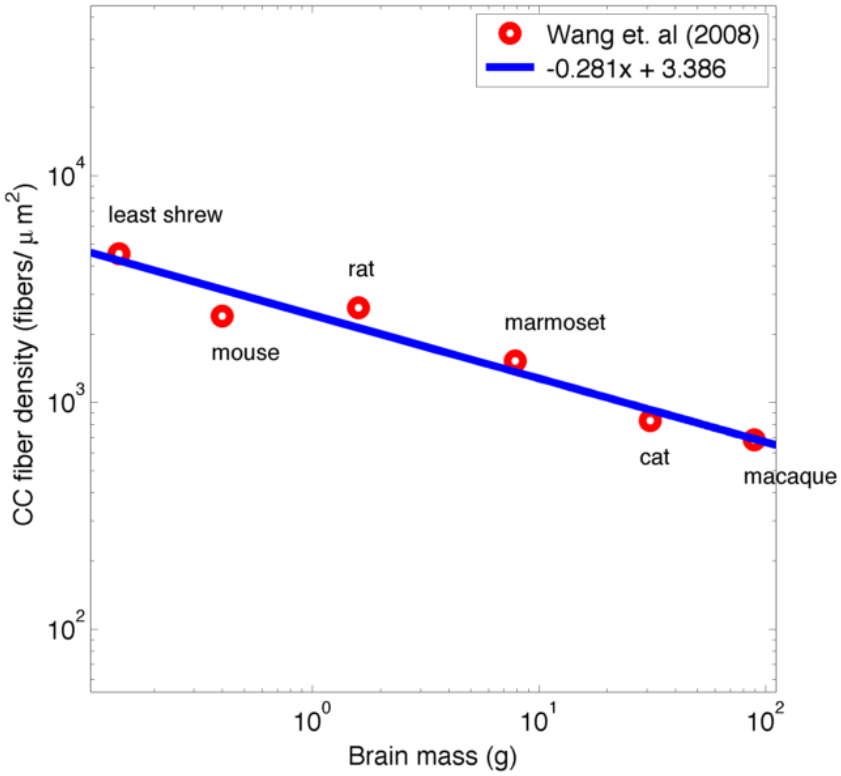

Figure 6.4: Allometric regression of callosal fiber density using data from S. S. H. Wang et al. (2008), on log-log axes. Callosal axon density decreases with brain size, consistent with data showing more myelination and thicker axons in species with larger brains (see text for details). Note the difference in offset parameter here (3.386) from that in Table 6.1 (0.386). Since these are actually exponents, this is a factor of 10^3 that was needed to convert to units of $fibers/mm^2$.

Using data from S. S. H. Wang et al. (2008) to perform an allometric regression, I find that callosal fiber density decreases with an exponent of -0.28 with respect to brain mass ($r^2 = 0.909$; see Figure 6.4).

6.3.3 Discussion

The negative allometry of corpus callosum density is consistent with the overall literature showing greater myelination and thicker axons in species with larger brains (S. S. H. Wang et al., 2008; Caminiti et al., 2009). One potential objection to the methods above is its use of small-brained animals to estimate callosal fiber density. The largest brain used by S. S. H. Wang et al. (2008) is the rhesus macaque monkey brain ($89g$), 15x smaller than the average human brain ($1350g$). Though the regression data span almost three orders of magnitude, it is worthwhile to compare the extrapolation of the regression to human data from the literature.

6.4 Analysis 2: Placing human callosal data in the context of animal data

In order to compare the allometric regression to human data, I searched for human electron microscopic data in the literature. Though a few studies have been published using a light microscope (Tomasch, 1954; Luttenberg, 1965; Aboitiz et al., 1992; Riise & Pakkenberg, 2011; Hou & Pakkenberg, 2012), I only found information about one small human sample that has been imaged using an electron microscope (Aboitiz et al., 1992). In this sample a raw density estimate was not reported; instead, density from a light microscope ($371.7 fibers/\mu m^2$) was reported with an estimate of 20% additional fibers found using electron microscopy. In addition to, there are confounds with the data from S. S. H. Wang et al. (2008) of tissue fixation and sample age. Aboitiz et al. (1992) reported 35% tissue shrinkage (vs. 0% for S. S. H. Wang et al. (2008)) and a sample age of 45 years old (vs. "young adult" samples for S. S. H. Wang et al. (2008)).

Factors to correct for imaging and shrinkage were presented, and so only the

age difference needs to be addressed. Indications from the literature are that an age correction towards a younger age should increase density. Callosal density decreases in early post-natal development (cats: Berbel and Innocenti (1988); macaques: LaMantia and Rakic (1990a)) as fibers are pruned, axon diameters increase, and myelination occurs. Though unreported in the original publications, an analysis of adult data in macaques (LaMantia & Rakic, 1990a) suggests that the decrease in axon density continues beyond sexual maturity (see Figure 6.5a). Thus, a correction for age seems necessary.

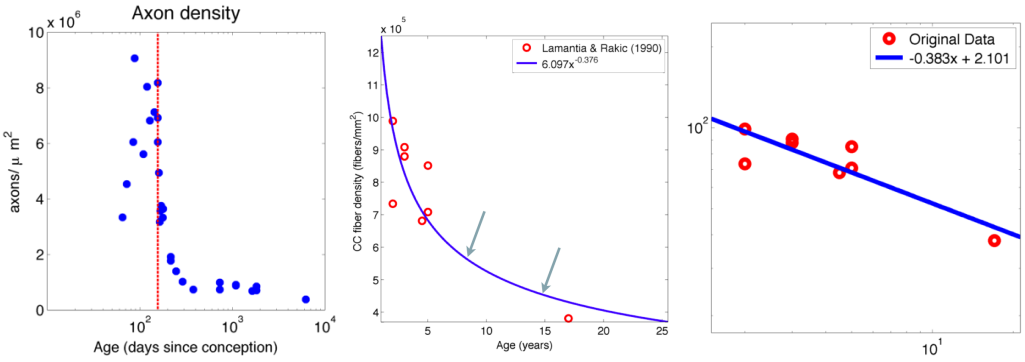

Figure 6.5: Changes in axon density for macaques (a) across their lifespan (red line=birth; no data on the left-most area indicates callosum has not begun developing yet). (b) Same data as in (a), but zoomed into the adult samples, plotted on cartesian axes, and plotted with the computed allometric regression (blue line). The average adult macaque age (left arrow) and the human sample age (45 years old) mapped onto macaque lifespan (right arrow; see text for details) are then added. (c) This log-log plot with the same adult sample and allometric regression shows both the relatively good fit ($r^2 = 0.614$) and how the slope of the line is driven largely by the single datapoint in the lower right corner. See the text for detailed methods. Data from LaMantia and Rakic (1990a); LaMantia and Rakic (1990b).

Allometry has been used much less extensively in development and aging, but validation of the procedure exists. R. D. Martin (1983) investigated how *inter*-species allometric scaling compared with with *intra*-species scaling over the lifespan. He concluded that development can be broken into 3 stages that each obey their own allometric scaling laws: pre-natal development, post-natal development, and adulthood. R. D. Mar-

tin (1983) and Clancy et al. (2007) both suggest that these developmental scaling laws are due to maturational changes tightly correlated with species-specific aging; Clancy et al. (2007) show that these developmental ages can be mapped across species[3].

Before performing the comparison between the human data, I cautiously expected the human data to match or exceed the allometric regression. The caution came from the fact that the human data is only a single sample and differs from the animal data in sample age and tissue processing, which might introduce variability into the result. The expectation of an equal or higher density for the human data than predicted from the regression is based on a number of findings indicating that humans have more small-diameter fibers than would be expected for other species. First, corpus callosum size in humans correlates with small diameter fiber count (Aboitiz et al., 1992), but not in the smaller-brained macaque monkey (Olivares et al., 2001)–indicating a larger proportion of small diameter axons. Second, small diameter fibers are associated with association cortices such as temporal and prefrontal cortices (Aboitiz & Montiel, 2003), and comparative studies suggest that the major areas for human cortical expansion is in association cortices (Rilling, 2014). Finally, Caminiti et al. (2009) compared axon diameter distributions (ADD) between macaque, chimpanzee, and human brains and found that while the chimpanzee ADD compensates for the larger brain size, the human one does not.

6.4.1 Methods

I apply three corrections to the light microscope human data. Aboitiz et al. (1992) reported 20% additional fibers found using electron microscopy over light microscopy. Second, Aboitiz et al. (1992) reported 35% tissue shrinkage. These first two multiplicative

[3] An online tool implements their mappings for many species:
http://bioinformatics.ualr.edu/ttime/translatetime_primates_php.php

corrections were reported and used in the original paper. The third correction is a novel correction for differences across samples due to age.

I use allometric scaling to correct for differences in sample age. Electron microscopic data of the macaque corpus callosum over pre- and post-natal development (LaMantia & Rakic, 1990b) and into adulthood (LaMantia & Rakic, 1990a) seem to be consistent with the division into three developmental stages, with the onset of the third around 1 year of age (see Figure 6.5a). Thus, I attempt to quantitatively account for age differences between the samples by deriving an allometric curve from macaque electron microscopy data, then map humans onto the macaque allometric curve to find a common point of comparison between the two samples, and use the differences in position on the allometric curve to adjust the reported density data for the human sample.

I estimate callosal density changes as a function of age in macaque monkeys by performing an allometric regression between age and callosal density on adult macaque data from LaMantia and Rakic (1990a) (see Figure 6.5c). Macaque "young adult" average age of 5.2 years was obtained from the adult samples from LaMantia and Rakic (1990a). I then followed the methods of Finlay, Darlington, and Nicastro (2001) for cross-species remapping to map the human sample age onto the macaque lifespan, as follows.

First, I obtained values for sexual maturity and average age of death for the two species (macaque: sexual maturity at 4 years old (yo), lifespan 25 yo, human: sexual maturity at 15 yo, lifespan 73 yo (Chudler, n.d.)). Then I found the percentage the human lifespan between sexual maturity and death that 45 years old corresponded to by using the following equation: $pct = (age_{human} - 15)/(73 - 15)$. I then mapped that percentage onto the monkey span using the following equation: $age = 4 + pct * (25 - 4)$. Together, these two equations give:

$$macaque\ age\ estimate_{human\ sample} = 4 + [(25-4) * \frac{age_{human} - 15}{73-15} \qquad (6.4)$$

After having the human age mapped onto the macaque lifespan (see Figure 6.5b) I measured the densities for the average macaque age (representing a "young adult") and human age, then divided the two to get a multiplicative factor to correct the human density for the age difference.

In order to compare the (corrected) human sample to the value predicted by the allometric regression based on S. S. H. Wang et al. (2008), I plug in the human brain weight into the callosum fiber density allometric equation estimated in Analysis 1 ($density = 2.43 * 10^3 * BWT^{0.280}$). An average human brain weight of $1350g$ is used for this comparison (Chudler, n.d.).

6.4.2 Results

Plugging a value of $1350g$ into the allometric equation, I obtain an estimate of $309.1 fibers/\mu m^2$ for the fiber density of the human corpus callosum. Aboitiz et al. (1992) reported an (uncorrected) fiber density in the human corpus callosum of $371.7 fibers/\mu m^2$ (their Table 1); applying their published corrections for imaging technique increases their estimate by a factor of 1.2; correcting for shrinkage reduces their estimate by $1/0.65$. Applying these two corrections gives a value of $288.6 fibers/\mu m^2$, 7% lower than the allometry-based estimate. This is the pre-age-correction baseline difference.

As shown in Figure 6.5c, the regression on age gives an equation $y = 6.1 * x^{-0.386}$. The fit is reasonable ($r^2 = 0.6140$), and the trend is extremely clear (decreasing axon density with age). The curvature for later ages is driven by the single older sample (Figure 6.5b and c), and so quantitative results using this regression should be interpreted with

care. Using the methods above to map human and "young adult" ages onto this curve, I estimate that human age 45 years old corresponds to macaque age of 14.8 years old (see Figure 6.5b). The ratio of callosal density for the "young adult" macaque sample and older human sample gives a value of 1.2, indicating that a younger human sample likely would increase the measured density by about 20%.

When I multiply the shrinkage- and imaging-corrected density ($288.6 fibers/\mu m^2$) by the 1.2 age-correction factor, the corrected human data reported by Aboitiz et al. (1992) ($346.3 fibers/\mu m^2$) is approximately 11.5% greater than the estimate from the regression ($309.1 fibers/\mu m^2$).

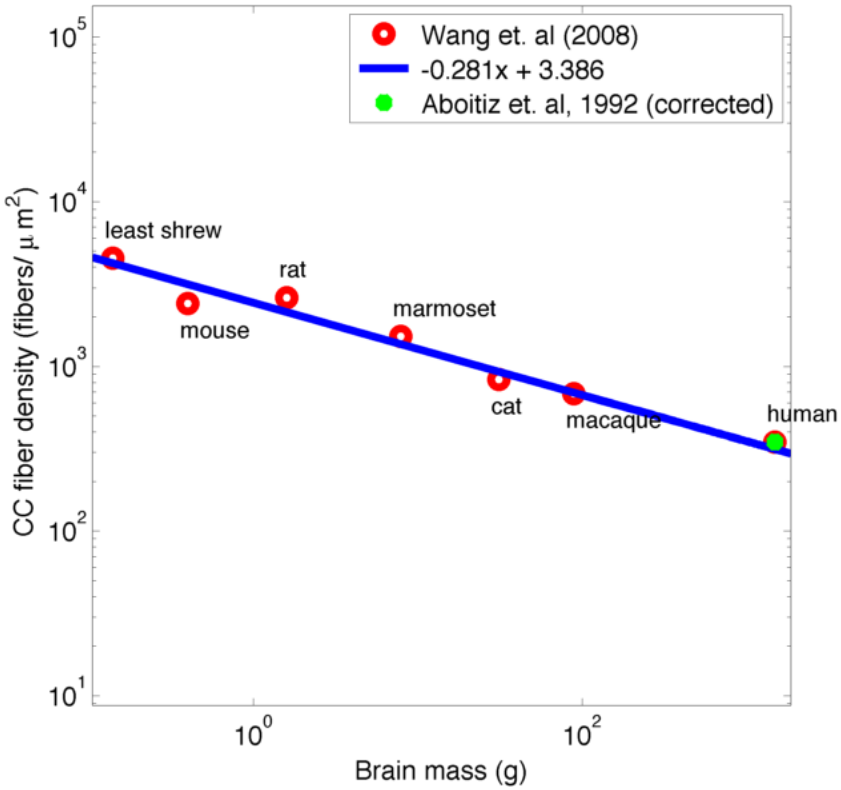

Figure 6.6: Corrected human density estimate plotted on the regression line derived from animal data. Data from Aboitiz et al. (1992); S. S. H. Wang et al. (2008).

To compare how the human variability compares with the other data, an allometric

regression was recomputed with the corrected human data. With this data point, the regression equation changes to $2.43 * BWT^{-0.274}$ with $r^2 = 0.928$. This is a small (2.5%) change in exponent, virtually no change in multiplicative constant ($< 1\%$), and an improvement in the r^2 value. These indicate that the human data are within the variation expected from the other animal data.

6.4.3 Discussion

Age correction suggest that the regression equation for callosal axon density may be conservative, but is overall very good (within 11.5% of the estimate). Though it is clear that some age correction is needed, the estimate of 20% age difference in fiber density needs further validation, given the lack of human data to estimate a human-specific curve and the sparsity of the animal data available to reliably estimate the curve.

It is worth noting that the widely cited estimate of 200 million fibers in the human corpus callosum is taken from this aged human sample. Due to the age of the sample, this estimate clearly underestimates the human callosal fiber count for young adults. Applying the same age correction to this total count I estimate $1.2 * 200 = 240$ million fibers in the human corpus callosum, 20% more than previously reported.

6.5 Analysis 3: Estimating relative fiber counts from Rilling and Insel (1999a).

Rilling and Insel (1999a) estimated grey matter surface area and corpus callosum surface area and made an inference about interhemispheric and intrahemispheric connectivity from the data. At least two things prevented them from estimating actual connectivity from their surface area data using these equations. First, at the time of their

publication, data had been published and allometric regressions performed for all quantities above except one–connection density within the corpus callosum. Second, though the regressions had been performed on all other variables, some papers only reported the allometric exponent (B in $y = A * x^B$, or $log\ y = A + B * log\ x$ when transformed into log-log space for the linear regression)–sufficient to examine scaling relationships, but insufficient for quantitative estimates of other values.

Both of these issues have been addressed. As shown above, since the time of Rilling and Insel (1999a)'s publication, electron microscopy data of callosal fiber density has been reported for 6 species (S. S. H. Wang et al., 2008). Solving the second issue was trickier. If all of the data from these publications were publicly available, it would be possible to compute parameters for each allometric regression and plug all quantities into the equations. Unfortunately, no original data was available from any authors contacted; instead, I use the same basic imaging techniques outlined in Section 6.3.1 to estimate the data and estimate estimation error. I also use data from tables where I can, and I cross-reference and combine results across the same lab where applicable.

A third reason why one might not perform the analysis that follows is that it is extremely precarious to combine these data mathematically across studies. Choices such as species sampled, tissue preservation and processing, and imaging techniques can all have large effects on individual allometric estimates; because of this, these scaling laws are usually understood more qualitatively than quantitatively. Though I have seen some papers combine data across studies (Zhang & Sejnowski, 2000; Changizi, 2001; Karbowski, 2003; Changizi, 2009), most combine exponents through very rough qualitative means rather than through the quantitative plug-and-play procedures here. I have not seen any quantitative examinations of either approach, though I approach both with caution.

I choose to follow the precarious mathematics because I believe Rilling and Insel

(1999a)'s interpretation of their data doesn't account for important scaling differences between the corpus callosum and intrahemispheric inter-area connections, and that when this is accounted for, their data lead to the unlikely (and opposing) hypothesis that fiber connections in callosal inter-area connections are proportionally increasing vs. intrahemispheric inter-area connections. In addition, the authors implicitly used similar computational procedures to come to their conclusions.

In order for the scaling exponent of surface areas to represent the scaling exponents of actual connectivity, as Rilling and Insel (1999a) did, one must assume that the rest of the quantities in Equations 6.1 and 6.2 scale with unity. This is the same as assuming that Equation 6.5 (below) is true, where each quantity is a power law of brain volume, and therefore the exponents add and are equal on each side of the equation. In order to test such an assumption, one would have to plug values into the equations, just as I propose doing in this analysis[4].

$$[Thickness_{grey}] * [Neuron\ Density_{grey}] * [\%\ Neurons_{project\ to\ white\ matter}] = constant * [Axon\ Density_{callosum}] \tag{6.5}$$

In order to give the reader a deeper insight into this data analysis, after discussing the methods I walk through each dataset I collected and decisions I made in which quantities were used from what publications.

[4]Some of the downsides can be mitigated by having a single lab collect these data, but even then their collection procedures will differ from the collection procedures of Rilling and Insel (1999a), and so introduce cross-technique variance.

6.5.1 Methods

Data Acquisition

Many of the data used here are between 20 and 60 years old; raw data are no longer available. Even for newer data, requests for raw data have either elicited no response, or the data remain inaccessible for other reasons. In order to use these valuable, published data, I developed a suite of simple computer vision techniques and manual data mark-up to extract data from published histograms and scatter plots. Using these techniques, I have been able to reproduce statistical results usually within 1% error (and always within 2%) of the published analyses and allometric regressions. All code, parsed data, and validation procedures are available freely online[5].

The data used in this analysis were exclusively from scatter plots (no histograms), and so I used the same general methods outlined in Section 6.3.1. Table 6.1 summarizes the datasets selected and estimates of "plucking error" for each.

Data Analysis

Data were analyzed through reduced major axis regression on log-log plots (i.e. allometric regression), which operates under the assumption that relationships between parts of the brain are scale-free (i.e. that the relative relationship between the quantities remains the same across all sizes). Scale-free relationships obey power laws, and so are linear in log-log space. All allometric regressions I computed had excellent fits (except where indicated otherwise in the text, $0.87 \leq r^2 \leq 0.99$ for all regressions).

[5] https://github.com/bcipolli/CallosalScaling
[6] See Section 6.5.1 for details.
[7] See Section 6.5.1 for details.
[8] Error could not be estimated, as no data analysis values were reported for this.

Table 6.1: Regression equations computed from "plucked" data or taken directly from the literature (when reported). "Plucking error" was computed by comparing computations published in the paper to the same computations with the "plucked" data. "Exact" indicates an equation pulled directly from the publication. BV (brain volume, cm^3) and BWT (brain weight, g) are the common comparison variables to examine scaling laws.

Quantity	Regression equation	Reference	"Plucking" Error
Grey matter volume	$GMV = 0.538 * BV^{0.969}$	Rilling and Insel (1999a, 1999b)	N/A
Grey matter density	$GMD = 9.59 * 10^4 * BWT^{-0.32}$	Tower (1954)	$< 1\%$
Callosal surface area	$CCA = 4.62 * BV^{0.702}$	Rilling and Insel (1999a)	N/A
% projecting	$PCT = 0.64 * BV^0$	None	N/A[6]
Brain weight (g)	$BWT = 0962 * BV^{1.024}$	(Rilling & Insel, 1999b; Chudler, n.d.)[7]	N/A
Callosal axon density	$CAD = 2.43 * BWT^{-0.28}$	S. S. H. Wang et al. (2008)	N/A[8]

Data Selection

Each dataset selected, including data from Rilling and Insel (1999b, 1999a), were selected to cross-validate both within a paper and across papers. A number of internal consistency checks were computed to validate that data were "plucked" in a meaningful way and that errors or inconsistencies in publications (such as unit conversions or typographic errors) were located and either fixed or omitted.

Grey matter volume Grey matter volume can be computed directly, or computed as the product of surface area and thickness. Rilling and Insel (1999a) estimated grey matter surface area from MRI scans and reported it in a scatter plot. Rilling and Insel (1999b) report grey matter volume directly in a table for a similar set of species and individuals. In fact, for 7 of 9 species, the two publications perfectly match the number of samples for each gender and average brain volume, indicating that for these species, data can be combined across the two publications.

I chose to use grey matter volume directly from Rilling and Insel (1999b) for a number of reasons:

- The data were available in a table vs. parsed from a plot (though I was able to replication regressions from the plot with error $< 1\%$)
- The estimation procedure for volume (counting thresholded pixels in individual scans, interpolating between scans) vs. surface area (manual tracing and addition within scans, then interpolating between scans) seemed more robust, as the interpolation for area made assumptions about shape whereas interpolation for volume made no such assumptions.
- When I computed the regressions for grey matter surface area vs. grey matter volume, the grey matter volume estimate (exponent = 0.969) agreed with previously reported values and estimations on theoretical grounds (exponent ≈ 1). The allometric regression for grey matter surface area did not (exponent = 0.754) match either empirical nor theoretical predictions (exponent ≈ 0.889) (Changizi, 2001, 2009)[9].

The choice to use grey matter volume means that species-average data were computed across this entire analysis. Species-average data are often used to help avoid large statistical problems, as variation within an individual species is dwarfed by variation across species. Thus, multiple data points per species in a regression act as anchors for the regression, giving more statistical confidence than warranted and, if the number of samples per species are not perfectly balanced, potentially weighting specific species data more than others in the regression. I had *a priori* decided to use species-average data to avoid these issues, and so I did not consider this a problem.

[9]The poor allometric regression for the grey matter surface area was driven largely by an unexpectedly small surface area for the human data point, compared to the volume reported. The dependence of the anomalous regression on a single data value was another red flag.

Grey matter density I used data from Tower (1954) and obtained regression coefficients within 1% of those reported in the publication (exponent=0.32). This value is most problematic, however. Herculano-Houzel (2011) reports that neuron density is not preserved across mammals; cross-family differences (for example, between rodents and primates) can be large. Herculano-Houzel (2011) estimate neuron density in primates to scale with cortex weight, but do not report a comparison with brain weight (which itself correlates with cortex weight). This seems inconsistent with their previous report of no correlation of brain size and neuron density in primates (Herculano-Houzel, Collins, Wong, & Kaas, 2007).

Tower (1954)'s data is consistent with a second publication (see Changizi (2001) for a review), included a wide range of species, and has been used in many papers previous to Herculano-Houzel (2011)'s publication, so I felt tentatively comfortable to use this value.

Callosal surface area This quantity was reported in Rilling and Insel (1999a) in both Table 1 (species-wise) and Figure 1b (individual-wise). Though I was able to obtain data from Figure 1b with little error ($< 1.5\%$), because I chose to use species averages, I used the data from their Table 1.

% projecting This value is problematic as well. Zhang and Sejnowski (2000) and Changizi (2009) assume this value is constant. Herculano-Houzel, Mota, Wong, and Kaas (2010) make a complex computational argument and estimate this to scale with an exponent of -0.159. Though I find problems with their method and with the plausibility of the reported value (discussed below), it is worth noting that regardless of these issues, an actual value (if constant) or equation (if a function of brain size) is unavailable in the literature.

The analysis of Herculano-Houzel et al. (2010) assumes that axon diameter

distributions (ADDs) are constant across brain size; in my review of the literature this contradicts the callosal data reviewed in Section 6.4. Note here, as discussed above, that only electron microscopy data are appropriate for this measurement. Thin, unmyelinated fibers are missed by using a light microscope, and their high packing density can have a significant effect on average axon diameter. No electron microscopic data have been published for intrahemispheric white matter ADDs, but there are no reasons to expect such fibers would be missing from intrahemispheric fiber tracts, particularly given how similar ADDs measured with a light microscope for intrahemispheric (Innocenti et al., 2013) and interhemispheric (Aboitiz et al., 1992; Caminiti et al., 2009) are. Finally, the authors cite Olivares et al. (2001) as showing increasing axon diameter with brain size. In fact, Olivares et al. (2001) show a negative exponent (≈ 0.2); Herculano-Houzel et al. (2010) suggest that it is small enough that it could be ignored. This logic seems flawed; using the same logic, then their exponent of $0.159 +/- 0.113$ could also be ignored.

Even accepting the assumptions behind the exponent, according to the basic estimation that follows, the reported exponent does not have a plausible value. Herculano-Houzel et al. (2010) report using brains ranging in weight from about 1 gram (tree shrew) to 1350 grams (human) in their analysis. Assuming a maximum of 80% of cortical neurons projecting into the white matter (all cortical pyramidal cells) in the tree shrew, we have enough data to use the allometric equation $y_{percent} = A * x^{B}_{brain\ weight}$ to get a sense of what $y_{percent}$ value this exponent would predict for humans. Solving the simple system of simultaneous equations 6.6 and 6.7 (below) returns an estimate of about 25% neurons projecting into the white matter for humans. This seems implausibly low, and does not represent a "slight" reduction in the percentage of neurons projecting across species as reported by Herculano-Houzel et al. (2010).

$$80 = A * 1^{-0.159} \tag{6.6}$$

$$PCT_{human} = A * 1350^{-0.159} \tag{6.7}$$

In order to keep the model simple, and given the scaling value was driven by an assumption about average axon diameter which I don't agree with, I made the simplifying assumption that this value is constant[10]. Once the value is a constant, then the actual value does not matter in the relationship between total fiber count and callosal fiber count, as in a log-log plot a constant factor becomes a change to the y-intercept and does not affect the exponent. The only computation examined that is dependent on the true value of this variable is the relative fiber count in interhemispheric vs. intrahemispheric inter-area connections (see Section 6.6.1 and Equation 6.12).

A value of 0.64 is used as about 80% of neurons are pyramidal cells, and "most" pyramidal cells project into the white matter (Zhang & Sejnowski, 2000). An informal poll[11] found 80% to best evoke the word "most", and so I set percent projecting to $0.8 * 0.8 = 0.64$.

Brain weight I used species brain volumes reported in Table 1 of Rilling and Insel (1999b). Some regressions used brain weights. To map brain volumes to brain weights, I looked up corresponding average weights for the species on a website that collected weights from a number of textbooks (Chudler, n.d.) and computed an allometric regression. Note that most people assume these values are interchangeable, and the computed

[10] I have re-run the analyses in this paper with different constant values for $[\%\ projecting]$ (0.80, 0.64, 0.30). I also re-ran using the allometric equation derived from equations 6.6 - 6.7. Changing the constant value only changes the relative number of fibers in a callosal vs. intrahemispheric inter-area connection (lowers to 2x or raises to 8x). Using the allometric equation added curvature Figure 6.8, and so could change the main results of this paper.

[11] $N = 1$ (me)

regression bears this out ($r^2 = 0.972$). I re-ran all analyses with the assumption that brain weight (g) and volume (mm^3) are the same, and the results were quantitatively extremely similar and qualitatively indistinguishable.

6.5.2 Results

Plugging in values from Table 6.1 into Equations 6.1 and 6.2, I compute the total number of callosal fibers to scale as the 0.643 power of the total number of white matter fibers (see Figure 6.7).

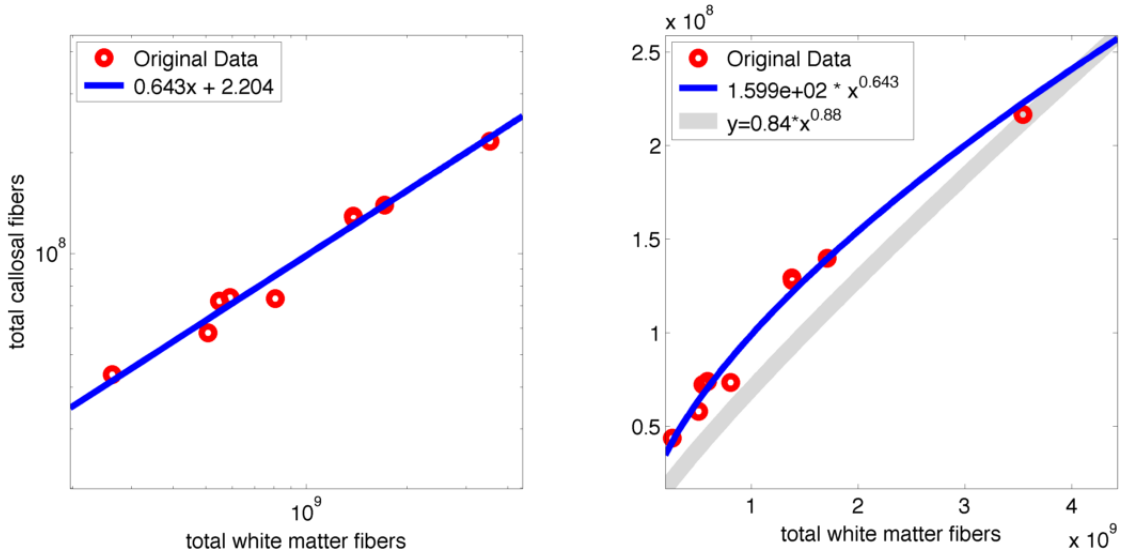

Figure 6.7: Log-log and euclidean plots of allometric regression for total white matter fibers vs. total callosal fibers. Estimates of connectivity computed from Rilling and Insel (1999a) data are in red, computed allometric regression is in blue. Grey corresponds to the regression equation estimated by Rilling and Insel (1999a). The regressions are plotted together to visually show the differences in scaling (curvature); note that the actual values output by their equation are not meaningful in its usage here.

6.5.3 Discussion

This result (exponent = 0.643) is drastically different than that estimated by Rilling and Insel (1999a) (exponent = 0.88) but is much closer to what was estimated in Section 6.2 (exponent = 0.66) and elsewhere (Changizi, 2001). The estimate in Section 6.2 is based on the difference between the homotopic connectivity of the callosum and the positive scaling of intrahemispheric inter-area connections.

In order to examine whether the scaling difference in inter-area connections can fully explain the scaling exponent of the fiber counts is explored in the final analysis.

6.6 Analysis 4: Explaining results through the homotopic connectivity of the corpus callosum

White matter fiber tracts connect as bundles of fibers between two cortical areas. When considering a single cortical area, callosal connectivity is largely to one other cortical area (the homotopic area in the other hemisphere (Aboitiz & Montiel, 2003)), whereas intrahemispheric connectivity connects many other cortical areas. Critically, while interhemispheric connections remain homotopic with brain size, the number of cortical areas that a single cortical area connects to increases with brain size, partly driven by an increase in the number of cortical areas in larger brains (Changizi & Shimojo, 2005) and potentially related to "efficient interconnectedness" (Changizi, 2009).

This suggests that any individual inter-area connection–whether interhemispheric or intrahemispheric–is a proportionally smaller amount of the total connectivity with increasing brain size, despite the fact that the size of each area, and number of fibers within that inter-area connection is likely increasing with brain size (Changizi, 2001, 2009).

6.6.1 Methods

In order to examine whether this effect can explain the above apparent reduction in interhemispheric connectivity, I directly compared the scaling of fiber connections to the scaling of inter-area connections. For the fiber ratio, I was able to avoid using the estimated scaling equation for the number of cortical areas (Changizi & Shimojo, 2005) by computing ratios of per-area quantities. The scaling equation for the number of cortical areas was not well-fit by a power-law equation and the value of its parameters has not been verified in other studies. I also chose to compare callosal connectivity to intrahemispheric connectivity (rather than comparing callosal connectivity to total connectivity, which callosal connectivity is a part of). Subtracting out a quantity from the total has shown to be a more effective method for doing allometric regression, and was used in some (but not all) of the original Rilling and Insel (1999b) analyses.

$$\begin{aligned} Connection\ ratio(per\ area) &= \frac{Callosal\ inter\text{-}area\ connections}{Intrahemispheric\ inter\text{-}area\ connections} \\ &= \frac{1}{inter\text{-}area\ connections(per\ area)-1} \end{aligned} \tag{6.8}$$

$$\begin{aligned} Fiber\ ratio(per\ area) &= \frac{\#\ callosal\ \ fibers\ (per\ area)}{\#\ intrahemispheric\ \ fibers\ (per\ area)} \\ &= \frac{\#\ callosal\ \ fibers}{\#\ total\ \ fibers-\#\ callosal\ \ fibers} \end{aligned} \tag{6.9}$$

In order to compare these scaling laws, I regressed them against each other (as done in Rilling and Insel (1999a) and in Analysis 1 above). In all regressions performed, allometric regression exponents were close to one, and so linear regressions

were computed as well to test whether allometric or linear regression was a better fit. However, since computing linear regressions opens up the possibility of non-zero y-offsets (i.e. that the curves do not intersect with the origin), I also estimated best fits for exponential relationships with a y-offset ($y = A * x^B + C$) using the Nelder-Mead optimization procedure in MATLAB[12].

Table 6.2 contains the quantities used in equations 6.8-6.9.

Table 6.2: Values used in equations 6.8-6.9.

Quantity	Regression equation	Reference
Callosal inter-area conns (per area)	$CAC = 1$	assumption
Inter-area conns (per area) (Intrahemispheric)	$TAC = 4.11 * BV^{0.31}$	Changizi and Shimojo (2005)
Callosal fibers	$CF = 1.126 * 10^7 * BV^{0.414}$	estimated from Equation 6.1
Total white matter fibers	$TWMF = 3.33 * 10^7 * BV^{0.649}$	estimated from Equation 6.2

If the relationship between relative fiber count scaling and relative inter-area scaling is linear, this would suggest that the scaling of the number of fibers per intrahemispheric and interhemispheric inter-area connection is the the same. Because an allometric function for fiber counts was estimated above, and an allometric function for per-area inter-area connections is available (Changizi & Shimojo, 2005), it is possible to compute an estimate of the relative fiber counts for callosal vs. intrahemispheric inter-area connections.

Using Equations 6.8-6.9 and basic algebra, the following equations are obtained (where IAC stands for inter-area connection):

[12] see https://github.com/bcipolli/CallosalScaling/blob/c3e72194cae535acd3b6cbd7ea01f67ad9a10759/_lib/guru/allometry/allometric_regression_offset.m

$$\textit{total fibers per IAC } (\textit{callosal}) = \frac{\textit{total callosal fibers}}{1 * \#\textit{ areas}} \tag{6.10}$$

$$\textit{total fibers per IAC } (\textit{intra-}) = \frac{\textit{total intra- fibers}}{[\#\textit{ inter-area cnxs } (\textit{per area})] * [\#\textit{ areas}]} \tag{6.11}$$

$$\begin{aligned} \textit{callosal relative fiber count} &= \frac{\#\textit{ fibers per callosal area cxn}}{\#\textit{ fibers per intra- area cxn}} \\ &= \frac{\textit{total callosal fibers}}{[\#\textit{ intra- fibers}]/([\textit{inter-area cxns } (\textit{per area})] - 1)} \end{aligned} \tag{6.12}$$

Just as before, by computing the ratio of callosal and intrahemispheric quantities, the allometric equation for the number of cortical areas cancels out. Note that, for this regression only, the percentage of neurons that project into the white matter is critical (see this variable's value and notes about the value's selection in Table 6.1). Variations in that value are noted in the discussion below.

6.6.2 Results

For the regression of relative fiber scaling and relative inter-area scaling, an equal fit (log-log: $r^2 = 0.927$; linear: $r^2 = 0.928$) is obtained with linear regression (assumed exponent = 1) and allometric regression (exponent = 1.207). Though the allometric is not so far from unity, the discrepancy between the allometric and linear exponents leave open the question of whether this relationship is linear or not. The unconstrained optimization (Nelder-Mead method) returns an exponent of 1.039 ($r^2 = 0.929$) when run on the untransformed data, lending support that the data have a linear relationship.

Regressing the expressions in Equations 6.10 vs. 6.11 also returns good fits for both allometric (exponent = 1.222, $r^2 = 0.977$) and linear regressions ($r^2 = 0.980$).

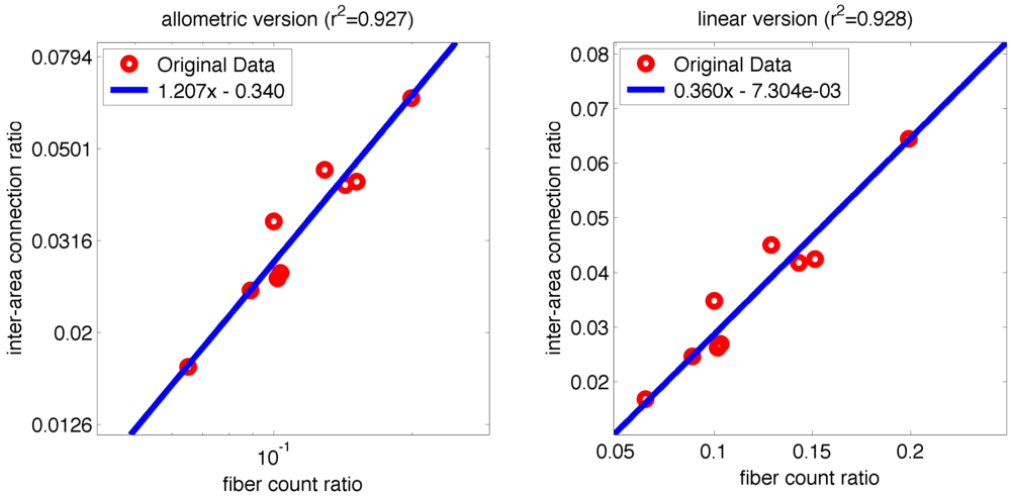

Figure 6.8: Regression for fiber ratio vs. inter-area connection ratio using species data. Both have similar fits.

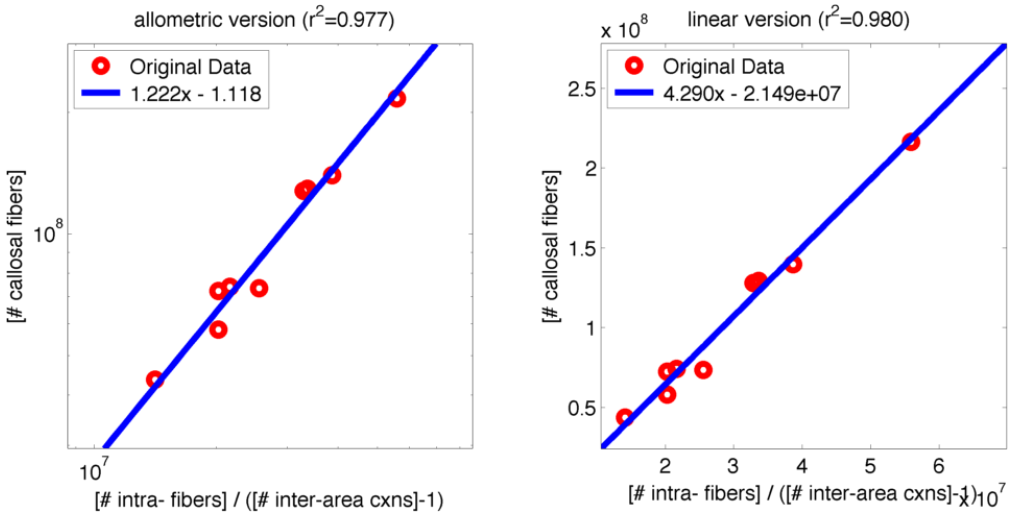

Figure 6.9: Regressions for callosal fiber count (per inter-area connection) vs. intrahemispheric fiber count (per inter-area connection). The allometric and linear regressions have very similar fits. The multiplicative constant in the linear regressions indicates the relative number of fibers in average callosal vs. intrahemispheric inter-area connections.

The unconstrained optimization returns an exponent of 1.0343, again consistent with the results from the first regression. The multiplicative value of the linear regression (4.3; see the legend in Figure 6.9b) gives the relative strength of callosal connections vs. intrahemispheric connections.

Given that the equations used in first and second regressions are simple algebraic manipulations of each other, I expected the regressions to show similar results. This is what was found for the allometric regression (exponents 1.222 and 1.207) and unconstrained optimization (exponents 1.034 and 1.039).

6.6.3 Discussion

What drives the relative reduction of callosal fiber count? We saw in Analysis 3 that callosal fiber count scales more slowly than total white matter scaling. The linearity of the first regression here is consistent with the hypothesis that this effect can be explained completely by the differential scaling of callosal vs. intrahemispheric inter-area connections, and that there is no differential scaling of fiber counts within each inter-area connection.

Fiber ratio and inter-area connection ratio showed a linear relationship; there is no exponential component of their relationship. Instead, their relationship is a constant multiplicative factor over brain sizes. This means that the fiber scaling differences found in Analysis 1 are completely explained by changes in the relative numbers of inter-area connections. In other words, we expect the proportion of interhemispheric inter-area connections will decrease with brain size–there is always only one per cortical area (the connection to the homotopic area in the other hemisphere) while we know that the number of areas, and intrahemispheric inter-area connections are both increasing (Changizi & Shimojo, 2005). The exponential rate at which that relationship changes is the same exponential rate at which we computed the number of interhemispheric vs. intrahemispheric fibers to be changing. There is no evidence of selective reduction in the number of fibers per inter-area connection as suggested by Rilling and Insel (1999a); increases or decreases in fiber counts exactly correspond to increases or decreases in inter-area connections.

Relative fiber count of inter- vs intrahemispheric inter-area connections Comparison of fiber counts, on a per-inter-area connection basis, also showed a linear relationship. This again supports the idea that the same scaling laws apply to both fiber types. Callosal fibers showed 4.3x more fibers per inter-area connection than intrahemispheric connections, suggesting a special role for interhemispheric fibers. This result is even stronger in the light of recent findings from Henry Kennedy's lab. They have published compelling data that suggest fiber count decreases as an exponential function of distance (Markov et al., 2013). Because callosal connections are on average longer than intrahemispheric connections (Lewis et al., 2009), our a priori expectation should be that callosal fiber counts would not be equal, but would be relatively lower when compared to intrahemispheric fiber counts (per inter-area connection).

If we accept this consistent relationship, then the slope of the regression represents the relative number of fibers in a callosal inter-area connection vs. an intrahemispheric inter-area connection. The slope value is 4.3x both in the linear and unconstrained 3-parameter optimization, suggesting that callosal inter-area connections have about 4.3x more connections than the average intrahemispheric inter-area connection (Figure 6.9). This 4.3x factor is preserved across all brain sizes.

Note that the percent of fibers projecting into the white matter was guessed at, using 80% of cortical neurons as pyramidal cells and 80% of those projecting into the white matter. This seems a relatively conservative estimate. Any percentage lower than that would simply weight callosal connections more than 4.3x.

Potential explanations for a non-linear relationship The possibility remains that the relationship between fiber and inter-area connection scaling is not a linear relationship. A potential interpretation of the 1.2 exponent value is that it reflects the scaling of non-homotopic connectivity in the corpus callosum. I assumed that all connections are

homotopic, but we know that is not strictly true. In addition, it seems likely that there will be a positive scaling of non-homotopic connections with brain size, as the number of non-homotopic areas increases with brain size (Changizi & Shimojo, 2005).

It is also worth noting that the possibility of the percentage of projecting neurons decreasing with brain size, as suggested by Herculano-Houzel et al. (2010), would not explain away a positive exponent, but rather would exacerbate it.

Summary These analyses suggest that callosal connections are both very typical and very special. There is no evidence for a selective decrease in callosal connections; rather callosal connections scale just like intrahemispheric connections. Across species, callosal connections severely break the exponential distance relationship; despite being on average longer connections, the number of fibers is 4.3x greater in a callosal inter-area connection than in an intrahemispheric inter-area connection.

6.7 General discussion and conclusions

In this paper, I used data extracted from the literature to investigate allometric scaling of total and interhemispheric white matter fibers and inter-area connections across primate species. Along the way, I found:

- Callosal fiber density scales proportional to brain mass with an exponent of -0.28.
- There is good evidence for age-related decreases of fiber density in macaque monkeys.
- I estimated a 20% age-related correction for human callosal density data reported in the literature, due to older samples in for humans vs. animals.

- From this correction, I estimate that young adult humans have ~ 240 million callosal fibers. This 20% increase is consistent with what is predicted from the callosal fiber density regression.

These findings allowed us to examine cross-species scaling of the proportion of total and interhemispheric white matter fibers. I found:

- Interhemispheric fibers scale as the 0.64 power to total fibers, much smaller than the 0.88 power previously estimated (Rilling & Insel, 1999a).

- The scaling of interhemispheric vs. intrahemispheric fiber counts seems to match the scaling of interhemispheric vs. intrahemispheric fiber tract bundles between areas, suggesting that the above is due purely to the homotopic nature of interhemispheric connectivity.

- When estimating bundle sizes, despite on average being longer connections, callosal fiber bundles contain 4.3x more axons than the average intrahemispheric connection.

6.7.1 Potential challenges and caveats

As outlined throughout the paper, there are a number of challenges in this type of estimation:

- Without direct access to source data, it is hard to know what data is best to use.

- Allometric regressions are highly-dependent on variables that I don't have control over when collecting data across the literature.

- There is a lack of convergence in the literature about the allometric relationship for both neural density and the percentage of neurons sending projections into the white matter fiber, both of which affect the analyses here.

- Allometric and linear regressions equally explained the data with different exponents; which choice reflects the true relationship in the data? The use of the non-parameterized optimization procedure gave weak evidence in favor of the linear regression, and there is theoretical reasoning behind the linear regression, but there is no stronger evidence in support of using either regression at the moment.

6.7.2 Applicability to other large-brained species

Not only does this work clarify the role of the corpus callosum in humans, but it also re-calibrates expectations for other large-brained animals. With a dissociation between brain size, lateralization, and independence, there is no reason to expect reduced interhemispheric communication, nor lateralization, in large-brained species such as elephants and cetaceans. In animals such as cetaceans where a reduced corpus callosum is clear (Tarpley & Ridgway, 1994), this should be viewed as unexpected and a specialization. In dolphins, relatively independent hemispheres may allow them maintain a constant state of alertness and ability to surface to breathe, even during their unique sleep pattern where only one hemisphere enters sleep at a time (Ridgway, 2002).

6.7.3 Conclusions

I have argued elsewhere that the special conditions of human development lead to a unique developmental trajectory of white matter, particularly the corpus callosum, which affects the development of lateralization (Chapter 5). I believe the results in this paper, in tandem with our previous results, put a focus back on the human corpus callosum and its role in human lateralization and cognition.

This paper makes a number of testable predictions about the corpus callosum across many species. I welcome collaborators with access to freshly deceased human,

cetacean, or other brains to collaborate with us in testing the hypotheses outlined in this paper.

6.8 Acknowledgments

Author contributions: I conceived of, implemented, and analyzed all computational simulations and analyses. Garrison Cottrell advised on the project and provided feedback on this manuscript.

This work was partly funded by a Center for Academic Research and Training in Anthropogeny (CARTA) fellowship, as well as by NSF grant SMA 1041755 to the Temporal Dynamics of Learning Center, an NSF Science of Learning Center

Chapter 7

Inter-chapter connectivity

In the preceding chapters I describe computational models that support neurodevelopmental explanations for lateralization of visual processing and robust cross-species interhemispheric communication. Interactions between lateralization and interhemispheric communication are briefly and abstractly touched on (Chapter 5), but an integrated account of visual asymmetries and interhemispheric interactions is not addressed directly nor speculated on. This chapter is an attempt to place the research in this thesis into a broader context of existing models and, by doing so, speculate on a direct relationship between lateralization of visual processing and interhemispheric communication. I will do so by reviewing two related models from the literature, examining how the models covered in Chapters 2 - Chapters 6 compare and contrast, and then offer a speculative integrated neurodevelopmental theory of visual asymmetries and interhemispheric communication. I conclude by relating the results and speculations of this thesis to lateralization more broadly. By doing so, I hope to set the stage for future research based on the findings within this thesis and my broader understanding of the literature.

7.1 Relation to the Double Filtering by Frequency (DFF) model

The double-filtering by frequency (DFF) model is a neural network model that implements Ivry and Robertson (1998)'s proposal that visual asymmetries in processing Navon stimuli or spatial frequency gratings arise from symmetric early visual processes being differentially biased by top-down task demands. The top-down mechanism operates by selecting task-related frequencies (the first "filtering" stage), then each hemisphere applies a differential bias on that task-related frequency band. In contrast, the differential encoding (DE) model described in Chapters 2 - Chapters 6 is an implementation-level model; it does not postulate a direct relationship between spatial frequency filtering and lateralization, but instead suggests that an asymmetry in the connection spread of long-range lateral connections drives encoding differences between the hemispheres that affect representation of configural information, contour information, and spatial frequency information in ways that can account for asymmetries in behavioral task performance.

Both models show a relationship between spatial frequency filtering and reaction time data in local/global processing. Both are consistent with data showing modulation of lateralization in attention. Is the differential encoding model an implementation of the double-filtering by frequency model? I believe there are a number of factors that not only differentiate the two models, but make them irreconcilable.

First, the two models have very different relationships with spatial frequency filtering. In the DFF, spatial frequency filtering is the fundamental asymmetric operation that differs between the hemispheres, while in the DE the fundamental asymmetric operation is in integration across receptive fields of contour and configural information via long-range lateral connections. In the DE, spatial frequency processing differences only arise as a byproduct of a bias in contour processing. The DE's focus on contour

processing, rather than more abstract spatial frequency processing, could be consistent with findings that studies manipulating spatial frequencies directly have extremely variable effects, as their effect on contour processing is itself variable and highly dependent on the manipulation found in each study. Stimulus variations that eliminate spatial frequency power differences in local and global levels, but maintain contour contrast, could therefore differentiate between the two models (see Section 8.1 for a proposal of such an experiment).

Second, the DE postulates multiple loci for visual processing asymmetries (see Section 3.4), whereas the DFF makes absolutely no claims. This is best illustrated by the differing approaches to explaining the putative "relative frequency" data of Christman et al. (1991). In the DE, top-down information feeds into multiple visual areas, each of which can have their own spatial frequency biases. The area most strongly selected for a classification task depends on the spatial scale of the task-related discrimination, as presumably an area that has receptive field sizes large enough to process features at that scale would be selected. In the DFF, top-down control acts as a central filter on the spectrally-processed visual information. Whether that spectrally-processed information exists in a single cortical area or not, and whether this filtering happens in a single cortical area or not, are both unanswered questions. However, given the great pains to share mechanisms over modalities, it would be surprising for the DFF to claim that either level (bottom-up processing of spatial frequency information or top-down modulation of that frequency information) involves multiple cortical areas.

The DE hypothesis of multiple cortical areas being involved in the "relative frequency" effect is supported by findings in the literature and further simulations we've run. Hopf et al. (2006) found that the spatial scale of a discrimination indeed activated different visual areas, with larger spatial scales activating areas later in the ventral visual processing stream, consistent with the increasing receptive field size in later areas.

Relevant to the DE, Amir et al. (1993) showed that both the absolute length of long-range lateral connections, and what percentage of the visual field that they span, increase the further one traverses down the visual hierarchy. In additional simulations, we have shown that these length differences are consistent with no lateralization in early visual areas (supported by data reviewed in Sergent (1982)'s original formulation of the spatial frequency hypothesis) and lateralization at different spatial scales in different cortical areas in the visual hierarchy. None of these findings are addressed by Ivry and Robertson (1998)'s model, nor are they compatible with the DFF neural network model outlined in the publication.

A third difference between the DFF and DE is how each model approaches lateralization across modalities. As referenced above, the DFF model aims to account for auditory lateralization of frequency processing through the same mechanism as visual lateralization. The DE model is based on the idea that a modality-specific mechanism is critical to characterizing and understanding lateralization. The role of long-range lateral connections in audition has not been well-characterized to my knowledge, and it remains unclear whether a modality-specific mechanism that could account for auditory frequency lateralization and allow top-down modulation exists (though see Section 7.5). The DE postulates that differential timing of hemispheric maturation interacts with visual acuity changes to cause the postulated connectivity difference in visual cortex. It is likely that this same differential maturation would affect other modalities, but how it affects them would be very modality-specific. For example, infants receive low-pass filtered auditory input in the womb (Smith, Gerhardt, Griffiths, Huang, & Abrams, 2003); given a faster maturing right hemisphere in the womb (N. Geschwind & Galaburda, 1985), one might find asymmetries in learned structure within the right hemisphere.

A final difference between the two models is how they address interhemispheric interactions. The DFF is not only silent about interhemispheric interactions, but because

the model lacks physiological mechanisms for spatial frequency filtering, it is not possible to generate any prediction about how interhemispheric communication mechanisms could interact with spatial frequency filtering. While the DE has not incorporated any interhemispheric integrations to date, its explicit physiological methods make incorporating interhemispheric connections more straightforward. In addition, because the DE contains an explicit developmental trajectory, interactions with development of the corpus callosum can be described (and is, in Section 7.2). Finally, recent evidence suggests that callosal connections share function and physiology with long-range lateral connections (Schmidt, 2013), making the feasibility of combining them into a single computational model more plausible.

Relation to Contour Processing

The core difference between frequency filtering and the differential encoding (DE) model is captured in the relationship of the DE to contour processing. I have argued that global-level processing, configural face processing, and contour processing all use neighbor information via long-range lateral connections. I've shown modeling data suggesting that asymmetric processing of these stimuli may come from a right hemisphere (RH) bias for shorter long-range lateral connections, which bias the RH for capturing these neighbor relationships inherent in contour and configural processing.

A number of neurophysiological and behavioral findings support a relationship are consistent across global figures, face processing, and contour processing, consistent with the hypothesis of a shared mechanism between them. While a RH advantage for global figures has been well established, As reviewed by Gazzaniga (2000), seemingly related abilities, such as in illusory contour processing or amodal completion - contour completion in the face of occluders - show a right hemisphere advantage (De Renzi & Spinnler, 1966; Wasserstein, Zappulla, Rosen, Gerstman, & Rock, 1987; J. Hirsch et

al., 1995). Volberg (2014) was the first to test lateralization of contour processing and found a RH advantage. Both show similar protracted developmental timelines (Altschuler et al., 2013), and both are reduced in autism Behrmann et al. (2006), a developmental disorder thought to affect connectivity mechanisms. Roux and Ceccaldi (2001) find age-related decline in local/global interference, consistent with Roudaia, Bennett, and Sekuler (2008) 's finding of age-related decline in contour processing, which requires ignoring conflicting local elements and parsing out a consistent global contour.

A few studies suggest a shared mechanism more directly. Volberg, Wutz, and Greenlee (2013); Pitts and Martinezzr (2014) both report that contour processing is modulated by task demands, consistent with studies on global form processing reviewed in Ivry and Robertson (1998) and with the DFF theory. At a deeper, more specific level, Li et al. (2008) showed that contour processing in macaque monkeys involves a feedback circuit between V1 and V4. When Volberg and Greenlee (2014) adapted Li et al. (2008)'s study to an EEG paradigm in humans, they associated the lateral occipital complex (LOC) with grouping mechanisms. These same LOC areas have been associated with face (Behrmann & Plaut, 2013) and global form (Hopf et al., 2006) processing.

The picture is not crystal clear, however. Gazzaniga (2000) reviews other studies that suggest separable mechanisms. (Wasserstein et al., 1987) reports right hemisphere dominance for illusory contour processing, but no relation to a facial discrimination task. Corballis, Funnell, and Gazzaniga (1999) found dissociations between illusory contour processing and amodal completion in two split brain subjects, also suggesting that there may be multiple mechanisms in play.

None of these studies definitively link contour processing, face processing, and global form processing, but their convergence lends support to the idea and suggests that further study is warranted.

7.2 Integration with Plaut and Behrmann (2011)

The most complete current theory on the development of lateralization of face and word recognition comes from (Plaut & Behrmann, 2011; Behrmann & Plaut, 2013). This theory builds off of literature suggesting a competitive relationship between face and word recognition, rather than an innate source of lateralization. Data used to argue the point include typical developmental trajectory of lateralization in relation to reading, cross-cultural studies of lateralization with relation to reading, and neuroimaging studies of reading recognition in prosopagnosia. Plaut and Behrmann (2011) also present a neural network model to support their idea that visual recognition of words is lateralized to the left fusiform gyrus, and therefore face recognition to the right fusiform gyrus. Core ideas to the model include that while faces and words require high-acuity visual discriminations, they have very different representations. This causes competition for resources that the brain resolves via lateralization, with visual word forms lateralized to the left hemisphere to efficiently express their dependency on left lateralized phonetic representations.

Potential issues with the model

I find the data this theory is based on to be very compelling, and overall I think the competitive view of lateralization fits with the data. However, a number of questions remain unanswered with their theory. What are the neuroanatomical substrates of the left and right hemisphere specializations? Are these neuroanatomical asymmetries only found in the late-stage fusiform areas, or could lateralization in earlier stages of visual processing account for the lateralization in the fusiform areas? Are these asymmetries modulated by stimulus strength and attention? If so, how?

Another challenge for the theory comes from questions about the relationship

between visual processing asymmetries of faces and words with that of other stimuli, such as Navon figures and spatial frequency gratings. Does lateralization in local/global processing or spatial frequency gratings relate to those of words and faces? If so, why are findings in visual lateralization so weak (67% of published studies; Van Kleeck (1989)) and variable across participants when population-level language lateralization is so strong (90% of the population) and unequivocal across studies? If not, what separates the mechanisms within the ventral visual stream?

A final set question surround the idea that visual word forms are lateralized to the left hemisphere due to left lateralization of productive language capabilities and specifically phonetic information. As discussed in Chapter 5, timing considerations are unlikely to lead to lateralization, particularly in the later stages of development when large-scale connection pruning is likely complete. Language lateralization is thought to depend crucially on the need for fast processing, but what processing requires such fast time scales that would lead to semantic and visual recognition of words also being left lateralized? A specific need based on timing is never presented, nor are neural data that show such a need cannot be fulfilled with long-distance connectivity. Finally, there is some evidence of RH lateralization of face processing in the rhesus macaque monkey (Hamilton & Vermeire, 1988; Vermeire, Hamilton, & Erdmann, 1998). Consistent with the human data, such lateralization is experience-dependent; unlike the human data, in rhesus macaque monkeys the RH lateralization cannot be driven by language lateralization. How might the model account for these data?

Clear overlap between the theories

Plaut and Behrmann (2011) postulate that interhemispheric competition is critical to lateralization of faces and visual word forms. This is consistent with my findings that the human corpus callosum is not selectively decreased in humans, but instead

may over-represent thin, slow fibers (Chapter 5)–just the types of fibers found between association areas such as the fusiform face area (FFA) and the visual word-form area (VWFA) (Aboitiz et al., 1992; Aboitiz & Montiel, 2003). It is also consistent with the analysis in Chapter 5 that the relative slowness of these fibers does not pose a challenge to interhemispheric collaboration.

The developmental trajectory of the corpus callosum is grossly consistent with the development of face recognition and word reading abilities. Lateralization is initially not present, consistent with immature interhemispheric connections leading to reduced interhemispheric competition (Chapter 5). Over time, maturation of these fibers would lead to increased interhemispheric communication and facilitate competition. Though maturation of some callosal fibers happen early during development, thinner association fibers tend to begin maturing later and mature for a longer period, consistent with a protracted trajectory for lateralization of face and visual word-form recognition.

Potential issues in integrating with this thesis

The differential encoding (DE) model is able to account for local/global (Chapter 2), spatial frequency and face recognition asymmetries (Chapter 3), with the hope to extend to word recognition. It postulates an asymmetry in connectivity of long-range lateral connections within retinotopic within extrastriate visual areas, causing stronger asymmetries with activation of this system due to weak stimulus strength (low contrast or brief duration) (H. A. Swadlow & Alonso, 2009) or from top-down task demands, particularly as they relate to contour or configural processing (C. D. Gilbert & Li, 2013).

These results seem overall consistent with the data from Plaut and Behrmann (2011). One potential point of difficulty in integrating the data across models is how the differential encoding model, focused on retinotopic visual cortex, might relate to asymmetries in the fusiform gyrus, located later in the ventral visual stream and thought

to contain representations that are less variant to stimulus position than retinotopic cortex.

Development poses an additional challenge in integrating the two theories. Plaut and Behrmann (2011) provide good data suggesting that development of lateralization for faces and visual word forms is inter-dependent, and therefore such lateralization is not obligatory, but instead based on experience with visual word forms and reading. The differential encoding (DE) model, on the other hand, postulates that lateralization of visual processing occurs early in typical human development due to an interaction between changing visual acuity and a difference in the timing of visual maturation through connection pruning (Chapter 4).

Potential ways to overcome issues

Proposing a shared developmental schedule

Developmental data show that long-range lateral connections tend to stabilize after initial pruning. For example, cats reared in an environment with vertical stripes do not attain full visual perceptual abilities after being shifted to a fully enriched environment if the shift is made after the critical period (H. V. Hirsch & Spinelli, 1970; L. E. White & Fitzpatrick, 2007). I performed simulations with our developmental model to test how further visual experience would affect the model when connectivity is held static but further perceptual learning occurs (through changes in synaptic strengths). I found that virtually all spatial frequency differences between the hemispheres (reported in Chapter 4) were lost (Cipollini, unpublished observations).

I propose the following developmental progression: long-range lateral connections in post-sensory visual areas are differentially pruned early in development, starting between 3 and 6 months of age (Gerhardstein, Kovacs, Ditre, & Feher, 2004; Baker, Tse, Gerhardstein, & Adler, 2008) and completing around 13 months of age (Burkhalter, 1993;

Norcia et al., 2005), due to an interaction between visual acuity changes (Norcia, Tyler, & Hamer, 1990) and an earlier maturation of the right vs. left hemisphere (N. Geschwind & Galaburda, 1985; Hellige, 1993; Chiron et al., 1997). Testing this asymmetry early in development would be challenging, as the asymmetries are not found in basic sensory detection tasks or others that more directly access early visual areas, as these areas have connection lengths too short to show a functional asymmetry.

After this period of axon elimination, experience-dependent plasticity continues to reshape these connections (Luhmann, Martinez Millan, & Singer, 1986; L. C. Katz & Callaway, 1992; R. A. W. Galuske & Singer, 1996) reduces asymmetry between the hemispheres. The connection asymmetry would remain latent, but any processing asymmetry would likely be too weak to reliably detect in most individuals or across the population. This is consistent with studies showing that shifting from a deprived to fully enriched visual environment does not change visual perceptual abilities if the shift is made after the critical period (H. V. Hirsch & Spinelli, 1970). The visual perceptual abilities are thought to be driven by long-range lateral connections, which show differential connectivity patterns based on the deprived environment (H. V. Hirsch & Spinelli, 1970); the critical period for these abilities is likely driven by connection pruning.

Immature interhemispheric fibers during this time would prevent the hemispheres from interacting in ways that might abolish their differential sensory development. After the critical period, the maturing interhemispheric fibers would enable more robust interhemispheric interactions and allow competition for representation (Plaut & Behrmann, 2011; Scherf, Behrmann, Humphreys, & Luna, 2007). Rather than visual word forms being lateralized to the left hemisphere to be localized with language (Plaut & Behrmann, 2011), I postulate that this is due to the postulated latent connectivity pattern differences that bias the right hemisphere for learning low spatial frequency information such as global-level contours and configural information at the cost of more detailed high-

frequency feature information, thus biasing word-form learning to the left hemisphere.

Over time, visual learning in contour processing continues, with evidence of plasticity in neuroscience through at least 4 years of age(Kaldy & Kovacs, 2003), and continued psychophysical development in ages 5 - 14 (Kovacs, Kozma, Fehr, & Benedek, 1999).

Proposing a relationship between IT and retinotopic connectivity asymmetries

There are a number of ways that an asymmetry in retinotopic visual cortices could lead to asymmetries in activation of the fusiform gyrus during face or visual word form recognition. One possibility is that the long-range lateral network is more active during development than adulthood. This could be due to a number of factors. Learning is effortful, particularly word learning, and that attentional engagement activates the long-range lateral connection network. These networks may also simply be more active during development, as feed-forward visual processing may proceed more slowly and may engage lateral networks more robustly during perceptual learning. On this idea, a heavier involvement of long-range lateral connections during the development of the fusiform areas could lead to their lateralization. After perceptual learning and individuals become face and word form experts, long-range lateral connections would only be selectively engaged due to stimulus strength and task demands. However, higher-level representations of faces and words would already be lateralized within the fusiform gyrus, and would no longer need active engagement of long-range lateral connections to be expressed.

Another possibility is that connection differences in the fusiform gyrus could lead to these types of differences. Representations in the inferior temporal lobe are less variant to stimulus position, but they are not invariant. It is possible that there is a component of the functional maps of the FFA and VWFA that represent retinotopy. In this case,

differences in long-range lateral connection may be latent in these areas and may be capable to bias perceptual learning directly.

A final possibility is that the face processing pathway is relatively independent of the pathway that produces local/global lateralization. In support of this idea, Kimchi (1992) of reviewed local/global and (w)holistic processing results and concluded that they likely describe different processes. There is a lot of evidence linking face processing and holistic processing, so this conclusion suggests that local/global and face processing are likely different processes. More directly, Dale and Arnell (2013) found that while local/global and face preferences showed stable individual differences, the two tasks did not share variance.

Nonetheless, some mechanism must link the two. A developmental model such as the one suggested in this section could account for these results. The interaction between the two systems could be unique to development. In such a model, after interacting during development, the two systems would share a common lateralization. However, after being decoupled late in development, the two systems could take different domain-specific trajectories. For example if face lateralization is present in the FFA and local/global lateralization is present in V4, then we might see a more direct interaction between V4 and the FFA during development. After development, that interaction would be lost, and the interactions of the FFA with the visual word-form area (VWFA) could then drive the FFA to keep some general aspects of lateralization, but also change the FFA's processing such that the neural coding becomes more and more decoupled from V4 representations.

7.3 Summarizing the theory

The DE is an implementational theory that posits a difference in the long-range lateral connections in extrastriate retinotopic visual areas drive lateralization in contour

and configural processing. The model shows spatial frequency differences only because contour and configuration information are usually stored in the low spatial frequencies. These long-range lateral connections are most active with low stimulus strength (brief presentation, low contrast), matching findings from the literature. Stimulus size and retinal position matter because the areas are retinotopic, also consistent with the literature.

The asymmetry in long-range lateral connectivity develops during early visual maturation, where earlier right hemisphere maturation leads to connection pruning under poor visual acuity, causing short-range connections to be over-represented after pruning. This is due to the surprising relationship between shorter long-range lateral connections and better contour processing. The left hemisphere also shows a bias for shorter-range lateral connections, but a lesser bias than the right hemisphere due to its greater experience with high-acuity visual input.

After initial developmental bias of these connections, symmetric visual input overpowers any small bias in information encoding between the hemispheres. The connectivity different remains latent, however. When the individual encounters stimuli that compete with existing representations in the brain (such as when learning to read, words may compete with faces because they have diagnostic information coded in very different ways), the neural encoding will self-organize into more separable maps. When the corpus callosum matures more completely, one good way to segregate these resources is across the hemispheres, and lateralization will emerge. Representations for objects such as faces will be learned more quickly by the right hemisphere due to the shorter connections favoring contour and configural processing.

7.4 Potential shortcomings of the theory

This theory depends crucially on left and right hemispheres developing at different rates. The empirical support for this is relatively weak (N. Geschwind & Galaburda, 1985; Hellige, 1993; Chiron et al., 1997). Though no justification has been given in this thesis why the hemispheres may develop asymmetrically, I believe there are good reasons for it. The right hemisphere exhibits lateralized connectivity to the autonomic nervous system ((Bud) Craig, 2009), negative affect (Craig, 2005) and generally shows preferences for faster processing (Bar, 2004; Howard & Reggia, 2007). Some authors have suggested a link between RH abilities and the "fight-or-flight" response of the sympathetic nervous system, and an explicit link between faster, low-frequency processing and the "fight-or-flight" response has been found in some baby chickens (Rogers & Andrew, 2002).

There is a potential link between earlier development of the sympathetic system responses across all animals and right hemisphere functions. If this were the case, then one would expect asymmetric timing in the development of the hemispheres across mammals, not just in humans. If true, this would also be consistent with findings of lateralization in visual processing of rhesus macaques (Hamilton & Vermeire, 1988; Vermeire et al., 1998).

Another potential shortcoming of the theory is in the specific timing of the developmental trajectory of callosal and interhemispheric fibers, specifically in the myelination of such fibers. Recent advances in neuroimaging allow the developmental trajectory of myelination to be discovered at a more detailed level. Though the research here represents a proof-of-concept on developmental dependencies between lateralization and interhemispheric communication, as more research is done, these qualitative investigations can become more quantitative. It is worth noting, however, that care must be taken in these quantifications. Both callosal and intrahemispheric connectivity are not unitary

things, and separating maturation of thick, fast fibers from thin, slow fibers is essential for any investigation of the effects described in this paper.

7.5 Extending beyond vision

I believe that many of the principles contained within this theory will extend to other aspects of lateralization, including language and handedness. It is clear that while some aspects language lateralization and handedness may be found even without callosal development (Paul et al., 2007), other aspects (such as prosodic integration) are not. In addition, in typically developing humans, lateralization of language and handedness increase over time (Petitto et al., 2012), again consistent with a role for the corpus callosum in establishing adult-like lateralization. Much more work must be done to carefully understand these underlying suggestions.

The differential encoding model may be extended beyond vision in two ways. First, the differential encoding model simply describes how neighbor information is combined across cortical maps. In this work I focused on retinotopic maps; however, somatotopic, tonotopic, and higher-level object or other maps may be applied through the same principles. The limiting factor in many cases, such as higher-level auditory areas such as Wernicke's area, is that we may not know the functional map to which this encoding difference may apply.

The second way that the differential encoding model can be extended is to focus on how connection spread affects time instead of space. In space, I've argued that the greater spatial correlations of nearby neighbors (such as contours) is captured better by shorter connections, while longer connections allow focusing more on local features. In time, a similar argument can be made: shorter-range connections may sample correlations relationships in time, while longer-range connections focus on features that are local in

time. Thus, longer connections would sample shorter time-scales (more local in time) while shorter connections would successfully integrate over a time envelope.

In fact, there is some consistency in this functional assessment and the biology of auditory and visual systems. An association between mini column spacing and inter-patch spacing has been found in auditory cortex (Seldon, 1981a; R. A. Galuske et al., 2000), with wider spacing of both in the left hemisphere auditory cortex as compared to right. In auditory cortex, this has been associated with lateralization in temporal processing, with wider left hemisphere connectivity associated with temporal discrimination at a faster time-scale. Notably, neither of these differences were found in primary auditory cortex. Recently, wider left hemisphere mini column spacing has been found in the fusiform gyrus (Chance et al., 2013). We predict greater spacing of long-range lateral connections, and show that these are associated with higher-frequency processing.

These are just two of many ways that these findings could be extended to other systems.

Chapter 8

Preliminary Extensions and Future Work

Though the work here has focused rather narrowly on lateralization of visual processing and the corpus callosum, the research touches on more general principles on the computational role of long-range lateral connections, the developmental trajectory of white matter connectivity, the role of conduction delays in neuroscience, and approximating human data using allometric regressions.

A number of projects have been conceived, proposed, or even begun during the course of this dissertation. For most projects, I outline the motivation and general direction. For those with work completed, I give a bit of detail on the data (to date) and potential directions. For those with proposals, I've included the relevant part of each proposal here.

8.1 Follow-ups to the Differential Encoding model

Neuroanatomical collaboration in extra-striate visual cortex

The first type of follow-up study could involve finding a collaborator to search the human brain for asymmetry in long-range lateral connections. The prediction of the model currently is that differences in long-range lateral connections should appear in any retinotopic visual area with an average connection length such that variations could lead to visual processing asymmetries.

Absolute and relative length of long-range lateral connections increase as one goes higher in the visual hierarchy (Amir et al., 1993). When I used data from Amir et al. (1993), I found that areas early visual area V1 has long-range lateral connections that span too little of the visual field to show any asymmetries with the 20% difference in spatial spread reported by R. A. Galuske et al. (2000). I found that retinotopic area V4 does have long enough connections where asymmetries could occur. Interestingly, C. D. Gilbert and Li (2013) postulate that an interaction between V4 and V1 can explain many aspects of contour processing. Therefore, V4 may be the most reasonable area to target for histology.

Similar processing methods to R. A. Galuske et al. (2000), who found the original connection distance difference between the hemispheres in Brodmann area 22, could be used in such a study.

Accounting for current results with a unified model

Currently, there are three different training paradigms used in generating the differential encoding results in this paper:

- The original technique selects autoencoder connections from a Gaussian distri-

bution, then trains the autoencoder model only on the task-relevant images (see Chapters 2 and 3). Though this model accounts for the most behavioral results, it approaches human vision least.

- The natural images technique also selects autoencoder connections from a Gaussian distribution, but uses a dataset of natural images to train the autoencoder (van Hateren & van der Schaaf, 1998) and extracts hidden unit encodings using task-relevant images (Chapter 4). This model uses a log-polar transform of the data in order to model the overrepresentation of central vision in retinotopic visual cortices. This model is much more like human vision, in that it uses task-independent visual features to compute encodings and uses neuroanatomical facts to more closely model those features, but has only been used to model one behavioral paradigm (Sergent, 1982). The results were promising; this model shows smoother and more consistent spatial frequency filtering properties than the original technique and can be trained once, then its encodings on any novel set of stimuli can be extracted and tested on any behavioral task.

- The developmental technique uses developmental pruning during asymmetric visual experience and learns asymmetric connection patterns. It then follows the natural images technique. Those this model is the most constrained, makes the fewest assumptions, and shows the expected spatial frequency encoding differences, but hasn't been used to model any task-related differences.

A clear step forward would be to use the developmental technique to account for all of the behavioral results. The developmental technique should include many of the benefits of the natural images technique, as it also uses natural images during its training, shows more robust frequency encoding properties, and only needs to be trained once. However, as seen in Chapter 4 and discussed in Section 7.2, spatial frequency encoding

differences in the developmental model are likely too small to show the behavioral asymmetries shown. A couple of options are available:

- While exploring developmental model parameters, I noted that although the post-training lateralization was weak in the network, training parameters could be changed to increases that asymmetry. Two parameters were particularly effective. First, the difference in spatial frequency content of training images could be increased between the hemispheres. Second, increasing both the initial spatial spread of connections and initial number of connections per hidden unit increased the asymmetries in the networks after training. Though these parameter changes are unlikely to reflect visual experience or neurally plausible parameters, the network would be more likely to show behavioral asymmetries.

- Plaut and Behrmann (2011) suggest that interhemispheric competition between representations leads to complementary lateralization of words and faces, and Reggia and Schulz (2002) suggest that inhibitory interhemispheric connections can accomplish this best. One way to enhance developmental asymmetries in these networks would be to interconnect the two model hemispheres with inhibitory connections after training completed, then to continue training with those connections. This is similar to the developmental trajectory postulated in Chapter 7, where early on the hemispheres are more independent due to immature, noisy axons, and then lateralization in face and word processing comes online as the corpus callosum matures and children learn to read.

Contrast Balancing

One of the most exciting suggestions in this thesis is that the fundamental visual lateralization ability may not be about spatial frequency processing abstractly, but instead

about contour processing via long-range lateral connections. Instead, spatial frequency processing differences only arise as a byproduct of a bias in contour processing. This could explain why studies manipulating spatial frequencies directly have extremely variable effects, as their effect on contour processing is itself variable and highly dependent on the manipulation found in each study.

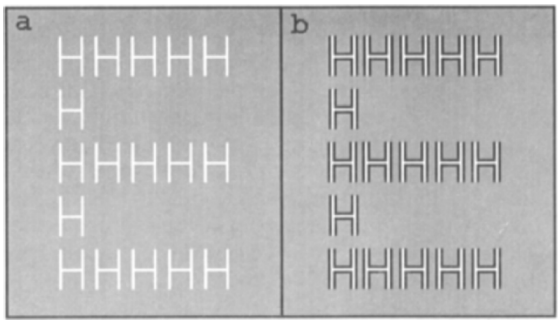

Figure 8.1: (a) A hierarchical letter stimulus. (b) The same stimulus with contrast balancing applied (Lamb & Yund, 1993). This eliminates the low spatial frequencies from the image while maintaining the global-level contour.

This dichotomy between spatial frequencies and contour processing has been studied in the behavioral literature under the label of "contrast balancing". In most studies using Navon figures, the external contour of the global-level figure has a higher contrast than that of the embedded local-level figures (Figure 8.1a). In contrast balancing studies (Lamb & Yund, 1993; Brand & Johnson, 2013), contrast differences at the global and local levels of a Navon stimulus are normalized by surrounding white local-level figures with black borders (Figure 8.1b). This eliminates the low spatial frequency information while keeping global-level contour information, dissociating the two types of information and allowing direct exploration of whether contour or spatial frequency information has primacy for various tasks.

Lamb and Yund (1993) found that while contrast balancing eliminated the global precedence effect (faster reaction times to global-level forms), suggesting that this effect

is mediated by low spatial frequency information. However, they found that other aspects of local / global processing were not affected, such as effects of attentional biasing towards local or global forms, and interference between a distractor at the non-queued level. Brand and Johnson (2013) found that contrast balancing also has specific effects on different types of scene perception. The overall conclusion was that while some aspects of local / global processing may be driven by spatial frequency processing, many others may not be.

This type of result offers a point of separation between the double filtering by frequency (DFF) model and the differential encoding model. The DFF model in principle cannot account for local/global processing results that are not related to spatial frequency differences. The differential encoding model does not implement spatial frequency processing; rather, it implements a neural mechanism that, in some cases shows spatial frequency filtering properties. However, looking at 2D spectrograms of frequency filtering, it's also clear that the differential encoding model is not a pure frequency filter; at a single spatial frequency (a circle on the 2D plot), some phases show spatial frequency filtering, others do not. Because the DE has a neural mechanism behind it's behavior, and not an abstract frequency filtering procedure, it could account for these results.

The proposal here is to implement one of the contrast-balancing studies from Lamb and Yund (1993) in the differential encoding model, to see whether the model can account for any of their results. The procedure is simple. First, I would train a differential encoding model on natural images. Then I would extract hidden unit encodings from the contrast-balanced stimuli used by Lamb and Yund (1993). Finally, I would train a classification network on the behavioral task that experimental subjects were tested on. I would compare behavioral differences between the left hemisphere and right hemisphere models to response-time differences on lateralized presentation to the right visual field

and left visual field, respectively. I would also look at whether the output images from each model hemisphere show differences in spatial frequency encoding.

I have no prediction how this model would perform. Though the model dissociates spatial frequency and performance on classification tasks requiring contour processing (I have seen models with little spatial frequency encoding differences show behavioral asymmetries and vice verse), the nature of that dissociation has not been characterized.

An exploration and analytic explanation of connection spread

What drives the unexpected association between short connection spread and low spatial frequency processing? How general is it, and is there an analytical way to describe it?

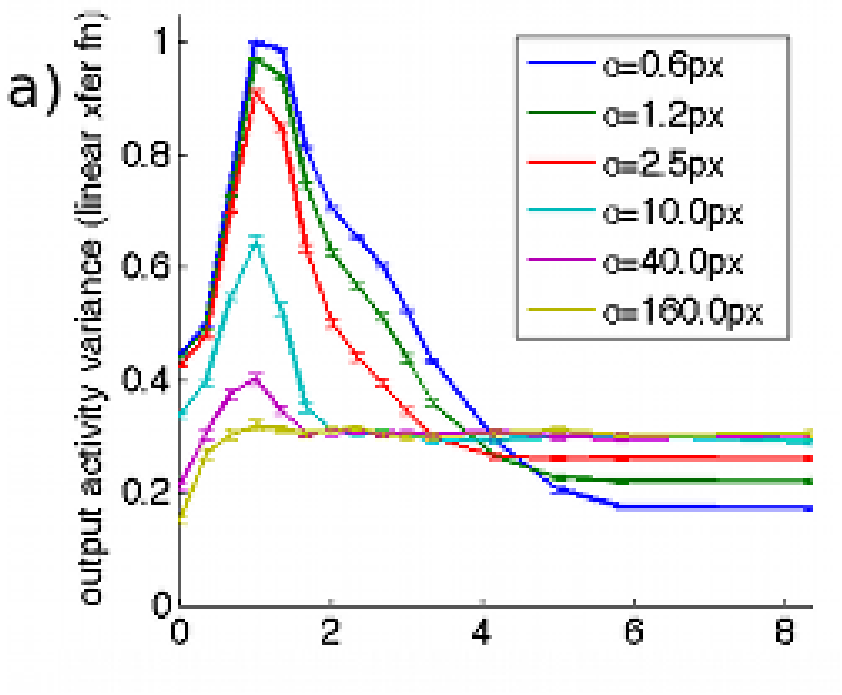

Figure 8.2: Spatial frequency vs. variance in output activation. As σ decreases, bias for low spatial frequency encoding increases, with a penalty for high spatial frequency information.

I've done some preliminary work exploring the connection association (see Appendix A for an abstract summarizing that work). I implemented a simple 2D neural network with a single output node, where input-to-output connectivity mirrored that of the differential encoding model (selected from a Gaussian PDF centered at the output unit location). This simplified network was developed under the view that the input to hidden unit connections represent the lateral propagation of activation to neighboring units.

The connections were given random weights with a non-zero mean. The output unit activation was computed for 64 different 2D sin wave gratings–8 different frequencies at 8 different phases. The output variance was plotted as a function of spatial frequency, with lines representing different spatial frequencies overlaid (Figure 8.2). Greater output variance was interpreted as showing greater encoding of each individual stimulus, and therefore better at global-level / contour-level discrimination. This work showed a very promising spatial spread-by-frequency interaction, where networks with smaller spatial spread showed greater variance over the lower frequency gratings, and lower variance over the higher frequency gratings–consistent with results found for the differential encoding networks.

Unfortunately, variance is a poor measure of encoding ability, and a more analytical analysis is be needed to approach a more general theory behind this phenomenon. The proposed work here is to implement these changes in the work. In addition, I would continue to explore the model from a sparsity or more general sampling perspective. Preliminary experiments suggested that the spatial frequency effects seen were not due to the spatial spread of connectivity per se, but rather due to changes in the connection density within a receptive field. This sampling perspective could be a way to investigate an analytical relationship between sampling density and spatial frequency processing that would be informative to a few fields of discipline, including computational neuroscience.

Reimplement the connection asymmetry in physiologically plausible models

The differential encoding model is an extremely simplified model of long-range lateral connections. This simplicity of the model allows mapping results from the neurocomputational domain into the cognitive domain, but it leaves open a question as to whether this connection asymmetry would drive contour processing differences in more physiologically realistic models. A number of alternative models of long-range lateral connections exist and all are more neurophysiologically plausible. A good test of the differential encoding model would be to reimplement the connection distance asymmetry in one of these models and analyze the contour processing and spatial frequency encoding differences in these models.

Dr. Steven Grossberg's lab has developed a neurophysiologically plausible model of long-range lateral connections that have shown numerous interesting visual processing behaviors, such as contour processing, illusory contours, and other grouping phenomena (Grossberg & Williamson, 2001; Grossberg, 2010). These models are very careful about the laminar structure of cortex, obey weight regularities, are attention-aware (Grossberg, 2010), and are sensitive to the same contrast changes that have shown to affect the level of asymmetry observed (Grossberg & Raizada, 2000). Unfortunately, Grossberg's models are generally thought to be challenging to understand and implement; I have had little luck understanding nor implementing them myself, nor in finding people who have been able to do so themselves. In addition, despite requests to the lab, no code has been made available to me for my research use.

Dr. Charles Gilbert and Dr. Wu Li have a long history of neurophysiological recordings of long-range lateral connections. Their recent publication detailed a theory about an interaction between V1 and V4 for top-down effects on contour processingPiech

et al. (2013)–with V4 having an average long-range lateral connection length that is long enough to show asymmetries. The model is very new and has not been tested on many images, and so a positive result in the model would be less meaningful than in Grossberg's model. However, the mathematical details of the model and analysis procedures are nicely detailed in their paper, making it more feasible to implement and modify this model.

Other models exist, including models that focus less on neurophysiology and more on low-level visual processing (e.g. Mely and Serre (2013)), that could explored more simply and extend the model to encompass more low-level vision.

8.2 Follow-ups for interhemispheric neural network models

Reimplementation of the developmental model in a spiking neural network framework

In Section 5, I explore effects of timing variability on learning. That model implements timing variability as noise on an instantaneous firing rate within a framework using rate-coded units. While I argue there for a mapping between spike-time variability and noise in the instantaneous firing rate, reimplementing this model in a spiking neural network (SNN) would allow direct investigation on how timing variability on conduction delays affects neural coding. The results of such an investigation could uncover unexpected side-effects and potential neural coding mechanisms that a rate-coded network might not be capable of. For example, SNNs have multiplexing capabilities that rate-coding networks must carefully implement, allowing a greater number of sub-networks that avoid overlapping in space and time (Izhikevich, 2006). The developmental trajectory

of such networks with noise variability could be of interest.

The major issue with implementing this project in a SNN that there is no well-accepted training algorithm for SNN. Most SNNs use spike-time dependent plasticity (STDP) to learn synaptic weights, or manually set synaptic weights and allow STDP dynamics to modify them. Without a training algorithm, training the network on a task such that performance could be assessed with and without interhemispheric connections is impossible.

The Neural Engineering Framework (NEF) (Eliasmith & Anderson, 2004) is a hybrid rate-coded / SNN framework. This framework contains a mathematical framework for deriving weights to do arbitrary function approximation using leaky integrate-and-fire neurons. This framework has been used to implement SPAUN, neural network model capable of accomplishing a number of cognitively interesting tasks through perception, task-selection, and motor selection and output mechanisms (Eliasmith et al., 2012). The framework has been extended to allow use of STDP, to try and capture spike time-related events after weight derivations. Unfortunately, the NEF has no developmental component–weights are computed directly, rather than stochastically learned, making the NEF inappropriate for developmental studies.

Progress is being made on training SNN using stochastic methods; when such an algorithm is available, then this work could be revisited.

Examine the effects of mixed interhemispheric transfer

As discussed in Chapter 1, interhemispheric transfer is quite heterogeneous. Early sensory/motor areas (vision, somato-sensation) tend to interconnect along the midline with thick, myelinated fibers–good for fast transmission (Aboitiz & Montiel, 2003; Doron & Gazzaniga, 2008). When examined across species, these fast fibers increase their size with brain size, indicating that speed is important (Olivares et al., 2001). On the other

hand, association cortices and prefrontal cortices interconnect diffusely across the corpus callosum, using thin fibers that are more frequently unmyelinated. These thin fibers do not change across species with different brain sizes, and so lead to longer conduction delays in larger brains.

Given the diversity of connectivity across the corpus callosum, it's easy to see that interactions over the corpus callosum can be highly task-dependent. For example, a stimulus presented centrally may make use of fast, midline callosal connections, whereas a stimulus presented laterally likely cannot.

I have attached a past proposal In Appendix B for a model capable to explore these effects. The model is a variation on Ringo et al. (1994)'s model and allows implementation of different types of interhemispheric transfer, including early sparse, fast transfer and later slow, diffuse transfer. Exploring such a model could give insight into how experimental paradigms such as lateralized presentation (where a stimulus is presented laterally to the left and right, and differences in behavior are attributed to differences in processing of the contralateral hemisphere) and the Poffenberger paradigm (where reaction time differences between presentation of stimuli to the ipsilateral and contralateral side as the response button are interpreted as interhemispheric transfer time) work.

With such work completed, then embedding asymmetries (such as differences in the spread of long-range lateral connections) into this framework could give more nuanced insight into

Examine the effects of axon diameter distribution

A more speculative, but important project could involve examining effects of having a distribution of conduction delays interconnecting cortical areas. In Chapter 5, I postulated that this distribution of conduction delays could lead to low-latency processing

and facilitate throughput when slower, broadband information arrives.

A previous association made is between shorter delays with a spike-time code and longer delays with a rate code (S. S. H. Wang, 2008). Other papers have associated shorter delays with "driver" synapses and longer delays with "modulatory" synapses (Sherman & Guillery, 1998; Sherman, 2007). Design of a hybrid system where a fast spike-time code facilitates processing of a slower rate code could be a neural computation framework fits with the distribution of delays as well as the suggestions by S. S. H. Wang (2008) and Sherman and Guillery (1998).

It is also known that, just as interhemispheric fibers covary in their transmission speed and function, so do intrahemispheric fibers (Innocenti et al., 2013). Thick axons are extremely expensive volumetrically (Harrison, Hof, & Wang, 2002; S. S. H. Wang, 2008), with white matter connectivity the major constraint on brain architecture in large-brained animals like humans (Zhang & Sejnowski, 2000; Changizi, 2009). There is an important role of thick, fast fibers in the brain, and computational modeling is a good place to explore what functional or energetic properties make the volumetric trade-offs worthwhile.

8.3 Extensions of the allometric analysis of the human corpus callosum

As mentioned in Chapter 1, surprisingly little data exist for the human corpus callosum. High-quality electron microscopic data exist for cats and monkeys in developmental and adulthood (Berbel & Innocenti, 1988; LaMantia & Rakic, 1990a; LaMantia & Rakic, 1990b) and show exciting patterns of great proliferation and massive pruning of thin, unmyelinated fibers in the corpus callosum, along with age-related changes to fiber density, fiber count, and myelination. Nonetheless, only a single sample of the human

corpus callosum has ever been imaged with an electron microscope and published–of a 45 year-old sample (Aboitiz et al., 1992). Only one developmental paper has been published (Luttenberg, 1965) and is marred by its use of a low-acuity light microscope, reporting fewer fibers in the human corpus callosum at birth (143 million) than reported in adulthood (200 million; Aboitiz et al. (1992)) and far below my best estimate of the fiber count at birth (800 million; see Section 5.7). It is clearly challenging to get access to freshly deceased in-tact human brains, then to have facilities to process and image them with an electron microscope–particularly of younger ages necessary to view comparable ages to animal data.

Having these data could be extremely valuable. Clearly they could clarify the development of human interhemispheric transfer, which I've speculated about in this thesis (see Section 5.7). The impact goes beyond that, however. The corpus callosum has become a testbed for diffused-based imaging. Because of its very clear fiber directionality without worries of crossing fibers, and the fact that histology of the corpus callosum is easier than all other white matter fibers, it's been used over and over to test new technologies.

For example, one of the latest uses of callosal imaging is in trying to derive axon diameter distributions from neural data directly, using histological samples from the rat corpus callosum as a point of comparison Assaf, Blumenfeld-Katzir, Yovel, and Basser (2008); McNab et al. (2012). However, current results still do not seem to match the histological samples well. Were we able to associate cellular-level neuroanatomy with MRI-based diffusion signals, it would be possible to estimate microstructural properties about white matter tracts from a combination of structural MRI and diffusion imaging. Currently, associations between diffusion imaging and microstructural properties are speculative and qualitative.

One potential use of allometry, however, is to predict axon diameter distributions

across the human lifespan from animal data. This project would combine cross-species developmental allometry (Clancy et al., 2007) with developmental and adult animal data (Berbel & Innocenti, 1988; LaMantia & Rakic, 1990a; LaMantia & Rakic, 1990b; S. S. H. Wang et al., 2008) to predict axon diameter distributions. These predictions would be informed by the existing human data (Luttenberg, 1965; Tomasch, 1954; Aboitiz, 1991; Aboitiz et al., 1992; Riise & Pakkenberg, 2011; Hou & Pakkenberg, 2012), and a combination of them could help fill in the missing smallest fibers that are missed by using a light microscope.

After such predictions are made, then a forward model for diffusion imaging could be created, to take a micro-structurally accurate model of the corpus callosum and to predict diffusion-based signal for that model. Forward models uniquely specify their deterministic measurements, and good forward models have been highly used in EEG analyses for constraining source localization–the inverse problem that is fundamentally ill-posed.

This project was submitted to the UCSD INC as a post-doc fellowship application. A detailed version of this proposal can be found in Appendix C.

Appendix A

Preliminary research: Analysis of an anatomically-based model of hemispheric asymmetry shows spatial frequency tuning[1]

We have developed a simple model of hemispheric asymmetry (Cipollini et al., 2012; Hsiao et al., 2013) based on data showing that there are anatomical differences in patch connectivity between the hemispheres. Specifically, the left hemisphere shows longer-range connections between cortical patches than the left. We model this using the simplest possible networks, autoencoders with differential connectivity distributions (Figure A.1). We think of the hidden units of this network as representing the interactions between nearby cortical patches. Surprisingly, this simple model is able to account for local/global effects in hierarchical letter perception, using Navon stimuli (large letters made of small ones). The LH model is faster at detecting local targets and the RH model

[1]This chapter was submitted as an abstract to the COSYNE 2013 conference.

is faster at global ones.

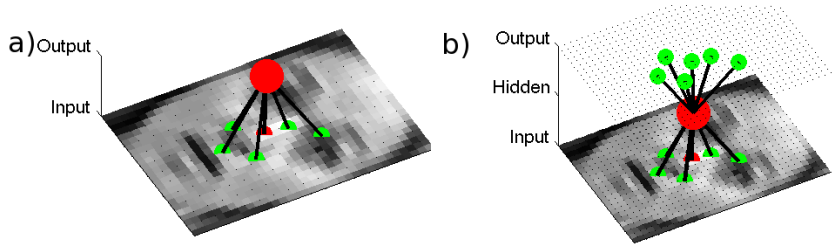

Figure A.1: (a) Two-layer neuron with a sparse receptive field. (b) The differential encoding model, an autoencoder with hidden units using this sparse receptive field. This model has been used to account for lateralization in visual processing by varying the spatial spread of the sparse connections.

Here we analyze the spatial frequency (SF) encoding properties of these networks. We implement three computational experiments, each showing that connections with a narrow spread show a strong LSF advantage, while connections with a wider spread show a weak HSF advantage. We show that this association is due to the lack of a center-surround structure and is modulated by overall connection density.

A.1 Methods and Results

In Experiment 1, we create a two-layer feed-forward neural network model, with a single output connecting to N input positions in a 2D image plane (20x20) (i.e., just the input and one hidden unit in Figure A.1). Connections are sampled from a Gaussian distribution centered over the output unit's position on the input. Each output in our model represents a single location in the input space; its connections to the input represent connections to nearby neighbors in the input space. In this experiment, the connection weights are random positive numbers, normalized such that the average output unit activity across all stimuli for a single network is approximately equal for all N and σ. Other weight configurations were tested, with no notable differences.

We test the SF tuning properties of these networks by varying the spread (σ) and number (N) of connections from the input to a single hidden unit, and then measuring the activity of this unit across 64 sine wave grating inputs (8 phases and 8 orientations), for each of 10 different SFs. We interpret greater variance as encoding more information, and therefore showing a greater encoding preference for that SF.

Figure A.2a shows SF preferences for 6 different values of σ with N=10 connections. We see greater encoding (higher variance) of LSFs as σ DECREASES, and small, consistent decrease in encoding HSFs. Figure A.2b shows SF preferences for 5 different values of N with σ=10px. The raw variance decreases with increasing N; further analysis shows that SF tuning sharpness increases. Together, this suggests that different densities of connections lead to different input encodings; for lateral connections, this means different contour processing where relative spread of connection varies: by position in the visual field and visual processing hierarchy.

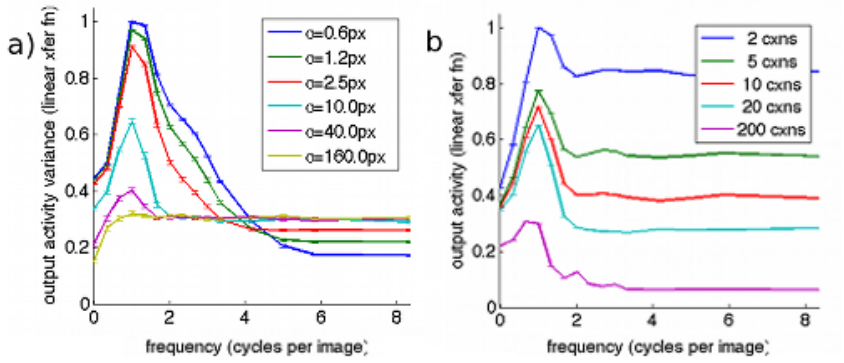

Figure A.2: Spatial frequency vs. variance in output activation a) [N=10] As σ decreases, bias for low spatial frequencies increases, with a penalty for high spatial frequency information. b) [σ=10px] As N increases, tuning becomes narrower and weaker.

In two further experiments, we create two autoencoders using these connectivity patterns (Figure A.1) and train them on 100 34x25 patches of natural images (van Hateren) using backpropagation of error. In Experiment 2, the two autoencoders select

connections to the input and output with different σ (4px vs 10px), and we measure how this affects the relative SF encoding of the networks. In Experiment 3, both autoencoders start with the same connection patterns, and we see how changing the SF content of training images affects what connections the network uses.

All networks have the same number of connections (N). Multiple instances of each network were randomly generated, and results averaged across networks.

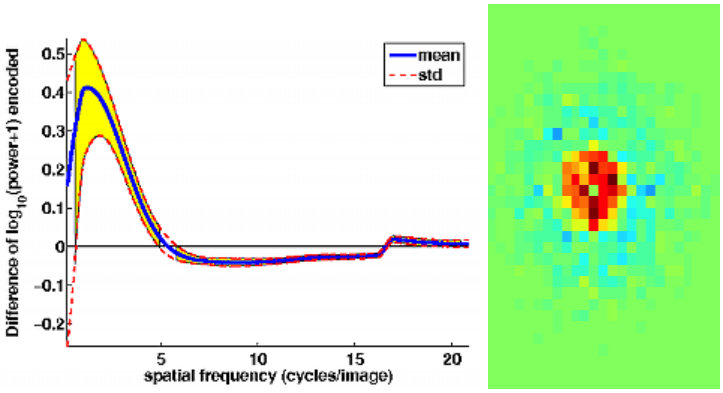

Figure A.3: (a) Spatial frequency encoding advantage for smaller spread (σ=4px) networks, compared to larger spread networks (σ=10px). Low spatial frequencies (left) show a positive advantage; High spatial frequencies (right) show a disadvantage. Mean in blue, stderr in dashed red, yellow indicates statistical significance. Inset: 2D power spectrum difference, used to compute the 1D spectrum difference. (b) Difference in connection distributions from hidden units to inputs [low-pass (LP)] - [high-pass (HP)]. The red center indicates more short-range connections for the LP-trained networks; the blue ring indicates more long-range connections for the HP-trained network.

In Experiment 2, after the two autoencoders sample connections (N=12) with different σ and trained to some error criterion, output images are extracted and their spectral power is computed and compared (Figure A.3a, inset). Figure A.3a shows that networks with smaller connection spread (σ=4px) show better LSF encoding, while networks with larger connection spread (σ=10px) show better HSF encoding.

In Experiment 3, the two autoencoders start with exactly the same connectivity pattern ($\sigma = 10$px, $N_{init} = 25$). One network is trained on low-pass filtered images; the

other on high-pass filtered images. While training the weights, we also prune the weakest connections ($N_{final} = 12$). After training, we pool the distribution of connections for hidden unit, and compare. The networks trained on low-pass images keep more of the short-range connections, while networks trained on high-pass images keep more of the long-range connections (Figure A.3b).

A.2 Discussion

Here we provide evidence that networks with no center-surround structure show an opposite association between spatial spread and SF tuning. We showed that the SF tuning was parameterized by both spread of connections (σ) and number of connections (N)–in other words, the connection density. Our tests with classic receptive fields (not detailed here) show that connection density only affects the broadness of SF tuning, but not the peak location as it does here.

We have shown elsewhere that, indeed, these networks can give rise to differences in contour processing. These SF biases introduced by these "patchy" connection networks can account for local/global, face, and grating visual processing asymmetries, and that these asymmetries plausibly arise from a developmental asymmetry in the timing of connection pruning (Experiment 3).

Appendix B

Proposed work: The role of multiple projection systems within the corpus callosum[1]

The only model architecture of interhemispheric integration that incorporates conduction delays and integration over time, published by Ringo et al. (1994), has a very odd set of results. After post-training lesioning of interhemispheric connections, the model shows good performance at early time-steps, then performance decays as over processing steps (see Figure 5.2). This decay occurs despite the fact that all intrahemispheric connections remain intact, each hemisphere has all the information necessary to solve the task itself, and each hemisphere is able to solve the task at early time-steps on its own.

These results don't make intuitive sense; interhemispheric integration shouldn't be necessary to maintain activity over time. Rather, interhemispheric integration should augment and modulate intrahemispheric activity (Innocenti, 2008). In addition, the results

[1] This proposal was originally written for my dissertation proposal and is repeated here for reference in future directions.

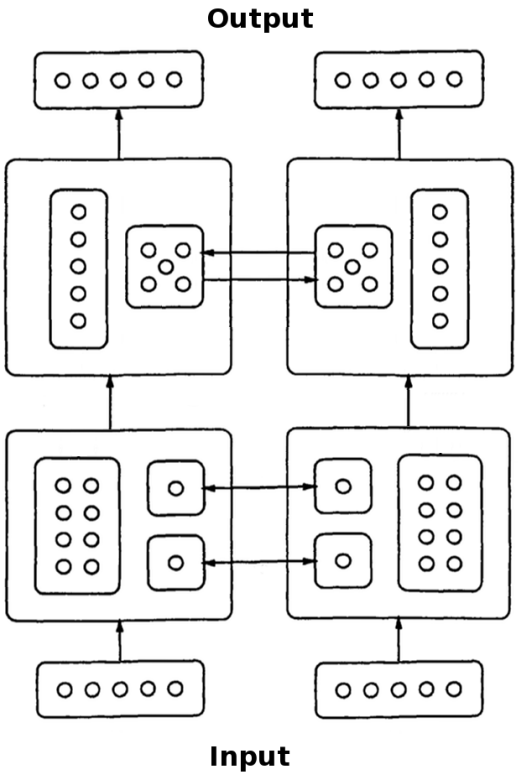

Figure B.1: Proposed architecture for investigating the interactions between the two callosal interhemispheric transfer systems.

are inconsistent with general observations from two methods of hemispheric-independent processing: the Wada test and split brain patients. In both cases, data suggest little change in behavior when one hemisphere operates independently of the other (ignoring, for the moment, asymmetries between the hemispheres), regardless if the independence is dynamic (i.e. Wada test; Paolicchi (2008)) or static (i.e. split brain; Gazzaniga (2000)).

The model work proposed here aims to mirror the structure and logic of Ringo et al. (1994) while addressing a number of features of their model and training paradigm that may underlie these unexpected results. In order to do so, the desired model behavior is first clearly defined. Then, in order to model callosal connectivity patterns more closely and address training issues, changes to the Ringo et al. (1994) modeling study are proposed. Finally, a set of experiments and expected results are given for the updated

model architecture, and interpreted according to the types of connectivity being modeled.

B.1 Desired Model Behavior

As discussed above, the general observation seems to indicate that, if a task can be completed with an isolated cerebral hemisphere, it will be. While this may be true when the hemispheres are forced to compute alone, in what cases will it be true when both hemispheres are computing and remain interconnected?

Transfer across the corpus callosum has recently been functionally divided into two systems (Aboitiz & Montiel, 2003; Doron & Gazzaniga, 2008). The first, termed the "primary"-type system in this proposal, features fast, sparse connections that connect along the midline, and are found in primary motor and sensory cortex. The second, termed the "association"-type system in this proposal, features slower, more diffuse connectivity, and represent the vast majority of fibers in the CC.

There are two cases to consider: First, if a task *cannot* be completed without information from both hemispheres, then at latencies too fast for interhemispheric integration to occur, subjects will perform at a level reflecting intrahemispheric processing only. With enough time for interhemispheric integration to occur, task performance should achieve high levels of accuracy. The amount of time necessary to achieve interhemispheric integration will be dependent on the position of the stimulus presentation (if near the midline, fast "primary"-type sensory fibers may contribute to fast interhemispheric transfer; if presented laterally to one side, the "primary"-type sensory fibers, which transfer only around the midline, will be ineffective and later, slower "association"-type transfer would be necessary) and the speed at which intrahemispheric bottom-up sensory processing occurs (which interhemispheric transfer must coordinate arrival of information with to allow integration to occur).

Second, in cases where a task *can* be completed without interhemispheric integration, the expectation is for interhemispheric transfer to take on a more facilitatory or modulatory role (Innocenti, 2008). In this case, output at short latencies should show high accuracy, reflecting intrahemispheric processing that has been able to complete regardless of the success or failure of interhemispheric integration. At later latencies at which interhemispheric integration has occurred, a small increase in performance is expected, but expected to be limited due to ceiling effects.

In the modeling work, the Ringo et al. (1994) procedure of training a model with interhemispheric connections intact, then lesioning those connections before testing will be used. The expectation for behavior in this case again follows these two cases. First, if a task *cannot* be completed without information from both hemispheres, after lesioning performance should reflect the ability to respond with only intrahemispheric of the isolated hemisphere's sensory input. Second, if a task *can* be completed without information from both hemispheres, then the hemisphere should initially show the same level of performance regardless of the state of the interhemispheric connections. After latencies where interhemispheric integration would have occurred, performance should remain at the same level, as no increase can occur since no new information arrives from the other hemisphere, and no decrease need occur, as the intrahemispheric processing can continue independent of the other hemisphere..

The model architecture I propose below is intended to provide these behaviors.

B.2 Model Architecture

A model architecture similar to the Ringo et al. (1994) architecture will be used (See Figure 5.1a), but with the following changes:

- *No recurrent connections within a layer*: Each unit in Ringo et al. (1994) model

is a leaky integrator, where activity shows a slow exponential decay with a time-constant shared by all units. Within-layer maintenance of activity will be implemented by adjusting this time-constant; no within-hemisphere dynamics will be considered, to simplify analysis and interpretation of the model.

- *No intra-hemispheric recurrent connections*: Though inter-area connectivity is highly recurrent/reentrant (e.g. Markov et al. (2010, 2013), without a specified functional role in solving the simple tasks used here, they simply make the network harder to train and analyze. By removing these connections and controlling network complexity, understanding of network complexity and behavior can be built carefully and iteratively.

- *Split outputs*: The design is to model interhemispheric integration at "cognitive" levels while manipulating conduction delay. Allowing integration at the output via backpropagation of error confounds the ability to manipulate interhemispheric integration. Splitting the output nodes forces interhemispheric integration to occur only across the specified interhemispheric connections. This design aspect follows that of Lewis and Elman (2008).

  In order to produce a unified output, one of two algorithms will be employed: either a horse-race algorithm will occur (where the first hemisphere to reach an activation threshold triggers a response), or an integration algorithm (where the combination of activation reaches an activation threshold and triggers a response). It is unclear which decision process reflects human instructions such as "respond as fast and as accurately as possible", though two sources point to a horse-race model:

  - One study testing unilateral and bilateral stimuli report that "bilateral presentations followed a race model with the superior right visual field (RVF)

dominating responses" (Zaidel & Rayman, 1994)

  - On further examination, conditions from Sergent (1982) which have at least one target and non-identical stimuli show a race effect (see Figure B.2).

- *Input duration*: In models that run in time, inputs can be kept "on" for any number of time-steps. It is unclear how long Ringo et al. (1994) kept their inputs on. I believe that, in order to achieve 100% training criterion on models that propagated activity over a large number of time-steps, inputs must have been kept "on" for all time-steps. In work derivative from this one, that input time will be manipulated, corresponding to stimulus exposure duration; in this study, the input will be kept "on" at all time-steps.

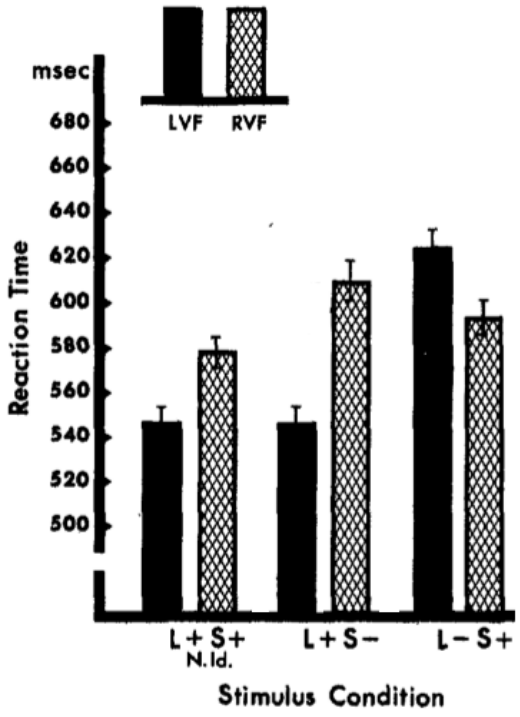

Figure B.2: Compare response with a (non-identical) target at both levels with performance for the preferred level for each VF (LVF/RH for L+S+ vs L+S-, and RVF/LH for L+S+ vs L-S+.

B.3 Training Paradigm

Ringo et al. (1994)'s training paradigm consisted in training networks to produce an output after a maximum number of time steps. Each data point in Figure 5.2 represents a set of independently trained and tested models, and not different latencies of a single set of models trained once and tested at different latencies. Human behavior shows a minimum time to response, and the ability to respond over longer delays. In addition, it is well-known that training networks over long numbers of time-steps can be problematic.

To address these issues, each instance of the model will be trained at multiple latencies to produce a correct response. This may help separate between interhemispheric processing differences and differences in maintaining information over time. Each model will also be tested (with interhemispheric connections removed) at each latency. During learning, latencies will be randomly interleaved. Alternately, a procedure of "starting small"–but in time–may be employed, where models are trained on short latencies first, and later on longer latencies, a la Elman (1993). This procedure makes sense for learning purposes, but isn't how people seem to learn–response times get shorter with age and experience.

In addition to a different training procedure, training stimuli will also be different, using the logic and stimuli of Lewis and Elman (2008). As described in Section 5.2.1, Lewis and Elman (2008) pointed out that, because input and output patterns were fully input into each model hemisphere, neither model needed to have any interhemispheric integration at all; either model hemisphere could solve the task independently of the other. To be able to better tease apart the roles of intrahemispheric processing and interhemispheric processing, Lewis and Elman (2008) modified the Ringo et al. (1994) architecture by splitting the input and output layers into two banks of five units each, and used pairings of 10-digit binary strings. Thus, each hemisphere only received half of the

10-digit input and only produced half of the 10-digit output pattern.

Left hemisphere			Right hemisphere		
Input		Target	Input		Target
1 0 0 0 1	→	**0 0 0 0 1**	**0 1 0 0 0**	→	**0 0 0 0 1**
0 1 0 0 0	→	0 1 1 1 0	0 0 1 0 0	→	0 1 1 1 0
1 1 1 1 0	→	1 0 0 0 1	1 0 1 0 1	→	1 0 0 0 1
1 0 0 0 1	→	**0 1 0 1 1**	**1 0 1 0 1**	→	**0 1 0 1 1**
1 1 0 1 1	→	1 0 0 1 1	0 0 1 0 0	→	1 0 0 1 1
1 1 1 1 0	→	1 0 1 1 0	0 1 0 0 0	→	1 0 1 1 0
0 1 0 0 0	→	1 0 1 1 1	1 0 1 0 1	→	1 0 1 1 1
1 1 1 1 0	→	1 1 0 0 1	0 0 0 0 0	→	1 1 0 0 1
1 1 0 1 1	→	1 1 0 1 0	0 1 0 0 0	→	1 1 0 1 0
1 0 0 0 1	→	**0 1 0 0 0**	**0 0 1 0 0**	→	**0 1 0 0 0**
1 1 0 1 1	→	1 1 1 0 0	1 0 1 0 1	→	1 1 1 0 0
0 1 0 0 0	→	1 1 1 0 1	0 1 0 0 0	→	1 1 1 0 1
1 0 0 0 1	→	**0 1 0 0 1**	**0 0 0 0 0**	→	**0 1 0 0 1**
0 1 0 0 0	→	1 1 1 1 1	0 0 0 0 0	→	1 1 1 1 1
1 1 1 1 0	→	0 0 1 0 0	0 0 1 0 0	→	0 0 1 0 0
1 1 0 1 1	→	0 0 1 1 0	0 0 0 0 0	→	0 0 1 1 0

Figure B.3: "Four-way ambiguous" input-output pairings, representing 50% of the total training input-output pairings. Each 5-digit input to a hemisphere could produce two different 5-digit outputs; only interhemispheric integration can disambiguate which of the two for that hemisphere to produce. Each 5-digit output could have been produced from two different 5-digit inputs; only interhemispheric integration of the 5-digit input to the other hemisphere disambiguates which input produced that output. Adapted from Lewis and Elman (2008)

Lewis and Elman (2008) then manipulated their input-output pairings such that 50% of the pairings required interhemispheric integration for a hemisphere to produce the correct 5-digit output ("ambiguous" patterns), and 50% of the pairings did not require any interhemispheric integration for a hemisphere to produce the correct 5-digit output. Figure B.3 shows examples of the "four-way ambiguous" patterns, where each hemisphere's 5-digit input specifies two possible 5-digit outputs, and only integration from the other hemisphere can specify which of the two is the correct one. In this same set of patterns, each 5-digit output of a hemisphere could be produced by two different 5-digit inputs to that hemisphere, with interhemispheric integration necessary to determine which of the two possible inputs had produced that output.

Using this dataset, chance performance for any individual hemisphere is $1/32$

(there are 32 possible outputs for a 5-digit binary string, and each hemisphere has 5 binary output units). However, chance performance on an "ambiguous" input to a single hemisphere is 50%, as the 5-digit input to a single hemisphere corresponds to only two possible outputs.

Experiments

The basic experimental paradigm will follow the form of Ringo et al. (1994): First, construct a network with particular interhemispheric delays between hidden units at the first and second hidden layers. These interhemispheric delays can take on two values; a faster value corresponding to the CC's "primary"-type system, and a slower value corresponding to the CC's "association"-type system. After constructing the network, train the model on the input/output pairings. Finally, after training has reached the training criterion, lesion the interhemispheric connections and test model performance.

Unlike Ringo et al. (1994), however, the following will be done:

- Ringo et al. (1994) always used the same interhemispheric delay for interhemispheric connections at the first and second hidden levels. Here, that will not be the case; the connectivity between the two banks of hidden nodes will be manipulated independently. This will allow for the analysis of all four possible interactions between "primary"-type and "association"-type systems in this model architecture. This is of theoretical interest, to characterize this model architecture's behavior more completely. This design may also be of practical interest, as each combination of interhemispheric delays may correspond to isolated interactions between intrahemispheric and interhemispheric processing of interest in cognitive neuroscience (see Figure B.5).

- While Ringo et al. (1994) only manipulated conduction delay to simulate slow

and fast connectivity, other aspects of the "primary"-type and "association"-type systems will be implemented. Besides manipulating the conduction delay, the number of units that have interhemispheric connections and their connectivity patterns will be manipulated as well. When the "primary"-type system is used at a hidden level, shorter conduction delays that connect topographically (to a "homologous" unit on the other side) will be used to implement interhemispheric connectivity at that hidden level. When the "association"-type system is used at a hidden level, longer conduction delays over a greater number of interhemispheric connections that connect diffusely with other interhemispheric units will be used to implement interhemispheric connectivity at that level.

This more accurately reflects the "primary"-type and "association"-type systems, where the "association"-type system trades off higher levels of connectivity with slow speeds.

Expected Results

Figure B.4 is an implementation of the model behaviors described in Section B.1. For all models, I expect patterns that can be completed intrahemispherically (50% of the dataset) to be unaffected by the elimination of interhemispheric fibers. This is in stark contrast to the Ringo et al. (1994) model, where all pattern input/output pairings could be computed intrahemispherically, and are only done so initially, with performance dropping off over time.

For patterns that require interhemispheric transfer to be completed, I expect that the pattern of results will depend on the configuration of interhemispheric integration systems at the two hidden layers. Intrahemispheric processing can eliminate most output patterns, and specify one of two possible patterns. The different configurations should

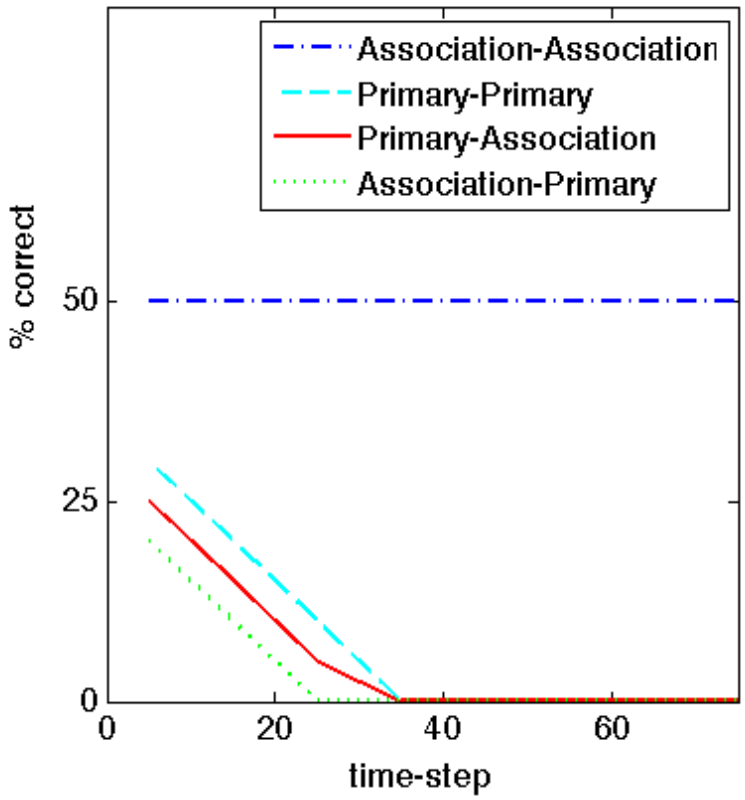

Figure B.4: Pattern of expected results on input/output pairings that require interhemispheric integration to differentiate between two possible output patterns. See text for explanations of labels and why curves are given these forms.

influence how quickly this process happens. Note that none of Ringo et al. (1994)'s models tested this condition, and none of these metrics are reported in Lewis and Elman (2008).

The following represent the four possible configurations (2 levels *x* 2 CC systems) of interhemispheric connections in the model, with the first label representing the CC system used at the first hidden layer, and the second label representing the CC system used at the second hidden layer (see Figure B.5 for examples).

- **Association-Association model** - Because interhemispheric integration happens slowly at both levels of hidden units, I expect intrahemispheric processing to

dominate, and therefore fast convergence to one of the two "confusable" output patterns. Performance cannot improve beyond 50%, as interhemispheric integration cannot occur, so that level of performance will be found at every time-step.

This corresponds to Ringo et al. (1994)'s 10-time-step model, except that initial performance should be at 50%. This performance may or may not degrade over time, depending on how the interhemispheric fibers affect processing.

- **Primary-Primary model** - Because interhemispheric integration happens quickly, I expect intrahemispheric processing to be less independent of interhemispheric integration, and slow or no convergence to one of the two "confusable" output patterns. Instead, performance should be at absolute chance levels ($1/32$).

  This corresponds to Ringo et al. (1994)'s 1-time-step model, except that initial performance should be below 50%, instead of below 100%. This performance should quickly degrade to chance levels.

- **Primary-Association model** - Because I expect the early fast transfer to cause difficulty in processing intrahemispherically, and because this problem processing intrahemispherically will propagate forward to the association area and affect its ability to process intrahemispherically, I expect this model to perform worse than the Association-Association and Association-Primary models. I do not have an expectation about whether this model will outperform the Primary-Primary model.

- **Association-Primary model** - Because of the early slow transfer should favor intrahemispheric processing, I expect this model to perform better than the Primary-Primary and Primary-Association models. Because of the later fast transfer, I expect representations at the second hidden layer to have more dependency on interhemispheric integration, and therefore for the model to perform worse than the Association-Association model.

B.4 Related Ideas

- To prevent interhemispheric connections from "driving" activity levels, instead of modulating them, and (correspondingly) In order to see good performance regardless of the presence or absence of the interhemispheric connections, the strength of the interhemispheric connections can be either fixed (e.g. Reggia, Goodall, and Shkuro (1998) to a small value, or have a maximum value implemented.

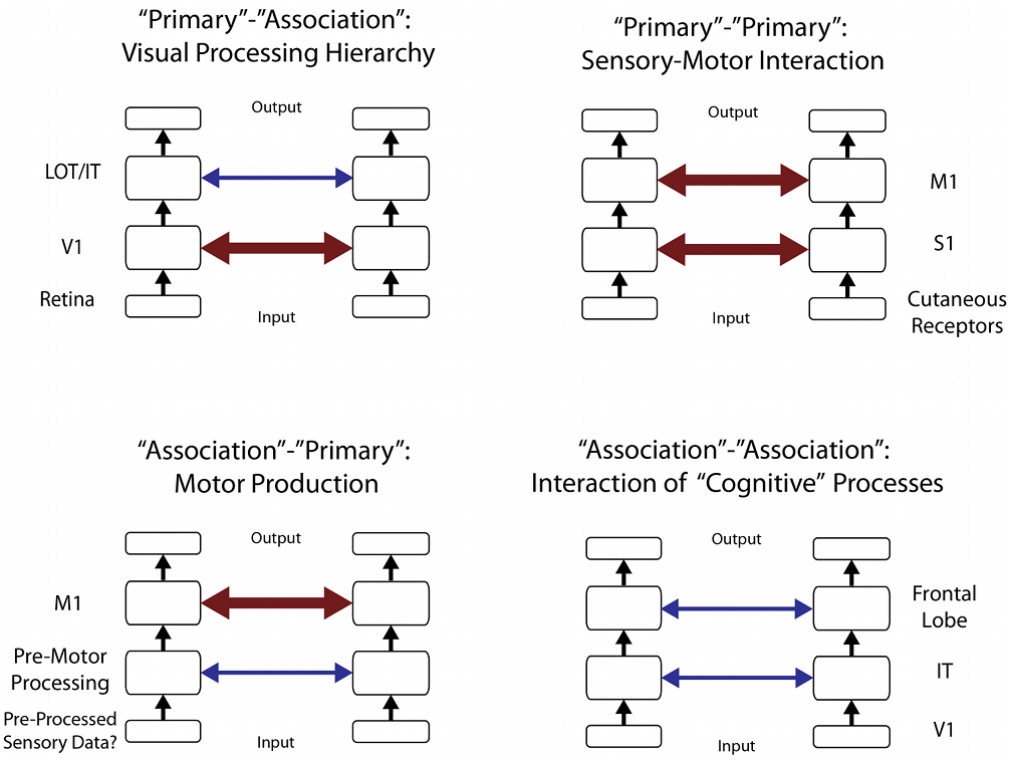

Figure B.5: Example mappings of each of the four model architectures to be tested.

Primary-Association: The most common interaction, going from sensory input through stages of a sensory processing hierarchy.
Primary-Primary: A fast, sensory-motor interaction, modeling direct connectivity between highly related input/output areas that both interconnect with fast, "primary"-type connectivity.
Association-Primary: Interaction of motor areas in selecting and executing a motor plan.
Association-Association: Any interaction between "cognitive" processing; probably most critical to model intrahemispheric feedback.

Note: Output banks are used for training purposes. For sensory processing models (primary-association and association-association), these represent (possibly different) behavioral outputs that are causing the sensory learning. For models with motor output, these represent unified behavioral outputs caused by lateralized motor production.

Appendix C

Preliminary research and proposed work: Investigating human interhemispheric connectivity across the lifespan through cross-species developmental allometry[1]

C.1 Introduction

DTI and related measures suffer from an inverse problem: though we can measure anisotropy in water diffusion, there is generally no unique solution as to the underlying microstructure causing these restrictions. Anatomical data, such as axon diameter distributions (ADD) can be used to constrain the solution space (Assaf, Freidlin, Rohde, & Basser, 2004; Assaf & Basser, 2005) or as validation for techniques aiming to measure

[1] This proposal was originally submitted for a post-doc fellowship application and is repeated here for reference in future directions.

them (Barazany, Basser, & Assaf, 2009; N. S. White, Leergaard, D'Arceuil, Bjaalie, & Dale, 2013). However, data on the basic microscopic constitution of cerebral white matter (axon diameter, degree of myelination, axon density and axon count) in humans are either missing or incomplete. If we had access to these data as a function of age, it may be possible to constrain this inverse problem and infer more specific microstructural changes from DTI data.

The corpus callosum (CC)–the predominant fiber tract directly interconnecting the two cerebral hemispheres–is an ideal structure for investigating this. The mid-sagittal extent of the CC is highly accessible, making it relatively well-studied in electrophysiology and anatomy, and is the most reliably and frequently imaged white matter tract. While some high-resolution anatomical data exist across species and developmental age in non-human animals, the data are incomplete for humans. Very few microstructural studies of the human CC exist, and those that do have used imaging techniques unable to discern the full distribution of fibers of the CC. Computational studies have shown that most quantitative aspects of human brains follow the same scaling patterns common across mammals (Changizi, 2009) and primates (Herculano-Houzel, Collins, Wong, & Kaas, 2008); perhaps the missing human data could be predicted from the more complete non-human animal data through allometric regression.

The CC also sits (literally) at a critical juncture in development and learning. Lateralization of the functions of the cerebral hemispheres is a hallmark of typical development in language (Petitto et al., 2012) and perceptual expertise (Dundas et al., 2012), and plays a role in virtually every function we think makes us human. What is the role of the CC in the development of functional lateralization, and how does its own developmental trajectory interact with that of the hemispheres? Developing computational models of the role of interhemispheric (IH) communication and lateralization in learning require being able to differentiate between changes in speed, reliability, and quantity of

IH connections–data which are inaccessible without the microscopic CC data mentioned above.

We believe that all of these questions are answerable through computational modeling. We aim to answer these questions using three computational techniques: (1) creating predictive models of the microstructure of the corpus callosum over data from an exhaustive literature review, (2) using a biophysically realistic forward model to virtually image our predictive model across the lifespan, then comparing these results to existing data measured in humans across the lifespan, and (3) using neural network modeling to examine the relationship between CC microstructure, interhemispheric transfer, and the development of lateralization.

C.2 Proposed Work

C.2.1 Predictive Modeling of CC microstructure across the typical human lifespan

Mammalian brains span over five orders of magnitude in size. Though the structure of the smallest brains differ from that of the largest, the relative differences in structure are predictable as a function of brain size (Jerison, 1982; Finlay et al., 2001; Changizi, 2009). These "allometric" scaling functions follow power laws, indicating they are "scale-free"–that the same relationship between quantities is independent of absolute size. Most microscopic (e.g. the # of synapses per neuron) and macroscopic (e.g. the total white matter volume) measures follow a power-law relationship with brain size[2]. These various allometric scaling functions can be related to each other, suggesting that

[2]Total brain weight and brain volume scale isometrically; thus use of either results in allometric relationships with extremely similar exponents. The core data we use are from S. S. H. Wang et al. (2008), who use brain weight; we follow their lead and convert brain volumes to estimated brain weights in publications where only brain volumes are reported.

they derive from more basic principles such as trade-offs between efficient wiring and interconnectedness (Changizi, 2009).

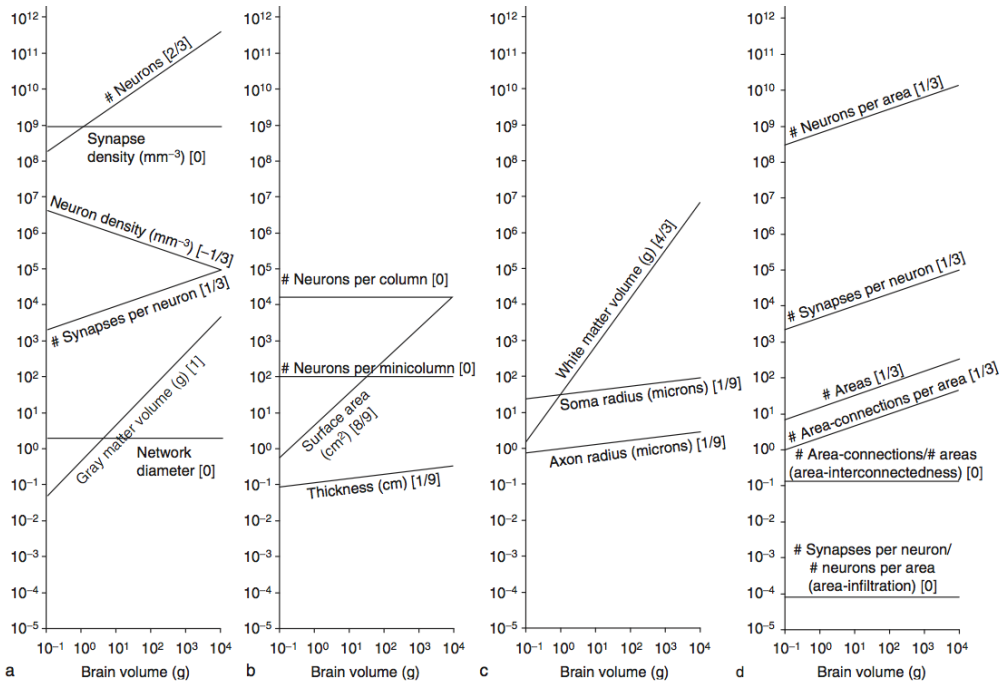

Figure C.1: Summary of allometric scaling curves across microscopic and macroscopic measures in mammals (Changizi, 2009).

In previous work, we used allometric scaling to examine changes in callosal connectivity as a function of brain size (Cipollini & Cottrell, in preparation). We found that callosal connections, on average, contain many more axons than the average intrahemispheric area-area connection. We also found that callosal connectivity is not selectively reduced with increasing brain size as is sometimes suggested (Rilling & Insel, 1999a). Rather, because callosal connections are largely homotopic, their proportion of the total white matter connectivity decreases with brain size at the same rate as each intrahemispheric area-area connection does, due to an increase of the total number of cytoarchitectonically-defined areas and area-area connections with increasing brain size (Changizi & Shimojo, 2005). These insights were accessible through allometric

regression of the mid-sagittal CC fiber density, enabled by recent high-resolution non-human animal data (S. S. H. Wang et al., 2008).

Here, we propose to use allometric scaling to examine neuroanatomical relationships not only across species, but also across development. Allometry has been used much less extensively in development, but validation of the procedure exists. R. D. Martin (1983) investigated how *inter*-species allometric scaling compared with with *intra*-species scaling over the lifespan. He concluded that development can be broken into 3 stages that each obey their own allometric scaling laws: pre-natal development, post-natal development, and adulthood. R. D. Martin (1983) and Clancy et al. (2007) both suggest that these developmental scaling laws are due to maturational changes tightly correlated with species-specific aging; Clancy et al. (2007) show that these developmental ages can be mapped across species[3]. Our own analyses of the CC in the macaque over pre- and post-natal development (LaMantia & Rakic, 1990b) and into adulthood (LaMantia & Rakic, 1990a) are consistent with the division into three developmental stages, with the onset of the third around 1 year of age (Figure C.4) (R. D. Martin, 1983)[4].

In order to accomplish our goal to predict diffusion MRI results in the mid-sagittal CC across the human lifespan, we must be able to predict the following quantities across the life-span: the axon diameter distribution (ADD), the proportion of myelinated fibers, the axon density, and the total axon count (see Equation C.2). Below, we describe the modeling methods for each, and show that they can give meaningful results across species at a single time-point, in young adults.

[3]An online tool implements their mappings for many species: http://bioinformatics.ualr.edu/ttime/translatetime_primates_php.php

[4]Hou and Pakkenberg (2012) found age-related changes in old age (65-90 years old) in humans. We will look at old age in humans separately using these same techniques.

Data Acquisition

Many of the data used here are between 20 and 60 years old; raw data are no longer available. Even for newer data, requests for raw data have either elicited no response, or the data remain inaccessible for other reasons. In order to use these valuable, published data, we have developed a hybrid suite of simple computer vision techniques and manual data mark-up to extract data from published histograms and scatter plots (described in detail elsewhere (Cipollini & Cottrell, in preparation)). Using these techniques, we have been able to reproduce statistical results usually within 1% error (and always within 2%) of the published analyses and allometric regressions.

Predicting the Axon Diameter Distribution (ADD)

Our plan is to model the axon diameter distribution (ADD) of the mid-sagittal CC from its initial fetal development through aging into the 90s. Data exist in humans for the fetus (Luttenberg, 1965), in adulthood (Tomasch, 1954; Aboitiz et al., 1992; Rabi, Madhavi, Antonisamy, & Koshi, 2007; Caminiti et al., 2009), and through aging into the 80s and 90s (Hou & Pakkenberg, 2012) but all were all collected with a light microscope[5], which is incapable of reliably imaging the smaller caliber fibers of the CC. High-resolution animal data exist[6], and previous work indicates a power-law relationship between brain size and axon diameters (Changizi, 2001). Here we outline mathematical modeling techniques for combining all the data to create a predictive model across the human lifespan.

First, we create a predictive model of ADDs across species at a similar develop-

[5] Aboitiz et al. (1992) report electron microscopic data for a single human sample but indicate that tissue preservation was likely poor. Our own quantitative analyses of the data suggest this sample is indeed unusual; we use those data with caution.

[6] Most useful here are a cross-species study in young adults (S. S. H. Wang et al., 2008), developmental studies in cats (Berbel & Innocenti, 1988) and macaque monkeys (LaMantia & Rakic, 1990b), and a study of adult macaques (LaMantia & Rakic, 1990a).

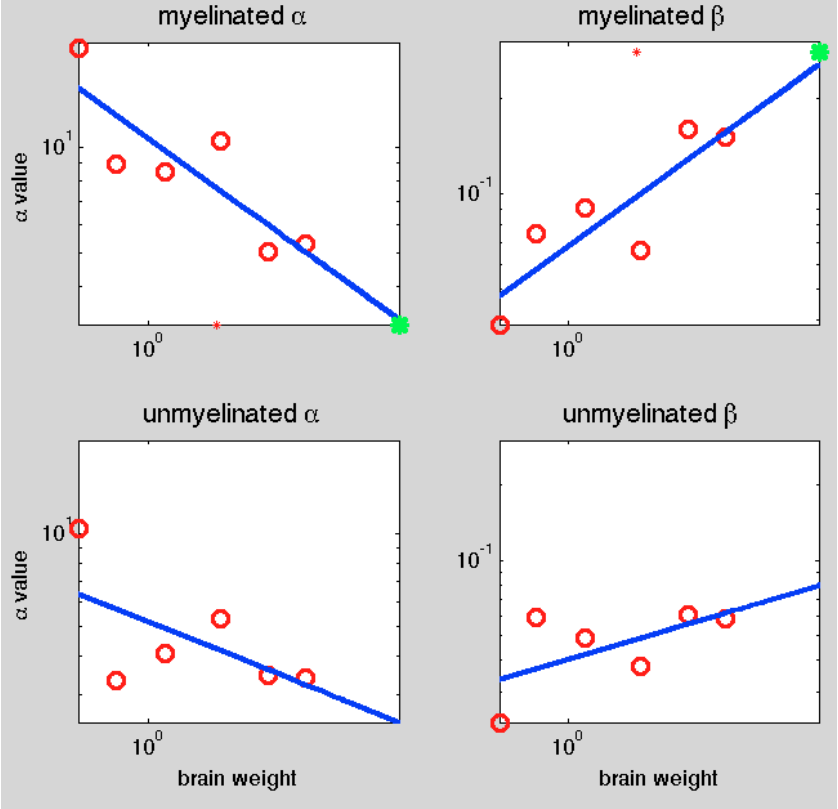

Figure C.2: Allometric regression of gamma-distribution parameters for myelinated and unmyelinated axon diameter distributions. Green stars in the first row indicate parameters for fitting human distributions. Cross-species data from S. S. H. Wang et al. (2008); human data from Aboitiz et al. (1992).

Note that Aboitiz et al. (1992) reported a single distribution mixed between myelinated and unmyelinated fibers. Since they reported over 90% to be myelinated, we compared the fitted curve only to the myelinated parameters (first row), and not to the unmyelinated parameters (second row).

mental age. We extract electron microscopy data on mid-centuryital CC axon distributions (AD) from S. S. H. Wang et al. (2008) (species: least shrew, mouse, rat, cat, macaque), separated by fiber type (myelinated and unmyelinated). We fit γ-distributions[7] to each ADD (Pajevic & Basser, 2013). We then create allometric (log-log) regressions for

[7] According to Pajevic and Basser (2013), there are only very slight differences in curve-fitting to ADDs between gamma, lognormal, and IUB (which they derived) distributions. We found that parameters for the IUBD distribution were less consistent across-species, while both gamma and lognormal distribution parameters gave very similar results.

each parameter of each fiber type (Figure C.2). We use data from S. S. H. Wang et al. (2008) and Aboitiz et al. (1992) to model the proportion of unmyelinated fibers (p_{unmye}) (described below).

ADDs for a species are computed as a weighted sum of myelinated and unmyelinated ADDs. γ-distribution parameters and the proportion of myelinated fibers are computed from the species-average brain weight; the two distributions are combined as :

$$\text{ADD} = (1 - p_{unmye}) * \gamma_{mye} + (p_{unmye}) * \gamma_{unmye} \tag{C.1}$$

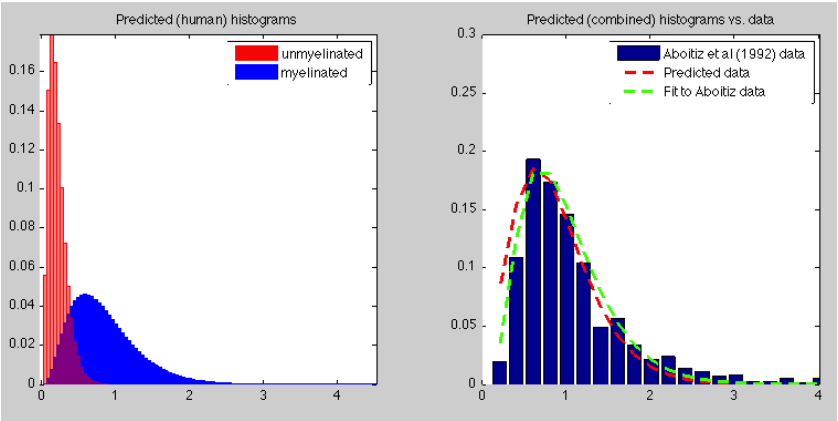

Figure C.3: (a) Predicted myelinated and unmyelinated axon diameter distributions (ADDs). (b) Predicted human CC ADDs (dashed red) vs. Aboitiz et al. (1992) human CC ADD (blue bars). Dashed green is the best-fit γ-distribution to the blue bars.

Preliminary results for macaques show good correspondence between predicted and measured myelinated axon distribution across studies (LaMantia & Rakic, 1990a). Preliminary results for humans predict a greater proportion of small myelinated fibers than reported (Figure C.3), broadly consistent with the fact that human data were collected with insufficient resolution to reliably image small-diameter fibers.

In order to model development, we will primarily use data from the cat (Berbel & Innocenti, 1988), supplemented with data from the macaque monkey (LaMantia &

Rakic, 1990b) and light microscopic data in humans (Luttenberg, 1965). As motivated above, developmental stages will be broken into three periods: pre-natal, post-natal, and adulthood. To extend the above procedures to development, the same fitting and regression procedures from above will be applied to each developmental stage individually, but generalizing across time instead of across species. We will then map developmental trajectories across species by stretching developmental trajectories in time to fit the dates of matching developmental milestones Clancy et al. (2007).

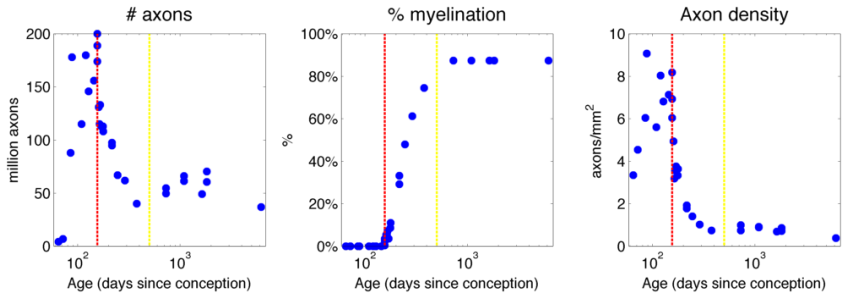

Figure C.4: (a) Number of axons, (b) percent myelination myelination, and (c) axon density over the macaque lifespan (data from LaMantia and Rakic (1990a); LaMantia and Rakic (1990b)). Red vertical line indicates birth (E156); yellow line is an eyeballed estimation of when developmental trajectory of all 3 quantities seems to change (346 days post-natal), consistent with R. D. Martin (1983)'s report for the macaque monkey (about 1 year old).

At each stage, we plan to corroborate predictions with all published ADD data, including light microscopic data across species. Though cross-lab comparisons can be challenging due to differing techniques, especially in tissue preservation and volumetric shrinkage of tissue, given the relative paucity of data this strong validation is necessary for producing reliable results. We expect one output of this work to be a spreadsheet of ADDs, explicit methods for their collection, and comments on whether a single study fits well with others of the same species or across species (and our thoughts as to why or why not).

Potential Challenges We identify three possible pitfalls in these procedures, and propose a possible solution for each.

Because the brain size of the non-human species used to fit these allometric regressions are much smaller than the human brain, large extrapolation errors may occur. In this case, instead of using human data for comparison to allometric predictions, the human data could be used to further constrain the cross-species curve-fitting. Though the proportion of small fibers in light microscopy is not accurate due to the low magnification, the relative proportions of the larger fibers to each other can presumed to be accurate. As part of the nonlinear fitting procedure, we can include the fits to these relative proportions in our cost function.

An additional challenge is that existing human samples are not young adults, but rather middle-aged to late-aged adults. Berbel and Innocenti (1988) have shown age-dependence in the mid-sagittal area (CCA), percent myelination (PMY), and fiber density (CCD) of the corpus callosum; we have found similar results for the CCA and CCD from data published in LaMantia and Rakic (1990a). It is unclear whether the fiber distribution is age-dependent in the third stage of the lifespan (adulthood). We will explore the possibility of obtaining individual subject data from (LaMantia & Rakic, 1990a) as one way to try and address this issue.

A final consideration here is that allometric regression may not be the appropriate relationship to consider here. If that is the case, less constrained regression procedures, such as Gaussian Process regression or general linear models, might be used in place of allometric regressions.

Predicting Proportion of Myelinated Fibers, Axon Density, and Axon Count

We have previously shown (in young adults) that axon density seems to follow an allometric power-law relationship (Cipollini & Cottrell, in preparation), perhaps due to

the relationships between brain size, axon diameter, cell size, and energetics (Changizi, 2001; S. S. H. Wang, 2008). This, combined with previous data on mid-sagittal callosal area (CCA) (Rilling & Insel, 1999a), allowed us to derive the allometric scaling of CC axon count (NCC) and its relationship to intrahemispheric axon count as well.

Deriving a relationship between brain size and proportion of myelinated fibers is trickier, however, as simple allometric regressions are not constrained to particular minimum and maximum values. Instead, we have previously modeled the relationship between brain size and the proportion of *unmyelinated* fibers using an exponential decay, which has provided better fits than logistic regression.

As described above, these procedures for young adults can be applied across the lifespan of a single species. The data from Berbel and Innocenti (1988) and LaMantia and Rakic (1990b) will again be used in conjunction of with human data from Luttenberg (1965), as well as CCA data from Rakic and Yakovlev (1968) to derive these relationships.

Potential Challenges The corpus callosum is not a uniform structure; fiber density, myelination, and diameter distribution vary across the anterior-posterior extent of the CC. The modeling above will initially be done across the callosum as a whole, rather than in individual sectors. Many studies measure a subset of callosal areas or report data across areas, making it impossible to model individual callosal sectors directly. However, despite the regional differences in callosal axon distribution, the combined distributions seem to show very regular properties (Pajevic & Basser, 2013).

LaMantia and Rakic (1990a) indicated that some sectors have very similar distributions and so can be considered together, constraining the problem. Some excellent data exist on the development and adult fiber composition of each callosal sector (LaMantia & Rakic, 1990b; LaMantia & Rakic, 1990a), and other data exist for dividing the callosum into sectors across species. One possible solution to the problem above is to try using

these specific data data to make individual sector predictions across species and lifespan. A second possible solution is to try and use these data to derive the ADD of each callosal sector as a species-independent function of the total CC ADD.

C.2.2 Validation via Diffusion MRI

Large-scale studies have collected data on water diffusion from across the human lifespan; this includes the PING study[8], a database containing, among other things, diffusion MRI data of people between the ages of 3 and 20. These data are largely from diffusion tensor imaging (DTI) which trades off assumptions about the distribution of fiber orientations for speed of acquisition. There is good evidence that diffusion is affected by axon diameter distribution (ADD), proportion of myelinated fibers (PMY), and axon density (CCD). However, because these values are currently not quantifiable in vivo (though see Barazany et al. (2009) and N. S. White et al. (2013)), relating diffusion MRI measures to underlying microstructure is an area of very active research.

Our predictions above encompass most parameters necessary for estimating the magnetic signal S due to water diffusion in a diffusion MRI paradigm. Intuitively, water diffusion is generally restricted by semi-impermeable cell membranes and by the size and density other molecules that it bumps into while diffusing. These two restrictions, generally referred to as *restricted* and *hindered* diffusion respectively, correspond to intracellular diffusion along an axon and extracellular diffusion within homogeneous fiber tracts like the CC.

In the mid-sagittal CC, which contains axons with relatively uniform direction and a relatively homogeneous extra-axonal space, a simple forward model of the magnetic signal intensity S can be derived. For generality, we also consider diffusion within the myelin itself:

[8] http://www.chd.ucsd.edu/research/ping-study.html

$$
\begin{aligned}
S = \lambda_h e^{-\mathrm{TE}*R_{2h}} * e^{-b*\mathrm{ADC}_h} \\
+ \lambda_r e^{-\mathrm{TR}*R_{2r}} * e^{-b*\mathrm{ADC}_r} \\
+ \lambda_m e^{-\mathrm{TE}*R_{2m}}
\end{aligned}
\tag{C.2}
$$

where h, r, and m refer to structures showing diffusion related to hindered, restricted, and myelin, λ is the volume fraction (proportion of total volume consisting of the particular medium), TE and TR are MRI acquisition parameters (the echo time and relaxation time, respectively), $R_2 = \frac{1}{T_2}$ is the "relaxation rate", or reciprocal of T2 relaxation, b quantifies how strongly diffusion is being induced, and ADC is the apparent diffusion coefficient (the average rate at which water is measured to diffuse in a particular direction given the MRI acquisition parameters). Note that in this equation, we assume that the ADC due to myelination is zero, i.e. that myelin is water-tight and contains no diffusing water.

Given our allometric regression models above and data from the literature, it is possible to fill in reasonable values for each quantity in Equation C.2. Our predictions of the microscopic structure of the corpus callosum, combined with simulations computing intra-axonal diffusion rates as a function of axon diameter (N. S. White et al., 2013), allow us to calculate the ADC_r from the ADD. ADC_h may also be estimated from data or taken from the literature. S. S. H. Wang et al. (2008) estimates that the proportion of the mid-sagittal CC area constituted by extra-axonal media (λ_h) is constant across species, $\approx 87\%$. With an estimate of this area, and the usual assumption that the thickness of myelinated is 0.7 times the diameter of the fiber it ensheathes, we will be able to compute all three volume fractions (λ_h, λ_r, λ_m).

Potential Challenges One major sticking point for a realistic forward model is R_2, the rate at which spins lose coherence. R_2 is a property of tissue, and it is unknown whether R_2 is a function of age nor how much it varies across participants. For our initial modeling, we will obtain gross estimates of R_2 by analyzing single-subject data across a number of b-values (strength of inducing diffusion). If this coarse-level validation of the allometric modeling proves to be informative, we will look at examining the relationship between R_2 and age through experiments varying how strongly diffusion is being induced (b).

A second area for closer investigation is the rate at which water passes through the cell membrane of unmyelinated cells (permeability), which has not been looked at closely in previous forward-modeling of water diffusion. The permeability of unmyelinated is linearly dependent on axon diameter. Because water diffusion in and out of the axon is perpendicular to the longitudinal direction of the axon, when unaccounted for it would appear as an (unexpected) contribution to hindered diffusion (ADC_h). This may be particularly important in species where forward models are tested (e.g. rats), where unmyelinated fibers account for more than 50% of the total fiber count in the mid-sagittal CC (Kim, Ellman, & Juraska, 1996; S. S. H. Wang et al., 2008).

C.2.3 Neural network modeling

In previous work, we adopted the framework of Lewis and Elman (2008) (Figure C.5), itself an adaptation of Ringo et al. (1994). This neural network is composed of leaky integrator units separated into three layers (input, hidden, output). Each layer is segregated into left and right "hemispheres" which interconnect only with units in its own hemispheresave for two nodes from the hidden layer of each "hemisphere", which fully interconnect with each other. Every connection has a time-delay, usually 1 time-step. The model is trained to output one binary string when presented another

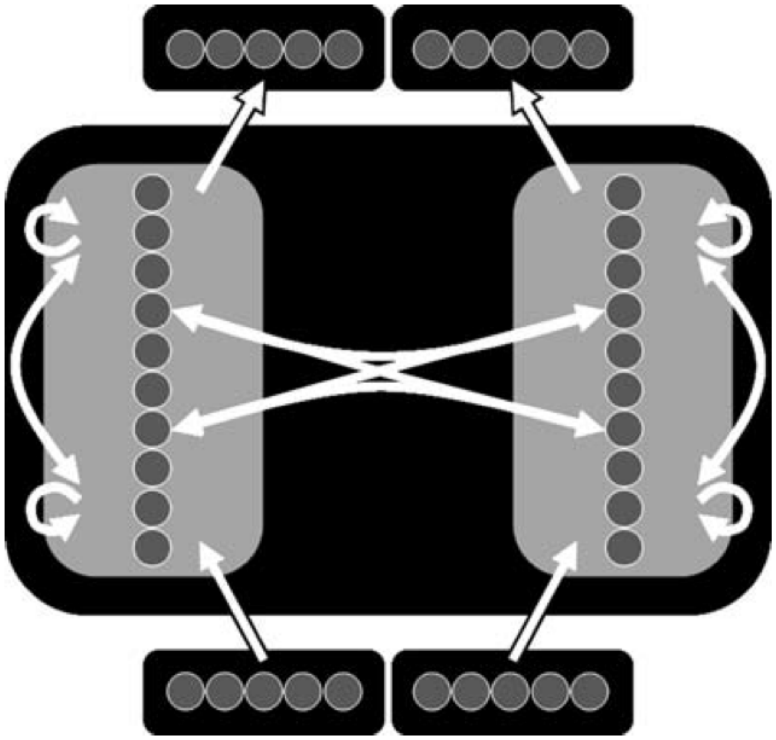

Figure C.5: Model architecture used in simulations(Lewis & Elman, 2008). Our simulations used 15 hidden units per "hemisphere" and 3 "callosal" connections, not 10 and 2 (respectively) as shown.

at input, for 32 random input-output parings. The network is said to have output a bit correctly if the output activation is within 25% of the expected output value. To examine the interdependence of the hemispheres, the network's "interhemispheric" (callosal) connections are removed; the increase in output error due to this lesion ("lesion-induced error") is used as an index of this interdependence.

We have used this modeling framework to show that unreliable IH signals, due to the preponderance of long, unmyelinated axons $<0.5\mu m$ in diameter present at birth (S. S. H. Wang, 2008) may reduce IH integration (Cipollini & Cottrell, 2013b). Subsequent analysis has indicated that the level of IH integration affects the spontaneous emergence of asymmetries. A developmental model which increases signal reliability (de-

crease signal noise) across training showed an early period of reduced interhemispheric interactions and as strong interhemispheric interactions after development as found in the same model trained without any noise.

Here we would like to use the developmental ideas from above to examine the relationship between callosal development, interhemispheric transfer, and lateralization. Lewis and Elman (2008) looked at how changes in head circumference and conduction velocity interacted. We would like to test a larger number of interacting factors separately to characterize their individual effects, then use them in a combined model to examine their interactions. These include changes to head size, conduction velocity due to axon diameter and myelination, total number of fibers, and transmission noise.

C.3 Summary

Here, we propose to use allometric scaling to fill in missing data of the microscopic structure of the mid-sagittal corpus callosum across the human lifespan. The model will be tested against existing diffusion MRI data, and its consequences for cerebral lateralization will be examined in a neural network framework. If successful, this model may help constrain the interpretation of microstructure from diffusion MRI data.

References

Aboitiz, F. (1991). *Quantitative morphology and histology of the human corpus callosum and its relation to brain lateralization*. Doctoral, UCLA.

Aboitiz, F., & Montiel, J. (2003). One hundred million years of interhemispheric communication: the history of the corpus callosum. *Brazilian journal of medical and biological research*, *36*(4), 409–20.

Aboitiz, F., Scheibel, A. B., Fisher, R. S., & Zaidel, E. (1992). Fiber composition of the human corpus callosum. *Brain Research*, *598*(1-2), 143–153.

Altschuler, T. S., Molholm, S., Butler, J. S., Mercier, M. R., Brandwein, A. B., & Foxe, J. J. (2013). The effort to close the gap: Tracking the development of illusory contour processing from childhood to adulthood with high-density electrical mapping. *NeuroImage*.

Amir, Y., Harel, M., & Malach, R. (1993). Cortical hierarchy reflected in the organization of intrinsic connections in macaque monkey visual cortex. *The Journal of Comparative Neurology*, *334*(1), 19–46.

Anderson, B., Southern, B. D., & Powers, R. E. (1999). Anatomic asymmetries of the posterior superior temporal lobes: a postmortem study. *Neuropsychiatry, Neuropsychology, and Behavioral Neurology*, *12*(4), 247–254.

Assaf, Y., & Basser, P. J. (2005). Composite hindered and restricted model of diffusion (CHARMED) MR imaging of the human brain. *NeuroImage*, *27*(1), 48–58.

Assaf, Y., Blumenfeld-Katzir, T., Yovel, Y., & Basser, P. J. (2008). Axcaliber: A method for measuring axon diameter distribution from diffusion MRI. *Magnetic Resonance in Medicine*, *59*(6), 1347–1354.

Assaf, Y., Freidlin, R. Z., Rohde, G. K., & Basser, P. J. (2004). New modeling and experimental framework to characterize hindered and restricted water diffusion in brain white matter. *Magnetic resonance in medicine*, *52*(5), 965–978.

Bailey, P., & Bonin, G. v. (1951). *The isocortex of man/il monographs in med sci 6: 1-2*.

Urbana, Ill.: Univ. of Illinois Press,.

Baker, T. J., Tse, J., Gerhardstein, P., & Adler, S. A. (2008). Contour integration by 6-month-old infants: Discrimination of distinct contour shapes. *Vision Research*, *48*(1), 136–148.

Bar, M. (2004). Visual objects in context. *Nat Rev Neurosci*, *5*(8), 617–629.

Barazany, D., Basser, P. J., & Assaf, Y. (2009). In vivo measurement of axon diameter distribution in the corpus callosum of rat brain. *Brain*, *132*(5), 1210 –1220.

Barbas, H., & Rempel-Clower, N. (1997). Cortical structure predicts the pattern of corticocortical connections. *Cerebral Cortex*, *7*(7), 635 –646.

Battaglia, P. W., Jacobs, R. A., & Aslin, R. N. (2003, July). Bayesian integration of visual and auditory signals for spatial localization. *Journal of the Optical Society of America. A, Optics, image science, and vision*, *20*(7), 1391–1397.

Behrmann, M., Avidan, G., Leonard, G. L., Kimchi, R., Luna, B., Humphreys, K., & Minshew, N. (2006). Configural processing in autism and its relationship to face processing. *Neuropsychologia*, *44*(1), 110–129.

Behrmann, M., & Plaut, D. C. (2013). Distributed circuits, not circumscribed centers, mediate visual recognition. *Trends in cognitive sciences*, *17*(5), 210–219.

Benninger, C., Matthis, P., & Scheffner, D. (1984). EEG development of healthy boys and girls. results of a longitudinal study. *Electroencephalography and Clinical Neurophysiology*, *57*(1), 1–12.

Berbel, P., & Innocenti, G. M. (1988). The development of the corpus callosum in cats: a light- and electron-microscopic study. *The Journal of comparative neurology*, *276*(1), 132–156.

Bolton, P., & Dewatripont, M. (1994). The firm as a communication network. *The Quarterly Journal of Economics*, *109*(4), 809–839.

Brand, J., & Johnson, A. (2013). Attention and spatial scale selection in scene categorization. *Journal of Vision*, *13*(9), 431–431.

Brodmann, K. (1909). *Vergleichende lokalisationslehre der grosshirnrinde in ihren prinzipien dargestellt auf grund des zellenbaues*. Barth.

Bryden, M. P., & Rainey, C. A. (1963). Left-right differences in tachistoscopic recognition. *Journal of Experimental Psychology*, *66*(6), 568–571.

(Bud) Craig, A. D. (2009). How do you feel - now? the anterior insula and human

awareness. *Nat Rev Neurosci*, *10*(1), 59–70.

Burkhalter, A. (1993). Development of forward and feedback connections between areas v1 and v2 of human visual cortex. *Cerebral Cortex*, *3*(5), 476–487.

Buxhoeveden, D. P., Switala, A. E., Litaker, M., Roy, E., & Casanova, M. F. (2001). Lateralization of minicolumns in human planum temporale is absent in nonhuman primate cortex. *Brain, Behavior and Evolution*, *57*(6), 349–358.

Caminiti, R., Ghaziri, H., Galuske, R., Hof, P. R., & Innocenti, G. M. (2009). Evolution amplified processing with temporally dispersed slow neuronal connectivity in primates. *Proceedings of the National Academy of Sciences*, *106*(46), 19551 –19556.

Catani, M., & Thiebaut de Schotten, M. (2008). A diffusion tensor imaging tractography atlas for virtual in vivo dissections. *Cortex; a journal devoted to the study of the nervous system and behavior*, *44*(8), 1105–1132.

Chance, S. A., Sawyer, E. K., Clover, L. M., Wicinski, B., Hof, P. R., & Crow, T. J. (2013). Hemispheric asymmetry in the fusiform gyrus distinguishes homo sapiens from chimpanzees. *Brain Structure and Function*, *218*(6), 1391–1405.

Changizi, M. A. (2001). Principles underlying mammalian neocortical scaling. *Biological Cybernetics*, *84*(3), 207–215.

Changizi, M. A. (2009). Brain scaling laws. *New Encyclopedia of Neuroscience*.

Changizi, M. A., & Shimojo, S. (2005). Parcellation and area-area connectivity as a function of neocortex size. *Brain, Behavior and Evolution*, *66*(2), 88–98.

Chiron, C., Jambaque, I., Nabbout, R., Lounes, R., Syrota, A., & Dulac, O. (1997). The right hemisphere is dominant in human infants. *Brain*, *120*, 1057-1065.

Christman, S. (1989). Perceptual characteristics in visual laterality research. *Brain and Cognition*, *11*(2), 238–257.

Christman, S., Kitterle, F. L., & Hellige, J. (1991). Hemispheric asymmetry in the processing of absolute versus relative spatial frequency. *Brain and Cognition*, *16*(1), 62–73.

Chudler, E. (n.d.). *Brain facts and figures.* Retrieved 2014-05-09, from http://faculty.washington.edu/chudler/facts.html

Cipollini, B., & Cottrell, G. W. (2013a). Sparse connectivity asymmetry in an autoencoder can explain visual hemispheric asymmetries in local/global, face, and spatial frequency processing. In *Proceedings of the 13th annual neural computation and*

psychology workshop. San Sebastian, Spain: Neural Computation and Psychology Workshop.

Cipollini, B., & Cottrell, G. W. (2013b). Uniquely human developmental timing may drive cerebral lateralization and interhemispheric coupling. In *Proceedings of the 35th annual meeting of the cognitive science society.* Austin, TX: Cognitive Science Society.

Cipollini, B., & Cottrell, G. W. (2014). A developmental model of hemispheric asymmetries of spatial frequencies. In *Proceedings of the 36th annual meeting of the cognitive science society.* Austin, TX: Cognitive Science Society.

Cipollini, B., & Cottrell, G. W. (in preparation). The enduring strength of callosal connections across brain size. *in preparation*.

Cipollini, B., Hsiao, J. H., & Cottrell, G. W. (2012). Connectivity asymmetry can explain visual hemispheric asymmetries in Local/Global, face, and spatial frequency processing. In *Proceedings of the 34th annual meeting of the cognitive science society.* Austin, TX: Cognitive Science Society.

Clancy, B., Finlay, B. L., Darlington, R. B., & Anand, K. (2007). Extrapolating brain development from experimental species to humans. *NeuroToxicology*, *28*(5), 931–937.

Corballis, P. M., Funnell, M. G., & Gazzaniga, M. S. (1999). A dissociation between spatial and identity matching in callosotomy patients. *Neuroreport*, *10*(10), 2183–2187.

Cottrell, G. W., Munro, P., & Zipser, D. (2012). Learning internal representations from gray-scale images: An example of extensional programming. In *Proceedings of the 9th annual meeting of the cognitive science society* (p. 61-473). Austin, TX: Cognitive Science Society.

Craig, A. B. (2005). Forebrain emotional asymmetry: a neuroanatomical basis? *Trends in Cognitive Sciences*, *9*(12), 566–571.

Dailey, M. N., & Cottrell, G. W. (1999). Organization of face and object recognition in modular neural network models. *Neural Networks*, *12*(7-8), 1053–1074.

Dailey, M. N., Cottrell, G. W., Padgett, C., & Adolphs, R. (2002). EMPATH: a neural network that categorizes facial expressions. *Journal of Cognitive Neuroscience*, *14*(8), 1158–1173.

Dale, G., & Arnell, K. M. (2013). Investigating the stability of and relationships among global/local processing measures. *Attention, Perception, & Psychophysics*, *75*(3),

394–406.

Daugman, J. G. (1985). Uncertainty relation for resolution in space, spatial frequency, and orientation optimized by two-dimensional visual cortical filters. *Journal of the Optical Society of America, A, Optics, Image & Science*, *2*(7), 1160–1169.

De Renzi, E., & Spinnler, H. (1966, June). Visual recognition in patients with unilateral cerebral disease. *The Journal of nervous and mental disease*, *142*(6), 515–525.

Dhar, M., Been, P. H., Minderaa, R. B., & Althaus, M. (2010). Reduced interhemispheric coherence in dyslexic adults. *Cortex*, *46*(6), 794–798.

Di Lollo, V. (1981). Hemispheric symmetry in duration of visible persistence. *Perception & Psychophysics*, *29*(1), 21–25.

Doron, K. W., Bassett, D. S., & Gazzaniga, M. S. (2012). Dynamic network structure of interhemispheric coordination. *Proceedings of the National Academy of Sciences*, *109*(46), 18661–18668.

Doron, K. W., & Gazzaniga, M. S. (2008). Neuroimaging techniques offer new perspectives on callosal transfer and interhemispheric communication. *Cortex*, *44*(8), 1023–1029.

Dundas, E. M., Plaut, D. C., & Behrmann, M. (2012). The joint development of hemispheric lateralization for words and faces. *Journal of experimental psychology. General*.

Eliasmith, C., & Anderson, C. H. (2004). *Neural engineering: Computation, representation, and dynamics in neurobiological systems*. MIT Press.

Eliasmith, C., Stewart, T. C., Choo, X., Bekolay, T., DeWolf, T., Tang, Y., & Rasmussen, D. (2012). A large-scale model of the functioning brain. *Science*, *338*(6111), 1202–1205.

Elman, J. L. (1993). Learning and development in neural networks: the importance of starting small. *Cognition*, *48*(1), 71–99.

Ermentrout, G. B., Galan, R. F., & Urban, N. N. (2008). Reliability, synchrony and noise. *Trends in neurosciences*, *31*(8), 428–434.

Faisal, A. A., & Laughlin, S. B. (2007). Stochastic simulations on the reliability of action potential propagation in thin axons. *PLoS Computational Biology*, *3*(5).

Faisal, A. A., Selen, L. P. J., & Wolpert, D. M. (2008). Noise in the nervous system. *Nature Reviews Neuroscience*, *9*(4), 292–303.

Faisal, A. A., White, J. A., & Laughlin, S. B. (2005). Ion-channel noise places limits on the miniaturization of the brain's wiring. *Current biology: CB*, *15*(12), 1143–1149.

Fendrich, R., & Gazzaniga, M. S. (1990). Hemispheric processing of spatial frequencies in two commissurotomy patients. *Neuropsychologia*, *28*, 657–663.

Fink, G. R., Halligan, P. W., Marshall, J. C., Frith, C. D., Frackowiak, R. S., & Dolan, R. J. (1997). Neural mechanisms involved in the processing of global and local aspects of hierarchically organized visual stimuli. *Brain*, *120*(10), 1779 –1791.

Finlay, B. L., Darlington, R. B., & Nicastro, N. (2001). Developmental structure in brain evolution. *The Behavioral and brain sciences*, *24*(2), 263–278; discussion 278-308.

Fransson, P., den, U., Blennow, M., & Lagercrantz, H. (2011). The functional architecture of the infant brain as revealed by resting-state fMRI. *Cerebral Cortex*, *21*(1), 145–154.

Fries, P. (2005). A mechanism for cognitive dynamics: neuronal communication through neuronal coherence. *Trends in Cognitive Sciences*, *9*(10), 474–480.

Galuske, R. A., Schlote, W., Bratzke, H., & Singer, W. (2000). Interhemispheric asymmetries of the modular structure in human temporal cortex. *Science (New York, N.Y.)*, *289*(5486), 1946–1949.

Galuske, R. A. W., & Singer, W. (1996). The origin and topography of long-range intrinsic projections in cat visual cortex: A developmental study. *Cerebral Cortex*, *6*(3), 417–430.

Gazzaniga, M. S. (2000). Cerebral specialization and interhemispheric communication: Does the corpus callosum enable the human condition? *Brain*, *123*(7), 1293–1326.

Gerhardstein, P., Kovacs, I., Ditre, J., & Feher, A. (2004). Detection of contour continuity and closure in three-month-olds. *Vision Research*, *44*(26), 2981–2988.

Geschwind, D., & Rakic, P. (2013). Cortical evolution: Judge the brain by its cover. *Neuron*, *80*(3), 633–647.

Geschwind, N., & Galaburda, A. M. (1985). Cerebral lateralization. biological mechanisms, associations, and pathology: I. a hypothesis and a program for research. *Archives of neurology*, *42*(5), 428–459.

Gilbert, C., & Bakan, P. (1973). Visual asymmetry in perception of faces. *Neuropsychologia*, *11*(3), 355–362.

Gilbert, C. D. (1992). Horizontal integration and cortical dynamics. *Neuron*, *9*(1), 1–13.

Gilbert, C. D., & Li, W. (2013). Top-down influences on visual processing. *Nature Reviews Neuroscience*, *14*(5), 350–363.

Glasser, M. F., Goyal, M. S., Preuss, T. M., Raichle, M. E., & Van Essen, D. C. (2014). Trends and properties of human cerebral cortex: Correlations with cortical myelin content. *NeuroImage*, *93P2*, 165–175.

Goffaux, V., Hault, B., Michel, C., Vuong, Q. C., & Rossion, B. (2005). The respective role of low and high spatial frequencies in supporting configural and featural processing of faces. *Perception*, *34*(1), 77–86.

Gollin, D., & Rogerson, R. (2014). Productivity, transport costs and subsistence agriculture. *Journal of Development Economics*, *107*, 38–48.

Graham, L. E., Cook, M. E., & Busse, J. S. (2000). The origin of plants: Body plan changes contributing to a major evolutionary radiation. *Proceedings of the National Academy of Sciences*, *97*(9), 4535–4540.

Grossberg, S. (2010, September). Linking attention to learning, expectation, competition, and consciousness. *CAS/CNS Technical Report Series*, *0*(007).

Grossberg, S., & Raizada, R. D. (2000). Contrast-sensitive perceptual grouping and object-based attention in the laminar circuits of primary visual cortex. *Vision Research*, *40*(10-12), 1413–1432.

Grossberg, S., & Williamson, J. R. (2001). A neural model of how horizontal and interlaminar connections of visual cortex develop into adult circuits that carry out perceptual grouping and learning. *Cerebral Cortex*, *11*(1), 37–58.

Gunz, P., Neubauer, S., Maureille, B., & Hublin, J.-J. (2010). Brain development after birth differs between neanderthals and modern humans. *Current Biology*, *20*(21), R921–R922.

Gurkan, C., Koulov, A. V., & Balch, W. E. (2007). An evolutionary perspective on eukaryotic membrane trafficking. In *Eukaryotic membranes and cytoskeleton* (pp. 73–83). Springer New York.

Hagler, D. J., Ahmadi, M. E., Kuperman, J., Holland, D., McDonald, C. R., Halgren, E., & Dale, A. M. (2009). Automated white-matter tractography using a probabilistic diffusion tensor atlas: Application to temporal lobe epilepsy. *Human Brain Mapping*, *30*(5), 1535–1547.

Hamilton, C. R., & Vermeire, B. A. (1988). Complementary hemispheric specialization in monkeys. *Science*, *242*(4886), 1691–1694.

Han, S., Weaver, J. A., Murray, S. O., Kang, X., Yund, E. W., & Woods, D. L. (2002). Hemispheric asymmetry in Global/Local processing: Effects of stimulus position and spatial frequency. *NeuroImage*, *17*(3), 1290–1299.

Harrison, K. H., Hof, P. R., & Wang, S. S.-H. (2002). Scaling laws in the mammalian neocortex: does form provide clues to function? *Journal of Neurocytology*, *31*(3-5), 289–98.

Heinze, H. J., Hinrichs, H., Scholz, M., Burchert, W., & Mangun, G. R. (1998). Neural mechanisms of global and local processing. a combined PET and ERP study. *Journal of Cognitive Neuroscience*, *10*(4), 485–498.

Hellige, J. B. (1993). *Hemispheric asymmetry: What's right and what's left*. Harvard University Press.

Hellige, J. B. (2006). Evolution of brain lateralization in humans. *Cognitie, Creier, Comportament/Cognition, Brain, Behavior*, *10*(2), 211–234.

Herculano-Houzel, S. (2011). Not all brains are made the same: new views on brain scaling in evolution. *Brain, behavior and evolution*, *78*(1), 22–36.

Herculano-Houzel, S., Collins, C. E., Wong, P., & Kaas, J. H. (2007). Cellular scaling rules for primate brains. *Proceedings of the National Academy of Sciences*, *104*(9), 3562–3567.

Herculano-Houzel, S., Collins, C. E., Wong, P., & Kaas, J. H. (2008). Cellular scaling rules for primate brains. *Proceedings of the National Academy of Sciences*, *104*(9), 3562 –3567.

Herculano-Houzel, S., Collins, C. E., Wong, P., Kaas, J. H., & Lent, R. (2008). The basic nonuniformity of the cerebral cortex. *Proceedings of the National Academy of Sciences*, *105*(34), 12593–12598.

Herculano-Houzel, S., Mota, B., Wong, P., & Kaas, J. H. (2010). Connectivity-driven white matter scaling and folding in primate cerebral cortex. *Proceedings of the National Academy of Sciences*, 201012590.

Hirsch, H. V., & Spinelli, D. N. (1970). Visual experience modifies distribution of horizontally and vertically oriented receptive fields in cats. *Science (New York, N.Y.)*, *168*(3933), 869–871.

Hirsch, J., DeLaPaz, R. L., Relkin, N. R., Victor, J., Kim, K., Li, T., ... Shapley, R. (1995). Illusory contours activate specific regions in human visual cortex: evidence from functional magnetic resonance imaging. *Proceedings of the National Academy of Sciences*, *92*(14), 6469–6473.

Hoffman, J. E. (1980). Interaction between global and local levels of a form. *Journal of Experimental Psychology: Human Perception and Performance*, *6*, 222–234.

Hopf, J., Luck, S. J., Boelmans, K., Schoenfeld, M. A., Boehler, C. N., Rieger, J., & Heinze, H. (2006). The neural site of attention matches the spatial scale of perception. *The Journal of Neuroscience*, *26*(13), 3532–3540.

Hoptman, M. J., Zuo, X.-N., D'Angelo, D., Mauro, C. J., Butler, P. D., Milham, M. P., & Javitt, D. C. (2012). Decreased interhemispheric coordination in schizophrenia: A resting state fMRI study. *Schizophrenia Research*, *141*(1), 1–7.

Hou, J., & Pakkenberg, B. (2012). Age-related degeneration of corpus callosum in the 90+ years measured with stereology. *Neurobiology of Aging*, *33*(5), 1009.e1–1009.e9.

Howard, M. F., & Reggia, J. A. (2007). A theory of the visual system biology underlying development of spatial frequency lateralization. *Brain and Cognition*, *64*(2), 111–123.

Hsiao, J. H., Cipollini, B., & Cottrell, G. W. (2013). Hemispheric asymmetry in perception: A differential encoding account. *Journal of Cognitive Neuroscience*, 1–10.

Hsiao, J. H., Shahbazi, R., & Cottrell, G. W. (2008). Hemispheric asymmetry in visual perception arises from differential encoding beyond the sensory level. In *Proceedings of the 30th annual meeting of the cognitive science society.* Austin, TX: Cognitive Science Society.

Hsiao, J. H., Shieh, D. X., & Cottrell, G. W. (2008). Convergence of the visual field split: Hemispheric modeling of face and object recognition. *Journal of Cognitive Neuroscience*, *20*(12), 2298–2307.

Hutsler, J., & Galuske, R. A. W. (2003). Hemispheric asymmetries in cerebral cortical networks. *Trends in Neurosciences*, *26*(8), 429–35.

Innocenti, G. M. (2008). Dynamic interactions between the cerebral hemispheres. *Experimental Brain Research*, *192*(3).

Innocenti, G. M. (2011). Development and evolution: two determinants of cortical connectivity. *Progress in brain research*, *189*, 65–75.

Innocenti, G. M., Vercelli, A., & Caminiti, R. (2013). The diameter of cortical axons depends both on the area of origin and target. *Cerebral Cortex*.

Ivry, R. B., & Robertson, L. C. (1998). *The two sides of perception*. The MIT Press.

Izhikevich, E. M. (2006). Polychronization: computation with spikes. *Neural Computation*, *18*(2), 245–82.

Jerison, H. J. (1982). Allometry, brain size, cortical surface, and convolutedness. In E. Armstrong & D. Falk (Eds.), *Primate brain evolution* (pp. 77–84). Springer US.

Jernigan, T. L., Baar, W. F. C., Stiles, J., & Madsen, K. S. (2011). Postnatal brain development: structural imaging of dynamic neurodevelopmental processes. *Progress in brain research*, *189*, 77–92.

Kaldy, Z., & Kovacs, I. (2003). Visual context integration is not fully developed in 4-year-old children. *Perception*, *32*(6), 657–666.

Karbowski, J. (2003). How does connectivity between cortical areas depend on brain size? implications for efficient computation. *Journal of computational neuroscience*, *15*(3), 347–356.

Katz, L. C., & Callaway, E. M. (1992). Development of local circuits in mammalian visual cortex. *Annual Review of Neuroscience*, *15*(1), 31–56.

Katz, R., & Tushman, M. (1979). Communication patterns, project performance, and task characteristics: An empirical evaluation and integration in an R&D setting. *Organizational Behavior and Human Performance*, *23*(2), 139–162.

Kelly, A. M. C., Martino, A. D., Uddin, L. Q., Shehzad, Z., Gee, D. G., Reiss, P. T., ... Milham, M. P. (2009). Development of anterior cingulate functional connectivity from late childhood to early adulthood. *Cerebral Cortex*, *19*(3), 640–657.

Kim, J. H., Ellman, A., & Juraska, J. M. (1996). A re-examination of sex differences in axon density and number in the splenium of the rat corpus callosum. *Brain research*, *740*(1-2), 47–56.

Kim, J. H., & Juraska, J. M. (1997). Sex differences in the development of axon number in the splenium of the rat corpus callosum from postnatal day 15 through 60. *Developmental brain research*, *102*(1), 77–85.

Kimchi, R. (1992, July). Primacy of wholistic processing and global/local paradigm: a critical review. *Psychological bulletin*, *112*(1), 24–38.

Kitterle, F. L., Christman, S., & Hellige, J. B. (1990). Hemispheric differences are found in the identification, but not the detection, of low versus high spatial frequencies. *Perception & Psychophysics*, *48*(4), 297–306.

Kitterle, F. L., Hellige, J. B., & Christman, S. (1992). Visual hemispheric asymmetries depend on which spatial frequencies are task relevant. *Brain and Cognition*, *20*(2),

308–314.

Kovacs, I., Kozma, P., Fehr, ., & Benedek, G. (1999). Late maturation of visual spatial integration in humans. *Proceedings of the National Academy of Sciences*, *96*(21), 12204–12209.

Kriegeskorte, N., Mur, M., & Bandettini, P. (2008). Representational similarity analysis - connecting the branches of systems neuroscience. *Frontiers in Systems Neuroscience*, *2*.

Laakso, A., & Cottrell, G. (2000, March). Content and cluster analysis: assessing representational similarity in neural systems. *Philosophical Psychology*, *13*(1), 47–76.

LaMantia, A.-S., & Rakic, P. (1990a). Cytological and quantitative characteristics of four cerebral commissures in the rhesus monkey. *The Journal of Comparative Neurology*, *291*(4), 520–537.

LaMantia, A. S., & Rakic, P. (1990b). Axon overproduction and elimination in the corpus callosum of the developing rhesus monkey. *The Journal of neuroscience*, *10*(7), 2156–2175.

Lamb, M. R., Robertson, L. C., & Knight, R. T. (1990). Component mechanisms underlying the processing of hierarchically organized patterns: inferences from patients with unilateral cortical lesions. *Journal of Experimental Psychology. Learning, Memory, and Cognition*, *16*(3), 471–483.

Lamb, M. R., & Yund, E. W. (1993). The role of spatial frequency in the processing of hierarchically organized stimuli. *Perception & Psychophysics*, *54*(6), 773–784.

Levitt, J., & Lund, J. (2002). Intrinsic connections in mammalian cerebral cortex. In A. Schuez & R. Miller (Eds.), *Cortical areas: unity and diversity* (pp. 133–154). CRC Press.

Lewis, J. D., & Elman, J. L. (2008). Growth-related neural reorganization and the autism phenotype: a test of the hypothesis that altered brain growth leads to altered connectivity. *Developmental Science*, *11*(1), 135–155.

Lewis, J. D., Theilmann, R. J., Sereno, M. I., & Townsend, J. (2009). The relation between connection length and degree of connectivity in young adults: A DTI analysis. *Cerebral Cortex*, *19*(3), 554–562.

Ley, R. G., & Bryden, M. P. (1982). A dissociation of right and left hemispheric effects for recognizing emotional tone and verbal content. *Brain and Cognition*, *1*(1), 3–9.

Li, W., Piech, V., & Gilbert, C. D. (2008). Learning to link visual contours. *Neuron*, *57*(3), 442–451.

Luders, E., Cherbuin, N., Thompson, P. M., Gutman, B., Anstey, K. J., Sachdev, P., & Toga, A. W. (2010). When more is less: associations between corpus callosum size and handedness lateralization. *NeuroImage*, *52*(1), 43–49.

Luhmann, H. J., Martinez Millan, L., & Singer, W. (1986). Development of horizontal intrinsic connections in cat striate cortex. *Experimental Brain Research*, *63*(2), 443–448.

Luttenberg, J. (1965). Contribution to the fetal ontogenesis of the corpus callosum in man. ii. *Folia morphologica*, *13*, 136–144.

Markov, N. T., Ercsey-Ravasz, M., Essen, D. C. V., Knoblauch, K., Toroczkai, Z., & Kennedy, H. (2013). Cortical high-density counterstream architectures. *Science*, *342*(6158), 1238406.

Markov, N. T., Misery, P., Falchier, A., Lamy, C., Vezoli, J., Quilodran, R., ... Knoblauch, K. (2010). Weight consistency specifies regularities of macaque cortical networks. *Cerebral Cortex*.

Martin, M. (1979). Hemispheric specialization for local and global processing. *Neuropsychologia*, *17*(1), 33–40.

Martin, R. D. (1983). *Human brain evolution in an ecological context*. American Museum of Natural History.

Martinez, A., Di Russo, F., Anllo-Vento, L., & Hillyard, S. A. (2001). Electrophysiological analysis of cortical mechanisms of selective attention to high and low spatial frequencies. *Clinical Neurophysiology*, *112*(11), 1980–1998.

Martinez, A., Moses, P., Frank, L., Buxton, R., Wong, E., & Stiles, J. (1997). Hemispheric asymmetries in global and local processing: evidence from fMRI. *Neuroreport*, *8*(7), 1685–1689.

Marzec, M., & Kurczynska, E. (2014). Importance of symplasmic communication in cell differentiation. *Plant signaling & behavior*, *9*(1).

McNab, J., Witzel, T., Bhat, H., Heberlein, K., Keil, B., Cohen-Adad, J., ... Wald, L. (2012). In vivo human brain measurements of axon diameter using 300mt/m maximum gradient strengths. In *International symposium on magnetic resonance in medicine* (p. 20).

Mely, D. A., & Serre, T. R. (2013). Cortically-inspired inhibition subtends better contour

integration. *Journal of Vision*, *13*(9), 1038–1038.

Monaghan, P., & Shillcock, R. (2004). Hemispheric asymmetries in cognitive modeling: connectionist modeling of unilateral visual neglect. *Psychological Review*, *111*, 283-308.

Musacchia, G., Choudhury, N. A., Ortiz-Mantilla, S., Realpe-Bonilla, T., Roesler, C. P., & Benasich, A. A. (2013). Oscillatory support for rapid frequency change processing in infants. *Neuropsychologia*, *51*(13), 2812–2824.

Navon, D. (1977). Forest before trees: The precedence of global features in visual perception. *Cognitive Psychology*, *9*(3), 353–383.

Norcia, A. M., Pei, F., Bonneh, Y., Hou, C., Sampath, V., & Pettet, M. W. (2005). Development of sensitivity to texture and contour information in the human infant. *Journal of Cognitive Neuroscience*, *17*(4), 569–579.

Norcia, A. M., Tyler, C. W., & Hamer, R. D. (1990). Development of contrast sensitivity in the human infant. *Vision Research*, *30*(10), 1475–1486.

Oishi, K., Zilles, K., Amunts, K., Faria, A., Jiang, H., Li, X., ... Mori, S. (2008). Human brain white matter atlas: Identification and assignment of common anatomical structures in superficial white matter. *NeuroImage*, *43*(3), 447–457.

Olivares, R., Montiel, J., & Aboitiz, F. (2001). Species differences and similarities in the fine structure of the mammalian corpus callosum. *Brain, Behavior and Evolution*, *57*(2), 98–105.

Pajevic, S., & Basser, P. J. (2013). An optimum principle predicts the distribution of axon diameters in normal white matter. *PLoS ONE*, *8*(1), e54095.

Palmer, T. D. (2002). Adult neurogenesis and the vascular nietzsche. *Neuron*, *34*(6), 856–858.

Paolicchi, J. (2008). IS the wada test still relevant? yes. *Archives of Neurology*, *65*(6), 838–840.

Paul, L. K., Brown, W. S., Adolphs, R., Tyszka, J. M., Richards, L. J., Mukherjee, P., & Sherr, E. H. (2007). Agenesis of the corpus callosum: genetic, developmental and functional aspects of connectivity. *Nature Reviews Neuroscience*, *8*(4), 287–299.

Pearlmutter, B. A. (1989). Learning state space trajectories in recurrent neural networks. *Neural Computation*, *1*(2), 263–269.

Peterzell, D. H. (1991). On the nonrelation between spatial frequency and cerebral

hemispheric competence. *Brain and Cognition*, *15*(1), 62–68.

Peterzell, D. H., Harvey, J., L O, & Hardyck, C. D. (1989). Spatial frequencies and the cerebral hemispheres: contrast sensitivity, visible persistence, and letter classification. *Perception & Psychophysics*, *46*(5), 443–455.

Petitto, L., Berens, M., Kovelman, I., Dubins, M., Jasinska, K., & Shalinsky, M. (2012). The perceptual wedge hypothesis as the basis for bilingual babies phonetic processing advantage: New insights from fNIRS brain imaging. *Brain and Language*, *121*(2), 130–143.

Piech, V., Li, W., Reeke, G. N., & Gilbert, C. D. (2013). Network model of top-down influences on local gain and contextual interactions in visual cortex. *Proceedings of the National Academy of Sciences*, *110*(43), E4108–E4117.

Pitts, M. A., & Martinezzr, A. (2014). Contour integration: Sensory, perceptual, and attention/based erp components. *Cognitive Electrophysiology of Attention: Signals of the Mind*, 178–189.

Plaut, D. C., & Behrmann, M. (2011). Complementary neural representations for faces and words: A computational exploration. *Cognitive Neuropsychology*, *28*, 251275.

Poeppel, D. (2003). The analysis of speech in different temporal integration windows: Cerebral lateralization as 'Asymmetric sampling in time'. *Speech Commun.*, *41*(1), 245-255.

Proverbio, A. M., Minniti, A., & Zani, A. (1998). Electrophysiological evidence of a perceptual precedence of global vs. local visual information. *Cognitive Brain Research*, *6*(4), 321–334.

Qin, Y., & Zhang, X. (2012). Road to specialization in agricultural production: Evidence from rural china [2012 Conference, August 18-24, 2012, Foz do Iguacu, Brazil].

Rabi, S., Madhavi, C., Antonisamy, B., & Koshi, R. (2007). Quantitative analysis of the human corpus callosum under light microscopy. *European Journal of Anatomy*, *11*(2), 95–100.

Rakic, P., & Yakovlev, P. I. (1968). Development of the corpus callosum and cavum septi in man. *The Journal of Comparative Neurology*, *132*(1), 45-72.

Reggia, J. A., Goodall, S., & Shkuro, Y. (1998). Computational studies of lateralization of phoneme sequence generation. *Neural Computation*, *10*, 1277–1297.

Reggia, J. A., & Schulz, R. (2002). The role of computational modeling in understanding hemispheric interactions and specialization. *Cognitive Systems Research*, *3*(1), 87–

94.

Ridgway, S. H. (2002). Asymmetry and symmetry in brain waves from dolphin left and right hemispheres: Some observations after anesthesia, during quiescent hanging behavior, and during visual obstruction. *Brain, Behavior and Evolution*, *60*(5), 265–274.

Riedmiller, M., & Braun, H. (1993). A direct adaptive method for faster backpropagation learning: the RPROP algorithm. In *, IEEE international conference on neural networks, 1993* (pp. 586–591 vol.1). IEEE.

Riise, J., & Pakkenberg, B. (2011). Stereological estimation of the total number of myelinated callosal fibers in human subjects. *Journal of Anatomy*, *218*(3), 277–284.

Rijsdijk, J. P., Kroon, J. N., & van der Wildt, G. J. (1980). Contrast sensitivity as a function of position on the retina. *Vision Research*, *20*(3), 235–241.

Rilling, J. K. (2014). Comparative primate neuroimaging: insights into human brain evolution. *Trends in Cognitive Sciences*, *18*(1), 46–55.

Rilling, J. K., & Insel, T. R. (1999a). Differential expansion of neural projection systems in primate brain evolution. *Neuroreport*, *10*(7), 1453–1459.

Rilling, J. K., & Insel, T. R. (1999b). The primate neocortex in comparative perspective using magnetic resonance imaging. *Journal of Human Evolution*, *37*(2), 191–223.

Rimol, L. M., Panizzon, M. S., Fennema-Notestine, C., Eyler, L. T., Fischl, B., Franz, C. E., ... Dale, A. M. (2010). Cortical thickness is influenced by regionally specific genetic factors. *Biological Psychiatry*, *67*(5), 493–499.

Ringo, J. L., Doty, R. W., Demeter, S., & Simard, P. Y. (1994). Time is of the essence: A conjecture that hemispheric specialization arises from interhemispheric conduction delay. *Cereb. Cortex*, *4*(4), 331–343.

Roberts, J. A., & Robinson, P. A. (2008). Modeling distributed axonal delays in mean-field brain dynamics. *Physical review. E, Statistical, nonlinear, and soft matter physics*, *78*(5 Pt 1), 051901.

Robertson, L., Lamb, M., & Knight, R. (1988). Effects of lesions of temporal-parietal junction on perceptual and attentional processing in humans. *J. Neurosci.*, *8*(10), 3757–3769.

Rogers, L. J. (2009). Hand and paw preferences in relation to the lateralized brain. *Phil. Transactions of the Royal Society B: Biological Sciences*, *364*(1519), 943–954.

Rogers, L. J., & Andrew, R. (2002). *Comparative vertebrate lateralization* (1st ed.). Cambridge University Press.

Roudaia, E., Bennett, P. J., & Sekuler, A. B. (2008). The effect of aging on contour integration. *Vision Research*, *48*(28), 2767–2774. doi: 10.1016/j.visres.2008.07.026

Roux, F., & Ceccaldi, M. (2001). Does aging affect the allocation of visual attention in global and local information processing? *Brain and Cognition*, *46*(3), 383–396. doi: 10.1006/brcg.2001.1296

Rumelhart, D. E., Hinton, G. E., & Williams, R. J. (1986). Learning representations by back-propagating errors. *Nature*, *323*(6088), 533–536.

Schenker, N. M., Sherwood, C. C., Hof, P. R., & Semendeferi, K. (2007). Microstructural asymmetries of the cerebral cortex in humans and other mammals. In William D. Hopkins (Ed.), *Special topics in primatology* (Vol. Volume 5, pp. 92–118). Elsevier.

Scherf, K. S., Behrmann, M., Humphreys, K., & Luna, B. (2007). Visual category-selectivity for faces, places and objects emerges along different developmental trajectories. *Developmental Science*, *10*(4), F15–F30.

Schleicher, A., Amunts, K., Geyer, S., Morosan, P., & Zilles, K. (1999). Observer-independent method for microstructural parcellation of cerebral cortex: A quantitative approach to cytoarchitectonics. *NeuroImage*, *9*(1), 165–177.

Schleicher, A., Morosan, P., Amunts, K., & Zilles, K. (2009). Quantitative architectural analysis: A new approach to cortical mapping. *Journal of Autism and Developmental Disorders*, *39*(11), 1568–1581.

Schmidt, K. E. (2013). The visual callosal connection: A connection like any other? *Neural Plasticity*, *2013*, e397176.

Schneidman, E., Freedman, B., & Segev, I. (1998). Ion channel stochasticity may be critical in determining the reliability and precision of spike timing. *Neural computation*, *10*(7), 1679–1703.

Schwartz, E. (1985). On the mathematical structure of the visuotopic mapping of macaque striate cortex. *Science*, *227*(4690), 1065–1066.

Seidenberg, M. S., & McClelland, J. L. (1989). A distributed, developmental model of word recognition and naming. *Psychological Review*, *96*(4), 523–568.

Seldon, H. (1981a). Structure of human auditory cortex. i. cytoarchitectonics and dendritic distributions. *Brain Research*, *229*(2), 277–294.

Seldon, H. (1981b). Structure of human auditory cortex. II. axon distributions and morphological correlates of speech perception. *Brain Research*, *229*(2), 295–310.

Seldon, H. (1982). Structure of human auditory cortex. III. statistical analysis of dendritic trees. *Brain Research*, *249*(2), 211–221.

Sereno, M. I., & Allmann, J. M. (1991). Cortical visual areas in mammals. In A. G. Leventhal (Ed.), *The neural basis of visual function* (pp. 160–172). London: Macmillan.

Sergent, J. (1982). The cerebral balance of power: confrontation or cooperation? *Journal of Experimental Psychology. Human Perception and Performance*, *8*(2), 253–72.

Sergent, J. (1983). Role of the input in visual hemispheric asymmetries. *Psychological Bulletin*, *93*(3), 481–512.

Sergent, J. (1985). Influence of task and input factors on hemispheric involvement in face processing. *Journal of Experimental Psychology. Human Perception and Performance*, *11*(6), 846–861.

Sherman, S. M. (2007). The thalamus is more than just a relay. *Current Opinion in Neurobiology*, *17*(4), 417–422.

Sherman, S. M., & Guillery, R. W. (1998). On the actions that one nerve cell can have on another: Distinguishing ?drivers? from ?modulators? *Proceedings of the National Academy of Sciences*, *95*(12), 7121–7126.

Smith, S. L., Gerhardt, K. J., Griffiths, S. K., Huang, X., & Abrams, R. M. (2003). Intelligibility of sentences recorded from the uterus of a pregnant ewe and from the fetal inner ear. *Audiology and Neuro-Otology*, *8*(6), 347–353.

Specializations - SimCity wiki guide. (n.d.). Retrieved 2014-05-09, from http://www.ign.com/wikis/simcity/Specializations

Stark, D. E., Margulies, D. S., Shehzad, Z. E., Reiss, P., Kelly, A. M. C., Uddin, L. Q., ... Milham, M. P. (2008). Regional variation in interhemispheric coordination of intrinsic hemodynamic fluctuations. *The Journal of neuroscience*, *28*(51), 13754–13764.

Swadlow, H. (2000). Information flow along neocortical axons. *Time and the brain (Miller R, ed). Harwood Academic Publishers, Singapore*, 131–155.

Swadlow, H. A., & Alonso, J. (2009). Spikes are making waves in the visual cortex. *Nat Neurosci*, *12*(1), 10–11.

Tarpley, R. J., & Ridgway, S. H. (1994). Corpus callosum size in delphinid cetaceans. *Brain, Behavior and Evolution*, *44*(3), 156–165.

Tomasch, J. (1954). Size, distribution, and number of fibres in the human corpus callosum. *The Anatomical Record*, *119*(1), 119–135.

Tootell, R. B. H., Mendola, J. D., Hadjikhani, N. K., Liu, A. K., & Dale, A. M. (1998). The representation of the ipsilateral visual field in human cerebral?cortex. *Proceedings of the National Academy of Sciences of the United States of America*, *95*(3), 818–824.

Tower, D. B. (1954). Structural and functional organization of mammalian cerebral cortex: The correlation of neurone density with brain size. *The Journal of Comparative Neurology*, *101*(1), 19–51.

Trujillo-Ortiz, A. (n.d.). *gmregress - file exchange - MATLAB central.* Retrieved 2014-05-18, from http://www.mathworks.com/matlabcentral/fileexchange/file_infos/27918-gmregress

Tushman, M. L. (1978). Technical communication in r & d laboratories: The impact of project work characteristics. *Academy of Management Journal*, *21*(4), 624–645.

Uddin, L. Q., Supekar, K., & Menon, V. (2010). Typical and atypical development of functional human brain networks: insights from resting-state FMRI. *Frontiers in systems neuroscience*, *4*, 21.

Uylings, H. B., Arigita, E. J. S., de Vos, K., Pool, C. W., Evers, P., & Rajkowska, G. (2010). 3-d cytoarchitectonic parcellation of human orbitofrontal cortex: Correlation with postmortem MRI. *Psychiatry Research: Neuroimaging*, *183*(1), 1–20.

van Essen, D. C., Glasser, M. F., Dierker, D. L., Harwell, J., & Coalson, T. (2011). Parcellations and hemispheric asymmetries of human cerebral cortex analyzed on surface-based atlases. *Cerebral Cortex*, bhr291.

van Hateren, J. H., & van der Schaaf, A. (1998). Independent component filters of natural images compared with simple cells in primary visual cortex. *Proceedings of the Royal Society B: Biological Sciences*, *265*(1394), 359–366.

Van Kleeck, M. H. (1989). Hemispheric differences in global versus local processing of hierarchical visual stimuli by normal subjects: New data and a meta-analysis of previous studies. *Neuropsychologia*, *27*(9), 1165–1178.

van Rossum, M. C. W., O'Brien, B. J., & Smith, R. G. (2003). Effects of noise on the spike timing precision of retinal ganglion cells. *Journal of neurophysiology*, *89*(5), 2406–2419.

Vermeire, B. A., Hamilton, C. R., & Erdmann, A. L. (1998). Right-hemispheric superiority in split-brain monkeys for learning and remembering facial discriminations.

Behavioral neuroscience, *112*(5), 1048.

Vincent, P., Larochelle, H., Lajoie, I., Bengio, Y., & Manzagol, P.-A. (2010). Stacked denoising autoencoders: Learning useful representations in a deep network with a local denoising criterion. *J. Mach. Learn. Res.*, *11*, 3371–3408.

Vogt, C., & Vogt, O. (1919). *Allgemeine ergebnisse unserer hirnforschung* (Vol. 25). JA Barth.

Volberg, G. (2014). Right-hemisphere specialization for contour grouping. *Experimental Psychology*, 1–9.

Volberg, G., & Greenlee, M. W. (2014). Brain networks supporting perceptual grouping and contour selection. *Frontiers in Psychology*, *5*.

Volberg, G., Wutz, A., & Greenlee, M. W. (2013). Top-down control in contour grouping. *PloS one*, *8*(1), e54085.

Wang, P., & Cottrell, G. W. (2012). A computational model of the development of hemispheric asymmetry of face processing. In *Proceedings of the 35th annual conference of the cognitive science society.* Austin, TX: Cognitive Science Society.

Wang, S. S. H. (2008). Functional tradeoffs in axonal scaling: Implications for brain function. *Brain, Behavior and Evolution*, *72*(2), 159–167.

Wang, S. S. H., Shultz, J. R., Burish, M. J., Harrison, K. H., Hof, P. R., Towns, L. C., ... Wyatt, K. D. (2008). Functional trade-offs in white matter axonal scaling. *J. Neurosci.*, *28*(15), 4047–4056.

Wasserstein, J., Zappulla, R., Rosen, J., Gerstman, L., & Rock, D. (1987). In search of closure: Subjective contour illusions, gestalt completion tests, and implications. *Brain and Cognition*, *6*(1), 1–14.

Weissman, D., & Woldorff, M. (2005). Hemispheric asymmetries for different components of Global/Local attention occur in distinct temporo-parietal loci. *Cerebral Cortex*, *15*(6), 870 –876.

White, L. E., & Fitzpatrick, D. (2007). Vision and cortical map development. *Neuron*, *56*(2), 327–338.

White, N. S., Leergaard, T. B., D'Arceuil, H., Bjaalie, J. G., & Dale, A. M. (2013). Probing tissue microstructure with restriction spectrum imaging: Histological and theoretical validation. *Human Brain Mapping*, *34*(2), 327-346.

Witelson, S. F. (1985). The brain connection: the corpus callosum is larger in left-handers.

Science, *229*(4714), 665–668.

Witelson, S. F. (1989). Hand and sex differences in the isthmus and genu of the human corpus callosum a postmortem morphological study. *Brain*, *112*(3), 799–835.

Young, A. W., & Bion, P. J. (1981). Accuracy of naming laterally presented known faces by children and adults. *Cortex; a Journal Devoted to the Study of the Nervous System and Behavior*, *17*(1), 97–106.

Zaidel, E., & Rayman, J. (1994). Interhemispheric control in the normal brain: Evidence from redundant bilateral presentations. In C. Umilt & M. Moscovitch (Eds.), *Attention and performance 15: Conscious and nonconscious information processing* (pp. 477–504). Cambridge, MA, US: The MIT Press.

Zhang, K., & Sejnowski, T. J. (2000). A universal scaling law between gray matter and white matter of cerebral cortex. *Proceedings of the National Academy of Sciences of the United States of America*, *97*(10), 5621–5626.

Zilles, K., & Amunts, K. (2009). Receptor mapping: architecture of the human cerebral cortex. *Current Opinion in Neurology*, *22*(4), 331–339.